DEVELOPMENT OF MOLECULAR IMPRINTED POLYMER BASED VALINE BIOSENSOR FOR ELECTROCHEMICAL ANALYSIS

by
Aysel ARAT

Submitted to Graduate School of Natural and Applied Sciences
in Partial Fulfillment of the Requirements
for the Degree of Master of Science in
Biomedical Engineering

Yeditepe University
2022

DEVELOPMENT OF MOLECULAR IMPRINTED POLYMER BASED VALINE BIOSENSOR FOR ELECTROCHEMICAL ANALYSIS

APPROVED BY:

Assist Prof. Dr. Feride Şermin UTKU ……
(Thesis Supervisor)
(Yeditepe University)

Prof. Dr. Adil DENİZLİ ……
(Hacettepe University)

Prof. Dr. Ali Ümit KESKİN ……
(Yeditepe University)

DATE OF APPROVAL: …./…./2022

I hereby declare that this thesis is my own work and that all information contained within it was obtained and presented in accordance with academic rules and ethical conduct. As required by these rules and conduct, I have fully cited and referenced all material and results, and this thesis study contains no plagiarism. If any of the materials used in the thesis require copyright, the appropriate permissions have been obtained. There has been no use of material from this thesis in the awarding of another degree.

I accept any and all legal responsibilities that may arise in situations that are in conflict with these situations.

Name, Last name ……

Signature …..……..……..

ACKNOWLEDGEMENTS

First of all, I would like to express my endless thanks and respect to our great leader, Gazi Mustafa Kemal Atatürk, who gave me the right to receive education as a woman. I would like to thank my advisor, Assist. Prof. Dr. Feride Şermin UTKU, for giving me the opportunity to conduct research and development, and for her invaluable, caring and sincere guidance throughout my master's project. She patiently taught me the steps and rules of doing the right research.

Finally, I would like to thank my very dear father and my dear mother, who have always made me feel their support, love and faith in my heart despite being far away.

ABSTRACT

DEVELOPMENT OF MOLECULAR IMPRINTED POLYMER BASED VALINE BIOSENSOR FOR ELECTROCHEMICAL ANALYSIS

Molecule imprinting technique (MIP) is an important tool in the preparation of intelligent three-dimensional polymeric materials, which are highly selective and are able to recognize the structure of the analyte with a unique recognition feature. In this study, a sensitive and stable electrochemical valine MIP biosensor was developed on gold disc electrodes and tested for selectivity and specificity. A hydrogel with molecule imprinted valine was formulated and polymerized on gold electrode; followed by the removal of valine molecules from the electrode surface, creating valine recognition sites. The electrodes with different amounts of valine recognition sites were tested using cyclic voltammetry and electrochemical impedance spectroscopy in solutions containing different concentrations of valine. The current, voltage and impedance response of the electrode to varying valine concentration was investigated. In this study, ten different concentrations of valine receptors were imprinted on gold electrodes with the removal of the template molecule to form molecule-recognizing regions (Au-MIP) and template molecule not removed (Au-UMIP) and control electrodes without any imprinted template molecules (Au-NIP). A total of twenty one gold electrodes were analyzed in phosphate buffer solution (pH=5). Au-MIP electrodes imprinted at 0.3M displayed a linearly regressed increase in impedance in the 10^{-18} to 10^{-6} M dynamic range, with a LOD of 9.76E-17 M and LOQ of 7.18E-15 M. Valine imprinted electrode selectivity factor (α) was 3.96, 4.19, and 92.76 times higher for Valine than glycine, alanine and methionine, respectively. The imprinting factor (β) values indicated that the valine imprinted biosensor (MIP) was more selective for valine than the control electrode (NIP), in presence of the interfering molecules glycine, alanine and methionine, at a ratio of 4.13, 4.41 and 96.63 respectively. RSD percent for intra- and inter-day precision were obtained as 2.3 percent and 8 percent respectively. The valine imprinted electrodes had 98.69±9.32 percent stability on day-45 with a RSD percent of 9.44. Our results indicate that the MIP biosensor developed for electrochemical analysis has displayed higher specificity than the conventional electrochemical analysis methods.

ÖZET

ELEKTROKİMYASAL ANALİZ İÇİN MOLEKÜLER BASKILI POLİMER BAZLI VALİNE BİYOSENSÖRÜNÜN GELİŞTİRİLMESİ

Molekül baskılama tekniği (MIP), kendine özgü tanıma özelliği ile analitin yapısını tanıyan ve oldukça seçici olan akılı üç boyutlu polimerik malzemelerin hazırlanmasında önemli bir araçtır. Bu çalışmada, altın disk elektrotlar üzerinde hassas ve kararlı bir elektrokimyasal valin MIP biyosensörü geliştirildi ve seçicilik ve özgüllük açısından test edildi. Molekül baskılı valin içeren bir hidrojel, altın elektrot üzerinde formüle edildi ve polimerize edildi ve ardından valin molekülleri elektrot yüzeyinden uzaklaştırılarak valin tanıma bölgeleri oluşturuldu. Farklı miktarlarda valin tanıma bölgelerine sahip elektrotlar, farklı konsantrasyonlarda valin içeren çözeltilerde döngüsel voltametri ve elektrokimyasal empedans spektroskopi kullanılarak test edildi. Elektrodun değişen valin derişimine karşı akım, voltaj ve empedans yanıtları incelendi. Bu çalışmada, molekül tanıma bölgeleri (Au-MIP) oluşturmak için şablon molekülün çıkarılmasıyla, şablon molekülü çıkarılmamış (Au-UMIP) ve herhangi bir baskılanmış şablon molekülü (Au-NIP) olmadan kontrol elektrotları ile altın elektrotlar üzerine on farklı valin reseptörü konsantrasyonu baskılanmıştır. Toplam yirmibir farklı altın elektrot fosfat tampon çözeltisinde (pH=5) analiz edildi. 0.3M Au-MIP elektrotları, 9.76E-17 M LOD ve 7.18E-15 M LOQ ile empedansta 10-18 ile 10-6 M dinamik aralıkta doğrusal olarak gerileyen bir artış sergiledi. Valin baskılı elektrot seçicilik faktörü (α), valine için sırasıyla glisin, alanin ve metioninden 3.96, 4.19 ve 92.76 kat daha yüksekti. Baskılama faktörü (β) değerleri, glisin, alanin ve metiyonin moleküllerinin varlığında sırasıyla 4.13, 4.41 ve 96.63 oranında, valin baskılı biyosensörün (MIP) valin için kontrol elektroduna (NIP) göre daha seçici olduğunu göstermiştir. Gün içi ve günler arası kesinlik için RSD yüzdesi sırasıyla yüzde 2.3 ve yüzde 8 olarak elde edilmiştir. Elektrotların kararlılığının, 45. günde yüzde 98.69±9.32 ve RSD'nin yüzde 9.44 olduğunu göstermiştir. Sonuçlarımız, elektrokimyasal analiz için geliştirilen MIP biyosensörünün geleneksel elektrokimyasal analiz yöntemlerine göre daha yüksek spesifisite sergilediğini göstermektedir.

TABLE OF CONTENTS

LIST OF FIGURES

LIST OF TABLES

LIST OF SYMBOLS/ABBREVIATIONS

A	Instrument response
ABS	Acetic buffer solution
AFM	Atomic force microscopy
AIBN	Azobisisobutyronitrile
Ai	Response obtained from solution i
APS	Ammonium persulfate
Au	Gold
CS	Standard concentration
CV	Cyclic voltammetry
CX	Analyte
D	Coefficient of diffusion
DNA	Deoxyribonucleic acid
E	Half cell reduction potential
E^0	Standard half cell reduction potential
EGDMA	Ethylene glycol dimethylacrylate
EIS	Electrochemical impedance spectroscopy
FET	Field effect transistor
fmol	Femtomole
GC	Gas chromatography
HEMA	2-Hidroksietil metakrilat
HCl	Hydrochloric acid
Ip	Current density
ISFET	Ion-sensitive field-effect transistor
k	Constant of proportion
L	Liter
LOD	Lower limit of detection
LOQ	Lower limit of quantification
M	Molar
MAGA	Methacryloamidoglutamic acid
mg	Milligram
MIP	Molecular imprinted polymer

mL	Milliliter
mM	Millimolar
MS	Mass spectrometry
mV	Millivolt
n	Number of transmitting electrons
N	Normality
NAD	Nicotinamide adenine dinucleotide
NADP	Nicotinamide adenine dinucleotide phosphate
NIP	Non-imprinted polymer
OCP	Open circuit potential
PBS	Phosphate buffer solution
PGE	Pencil graphite electrode
pH	Potential of hydrogen
QCM	Quartz crystal microbalance
R_{ct}	Load transfer resistor
Rdx-PBS	Redox-phosphate buffer solution
RNA	Ribonucleic acid
rpm	Revolutions per minute
Rs	Solution resistance
SPR	Superface plasm resonance
S_m	Average witness signal
S_{bl}	Default witness deviation
V_S	Standard volume
V_T	Total volume
V_X	Analyte volume
YÜDETAM	Yeditepe University Experimental Research Center
3D	3 Dimensional
µA	Microamperes
µM	Micromolar

1. INTRODUCTION

Living organisms struggling to survive in nature perceive all the changes that take place in their environment over a certain time. In order to survive, they must keep up with these changes. This system of perception in living things is taken as a sample by researchers and attempted in a laboratory setting. Biosensors here were obtained as a result of the transformation in the laboratory setting of a biological event into an electrical signal. Living things divide the biological substances into their fundamental parts to allow the perception of stimuli that take place in life. These pieces and their relationships are then analyzed as a whole. By combining the systems obtained through this study, bio-sensor structures are developed (transformation of a biological event into an electrical signal) [1]. Biosensors have shown rapid growth with the technological advances of today. The fact that sensor technology covers the fields of study in such disciplines as chemistry, biology, material science, engineering and updates with new technologies has made a significant contribution to biosensor development.

Biosensors identify the substance to be analyzed and relate the changes which are caused by an interaction with magnitudes such as concentration, density and quantity. Biosensors which are active in the health sector in particular, are commonly used for the detection of pathogens such as viruses and bacteria, the measurement of body-harming substances or the detection of molecules that can be used as a marker for diseases. With molecular identification, biosensors are easily used in all fields without hospital requirements. These type of molecular biosensors are classified as POC (point of care) devices, but in diagnosis, diagnosis and monitoring of diseases, they are very efficient, easy-to-use, portable, fast, precise and inexpensive systems. Although molecules can be measured in different ways in biosensors, electrochemical methods are one of the most used. Electrochemical biosensors contain in their structures substances such as enzymes, cells, tissue and nucleic acids. It also responds to the level of the detected molecules, ions or compounds and delivers electrical signals. Concentration changes lead to changes in electrical properties, such as current, voltage or impedance.

Biosensors allow the conversion of biological responses into optical, thermal and electrical signals to different chemical substances used in biological research. As a result of the

advancement of electronic circuits, biosensors have become small structures over time. Thanks to nano-sized tests, biosensors are placed on chips. In addition, biological mechanisms have been developed in the field of electronics and different response capabilities [2].

Biosensors based on electrical analysis, and particularly biosensors using voltammetric sensing, molecular imprinted polymers can be sufficient tools due to their selectivity and sensitivity to enable early diagnosis of a variety of diseases. MIPs are typically obtained by bulk (3-D), a method in which a cross-linking agent is used to polymerize selected functional monomers (organic or inorganic material) [3]. Molecularly imprinting method generates molecular recognition regions for electrodes, which enable the molecule to be attached to those regions. Biosensors with high sensitivity and selectivity are produced in the creation of these recognition regions by using biomolecules at very low concentrations. With the molecularly imprinting process, the printing of suitable electrodes may be used to evaluate amino acids, hormones, enzymes, salt structures, vitamins or substances used as markers for disease.

Valine ($C_5H_{11}NO_2$) is an aliphatic and highly hydrophobic essential amino acid found in the DNA protein along with other amino acids. Valine molecules have a lot of potential for use in optical devices due to their chirality. Unlike other amino acids, such as alanine, the electronic properties of these crystals have received little attention. Furthermore, because two forms with different chirality exist, the effect of molecular structure on the physical and chemical properties of the crystal can be investigated. Valine is a branched essential amino acid, which promotes muscle growth and tissue repair [4].

This study provided valine-sensitive biosensor by imprinting valine on gold disk electrode (CHI 101) by means of a molecularly imprinting procedure previously not tried for valine molecules. While performing the molecularly imprinting of valine, Acrylamide/Bisacrylamide, TRIS-HCl and APS/TEMED were used. The CHI 101 Au working electrode with HCl and deionised water washed away valine molecules and valine-specific binding sites formed. Electronic impedance spectroscopy was used to analyze the changes in electrical properties occurring on the electrode by attaching the valine to the valine receptors of the gold working electrode. An impedimetric biosensor electrode was developed based on Cyclic Voltammetry (CV) and Electrochemical Impedance Spectroscopy (EIS) data extracted from the analysis. Using rat blood serum, the biosensor

was checked for feasibility for clinical use. This study was conducted to accurately and reliably evaluate the valine concentration in a solution containing many other molecules with high selectivity and sensitivity, using the key-and-lock mechanism.

1.1. AIM OF THE STUDY

In this project, it is aimed to develop a stable and useful biosensor that can easily detect valine by electrochemical impedance spectroscopy method.

Within the framework of evidence-based medical ethics, qualities and quantities of relevant organic and inorganic substances in body fluid, tissues and cells are evaluated in the diagnosis and diagnosis of diseases. Studying patient samples in clinical laboratories is a very complex and lengthy process. The laboratory process basically consists of three parts: pre-analytical phase, analytical phase and post-analytical phase.

It is aimed to develop a biosensor that will both facilitate the real-time qualitative and quantitative measurement of valine and other nano-sized cancer metabolites and shorten this process by making a MIP-based valine sensor using a gold disk electrode. It was decided to use pure gold electrode based MIP for the detection of valine molecule, which is one of the metabolites that can be used in early pancreatic cancer diagnosis. Qualitative and quantitative analysis of various nano-sized molecules associated with other types of cancer can be performed with this electrode, which can quickly measure real-time blood samples, without removing the patient from his/her environment, saving time and space [5].

1.2. BIOSENSORS

Living organisms must perceive changes in their environment and adapt to circumstances so that they can survive as soon as possible. These behaviors typically create a defensive shield against external hazards by using natural sensors that have a pure enzyme, tissue and microorganism function [6]. Biosensors were obtained by several researchers through the simulation of the detection process in living objects. If the enzyme electrode obtained in the studies containing glucose and oxygen is contacted to the biological solution, both compounds pass through the enzyme membrane. The solution oxidizes glucose into gluconic

acid by means of electrode oxygen. The enzyme electrode thus tests the volume of oxygen partial pressure decrease. These modifications are used by biological sensors to acquire physical data. Biological sensors (enzymes, antibodies, nucleic acid (deoxyribonucleic acid, ribonic acid), cells, tissues, artificial biological receptors) and selectively interacting physicochemical transducers (electrical electrodes), transistors, thermistors and fibers (optical fibres), piezoelectronic crystals to analyze physical signs. From these calculated physical signals, electrical signals are produced. Structures that work in this way are called biosensors [7]. Biological sensors operate by integrating the signal produced by the interaction of the detected sensors (electrodes, polymers, etc.) and transmitting it to the measuring device by means of a conducting system. Biosensors are able to assess quantitatively and qualitatively the substances that are to be studied in liquid or gaseous conditions [8]. Biosensors that are devices for the inspection and sensing of target-analyte materials in biological reactions consist of two main structures, interlinked biochemical and electrochemical properties. The biochemical component interacts with and recognizes the material to be studied. During this process, biochemical product can be produced. The data obtained as a result of the recognition event is converted into a readable numeric value in the electrochemical section of the biosensors [9]. Biosensors, which are classified as modern structures that combine the selectivity properties of biological molecules with the processing capabilities of advanced electronic methods, are used to classify a broad variety of applications with modern technology. During the selective, fast and consistent response to a substance with a biological or chemical effect, biosensors must have bioactive and biosensing materials. The analysts should be able to identify these materials and have near interaction with the transducer. Otherwise, complications occur when the sizes of the biosensors are processed. The scientific or technological uses of many branches of science gave rise to these constructs thanks to experience in scientific fields like biology, physics, chemistry and biochemistry. These structures possess numerous superior properties such as selectivity, reproducibility, stability and short response time [10].

1.2.1. STRUCTURE AND FUNCTIONS OF BIOSENSORS

The biomolecular structure that the analyser is able to detect and bioceptors that play a key role in the creation of the biosensors are highly sensitive biological structures that associate selectively with the material to be analysed. Biological molecules (e.g. antibodies, enzymes,

proteins, nucleic acids) or living biological systems (e.g. cells, tissues and microorganisms) can be used in the structures of bioreceptors. Today, the biosensors contain a wide variety of biocomponents and transducer substances and systems some of which are given in Table 1.1 [11].

Table 1.1. The components of biosensors [12].

Analyte (Sample)	**Biocomponent (Receptor)**	**Signal transmitting system**
Valine	Artificial receptor	Impedimetric
Hormones	Enzymes	Amperometric
Enzyme	Antibodies	Impedimetric
Glucose	Glucose oxidase	Amperometric
L-amino acids	Horserodis, peroxidase	Potentiometric
Coenzymes	Cell	Semiconductor
Substrate	Tissue sections	Optical
Activator	Receptors	Photometric
Inhibitor	Microorganisms	Fluorometric
Antibody-antigen	Nucleic acids	Fluorometric
Nucleic acid	Lipids	QCM
Microorganisms	Cell organelles	Microcentilevers

In general, the functioning mechanism of the biosensor is produced by combining it with a transduction unit that transmits the signal received from the interaction of the bioactive element, which optionally interacts with the analyzing substance and is used with measuring devices. Physical components such as amplifier, microprocessor, transistor, thermistor and digital imager may be included in the device depending on the system specifications. These physical components convert the biological functions of the biocomponents into physical signals based on their measuring capacity. The amperometrical and potentiometric electrodes are selected by considering the biochemical reaction involved. In the process of measuring and transmitting signal that occurs as a result of the interaction of the substance determining the bioactive element, electronic equipments such as electrochemical, optical, calorimetric and piezoelectric are used [13].

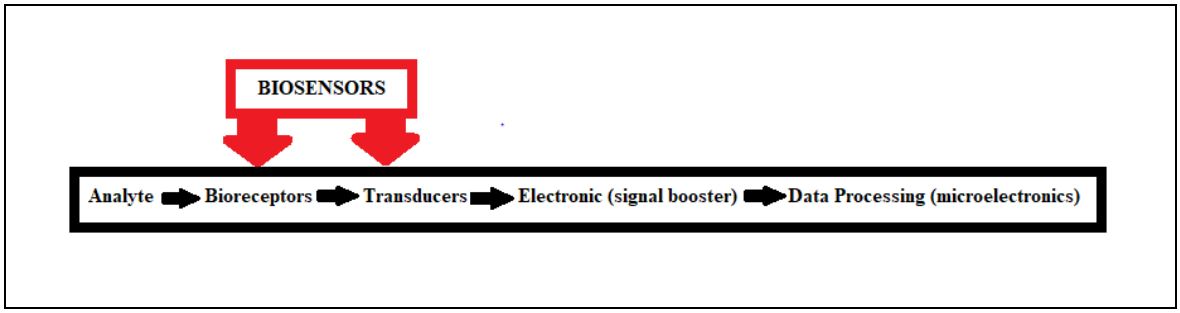

Figure 1.1. Components that make up a biosensor [41].

The substances to be analyzed are identified as analytes in biological sensor applications. Biomolecular receptors convert analytical materials into another type as shown in Figure 1.1. Enzymes and antibodies are widely used analytic substances during these phases. The first step in the process between enzyme substrates and antibody-antigen is to bind the analytes to the molecules of protein. Catalytic antibodies produced in recent years allow a chemical to react or alter the reaction speed without any changes. Polymerisation of small protein-structured substances results in the formation of large molecules enabling the formation of artificial receptors [14].

1.2.2. CLASSIFICATION OF BIOSENSORS

Biosensing technologies are applied via multidisciplinary research in biology, chemistry and engineering with biosensing materials, transducer devices and immobilization processes. Biosensors can also be categorized in different ways, based on biosensing materials, the technology and processing tools used. Depending on the biological sensing materials used, biosensors can be classified into three separate groups: biocatalytic, bioaffinity and microbial. The biocatalytic group comprises enzymes; the bioaffinity group contains antibodies, detectors, and nuclear acids; and the microbial group comprises microorganisms, cells, organels, and tissues [15,16].

Biosensors can be divided into two general categories when considered at the base of the interfaces between bio-sensing materials and transduction media: (a) direct biosensors detecting and quantifying the analyte directly in physical and chemical signals using any transducer, such as impedance, optical fiber, SPR (superface plasm resonance), SAW (Surface Acoustic Wave) or QCM (Quartz Crystal Microbalance) transducer; (b) indirect

biosensors, detecting chemical reactions in presence of analytes using electrochemical, impedance, optical transistors, QCM, calorimetric and magnetic transducers.

The same biosensor can be used directly or indirectly in various applications. Biosensors can be categorized as electrochemical, optical, piezoelectric, thermal and magnetic according to the various conversion tools used [17]. The types and operating principles of transducers are summarized in Tables 1.2 and 1.3.

Table 1.2. The types of biosensors based on biosensing materials.

Biosensor	**Operating Principle**
Enzyme sensors	Enzymes that accelerate the transition states of reactions by stabilizing them with amperometric, potentiometric, chemical radiation and thermal transducers are commonly used in enzyme sensors [18].
Immuno sensors	An antibody may be attached directly to the electrode surface of the transducer or an optical waveguide to provide a visible signal when the analyte is attached. The response signal increases in direct and sandwich formats but decreases as the analyte concentration increases in competitive formats [19,20].
Nucleic acid probe sensors	The genetic make-up of an organism and the presence of genes or mutated genes associated with genetic defects are studied by the nucleic acid samples. A nucleic acid test is a nucleic acid subdivision that precisely identifies and binds target nucleic acid by forming stable hydrogen bonds between the two nucleic acid sequences [21,22].
Microbe or cell based sensors	A microbial biosensor includes fixed microbial living cells and metabolic functions of the respiratory transducer-associated cell. The study to be controlled in this step may be either a substrate or an inhibitor [23,24].
Tissue-organelle based sensors	Biosensors based on tissue or organelles are more stable compared to enzyme biosensors. Sensors taken from animals and plants for transducer biosensors such as ISFET, electrical and optical fibers are fixed for short response periods, high sensitivity, large range of linear responses and natural selectivity [25].

Table 1.3. Classification based on the conversion tool applied.

Electrochemical biosensors	Electrochemical biosensors are sensors that calculate the produced electrical signals on the basis of the interaction between the test substance and the electrodes [26].
Amperometric sensors	The electrochemical cells use a constant potential in amperometric sensors and a reduction or oxidation reaction produces the related current [27].
Voltametric sensors	It is based on the calculation of resistance, capacity, conductance or impedance in the circuit [28].
Potentiometric biosensors	Potentiometric detection typically tests the voltage of an electrochemical reaction inside an electrochemical cell containing a biological sensing component, either by the action of the product or by its operation [29].
Conductivity/Capacitance/impedance biosensors	Biosensors of conductivity, capacity and impedance test different electrical field changes. These variations may include the electrical overall conductivity and the change in capability due to the fixed layer on

	the electrode surface, which may also be expressed in the impedimetric reaction [30].
Optic biosensors	It is the calculation of the change of optical properties according to the target analyte concentration [31].
Absorption and reflection biosensors	The absorption calculation is based on the use of analyte or reagent absorption properties in a permeable environment. Reflective biosensors test with the reagent and the analyte in an impermeable medium. In biosensors with enzymes, antibodies and DNA/RNA samples, absorption/reflection transducers are used [32].
Radiation biosensors	The sensing layer with fixed biosensing materials will detect the particular target analyte in the sample in the radiation biosensor. After the light propagation starts, the light is sent by the waveguide to the light detector [33].
SPR biosensors	The quantity of electrical charges on the sensor surface can be calculated in many ways such as wave-length shifts, angle, strength of reflectance and reflecting phase as the reflexion index of the specimens while staying steady with other parameters [34].
Optical fiber biosensors	An optical fiber is used as a straight transducer for directing the light and converting the light from the sample and controlling the device detection sample remotely [35].
Piezoelectric biosensors	The Piezoelectric biosensors use commercially available instruments such as quartz crystal microbalances based on theories developed in the field of electricity, mass and viscoelativity [36].
Thermal biosensors	By integrating the biosensing material in a physical transducer, such as a thermometer, thermopile or thermistor, thermic biosensors have been generated [37].
Magnetic biosensors	Magnetic sensors are small biosensors focused on the accurate detection of magnetic micro and nanoparticles by means of magneto-resistive effect in micro fluid channels [38].

1.2.3. DESIGN OF BIOSENSORS

The design of the biosensor involves the selection of the bioreceptor, the determination of the suitable transducer and the biologic component fastening on the transducer. In the meantime, new technologies, samples, operating conditions and outcomes are taken into account [39] as given in Table 1.4.

There are some known, unknown, organic and inorganic materials in the analytes used. Therefore, the analyte concentration can be increased by filtration, centrifugation and magnetic immuno-separation methods. Magnetic immunoseparation is preferred during biosensor studies, as the application is fast, simple and automatic. Magnetic nanoparticles and microparticles can be magnetically treated in the separation process using a permanent

magnet or an electromagnet. When manipulated cells remain in a magnetic system, they can be identified, sorted and filtered [40].

Table 1.4. Essential elements used in the design of biosensors [41].

Used technologies	Analytes	Operating Conditions	Outcomes
*Chemistry *Biochemistry *Biology *Molecular Biology *MEMS *NEMS *Microfluidic *Nanotube *Nanowire *Nanoparticle *Instrumentation	*Solid *Liquid *Gas *Organic-Inorganic Materials	*Online *Real-time *Continuous or discrete *Single or multiple targets *Automatic or semi-automatic *Benchtop or portable *In the field or in the laboratory	*Selectivity *Sensitivity *Measurement range and duration *Repeatability *Speed *Cost *Consistency *Stability

Certainity or selectivity are the most relevant parameters used in the performance of biosensors. The biosensor affinity only to the analyte is an indicator of its selectivity. The ratio of change in the output signal of the biosensor in response to a change in the concentration of the target analyte determines its sensitivity. The signal shift can be detected by exposing the biosensor to a standard solution containing various target analyte concentrations. Many factors affect a biosensor's sensitivity due to various biosensing materials and processing devices. The biosensor sensitivity is expected to remain unchanged and to deliver consistent and reliable numerical results [42].

The biosensor detection time starts with the loading of the sample and extends till the acquisition of the series of results. The response time of the biosensor is the time required to acquire a signal based on a defined equation. The reset time is the time needed to prepare a biosensor before the next example is loaded. Repeatability and reproducibility are critical in biosensor assessments due to the great variability in biological samples and biosensing elements. Temperature, humidity, pH and other factors influence biosensing elements over time. The lifespan of organic materials that deteriorate under these conditions is also a significant factor. In reality, a biosensor response signal can be expressed in months, days or even hours depending on the biosensor material used [43].

1.2.3.1. Bioreceptor Selection

The role of bioreceptors is to act as a molecular detector. By reacting with the analysis solution, they generate a physicochemical effect that the converter can detect. A biosensor selection should therefore be performed according to the molecule to be analyzed.

Bioreceptor enzymes are generally available on the market. Enzymes are also available for specific applications from one or more biological sources. They can be used alone or with NAD^+ and $NADP^+$ cofactors. Particularly when the formation of complex reactions is examined, the choice of bioreceptors for microorganisms or cells is more appropriate. These structural elements contain all the enzymes and cofactors required to replicate and compensate for losses in enzyme reactions when a proper culture is formed. The use of tissues and organelles, another type of bioreceptor, has an advantage by easily attaching them to the transducer and its strong structure [44].

1.2.3.2. Transducer Selection

The transducer, an element to determine whether a reaction has occurred between the analyte and the biosensor during the analysis process, should be selected depending on the type of reaction. Furthermore, another important point for the choice of transducer is the environment in which the biosensor is used. For example, a biocompatibility biosensor to be used in *in vivo* applications should be designed considering the possibility of toxic, metallic or polymeric components occurring, especially in long-term applications [44].

1.2.3.3. Immobilization of Bioreceptors

The most challenging stage in biosensor generation is the immobilization of the bioreceptors on the transducer. In order to maintain the maximum degree of interaction with the analyte and to ensure that the measurements taken are safe, biologically active molecules must be immobilised on the transducer. Animal and vegetable tissue have a membrane structure and are thus exempt from this regulation. Physical methods such as the arrest of the polymer gel matrix, microencapsulation in a semi-permeable capacity, physical surface adsorption and chemical methods such as covalent bonding, cross-linking of double or multifunctional reagents and chemical adsorption are possible in the immobilization of the receptors on the transducers [44-46].

Since enzymes are high molecular weight, sufficiently large proteins, they can easily be physically attached in polyacrylamide gel. Furthermore, enzymes can be fixed by dialysis

membranes on the electrode to prevent protein diffusion. Since fastening requires the enzymes to remain in solution for a long time, it has a negative effect on the activities of the enzymes. This is why more chemical fixation is being used today. Covalent or cross-links are used more widely among chemical fixation methods because they ensure that enzymes remain stable for a long time [44].

1.2.4. PERFORMANCE CRITERIA OF BIOSENSORS

Whether a prepared biosensor is in compliance with the goals can only be calculated after the performance requirements have been evaluated. Generally, biosensors are characterized by eight parameters.

1.2.4.1. Selectivity

Selectivity is one of the most important parameters for an ideal biosensor. Selectivity is the ability of biosensors to interact with the molecule that can only be assessed in the environment. The sensitivity of the biomolecule to the target analyte, which is one of the biosensor components, is not of concern to other analytes that may be present in the atmosphere and therefore does not produce incorrect results. Therefore, it is important to assess the interference rates of species which may invade the ecosystem and to take steps to prevent the attempt. Sensor interferences, biocatalyst interferences and pH are primarily influenced by the biosensor's selectivity.

1.2.4.2. Sensitivity

Sensitivity is characterized as a change of the biosensor output signal due to the biochemical reaction added to the measuring medium with the analyte concentration. The magnitude of this ratio is an indicator of biosensor sensitivity. The sensitivity of an excellent biosensor is desirable to remain constant and extremely sensitive throughout the entire biosensor lifespan.

1.2.4.3. Linearity

In studies conducted with the prepared biosensor the linear zone should be established where signal changes indicate a linear tendency with a changing analyte concentration by adding some analyte amounts to the measuring medium in order to obtain exact measurements [47].

1.2.4.4. Response Time

One of the main reasons for biosensor production and use is that they can produce realistic results in a short period of time. The response time is defined as the time elapsed before the signal changes are read as a measuring medium is applied to the item to be evaluated.

The biosensor response time depends on events in three main phases.

1. How easily the substrate material diffuses from the analytical media to the sensor surface,
2. How easily the biocatalyst with its active core reacts,
3. How easily the resulting product diffuses on the measured sensor surface.

The key factors which influence those three events are the mixing speed of the solution, the concentration of the substrate material, the concentration of the enzyme, the optimal pH, the temperature and whether any layer is used in the surface and its consistency. The increase in the mixing speed decreases the time of response, while the increased concentration in the substrate material contributes to its extension. Increasing the amount of the enzyme and reaching the maximum pH minimize the response time. As the increase in the amount of enzyme leads to thickening of the bioactive layer, this can increase the diffusion problem and extend the response time.This problem can be overcome by the use of highly specific enzyme preparations. Temperature has a positive effect on diffusion, and the response time is shortened. It should not be overlooked however that moving away from the optimum enzyme temperature causes a decrease in the activity of the enzyme [48].

1.2.4.5. Observability Limit

The smallest analyte concentration the prepared biosensor can react to at a certain confidence level is defined as the limit of observability. This constraint depends on the analytical signal size of the witness signal statistical deviation rate. In other words, as long as the analytical signal is not as large as *k* times the noise signal deviation, it is impossible to see the signal accurately. S_m, the average witness signal, is the smallest analytical signal to be determined and equivalent to S_{bl} and the default witness deviation, S_{bl}, times *k*.

$$Sm = Sbl + k(Sbl) \tag{1.1}$$

1.2.4.6. Stability

The stability of an enzyme electrode is one of the most important determinants of its functional usefulness in other variables under suitable conditions. Stability provides information on the lifespan of the biosensors and calculates how many tests the biosensor can carry out. Stability affected by the physical strength of the enzyme used; parameters of pH, temperature, humidity, climate, concentration of O_2, chemical and physical character of the polymer used to immobilize the enzyme are affected as well.

1.2.4.7. Repeatability

The same findings from experiments with the same electrode against the substrate material or with more than one sample with the same properties show that the biosensor results can be reproducible. Electrode activity, stability and purity are crucially significant when the sensor can achieve reproducible results. Standard deviation, correlation and correlation numerical measurements are used for measurement accuracy. If a standard calibration chart is to be avoided, standard methods of addition are implemented. The sample being analysed is measured along with a known standard the concentration of which is about twice the concentration of the unknown[48].

1.2.4.8. Lifetime

A biosensor must have a long lifespan, which helps it to retain its sensitivity under normal operating conditions. This period may depend on the total number of measurements made or the magnitude of the measured analyte concentration and is defined as a measure of the changes in activity of the biomolecule as a result of the measurements. Higher concentrations can lead to a faster reduction in sensitivity. Furthermore, in the analytical setting, other chemical species which inhibit activation can be present regardless of the analyte concentration. The length of time between storage and the use of the biosensor is also a significant aspect. The biological component might also have to be preserved in a special chemical environment in order to maintain its bioactivity, as the biosensor has to be kept in an environment appropriate for its structure. The biosensor life also affects parameters such as frequency of calibration, stability and repeatability [49].

1.3. ELECTROCHEMICAL MEASUREMENTS

Electrical effects are applied to the electrode solution system in electrochemical techniques and the response is measured. This response provides information on the system's properties. Nearly all electrochemical methods have potential, current and time parameters. These parameters are specified in the technical name. For example, rough information about the method can be obtained from potential-current, time-current and time-load parameter, in terms of voltammetry, chronoamperometry and chronocoulometry.

Electroanalytical methods are usually divided into two: static methods at equilibrium, where the net current is zero; and dynamic methods in which the net current is distant from equilibrium. Most techniques recognize currents and these are controlled mainly by potential or current. Potential and current are controlled with large amplitude or small amplitude techniques. Large amplitude techniques are more frequently used than others [50].

The advantages of electrochemical methods compared to other analysis methods are: being cheap, being selective, having the ability to work with very few samples, determining the lower limit of determination (LOD), having a wide linearity range, and having the ability to work with many different electrodes.

1.3.1. ELECTRODES USED IN ELECTROCHEMICAL ANALYSIS

Electrochemical experiments are conducted in a triple electrode device. The varying-potential electrode is called the working electrode. In triple electrode system, a wide range of working electrodes are used. These electrodes are: carbon glass, silver, gold, nickel, graphite, mercury, carbon paste, etc. The current generated by the reduction of the substances in the working electrode is known as the cathodic current and due to its oxidation the current is known as anodic current. Working electrode must be conductive and inert in the potential range studied. Negative potential limit of working electrode must be high and the desired geometric shape should be easily given and easy to process.

The reference electrode is the electrode whose potential remains constant during the experiment. Ag/AgCl or calomel saturated electrodes are typically used as reference electrodes. Tl/TlCl, Hg/HgO, $Hg/HgSO_4$ and $Ag/AgNO_3$ electrodes are also used for

voltammetry as reference electrodes. An ideal electrode of reference must be reversible and compatible with the Nernst equation, its potential should not change over time. Potential must not drift greatly with a small change in current and in temperature.

The counter electrode is the third electrode used in electrochemistry. While the potential difference between the working electrode and the reference electrode is evaluated in the triple elecrode system, it is confirmed that the current passes through the opposite electrode instead of the reference electrode. This prevents the potential of the reference electrode from being affected by the flow of current through the circuit. Platinum wire is the counter electrode commonly used [51].

1.3.2. CYCLIC VOLTAMMETRY (CV)

As the potential of a working electrode in a stationary solution with a conducting material is applied linearly with time, the current potential curve looks like a peak. This technique is known as cyclic voltammetry when the potential scanning is inverted to decrease again linearly after hitting a certain potential value in the forward direction. Potential scanning speeds in the forward and the reverse directions can be kept the same in cyclic voltammetry and can be used at different scanning speeds if necessary. Furthermore, forward and reverse scanning may be conducted once or several times.

When a fast potential scan for the electrode is performed, the potential approaches the normal reduction potential value and depletes the substance. The rate of depletion of the substrate on the electrode surface approaches potentially negative values and, as a result, increases the current value as more material is depleted. As the rate of depletion increases, the current starts to check the amount of material that diffuses to the surface of the electrode. The diffusion rate decreases, as the diffusion layer thickens over time. The current-potential relation in the voltammogram obtained by the cyclic voltammetry technique is shown in Figure 1.2.

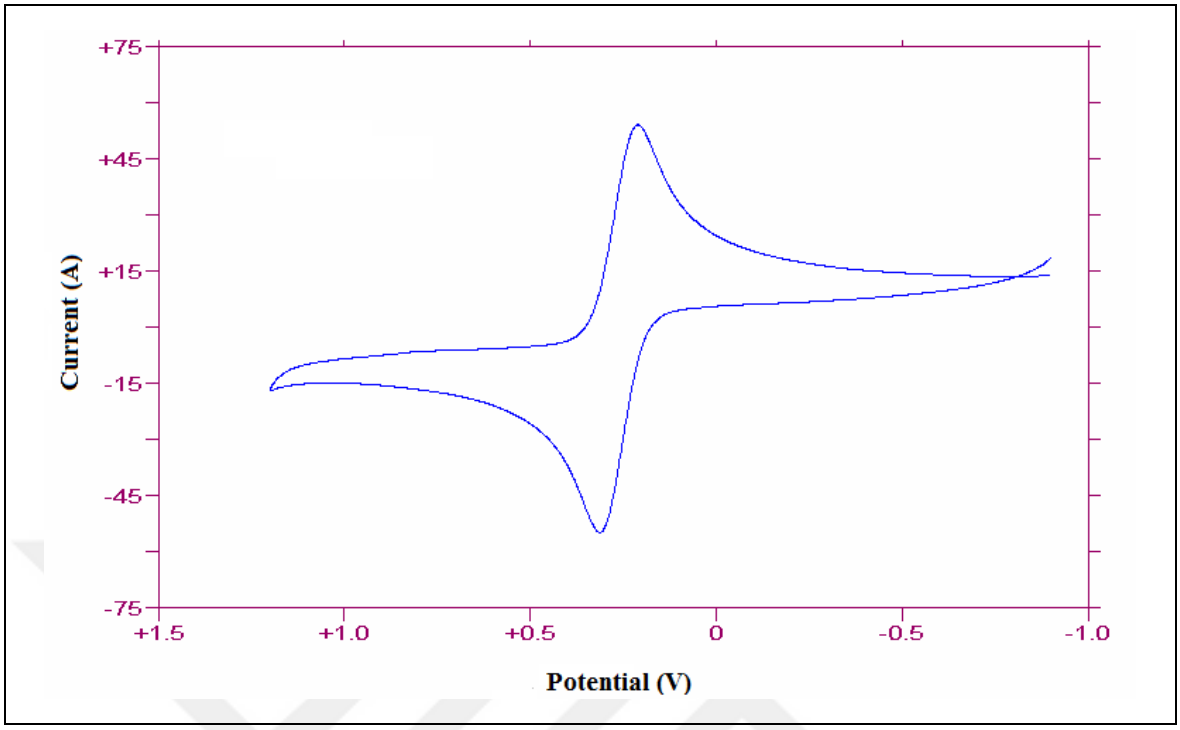

Figure 1.2. The current potential (I-V) curve obtained using cyclic voltammetry (CV) [87].

The presence and magnitude of chemical reaction and the amount of adsorption, diffusion and electron transmission can be calculated in the CV technology by adjusting the scanning speed as a function of change in peak height. In addition, the forward and reverse scan peaks and kinetic data can be collected to estimate the reaction mechanism.Alternating voltammetry is used in quantitative evaluation, surface modification, kinetics of electrode reactions investigation, presence of different physicochemical constants, research of adsorption incidents, electrode reaction mechanisms, and complex structure determination.

The electrode reaction in a reversible reduction reaction uses the cyclic voltametric technique;

$$O + ne^{-} \leftrightarrow R \tag{1.2}$$

Electrochemical reversibility applies in this regard to conditions in which the rate of transmission of electrons is high. However, very few mechanisms are reversible electrochemically. At first, the solution contains only the Oxidized-substance and there is no

chemical reaction except for electron transfer. Where the potential sweep speed is too slow, after a certain potential, the I-V graph achieves the limit current and the current becomes independent of the potential. With the increase in the potential scanning rate, the I-V graph is seen as a peak and as the scanning speed increases the peak height.

The [O] / [R] ratio depends on potential with the Nernst equation for a reversible reaction.

$$E = E^0 - \frac{RT}{nF} ln \frac{[R]}{[O]} \tag{1.3}$$

In the CV technique the voltammogram of a reversible $O + ne^- \leftrightarrow R$ reaction is as shown in Figure 1.2 and the potential time profile in Figure 1.3.

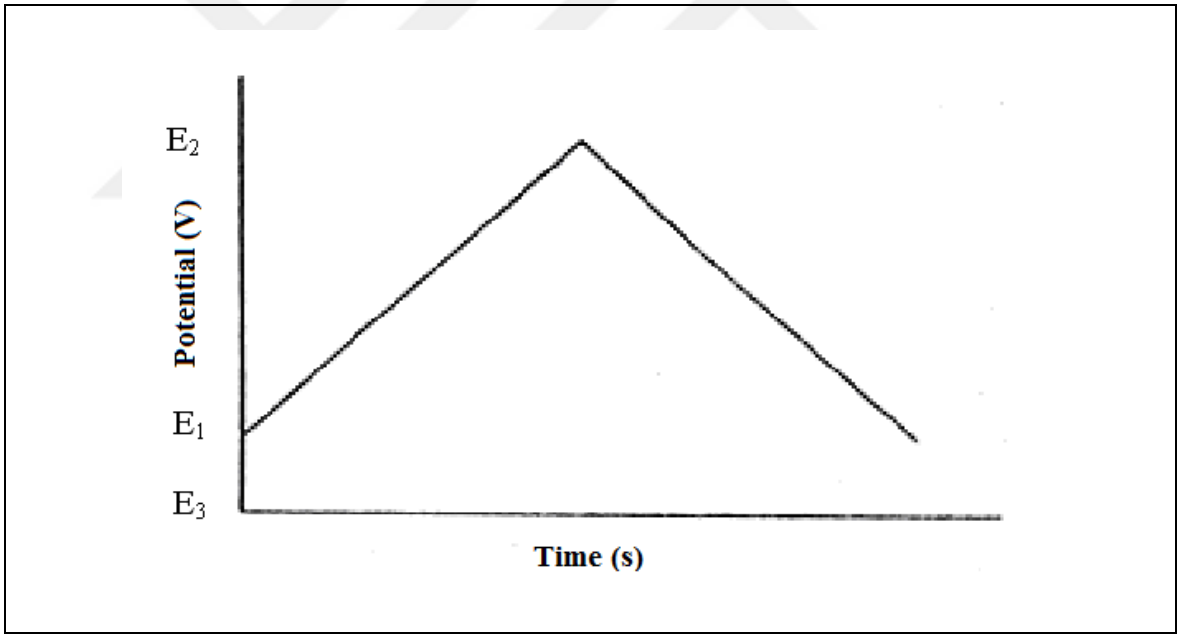

Figure 1.3. Potential scan and time curve for cyclic voltammetry [87].

The following equation is derived mathematically from Fick's Second Law considering the limits and scanning speed for the value of peak current I in CV at 25 °C. This is called the Randles-Sevick equation.

$$I_p = -(2{,}69x10^5)n^{3/2}C_0D^{1/2}v^{1/2} \quad (1.4)$$

I_p (A/cm^2) = Current density

v (V/s) = Scan speed

D (cm^2/s) = Coefficient of diffusion

C_o (mol/cm^3) = The concentration in mother liquor of O

n = Number of transmitting electrons

Reversibility tests can be performed using the CV data. The system can be reversed if the Ip-$v^{1/2}$ graph is linear and passes through the origin.

In reversible systems the transfer rate of electrons is higher than the mass transfer rate at all potentials and on the electrode surface Nernst Equation is valid. In irreversible systems, Nernst Equation is not valid because the rate of transmission of electron is not high enough. The type of the CV voltammogram varies from that of the reversible example. In irreversible systems, if the potential scanning rate is very low, the electron transfer rate is higher than the mass transfer rate, and the mechanism can be seen as reversible. The lack of anodic peak does not necessarily show that the transmission of the electron is irreversible. For example: in a very fast chemical reaction after the electron transfer step; in reverse scanning, no oxidation peak can be observed as the product can quickly be transformed into a different material [87].

1.3.3. ELECTROCHEMICAL IMPEDANCE SPECTROSCOPY (EIS)

In a circuit, the total resistance is called impedance. Impedance spectroscopy is an important technique for electrochemical structures and methods to be investigated. In comparison to electrochemical methods, electrochemical impedance spectroscopy can be used in both volume and interface studies along with time constants varying from minutes to microseconds. Furthermore, the impedance process is based on the electrochemical cell shift in which a small wave signal in equilibrium or constant state is calculated. A broad variety of parameters, such as applied potential, applied current or convection speed, can be used

for hydrodynamic electrodes. The key benefit of this approach is that the responses are roughly linear as long as the differences are small enough [50].

Impedance is primarily based on resistance calculation influenced by capacitive and inductive changes in the application of high frequencies. Impedance is a measure of the resistance of all circuit elements to electrical current. EIS is widely used to determine the interaction between bioreceptor and analyte. Especially in affinity-based biosensor applications, EIS is an advantageous method for connecting binding sites and signal transmission systems. In the triple electrode method, at least three values are needed depending on the equivalent circuit feature. This can be represented as the electrolyte solution between the electrode reference and the operating electrode resistance (Re), the double-layer capacitance C dl and the load transfer impedance (Zf) known as faradaic impedance. The accuracy of the EIS data is checked by identifying it with an equivalent electrical circuit. In model circuits, elements of circuits are typically found: resistors, condensers, inducers. General elements are shown in Table 1.5.

Table 1.5. Schematic representation of electrical general elements.

Impedance Element	**Voltage versus Current**	**Impedance**
Resistance (R)	$E=IR$	$Z=R$
Inductor (L)	$E=Ld_i/d_t$	$Z=j\omega L$
Capacitor (C)	$I=Cd_e/d_t$	$Z=1/j\omega C$

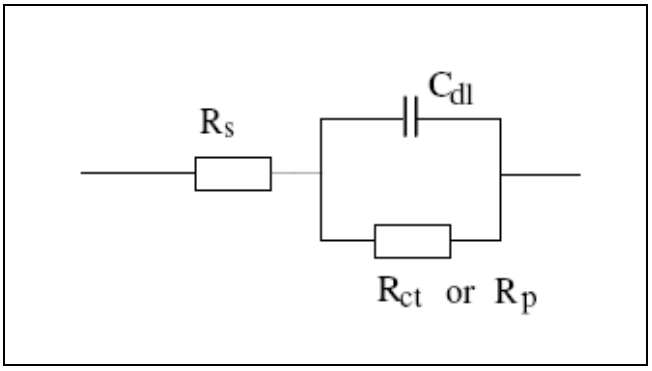

Figure 1.4. A schematic representation of the circuit of Randles [87].

The Randles circuit is the simplest EIS circuit. Solution resistance, double-layer condenser has a load or polarization condenser.The Randles circuit is shown in Figure 1.4.

Impedance tests are used corrosion studies, coating of metals, semiconductor electrods properties investigation, biosensor, conductive polymer characteristics investigation, biological systems, thin organic film properties determination, battery, and performance investigation of semiconductor polymers.

1.4. MOLECULAR IMPRINTING METHOD

Modern biotechs have seen the advent of critical and selective application areas in the fields of detection of illicit drugs and chemical warfare agents, as well as new demands and opportunities in clinical diagnosis, environmental analysis, food analysis and processing, including biomimetic receptor systems that are capable of precisely binding with the target molecule [52]. It was incredibly difficult to discover small target molecules such as inorganic ions. For this reason, numerous approaches have emerged and the molecular imprinting approach is one of them [53]. Due to their high selectivity of the target molecule, carriers prepared by molecular printing are promising. In 1972, Günter Wulff and his working group initially described molecular printing method and it was used to obtain highly selective binding places by arranging the three dimensional structures in synthetic polymers of functional groups [54].

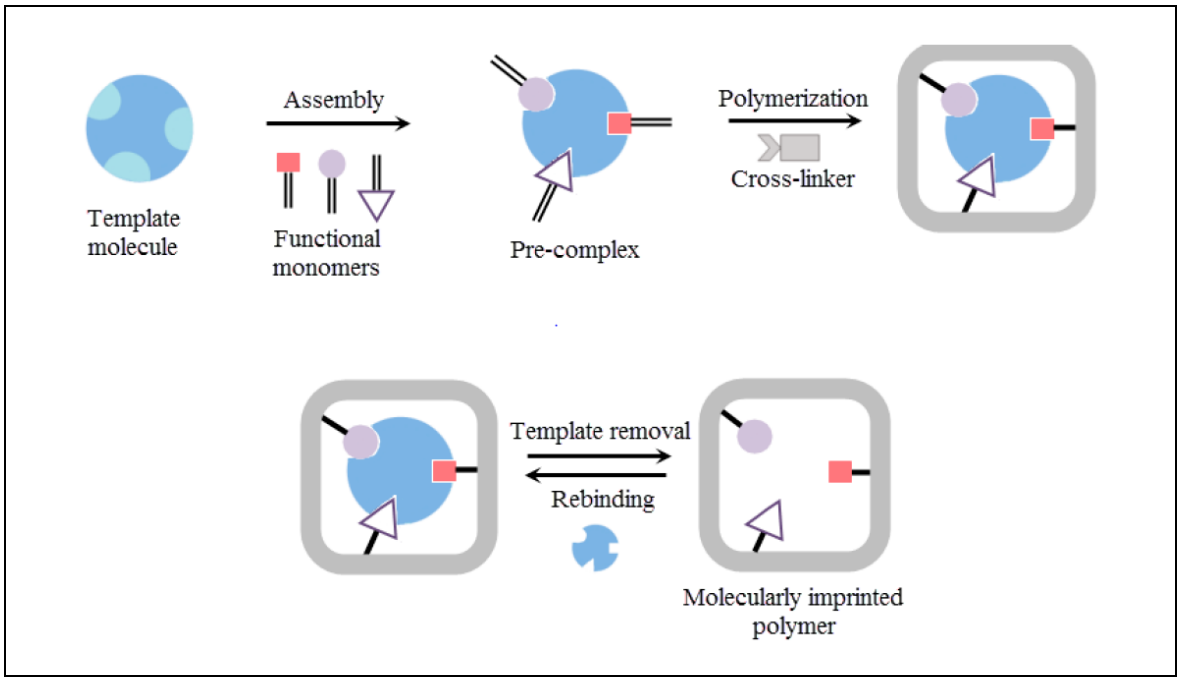

Figure 1.5. Molecular printing system schematic representation [55].

The application of the molecular imprinting approach to many analytes is one of the most important aspects. Small organic molecules are best classified such as drugs, pesticides, amino acids and peptides, nucleoid bases, steroids and sugars. Although it is difficult to imprint larger organic molecules with similar methods, they can be imprinted partially. There may be proteins, mineral and cell crystals [56-58]. Molecular imprinted polymers selectively identify the target molecule. The high mechanical strength, heat and pressure resistance, physical strength, high stability in presence of extreme conditions like acids, foundations, metal ions and organic solvents are very useful and the preparation process cost is low and simple. They thus retain their success for years under acceptable conditions [59-61].

The molecular printing method's characteristics permit it to be used for identification and separation in a number of fields, such as life, pharmaceutical and environmental sciences. In recent years, molecular identification of imprinted polymers has been extensively studied. The molecular printing technique seeks to arrange functional monomers by means of covalent or non-covalent interactions around a mould and then, through a suitable process, to produce solid materials with a chemical function (Figure 1.5). After the process, the structure forms cavities unique to the mold molecule by removing the mold molecule. An ideal material for processes such as separation, chemical determination and catalysis is therefore obtained.

Molecular imprinting technology produces precise positions of identification by template molecules in synthetic polymers. Two functional groups are normally present in the functional monomer. One of them interacts directly non-covalently or reversibly covalently with the mold, while the other will covalently bind with the crosslinker that does not interact with the mold. The choice of molar ratios of the monomer, crosslinker and template molecule and polymerized temperature is very critical when preparing molecular imprinted polymers [62].

Various molecular printing technologies have emerged today. One of them is the method, whereby compounds are formed using the same three-dimensional structure. Functionality arises from the fact that the functional groups are organized in the same way as the original. This technology is referred to as double printing. Another one is to fill small chemical compounds into the active area to take shape, as in the double printing process. The resulting

structure will be a copy that occludes this region and then it will be possible to test the behavior of this structure in a living cell.

Molecular imprinting method is classified into two major classes, covalent and non-covalent, by form of interaction between the target molecule and the monomer.

1.4.1. COVALENT PRINTING

The covalent printing process consists of a reversible covalent bonding of the Schiff base, ketal, esters, amides and boronic acids to form the target molecule and monomer complex. The functional monomer and the template molecule are connected with each other by covalent bonds before the polymerization process. Following the polymerisation, covalent bonds are broken and separated from the polymer to form a mold as shown in Figure 1.6. If the target molecule interacts with the impressed polymer, the same covalent bond is regenerated.

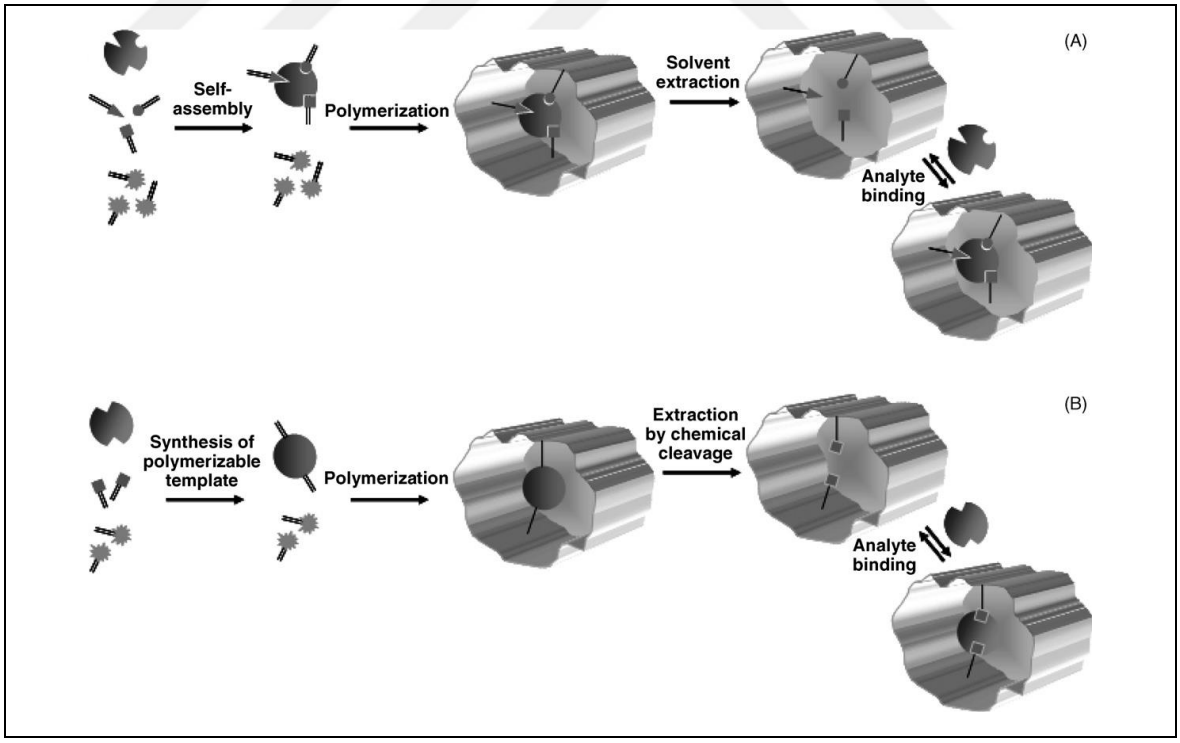

Figure 1.6. Schematic representation of the two production techniques of MIP. (a) Non-covalent printing. (b) Covalent printing [63].

Advantages :

1. As a stable mold monomer complex is formed, the binding sites are homogenously distributed.
2. Since the conjugates are made up of covalent bonds, polymerization conditions can be applied as required (for example, high temperature, high or low pH).

Disadvantages :

1. Problems also occur in the monomer-template conjugate synthesis, and the synthesis process is not economic.
2. The number of reversible attachments to the polymer of the target molecule is reduced.
3. Binding kinetics are sluggish because of the formation of the covalent bond.
4. The target molecule is difficult to extract after polymerisation [64,65].

1.4.2. NON-COVALENT PRINTING

Mosbach et al. have mentioned the absence of a covalent relation between the template molecule and functional monomer for molecular imprinting and the effectiveness of uncovalent interactions between the template molecule and functional monomer. Adding to the reaction mixture are random non-covalent interactions and active imprinting. The molecular bonding of a monomer prototype was achieved through hydrogen bonds and electrostatic interactions. This approach has succeeded in eliminating numerous medications, insecticides and other chemicals. Many scientists did not expect the imprinting effect to take place with such value in a very simple way. Scientists are persuaded that this approach is being used in a large molecular field and has begun to be used in their own laboratories [66,67].

The functional monomer and the template molecule are connected by non-covalent interactions (such as hydrogen bonding, electrostatic interactions and coordination bond formation). Following polymerisation, the mold molecule is separated with sufficient solvents from the polymer. Polymers with the target molecule are connected by non-covalent interactions. Due to the simplicity of mold removal process and the development of several

high affinity polymer regions, Non-covalent printing is a mostly preferred method for preparing molecular polymers.

The relation between the mold and the monomer forms unique bonding sites and copolymerizes with the crosslinker. Compounds with polar groups, such as hydroxyl, carboxyl, amino and amide, should be chosen as template molecules in non-covalent contact. The imprinted target molecules communicate with the polymer in both the imprinting and reconnection phase through non-covalent interactions (such as hydrophobic, hydrogen bonding, and metal coordination) [68, 69].

Advantages :

1. The covalent monomer template conjugate synthesis is not necessary.
2. After polymerisation, the molecule is quickly separated from the polymer since non-covalent interactions are less than covalent.
3. The kinetics of reconnection of the target molecule are simple.
4. Non-covalent printing is simpler than covalent printing and higher affinity binding sites than the formation of covalent binding [64].

Disadvantages :

1. Restricted polymerization conditions can be used to improve non-covalent interactions.
2. Functional monomers are overused to boost the stability of the formation of bonds and can contribute to the formation and reduction of non-specific binding sites [70, 71].

In the printing process, the molecular functional monomer, analyser (molecule or ion to be print), crosslinker, solvent and polymerisation initiator is used for efficient molecular imprinting.

1.4.3. COMPONENTS USED IN MOLECULAR PRINTING

1.4.3.1. Functional Monomers

The stability of the monomer-pattern complex is dependent on the selection of functional monomers. In order for a functional monomer to be useful, it must have a sufficient number

of functional binding sites. In order to increase the complex formation and molecular imprinting impact, it is critical that the functional monomers and the functional groups of the imprinted molecule or ion match [78].

1.4.3.2. Target Molecule

The molecule or ion to be imprinted in the molecular imprinting process interacts with monomers with the suitable functional groups, hence the molecule to be imprinted is highly crucial in this method. A polymerization-inhibiting or reaction-slowing group must be present in the molecule to be imprinted, and the imprinted molecule must be stable at high temperatures. The bonding interaction rises as the number of bonding groups in the template molecule increases. Molecules that can be imprinted include drugs, amino acids, carbohydrates, proteins, nucleoside bases, hormones, pesticides, coenzymes, and ions [79].

1.4.3.3. Cross-Linkers

Controlling morphology, stabilizing binding sites, and providing mechanical stability are all functions of crosslinkers in polymer matrixes, which are either gels, macroporous, or microgel powders. Crosslinkers and functional monomers must work together in order for imprinting to be successful. For example, if only one of the functional monomers or crosslinkers dominates polymerization, then copolymerization will not take place. The functional monomer and the crosslinker must be in stoichiometric balance. Crosslinkers display non-covalent interactions with functional monomers or template molecules in very large molar ratios, decreasing the efficiency of imprinting. The binding sites of the template molecules are relatively near to each other at low mole ratios. Due to the surrounding sites, the target molecule binding site is effectively blocked [80].

1.4.3.4. Solvents

Depending on the printing procedure, solvents are employed that are appropriate for the job. Polymerization in non-covalent imprinting polymerization is also tasked with enhancing molecule-functional monomer complex formation. For both imprinting and non-covalent interactions between the template and functional monomer, the choice of solvent is critical. Polymerization is also prevented from forming undesired byproducts since the heat is evenly distributed during the process.

1.4.3.5. Initiators

In free radical polymerization, a variety of chemical initiators with varying chemical characteristics are employed as radical sources. APS/TEMED, AIBN and ADVN are the most commonly utilized. It is impossible to reach high temperatures if the contacts between the monomer and the template molecule are relatively weak [78].

2. MATERIALS AND METHODS

2.1. MATERIALS

2.1.1. Instruments and Consumables

Table 2.1. Instruments and consumables used for electrochemical experiments.

Item	Brand	Production place	Catalogue no
Potentiostat galvanostat	Biologic	Seyssinet-Pariset/France	SP-200
Fridge	Arçelik	Sütlüce/Istanbul	No-frost
Ultrasonic bath	Isolab	Arnavutköy/Istanbul	621.05.006
Centrifuge	Isolab	Arnavutköy/Istanbul	603.06.001
Incubator	Nüve	Bahçelievler/Istanbul	EN120
Precision balance	Ohaus	New Jersey	Pioneer
Atomic Force Microscopy	Bio-Rad	California/USA	XE 100
Vortex mixer	Labnet	New Jersey	VX-200
pH meter	Thermo Scientific	Waltham,Massachusetts/US	Orion Versa Star
Vacuum filtration	Lab312	Şaşmaz/Ankara	RDVAC
Ag/AgCl reference electrode	Gamry	Warminster/USA	930-00015
PGE	Tombow	Tokyo/Japan	0.9-2B
Automatic pipette	Eppendorf	Hamburg/Germany	H427443J

2.1.2. Chemicals

Table 2.2. Chemicals used for electrochemical processes.

Item	Brand	Production place	Catalogue no
Acrylamide	Sigma	St. Louis, Missouri/USA	A8887
Bisacrylamide	Sigma	St. Louis, Missouri/USA	294381
EGDMA	Sigma	St. Louis, Missouri/USA	335681
HEMA	Daejung	Siheung/South Korea	4120-4400
TEMED	Biobasic	Toronto/Canada	TB0508
APS	Biobasic	Toronto/Canada	AB0072
TRIS-HCl	Sigma	St. Louis, Missouri/USA	10812846001
Valine	Biobasic	Toronto/Canada	VB0172
Choline Chloride	Sigma	St. Louis, Missouri/USA	C7017
Glycine	Fluka	Germany	50058
Alanine	Fluka	Germany	05160
Methionine	Alfa Aesar	Massachusetts/US	A10318
Potassium Ferricyanide	Sigma	St. Louis, Missouri/USA	702587

Sodium Chloride	Supelco	Istanbul	1552782804-134
Sodium Acetate Trihydrate	Isolab	Arnavutköy/Istanbul	969.013.0500
Potassium Chloride	Daejung	Siheung/South Korea	6566-4405
Disodium Hydrogen Phosphate	Fluka	Germany	71632
Potassium Dihydrogen Phosphate	Isolab	Arnavutköy/Istanbul	960.066.1000
Hydrochloric Acid	Sigma	St. Louis, Missouri/USA	30721
Nitric Acid	Isolab	Arnavutköy/Istanbul	951.04V.1000
Acetic Acid	Isolab	Arnavutköy/Istanbul	901.013.2500

2.1.3. Solutions

2.1.3.1. Acetate Buffer Solution (ABS)

1 L Acetic buffer solution (ABS) (pH 4.8) was prepared to optimize the electrodes with the anodization procedure during the preliminary preparation of the pencil graphite electrodes. 20 mM Sodium chloride (NaCl), 0.1 N sodium acetate trihydrate ($C_2H_3NaO_23H_2O$) and 0.1 N acetic acid (CH_3COOH) were made up to 1 L volume using distilled water.

2.1.3.2. Phosphate Buffer Solution (PBS)

0.137 M Sodium chloride (NaCl), 0.0027 M potassium chloride (KCl), 0.01 M disodium hydrogen phosphate (Na_2HPO_4) and 0.0018 M potassium dihydrogen phosphate (KH_2PO_4) were prepared by adding distilled water to the solution for 1 L Phosphate buffer solution (PBS). For the electrochemical analysis of the electrodes by making CV and EIS measurements, Rdx-PBS solution was obtained by adding 5 mM Potassium ferricyanide ($K_3[Fe(CN)_6]$) to 1 L PBS.

2.1.3.3. Different concentrations of valine solutions

To prepare solutions containing valine in different molarities, 11.25 mg of valine was dissolved in 20 mL of PBS and valine stock solution (solution 1) was obtained (PBS used in stock solution and diluted concentrations does not contain Rdx). The stock solution was serially diluted as given in Table 2.3 in order to determine the detection ranges of the molecularly imprinted valine electrode.

Table 2.3. Dilution of solution.

Solution number	Valine concentration	Dilution step
2	$7.16x10^{-6}$ M (E-6)	200 µl stock solution, 800 µl PBS
3	$7.16x10^{-7}$ M (E-7)	100 µl solution 2, 900 µl PBS
4	$7.16x10^{-8}$ M (E-8)	100 µl solution 3, 900 µl PBS
5	$7.16x10^{-9}$ M (E-9)	100 µl solution 4, 900 µl PBS
6	$7.16x10^{-10}$ M (E-10)	100 µl solution 5, 900 µl PBS
7	$7.16x10^{-11}$ M (E-11)	100 µl solution 6, 900 µl PBS
8	$7.16x10^{-12}$ M (E-12)	100 µl solution 7, 900 µl PBS
9	$7.16x10^{-13}$ M (E-13)	100 µl solution 8, 900 µl PBS
10	$7.16x10^{-14}$ M (E-14)	100 µl solution 9, 900 µl PBS
11	$7.16x10^{-15}$ M (E-15)	100 µl solution 10, 900 µl PBS
12	$7.16x10^{-16}$ M (E-16)	100 µl solution 11, 900 µl PBS
13	$7.16x10^{-17}$ M (E-17)	100 µl solution 12, 900 µl PBS
14	$7.16x10^{-18}$ M (E-18)	100 µl solution 13, 900 µl PBS

2.1.3.4. Preparation of the blood sample

Before starting the studies, Ethics committee approval was obtained from Yeditepe University, Faculty of Medicine, Experimental Research Center (YÜDETAM) to work with 6 Spraque Dawley rats, 12 weeks old and weighing approximately 400 g. Ketamine hydrochloride (100 mg/kg) and xylazine (7 mg/kg) were administered by intraperitoneal injection as a preanesthetic, analgesic and anesthetic agent. The depth of anesthesia was determined by monitoring the physiological response. After anesthesia, the blood sample was collected in blood tubes containing heparin to prevent coagulation by entering the vein by venous route. Blood samples were centrifuged at 4000 rpm for 15 minutes, blood plasma was separated, and stored in tubes at -20°C to be used in the study.

2.2. METHODS

Gold disc electrode (CHI101 Au) and pencil graphite electrode (PGE) were chosen as working electrodes. The PGEs were used to test the precision, reproducibility and stability of the electrodes. The molecular imprinted length of the pencil graphite electrodes was marked as approximately 2 cm, and measurements were made by immersing the electrodes 2 cm into the solution while performing the analysis.

2.2.1. The Experimental Setup

The electrodes were electrochemically analyzed using the experimental setup depicted in Figure 2.1. Part 1 of this setup is where the connections between the solution to be measured and the potentiostat device. The connection cables placed in the fixing mechanism allow for the transmission of the voltage to be supplied from the device to the electrodes as well as the transmission of the responses obtained from the electrodes to the device. Part 2 refers to the PBS solution in which the triple electrode assembly is placed and potassium ferricyanide analyses are performed. Part 3 is a galvanostat potentiostat that performs OCP, CV, and EIS analysis. The fourth component of the assembly represents the transfer of measurement results to the computer using the potentiostat device software. Finally, in the fifth section, there is a digital heater that allows measurements to be taken at 37^{o}C.

The platinum plate electrode as the counter electrode and the gold disc electrode as the working electrode were positioned in the Rdx-PBS solution at a distance of 2 cm as shown in Figure 2.2. The Ag/AgCl electrode was positioned as the reference electrode in the middle of the gold electrode and the platinum plate electrode. A thermometer connected to a digital heater was added to this system in order to keep the measurement temperature under control.

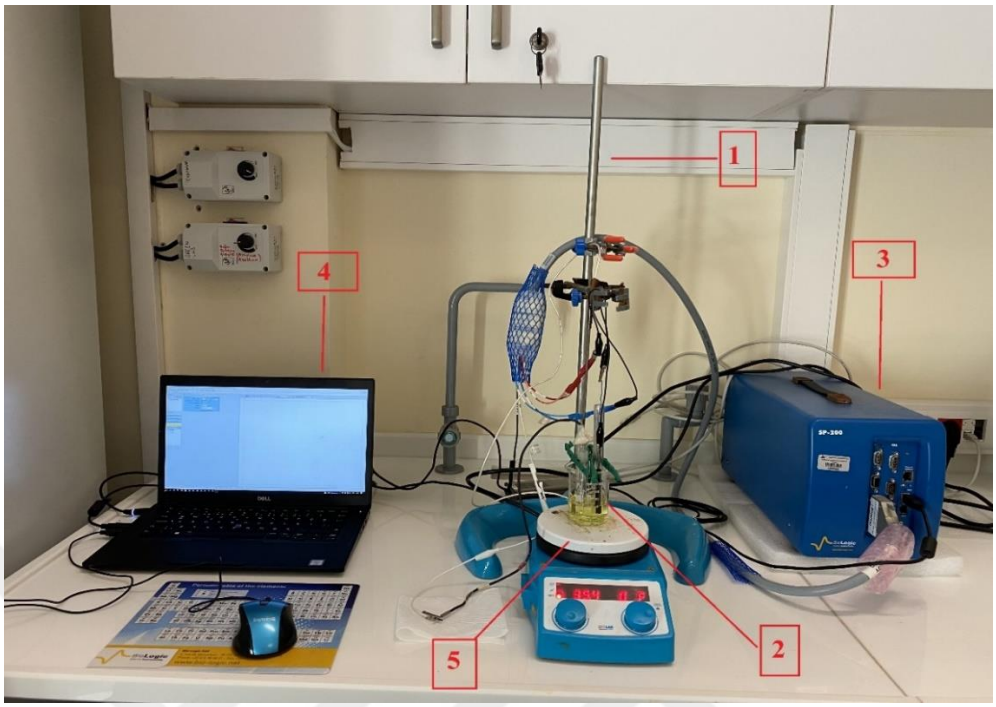

Figure 2.1. The experimental setup.

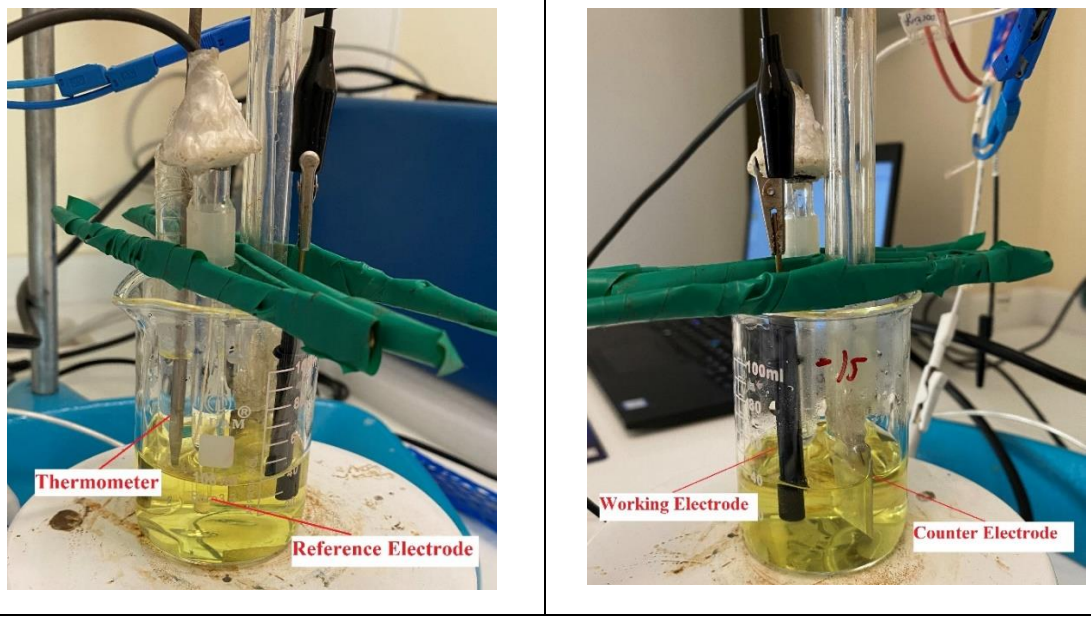

(a) (b)

Figure 2.2. Placement of (a) thermometer, reference electrode, (b) working electrode and counter electrode in Rdx-PBS solution.

2.2.2. Preparation of Electrodes

Graphite electrodes were optimized with a Potentiostat Galvanostat device in ABS solution by applying a voltage of +1.4 V for 60 seconds before being subjected to any treatment. In this process, PGE was used as the working electrode, Ag/AgCl as the reference electrode, and a platinum plate electrode as the counter electrode.

Graphite electrodes were prepared to find the correct hydrogel formulation with valine and choline molecules. Since there will be many trials, the easily accessible and inexpensive graphite electrode was preferred in the studies to find the right hydrogel formulation. Tombo 0.9 mm 2B pencil tip was chosen as pencil graphite electrode in this study.

As the Hydrogel formulation, 2 types of formulations were preferred. The first of these formulations contains Acrylamide/Bisacrylamide, EGDMA, HEMA, TRIS, APS and TEMED ratios. The other hydrogel formulation contains Acrylamide/Bisacrylamide, TRIS, distilled water, APS and TEMED ratios. As the results were obtained, the hydrogel formulation was modified by changing the component ratios and it was decided which formulation to continue.

Pencil graphite electrodes were divided into two groups as PGE unremoved molecular imprinting group (PGE-UMIP) and PGE molecular imprinting group (PGE-MIP) group.

The molecularly imprinted pencil graphite electrodes with 0.3 M valine consist of seven electrodes; PGE1-(polyHEMAcoEGDMA-0.3M-Val-MIP), PGE2-(TRIS-0.3M-Val-MIP), PGE3-(TRIS-0.3M-Val-MIP), PGE4-(TRIS-0.3M-Val-MIP), PGE5-(TRIS-0.3M-Val-MIP), PGE6-(TRIS-0.3M-Val-MIP) and PGE7-(TRIS-0.3M-Val-MIP).

PGE1-(polyHEMAcoEGDMA-0.3M-Val-MIP) electrode (polymer H513 contains 513 µl Acrylamide/Bisacrylamide (30 percent), 225 µl EGDMA, 61 µl HEMA, 179 µl TRIS (1.5 M, pH 4.8), 20 µl APS (10 percent) and 2 µl of TEMED), PGE2-(TRIS-0.3M-Val-MIP), and PGE3-(TRIS-0.3M-Val-MIP), PGE4-(TRIS-0.3M-Val-MIP), PGE5-(TRIS-0.3M-Val-MIP) electrodes with H600 (containing 600 µl Acrylamide/Bisacrylamide (30 percent), 250 µl TRIS (1.5 M, pH 4.8), 10 µl APS (10 percent) and 1 µl of TEMED). PGE6-(TRIS-0.3M-Val-MIP) with H767 (containing 767 µl Acrylamide/Bisacrylamide (40 percent), 200 µl TRIS-HCl (3.5 M, pH 4.8), 30 µl APS (10 percent) and 3 µl of TEMED) and PGE7-(TRIS-

0.3M-Val-MIP) electrode with H853 (containing 853 µl Acrylamide/Bisacrylamide (40 percent), 125 µl TRIS-HCl (3.5 M, pH 4.8), 20 µl APS (10 percent) and 2 µl of TEMED)

Two types of formulations were prepared. The first of these formulations contained Acrylamide/Bisacrylamide, TRIS, APS and TEMED. The binding of valine to the surface is via functional monomer (Acrylamide) and crosslinking agent (Bisacrylamide). Acrylamide/Bisacrylamide, TRIS-HCl, initiators (APS/TEMED) and 0.3 M valine were combined in an eppendorf tube. Valine imprinted eletrodes were prepared (Figure 2.3) and CV and EIS measurements of all electrodes were made in Rdx-PBS solution containing 5 mM $K_3[Fe(CN)_6]$ to find right hydrogel formulation ratios.

The second of these formulations contains Acrylamide/Bisacrylamide, EGDMA, HEMA, TRIS, APS and TEMED. Acrylamide/Bisacrylamide, EGDMA, HEMA, TRIS-HCl, initiators (APS/TEMED) and 0.3 M valine were combined in an eppendorf tube. After combining the amount of Acrylamide/Bisacrylamide and valine, it was kept in an ultrasonic bath at 37 degrees for 1 hour for the valine to incubate well. Then it was degassed by vacuum filtration and vortexed by adding EGDMA, HEMA and TRIS-HCl. Finally, APS/TEMED was added and the pencil graphite electrode was quickly dipped into this tube and left for 20 seconds for polymerization. The electrode, which was removed from the tube, was left to stand at room temperature for 15 minutes. In order to form valine-specific vacancies in the pencil graphite electrode, whose polymerization process was completed, removal of the valine from the imprinted polymer structure was achieved by keeping the electrodes in 0.1 M HCl solution for ten minutes. As a final step, the electrodes were washed twice for five minutes each by keeping them in eppendorf tubes containing water.

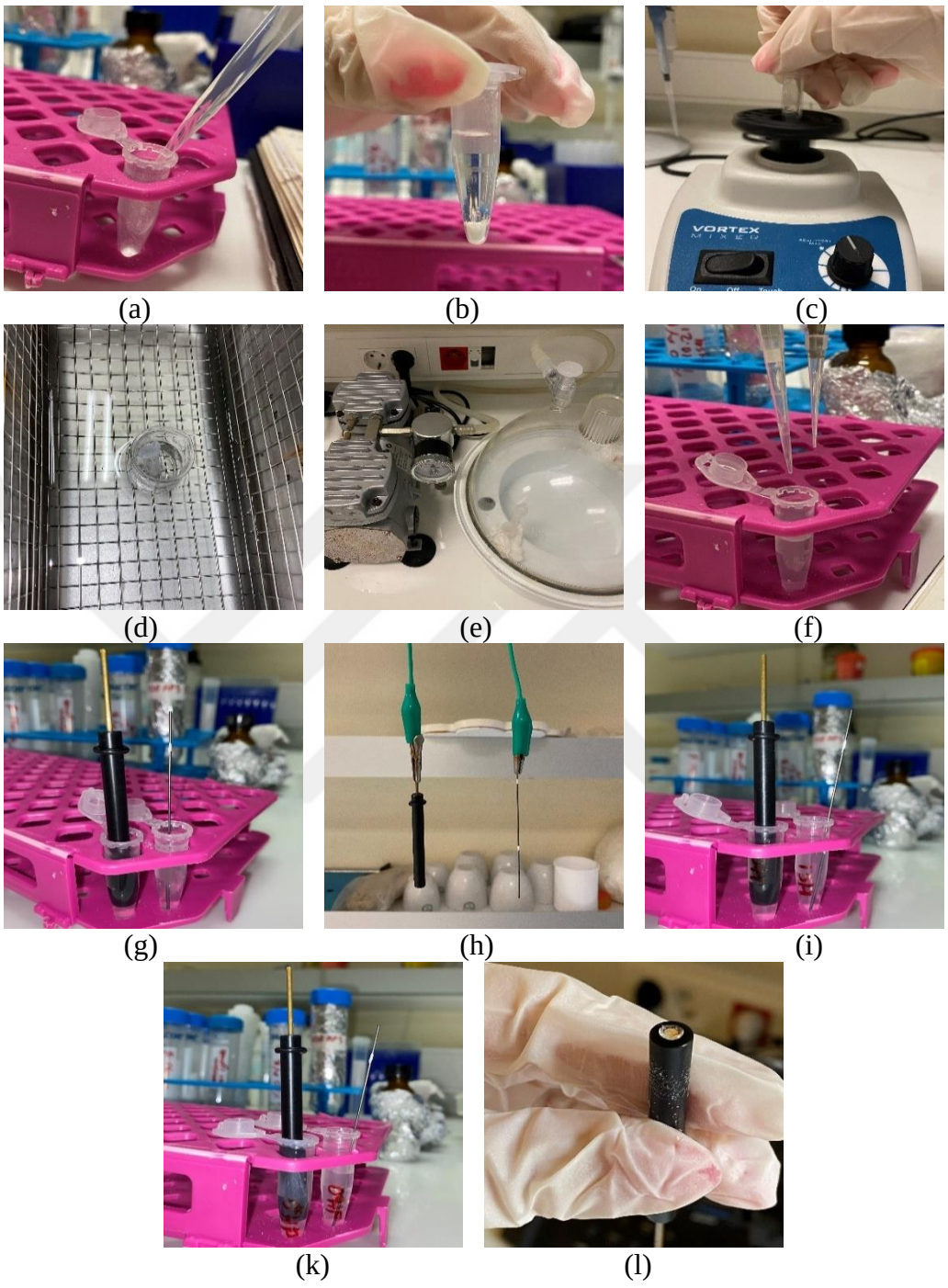

Figure 2.3. Molecular imprinting process. After combining the amount of Acrylamide/Bisacrylamide and valine (a-b), it was kept in an ultrasonic bath at 37 degrees for 1 hour for the valine to incubate well (c-d). Then it was degassed by vacuum filtration and vortexed by adding TRIS-HCl (e). Finally, APS/TEMED was added and the pencil graphite electrode was quickly dipped into this tube and left for 20 seconds for

polymerization (f-g). The electrode, which was removed from the tube, was left to stand at room temperature for 15 minutes (h). In order to form valine-specific vacancies in the pencil graphite electrode, whose polymerization process was completed, removal of the valine from the imprinted polymer structure was achieved by keeping the electrodes in 0.1 M HCl solution for ten minutes (i). As a final step, the electrodes were washed twice for five minutes each by keeping them in eppendorf tubes containing water (k). Thus, the valine imprinted electrodes were prepared (l).

These two formulations were also prepared to characterize the 0.2 M choline molecule imprinted PGE. Gold electrodes were prepared by choosing the best hydrogel formulation as a result of electrochemical studies on the pencil graphite electrode.

The Au electrode was first cleaned physically, chemically and electrochemically without any treatment. Cleaning steps are as follows:

1. Some Gamma alumina powder was taken and placed on the velvet surface. A few drops of distilled water were dropped on the alumina and mixed with a clean spatula tip until the alumina reached a gel consistency. Then, the Au electrode was moved slowly and in the same direction on the alumina in gel consistency. Thus, the layer on the surface and/or any other contamination was removed mechanically.
2. After rinsing the Au electrode with distilled water, it was kept in an ultrasonic bath in ethanol for 10 minutes. Then the electrode was rinsed with distilled water again and kept in an ultrasonic bath in distilled water for 10 minutes.
3. In order to electrochemically clean the surface of the Au electrode (CHI101 Au), cyclic voltammetry measurement was taken at 100 mV scan rate between +1 and -1 potentials in 0.1 N HNO_3 solution. In this process, CHI101 Au was used as the working electrode, Ag/AgCl as the reference electrode, and a platinum plate electrode as the counter electrode [72].

The gold electrode was prepared for electrochemical determination studies with valine and choline molecules. Electrodes were divided into three groups as Au unremoved molecular imprinting group (Au-UMIP), Au molecular imprinting group (Au-MIP) and Au non-imprinting group (Au-NIP).

The molecularly imprinted gold electrodes with valine consist of ten electrodes; 0.15M (Au-0.15M-Val-MIP), 0.2M (Au-0.2M-Val-MIP), 0.25M (Au-0.25M-Val-MIP), 0.275M (Au-0.275M-Val-MIP)), 0.3 M (Au-0.3M-Val-MIP), 0.325 M (Au-0.325M-Val-MIP), 0.35 M (Au-0.35M-Val-MIP), 0.4 M (Au-0.4M-Val) -MIP), 0.45M (Au-0.45M-Val-MIP) and 0.5M (Au-0.5M-Val-MIP).

Template molecule unremoved molecularly imprinted electrodes containing the same molarities of these ten electrodes were also prepared; 0.15 M (Au-0.15M-Val-UMIP), 0.2 M (Au-0.2M-Val-UMIP), 0.25 M (Au-0.25M-Val-UMIP), 0.275 M (Au-0.275M-Val-UMIP), 0.3 M (Au-0.3M-Val-UMIP), 0.325 M (Au-0.325M-Val-UMIP), 0.35 M (Au-0.35M-Val-UMIP), 0.4 M (Au-0.4M-Val) -UMIP), 0.45 M (Au-0.45M-Val-UMIP) and 0.5 M (Au-0.5M-Val-UMIP).

Au non-imprinting electrode was prepared as the control group (Au-NIP), because it did not contain valine.

H853 formulation and varying amounts of valine according to molarity were combined in an eppendorf tube. After combining the amount of Acrylamide/Bisacrylamide (40 percent) and valine, it was kept in an ultrasonic bath at 37 degrees for 1 hour for the valine to incubate well. Then it was degassed by vacuum filtration and vortexed by adding TRIS-HCl. Finally, APS/TEMED was added and the gold electrode was quickly dipped into this tube and left for 20 seconds for polymerization. The electrode, which was removed from the tube, was left to stand at room temperature for 15 minutes. In order to form valine-specific vacancies in the gold electrode, whose polymerization process was completed, removal of the valine from the imprinted polymer structure was achieved by keeping the electrodes in 0.1 M HCl solution for ten minutes. As a final step, the electrodes were washed twice for five minutes each by keeping them in eppendorf tubes containing water. Thus, the valine imprinted electrodes were prepared and the CV and EIS measurements of all electrodes were made in RdxPBS solution containing 5 mM K_3 $[Fe(CN)_6]$.

This formulation was also prepared to characterize choline molecule imprinted Au working electrodes prepared using the same methodology and procedural sequence as valine. Electrodes were divided into two groups as Au unremoved molecular imprinting group (Au-UMIP), Au molecular imprinting group (Au-MIP). The molecularly imprinted gold electrode with choline consists of one electrode; 0.2 M (Au-0.2M-Cho-MIP). Unremoved

molecularly imprinted electrode containing the same molarity of MIP electrode was also prepared; 0.2 M (Au-0.2M-Cho-UMIP). These choline electrodes were examined along with the valine electrodes under the AFM; and the AFM images of both MIP and UMIP of both polymers prepared using the valine and choline template molecules were compared.

2.2.3. Electrochemical Characterization

Electrodes were divided into three groups as Au unremoved molecular imprinting group (Au-UMIP), Au molecular imprinting group (Au-MIP) and Au non-imprinting group (Au-NIP). The pH, scan rate and response time studies were performed on the Au-0.3M-Val-MIP electrode to determine the operating conditions of the electrode.

Initially, the optimum pH was determined. CV and EIS measurements were conducted in Rdx-PBS at E-8 M concentration with a pH ranging from 5 to 10 (pH 5, pH 6, pH 7, pH 8, pH 9 and pH 10).

After the pH of the PBS, the scan rate was optimized. CV and EIS measurements were taken at the scan rate varying from 10 mV to 100 mV in Rdx-PBS (10 mV, 20 mV, 30 mV, 40 mV, 50 mV, 60 mV, 70 mV, 80 mV, 90 mV, 100 mV) prepared at the determined pH and containing E-8 M valine. CV measurements were taken at the determined pH and scan rate with response times of 0, 5, 10, 15, 20, 25 and 30 seconds.

After the operating conditions of the electrode were determined, alternating voltammetry measurements were made by applying potential between -500 and +500 mV (scan rate: 100 mV/s) to characterize the steps of electrode modification. Cyclic voltammetry plots were obtained in Rdx-PBS solution (pH 5) containing 5 mM K_3 [$Fe(CN)_6$], as seen in Figure 2.1. For impedance measurements, measurements were carried out in the frequency range between 1000 kHz and 10 mHz with 10 mV amplitude using the setup and solution in Figure 2.1.

The electrodes were initially electrochemically characterized (OCP, CV, and EIS) in a 100 mL volume of Rdx-PBS containing 5 mM $K_3[Fe(CN)_6]$ without valine concentration. Then, the electrodes were measured by adding the prepared valine solutions separately to 100 mL of Rdx-PBS, from the most dilute to the most concentrated solution, respectively. After the OCP, CV and EIS measurements made by adding E-18 M solution were completed, E-17 M

solution was added to a new 100 mL Rdx-PBS solution and the same measurements were repeated. These measurements in E-16, E-15, E-14, E-13, E-12, E-11, E-10, E-9, E-8, E- 7 and E-6 M solutions were made consecutively for one electrode. These steps were performed for all electrodes prepared in different molarities. The behavior of the electrodes in solutions containing valine at different concentrations was studied.

The Au-NIP electrode, which is the control group, was prepared by immersing the solution that does not contain the template molecule valine, and the other electrodes were prepared by immersing them in solutions containing valine at different molarities. While the surface of the Au-NIP electrode was coated only with Acrylamide/Bisacrylamide, the other group electrodes were coated with a polymer containing different amounts of valine (0.15 M, 0.2 M, 0.25 M, 0.275 M, 0.3 M, 0.325 M, 0.35 M, 0.4 M, 0.45 M, 0.5 M).

The electrodes were analyzed in solutions containing 13 different valine concentrations. The solutions were added to Rdx-PBS solution containing 5 mM $K_3[Fe(CN)_6]$, E-18, E-17, E-16, E-15, E-14, E-13, E-12, E-11, E-10, E-9, E-8, E-7 and E-6 M, respectively, were obtained by adding solutions containing valine. OCP, CV and EIS analyzes of the electrodes were made in Rdx-PBS solution. The responses of the electrodes to each solution were examined and the concentration ranges in which valine could be detected were determined. According to this measurements, lower limit of detection (LOD) and lower limit of quantification (LOQ) was calculated with equations 2.1 and 2.2.

$$LOD = \frac{3s}{m} \tag{2.1}$$

$$LOQ = \frac{10s}{m} \tag{2.2}$$

s : standard deviation of a low-concentration sample

m : slope of the regression curve

Selectivity analysis was performed to examine the responses of the electrodes to different molecules, aiming to demonstrate that the EIS and CV responses of the electrodes are valine specific. Selectivity analysis was performed using glycine, alanine and methionine. The

selectivity (α) and imprinting factor (β) values of valine imprinted and non-imprinted electrode was calculated with equations 2.3 and 2.4.

$$a = \frac{\text{response to template molecule}}{\text{response to interfering molecule}} \tag{2.3}$$

$$\beta = \frac{\alpha_{MIP}}{\alpha_{NIP}} \tag{2.4}$$

Precision, stability and reproducibility tests on 0.3 M valine printed PGEs were performed with CV measurements in Rdx-PBS solution containing E-8 valine concentration. A total of 18 electrodes were produced with six MIP, six UMIP and six NIP groups. CV measurements were made for each electrode by replacing 100 mL of new Rdx-PBS solution with fresh one. Six replicates were measured to evaluate the valine-imprinted sensor reproducibility. For this purpose, E-8 valine solutions were prepared and the change in sensor response was measured in six replicates before and after incubation. After each measurement, the MIP and NIP groups were cleaned with HCl and distilled water, while the UMIP group was cleaned with water only. The same printed electrode was used in the next measurement by immersing in the solution.

Intra-day and inter-day precision studies were performed with the same concentration of valine solution. Intra-day precision study was performed by taking measurements at three different times in one day. The response of the electrode was measured every three days for three weeks with Rdx-PBS containing the same valine concentration to determine the stability of the electrode. After the measurement on the twenty-second day, the electrode was stored in the refrigerator and measured again on the forty-fifth day. The electrode was stored in a refrigerator at 4 ^{o}C when not in use.

For intra-day precision tests, the mean values and standard deviations for the anodic peak current values of each electrode at three different times on the same day were determined. The mean and standard deviation values of an electrode on different days and of different electrodes on a specific day were calculated in the same way for inter-day precision and reproducibility tests. After finding the means for each electrode, the t-test was performed to express the significance of the difference between the means of the two groups. Consistency

was examined for between groups, within groups, and among groups. ANOVA test was applied in SPSS data analysis program for among groups. ANOVA test, which is a parametric test, is used to determine whether there is a statistically significant difference between the means of independent groups**.** The electrodes were then analyzed in blood plasma using the standard addition method to determine the amount of valine in blood. The sample utilized in the standard addition method is a complex mixture or a substance with an unknown concentration, other substances besides the analyte can influence the signal obtained. In such circumstances, as well as in analyses involving potentiometric/voltametric observations, this method is widely used. The standard added to the sample should be chosen to include a component close to the analyte, according to the calculation method based on a large number of measurements [73]. $2.5x10^{-7}$ mole/mL valine solution at a concentration closest to the amount of valine obtained by dilution of blood plasma was chosen for standard preparation. 0.5 mL of blood plasma was added to five beaker and then, 0, 5, 10, 15, and 20 mL of standard were added to each beaker, and RdxPBS solution was added to each beaker to make up to 30mL as shown in Figure 2.4.

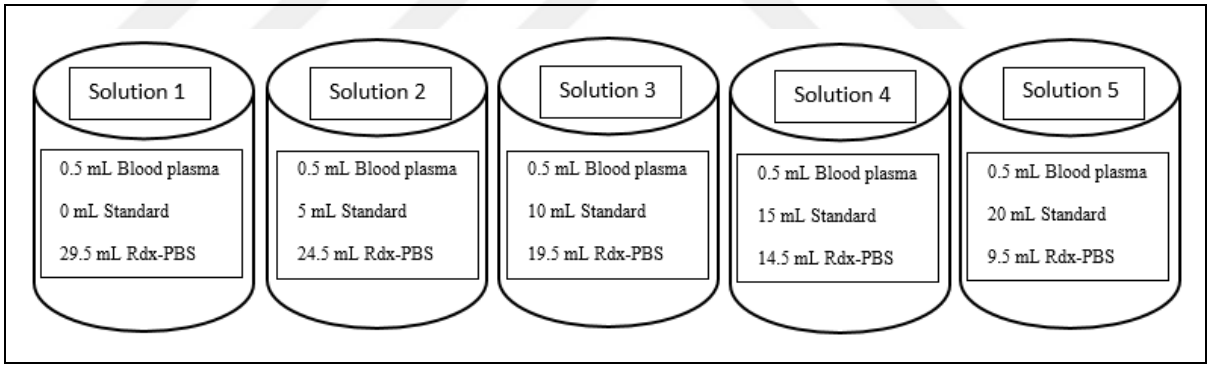

Figure 2.4. Solutions prepared for analysis of blood tests.

The responses of solutions to amounts of added standard were measured using OCP, CV, and EIS. The slope (m) and locations where it cuts the y-axis (b) were calculated using the data from the EIS graph in a line graph, and these values were used to calculate the amount of analyte in the solution [73].

$$A = \frac{(k * V_S * C_S)}{V_T} + \frac{(k * V_X * C_X)}{V_T} \tag{2.5}$$

A: Instrument response

V_S : Standard volume (variable, 0, 5, 10, 15, 20 mL)

C_S : Standard concentration

V_X : Analyte volume

C_X : Analyte

V_T : Total volume

k: constant of proportion

$$k = \frac{A_i}{A_1} \tag{2.6}$$

A_1 : Response from solution 1 (containing 0 mL standard)

A_i : Response obtained from solution i

The concentration (C_X) of the analyte can be calculated in two ways using this method:

- The impedance responses to the increased volume are plotted on a graph. The point where the line derived from this graph intersects the m and y axes is indicated as x if the slope of the line obtained from this graph is marked by b.

$$A = \mathrm{m} + V_S + b \tag{2.7}$$

$$m = \frac{(k * C_S)}{V_T} \tag{2.8}$$

$$b = \frac{(k * V_X * C_X)}{V_T} \tag{2.9}$$

$$\frac{b}{m} = \frac{(k * V_X * C_X)}{V_T} + \frac{V_T}{(k * C_S)} \tag{2.10}$$

$$C_X = \frac{(b * C_S)}{(m * V_X)} \tag{2.11}$$

- The instrument response and volume of the reference solution containing the analyte in an amount equal to the unknown analyte can be calculated by extrapolating the line generated based on the measurement results to the point where it intersects the x axis (Vs=0 point).

When A=0 ;

$$A = \frac{(k * (V_S * C_S))}{V_T} + \frac{(k * (V_x * C_X))}{V_T} = 0 \quad (2.12)$$

$$C_X = -\frac{((V_S)_0 * C_S)}{V_X} \quad (2.13)$$

At the end of the procedure, each analyzed electrode was first cleaned in 0.1 M HCl for ten minutes, followed by two five-minute washes in distilled water. In the second wash, it was first cleaned with 0.1 M HCl and then twice with distilled water for five minutes, making it ready for use again.

2.2.4. Characterization of Electrodes Using Atomic Force Microscopy

The atomic force microscope (AFM) or scanning force microscope is a scanning force microscope with extremely high resolution. A mechanical tip senses the surface and gathers information. Accurate and sensitive scanning is provided by piezoelectric devices on the electronic control, which offer modest but sensitive movements. Conductive levers can also be used to scan the electric potential at the sample surface. Current is delivered through the tip of the device in newer and more advanced versions to detect electrical conductivity or electron conduction at the surface.The AFM image is generated using a laser beam. Depending on the shape of the surface, the laser beam sent to it is reflected at varying angles, causing variances in the reflected laser beam. Surface recesses and protrusions are calculated using these deviations, and a topographic image of the surface is obtained. The roughness of the electrode surface and the ordered lattice at molecular resolution were observed in this work utilizing pictures produced by scanning a 100 nm^2 surface area [74].

3. RESULTS

3.1. HYDROGEL SOLUTION MODIFICATION

In this study, the first step in developing an impedimetric gold biosensor sensitive to valine was to create valine-sensitive recognition regions on pencil graphite electrodes using the MIP method. Molecular imprinted pencil graphite electrodes were used as synthetic valine receptors, and the responses of the polymer formed by this method to the change in PBS solution were examined by electrochemical method and hydrogel formulation was decided.

Two different electrodes were prepared to examine according to pH change; PGE1-(polyHEMAcoEGDMA-0.3M-Val-MIP) and PGE2-(TRIS-0.3M-Val-MIP). CV and EIS analyzes were performed on these two electrodes in Rdx-PBS solution containing E-8 M valine between pH 5 and 9, and pH change was investigated. The EIS behavior of PGE1-(polyHEMAcoEGDMA-0.3M-Val-MIP) and PGE2-(TRIS-0.3M-Val-MIP) electrodes was examined. The EIS response of the PGE1-(polyHEMAcoEGDMA-0.3M-Val-MIP) electrode were not adequate, so it was decided to proceed with the formulation of the PGE2-(TRIS-0.3M-Val-MIP) electrode. The pH at which maximum conductivity is displayed was determined. In the Nyguist diagrams an increase in the R_{ct} values, which increases the impedance and decreases the conductivity [75, 76]. In the PGE2-(TRIS-0.3M-Val-MIP) electrode, based on this information, the pH 5 result was determined as the most conductive pH of the electrode as shown in Figure 3.2.

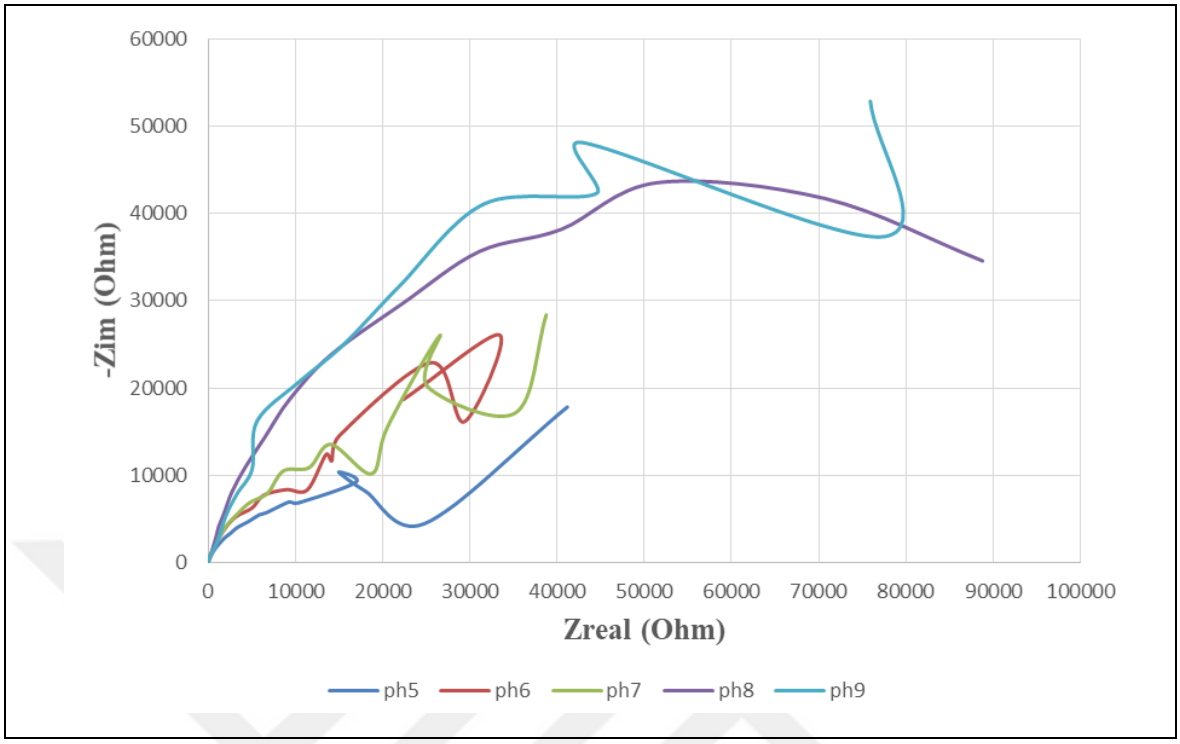

Figure 3.1. pH based EIS response of PGE1-(polyHEMAcoEGDMA-0.3M-Val-MIP) electrode in solutions with E-8 M valine.

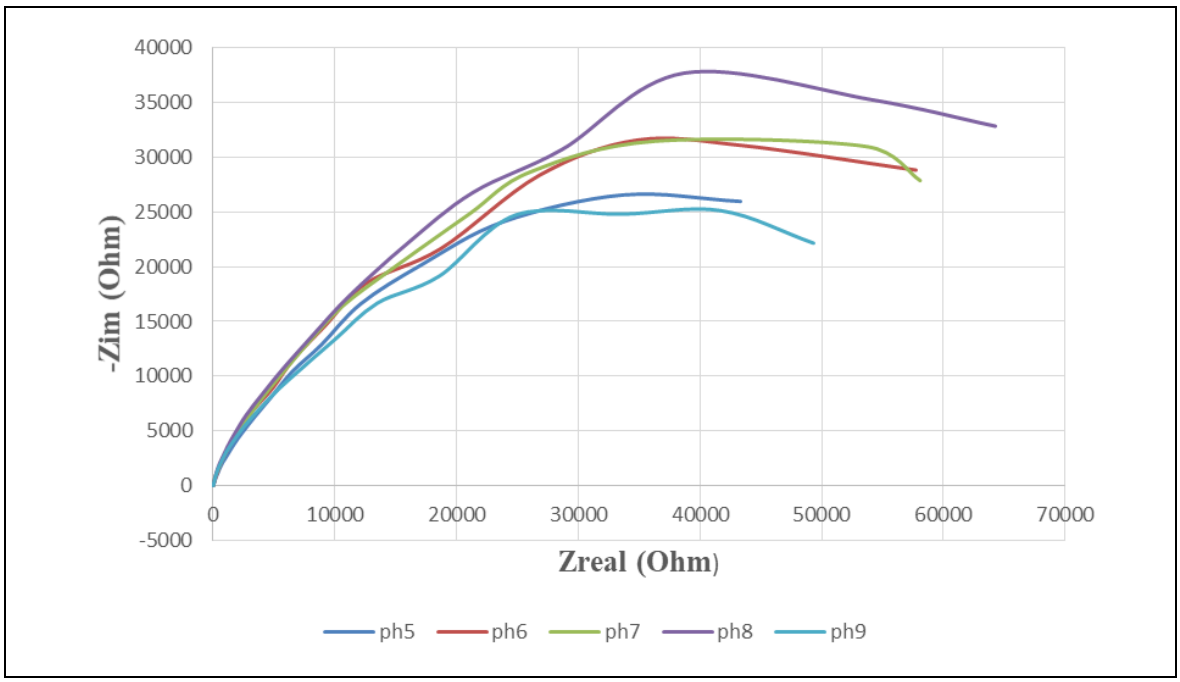

Figure 3.2. pH based EIS response of PGE2-(TRIS-0.3M-Val-MIP) electrode in solutions with E-8 M valine.

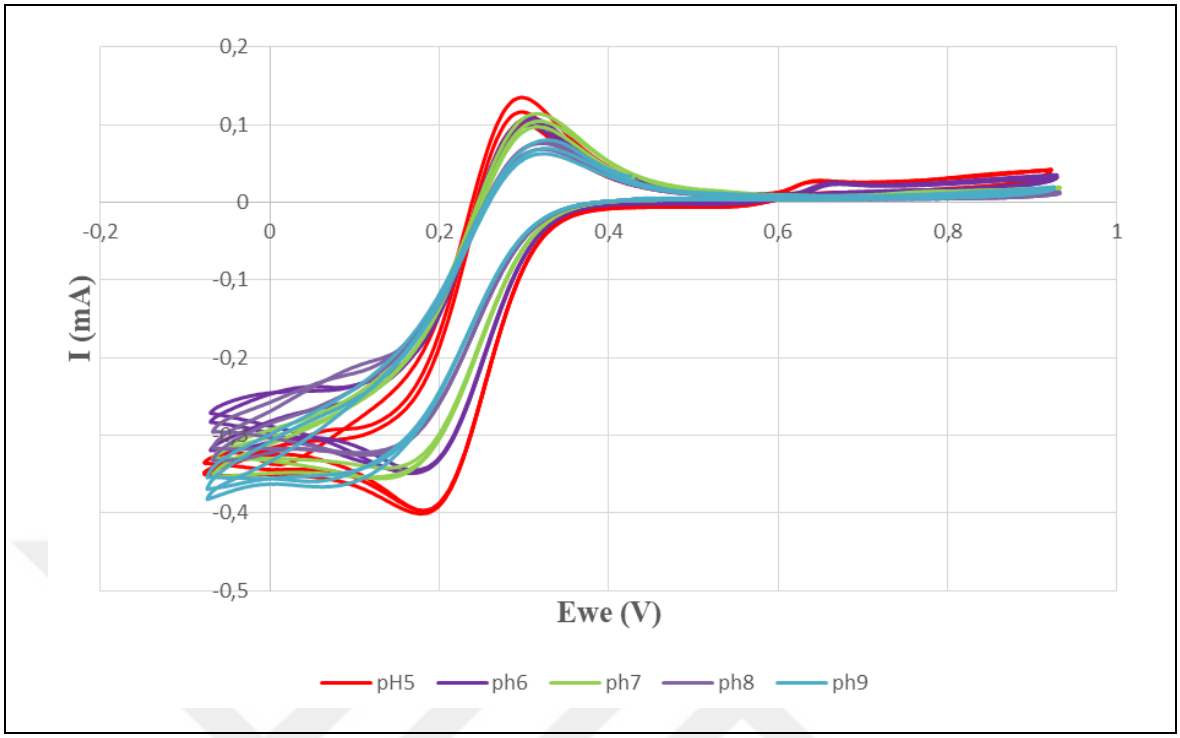

Figure 3.3. CV response of PGE2-(TRIS-0.3M-Val-MIP) electrode in solutions with E-8 M valine.

After selecting the pH 5, at which the polymer has maximum conductivity (Figure 3.3), the PGE3-(TRIS-0.3M-Val-MIP) electrode, which has the same hydrogel formulation ratios as the PGE2-(TRIS-0.3M-Val-MIP) electrode, was prepared by molecular imprinting with 0.3 M valine. EIS analyzes were performed at scan rates ranging from 10 mV to 100 mV in 100 mL of Rdx-PBS solutions containing E-8 M valine on the PGE3-(TRIS-0.3M-Val-MIP) electrode. As can be seen in Figure 3.4, the scan rates were selected as 60 mV and 80 mV, R_{ct} is displayed and the maximum conductivity is shown in the Nyguist graph of the PGE3-(TRIS-0.3M-Val-MIP) electrode. In order to make a comparison between 60 mV/s and 80 mV/s, measurements were taken at E-10 M, E-8 and E-6 M valine, and the scan rate at which the electrode best separated the concentrations was selected as shown in Figure 3.4.

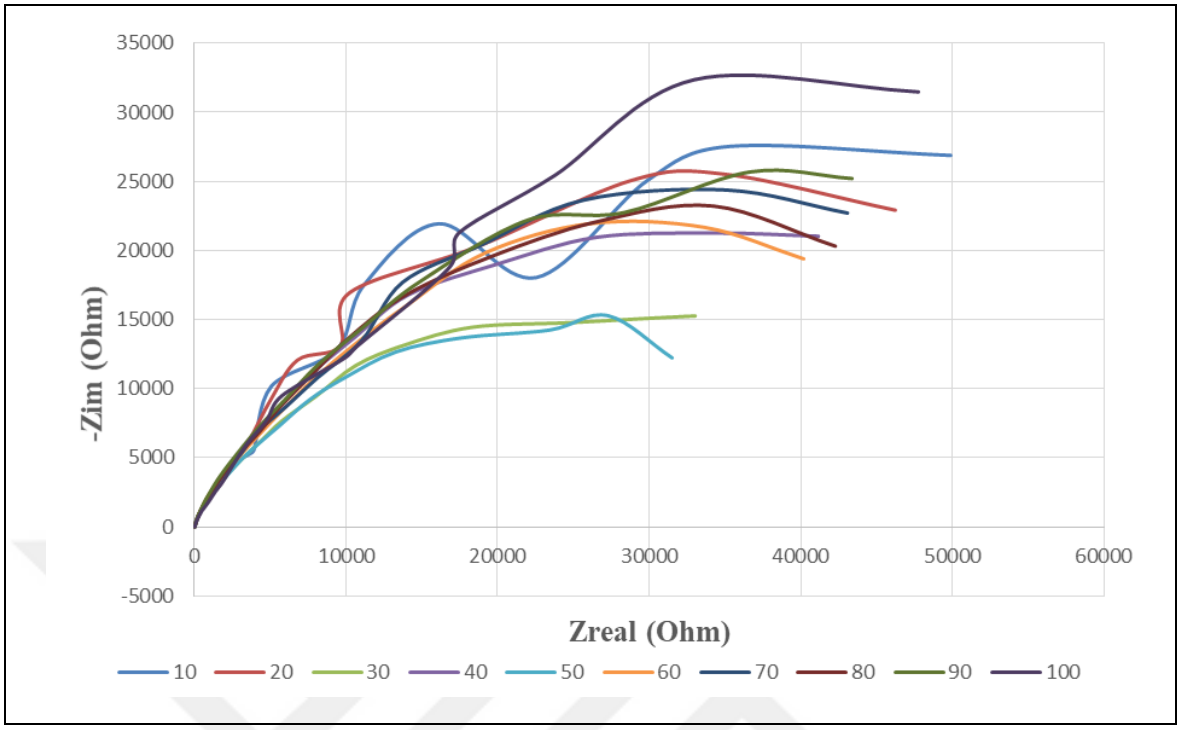

Figure 3.4. EIS response of PGE3-(TRIS-0.3M-Val-MIP) electrode in solutions containing E-8 M valine at pH 5 and different scan rates.

CV and EIS measurements of PGE3-(TRIS-0.3M-Val-MIP) electrode at 60 mV and 80 mV, respectively, was made in 100 mL of blank Rdx-PBS solution (NC), in 100 mL of Rdx-PBS solution containing E-10 M valine, in Rdx-PBS solutions containing E-8 and E-6 M valine. CV and EIS graphs changed depending on the concentration at both scan rates. The PGE3-(TRIS-0.3M-Val-MIP) electrode can be used at 60 mV scan rate to effectively separate the amount of valine in the range of E-10 M to E-6 M as seen in Figure 3.5 with 99.28 percent success (Figure 3.6).

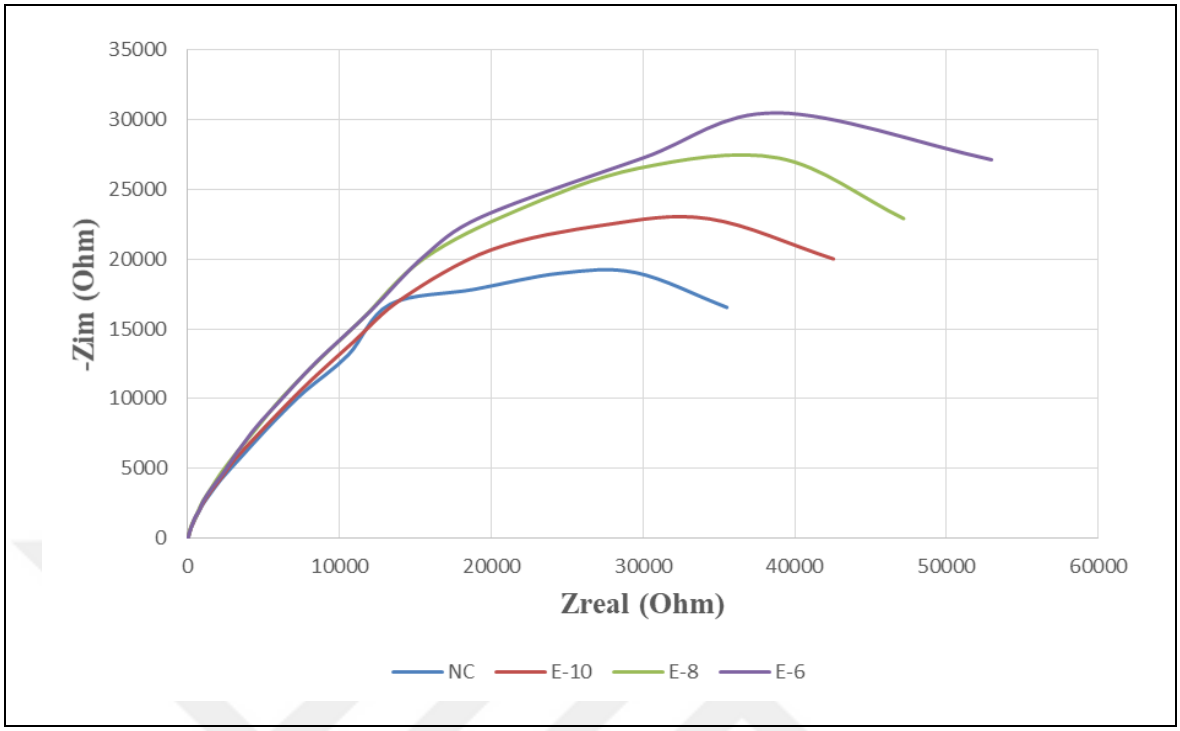

Figure 3.5. EIS response of PGE3-(TRIS-0.3M-Val-MIP) electrode in solutions containing E-8 M valine at pH 5 and 60 mV/s.

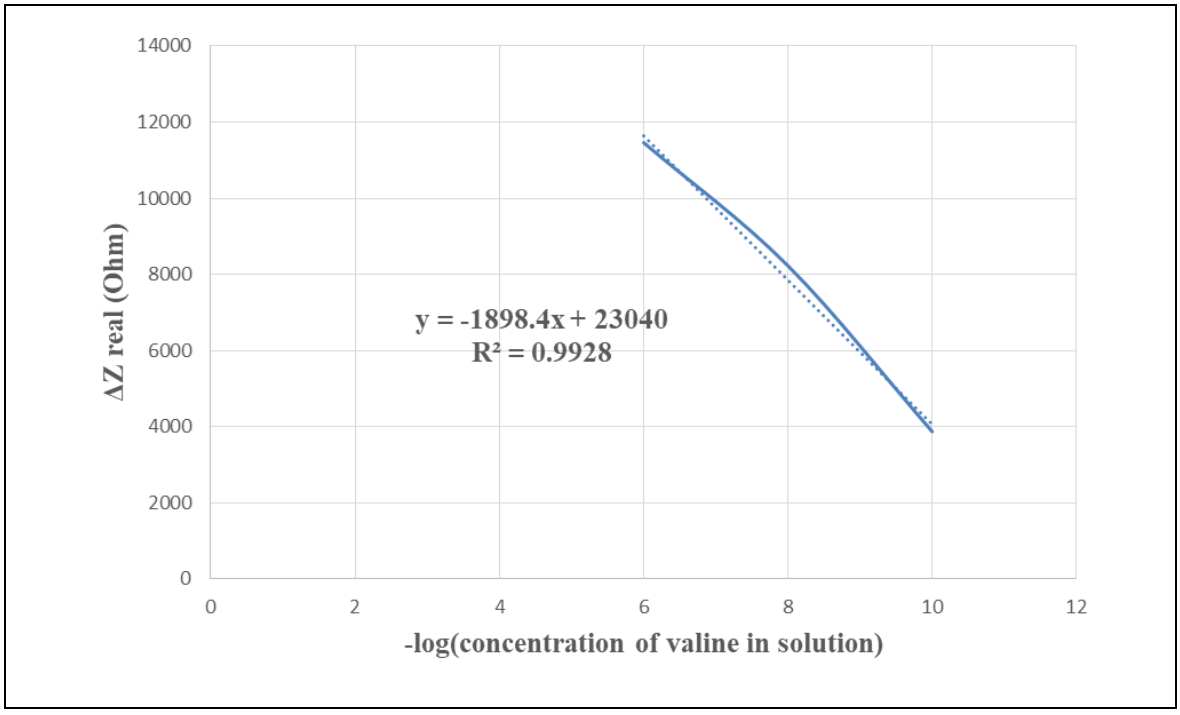

Figure 3.6. The regression curve of PGE3-(TRIS-0.3M-Val-MIP) electrode in solutions containing E-8 M valine at pH 5 and 60 mV/s.

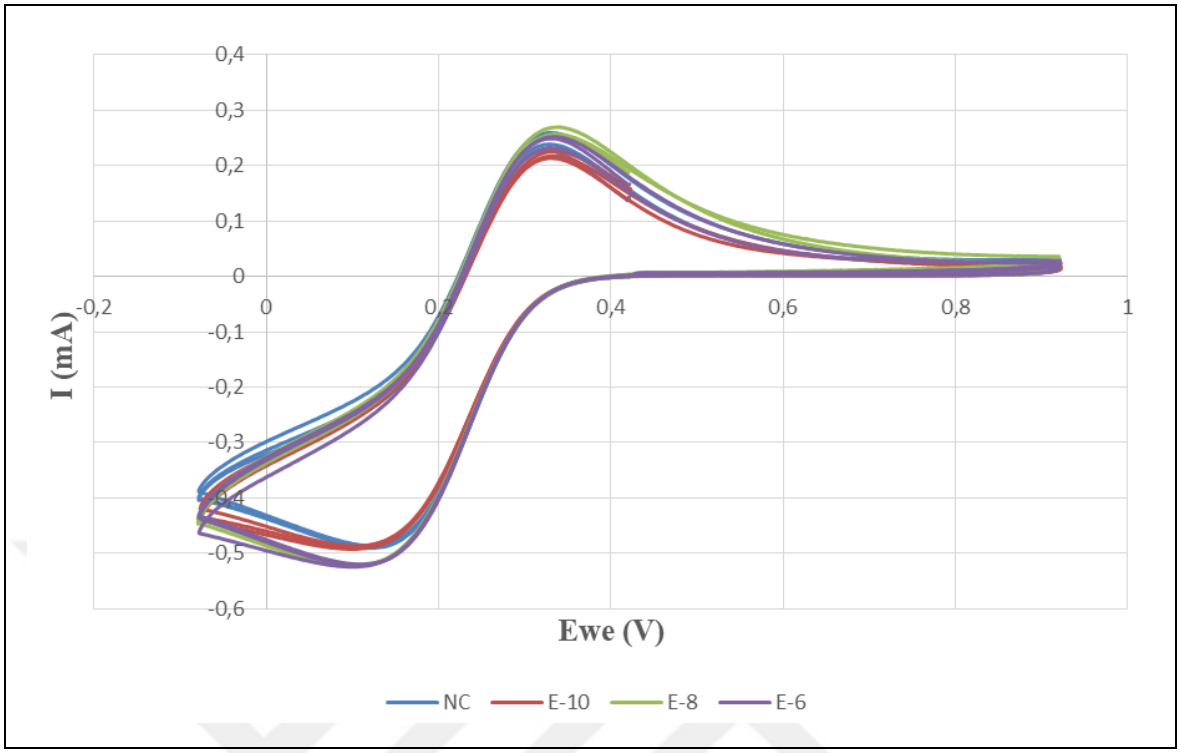

Figure 3.7. CV response of PGE3-(TRIS-0.3M-Val-MIP) in solutions containing E-8 M valine at pH 5 and 60 mV/s.

The EIS graphs of the PGE3-(TRIS-0.3M-Val-MIP) electrode at 80 mV scan rate indicate the separation due to varying valine concentration in the Rdx-PBS solution in the range of E-10 M to E-6 M as shown in Figure 3.8. The overlapping EIS curves of E-10, E-8, and E-6 molar solutions and the similar behavior of electrode indicates that sufficient separation cannot be made at these concentrations (Figure 3.8) with 67.85 percent success (Figure 3.9).

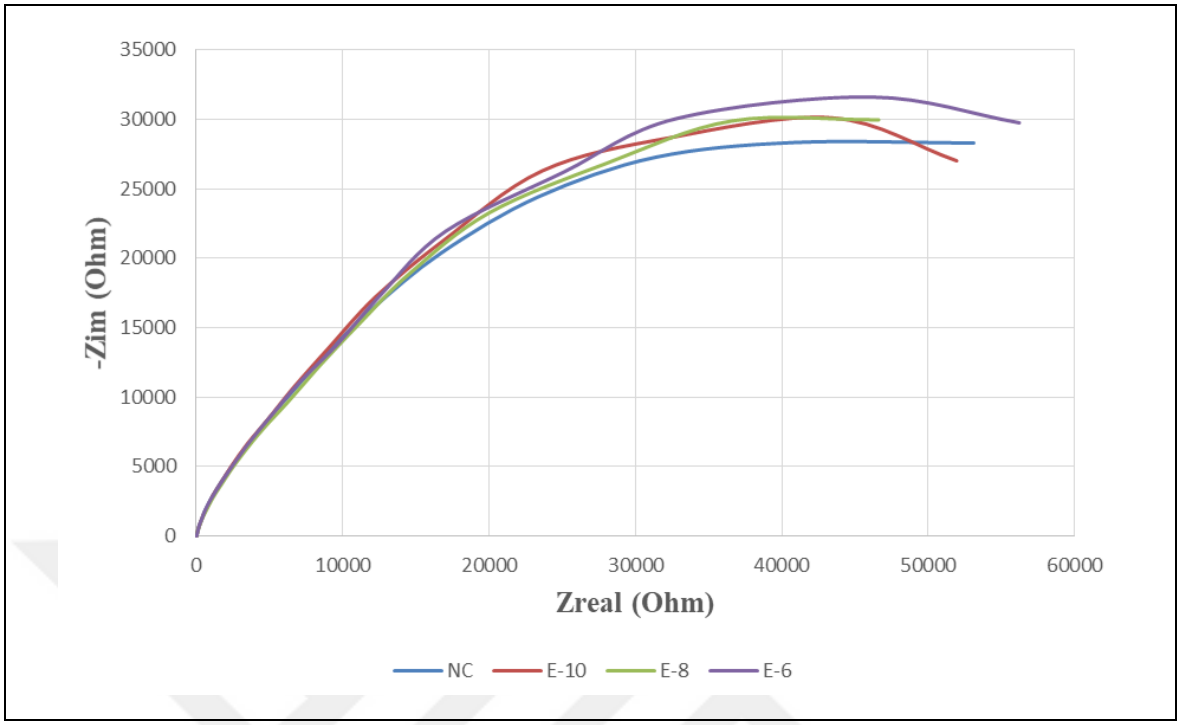

Figure 3.8. EIS response of PGE3-(TRIS-0.3M-Val-MIP) in solutions containing E-8 M valine at pH 5 and 80 mV/s.

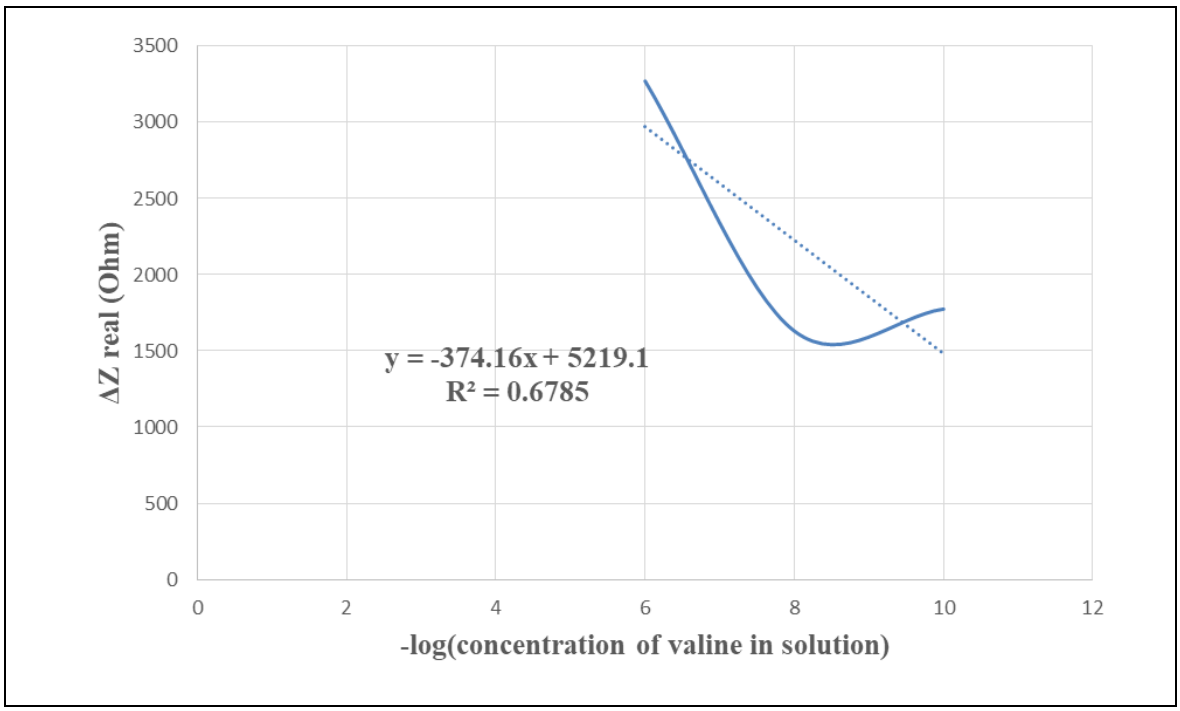

Figure 3.9. The regression curve of PGE3-(TRIS-0.3M-Val-MIP) electrode in solutions containing E-8 M valine at pH 5 and 80 mV/s.

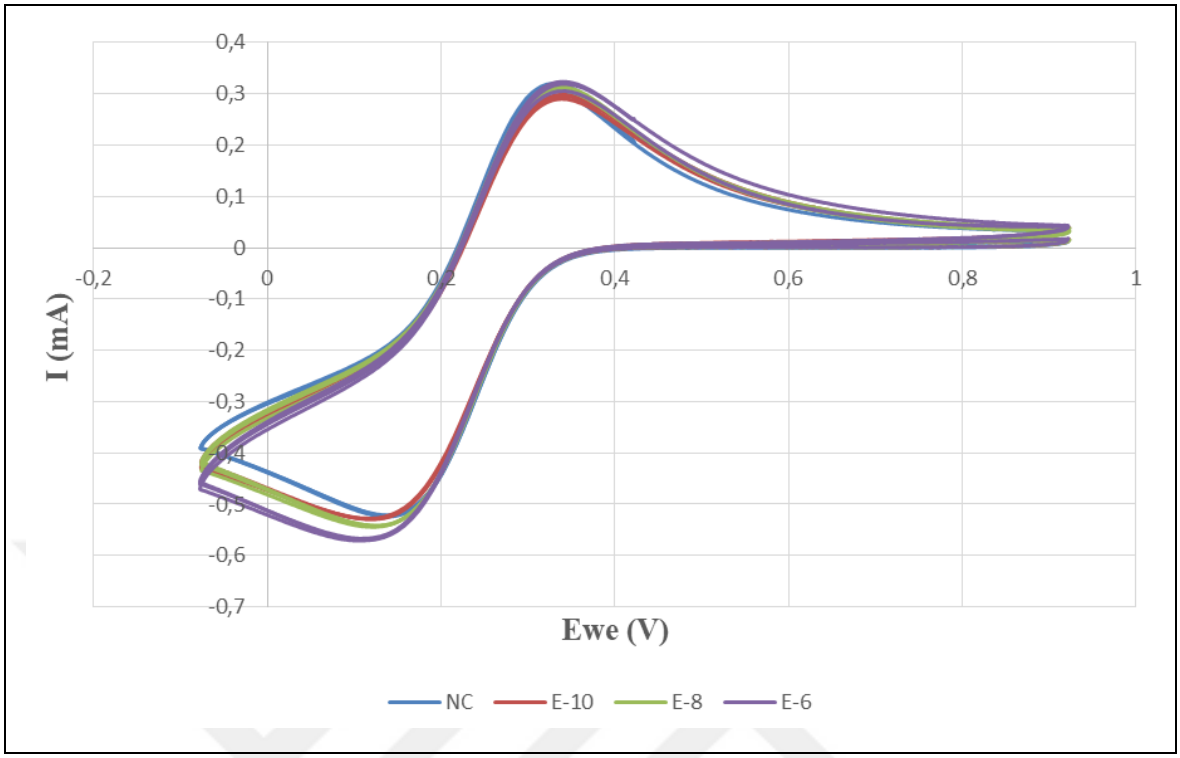

Figure 3.10. CV response of PGE3-(TRIS-0.3M-Val-MIP) in solutions containing E-8 M valine at pH 5 and 80 mV/s.

As a result of the above-mentioned findings, it was decided to continue the studies with the hydrogel formulation of the PGE3-(TRIS-0.3M-Val-MIP) electrode at pH 5 and a scan rate of 60 mV/s.

One of the main reasons for the production and use of biosensors is that they can produce realistic results in a short time. Response time is defined as the time it takes before signal changes are read while a measurement medium is applied to the item to be evaluated [47]. In order to determine the response time, the PGE4-(TRIS-0.3M-Val-MIP) electrode was produced. CV measurements were taken for each response time value at PGE4-(TRIS-0.3M-Val-MIP) electrode in the 100 mL Rdx-PBS solution which contains 100 µl E-8 M valine with response times of 0, 5, 10, 15, 20, 25 and 30 seconds. In the CV graphs in Figure 3.11, 30 sec response time was chosen as the most conductive response time with the highest increase in anode and cathode currents.

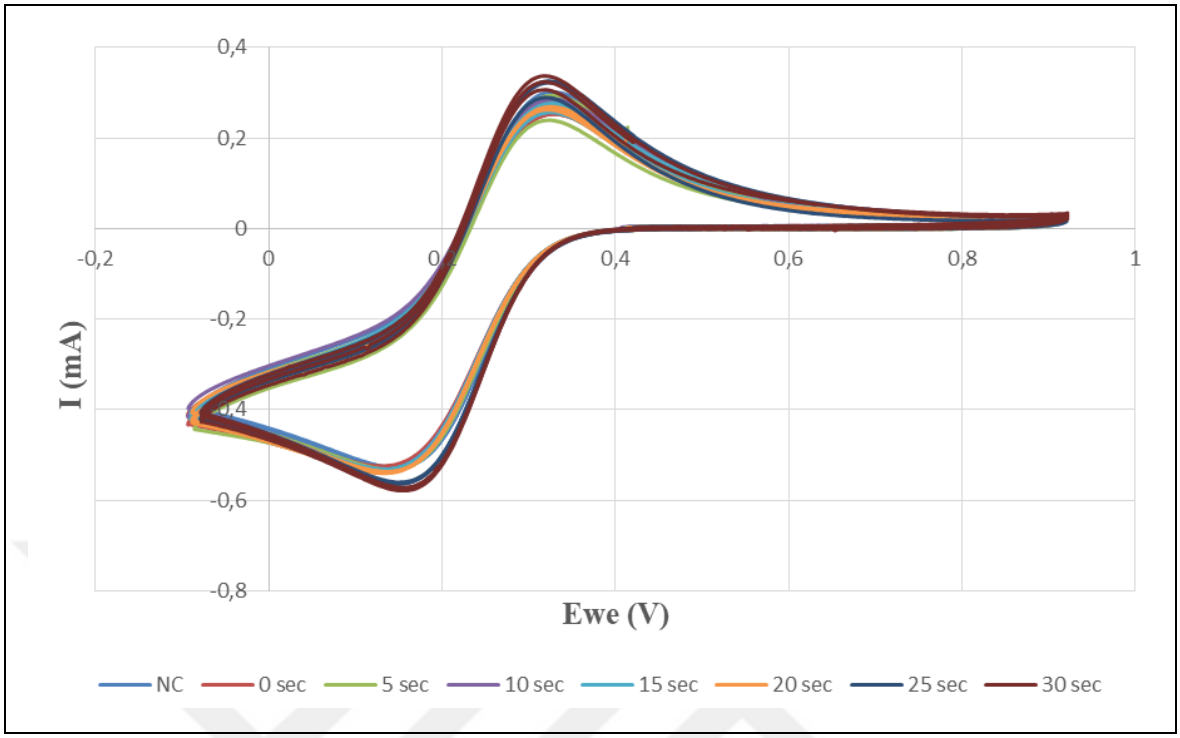

Figure 3.11. CV response of PGE4-(TRIS-0.3M-Val-MIP) electrode in solutions containing E-8 M valine with different response times.

EIS and CV measurements were made, in Rdx-PBS solution prepared at pH 5, at 60 mV/s scan rate and 30 s response time, respectively, in blank Rdx-PBS (no concentration), in solutions containing E-10, E-8 and E-6 M valine concentrations to PGE4-(TRIS-0.3M-Val-MIP) electrode as shown in Figure 3.12. The regression curve given in Figure 3.13 indicates that the PGE4-(TRIS-0.3M-Val-MIP) electrode can detect valine with 91.05 percent success.

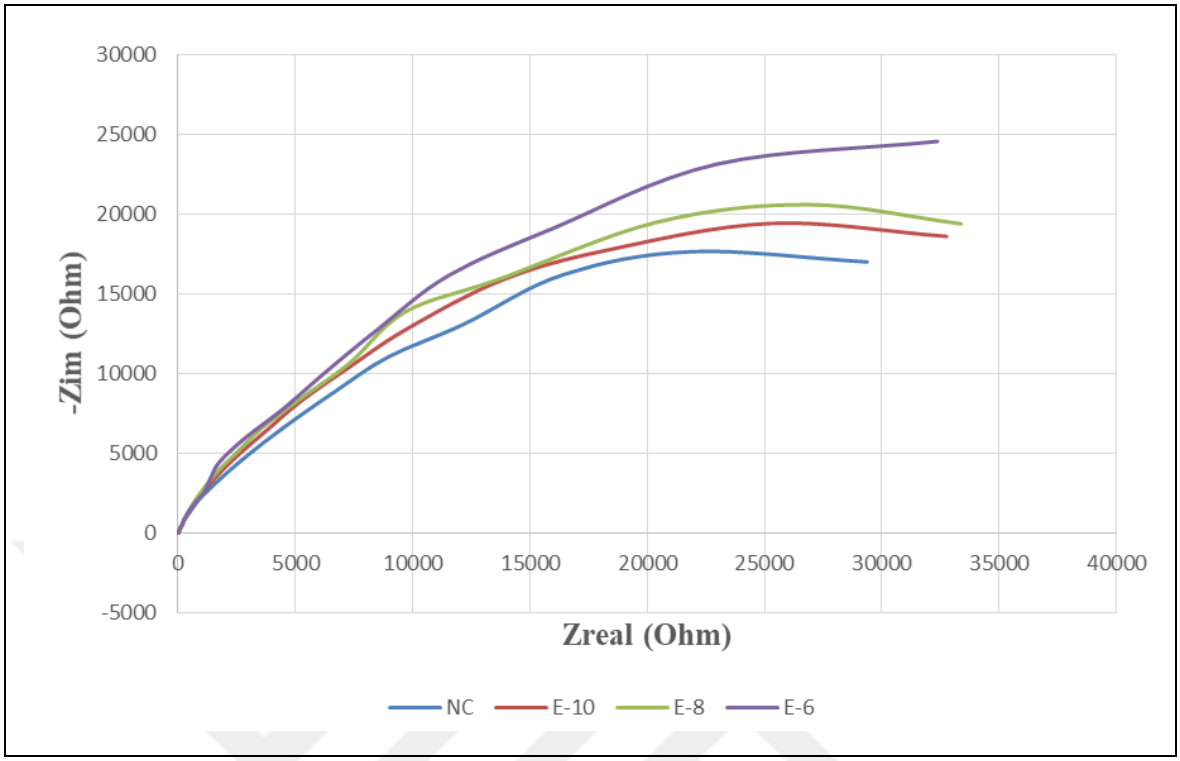

Figure 3.12. EIS response of PGE4-(TRIS-0.3M-Val-MIP) electrode.

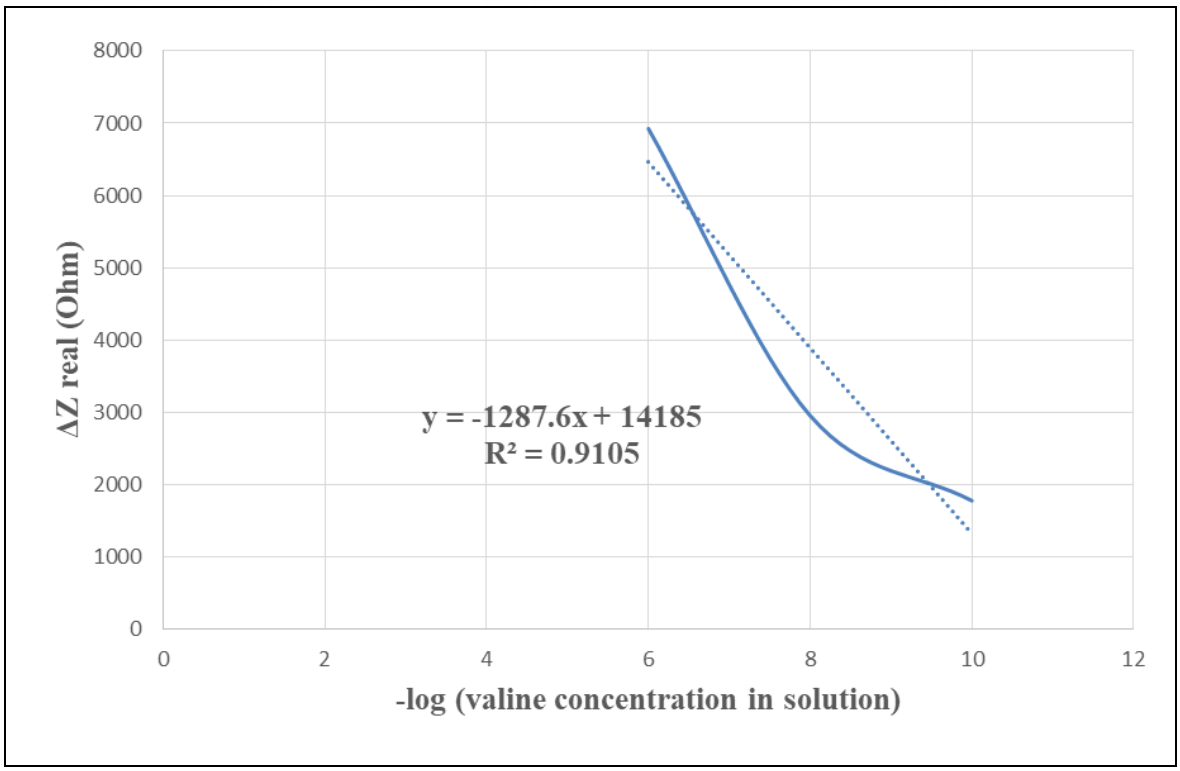

Figure 3.13. The regression curve of PGE4-(TRIS-0.3M-Val-MIP) electrode.

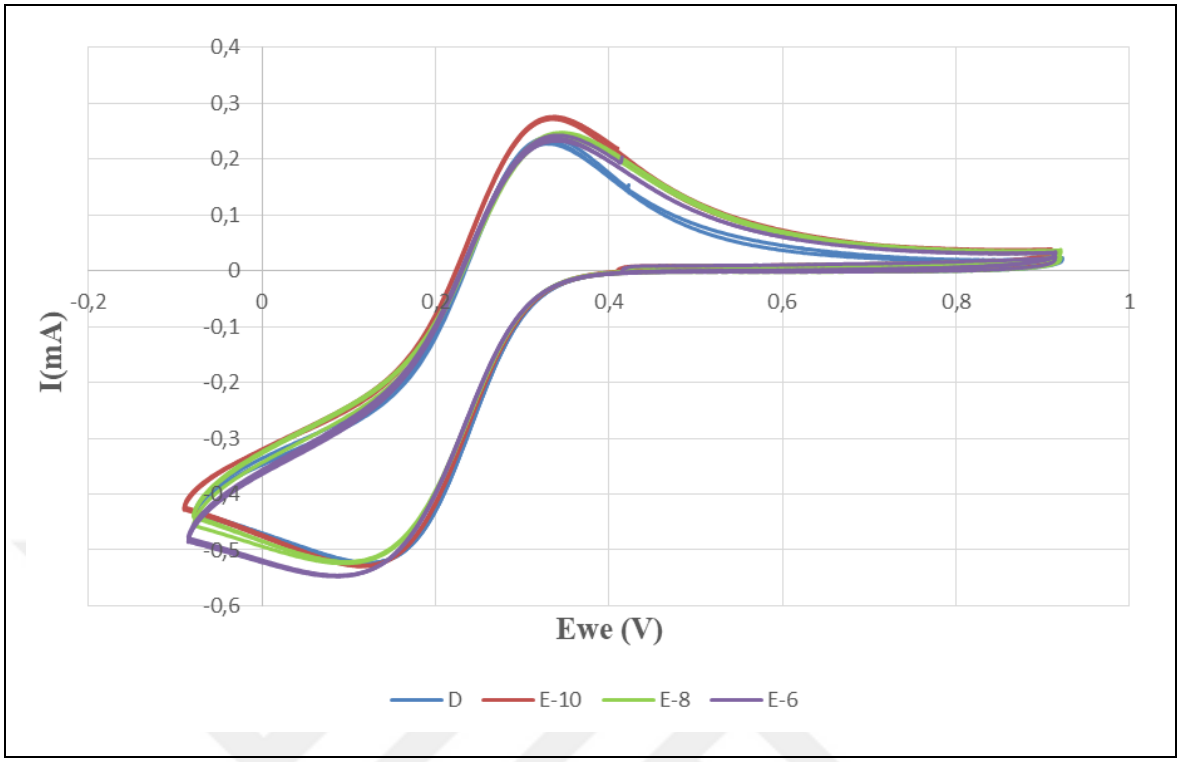

Figure 3.14. CV response of PGE4-(TRIS-0.3M-Val-MIP) electrode.

PGE5-(TRIS-0.3M-Val-MIP) and PGE1-(TRIS-0.3M-Val-UMIP) electrodes were prepared and EIS and CV measurements were made at pH 5, 60 mV scan rate and 30 sec response time, in blank Rdx-PBS and in E-12, E-11, E-10, E-9, E-8, E-7 and E-6 M valine (Figures 3.15, 3.17-3.18, 3.20).

The EIS data of the PGE5-(TRIS-0.3M-Val-MIP) electrode (Figure 3.15) shows that the valine molecule attaches to the valine receptors on the PGE electrode and the impedance of the electrode increases as expected, depending on the increasing valine concentration with 98.08 percent success (Figure 3.16). The EIS data of the PGE1-(TRIS-0.3M-Val-UMIP) electrode indicates that the saturated unremoved valine molecule on the electrode does not lead to an increase or decrease in the impedance of the electrode (Figure 3.18) with a low success of 14.51 percent (Figure 3.19).

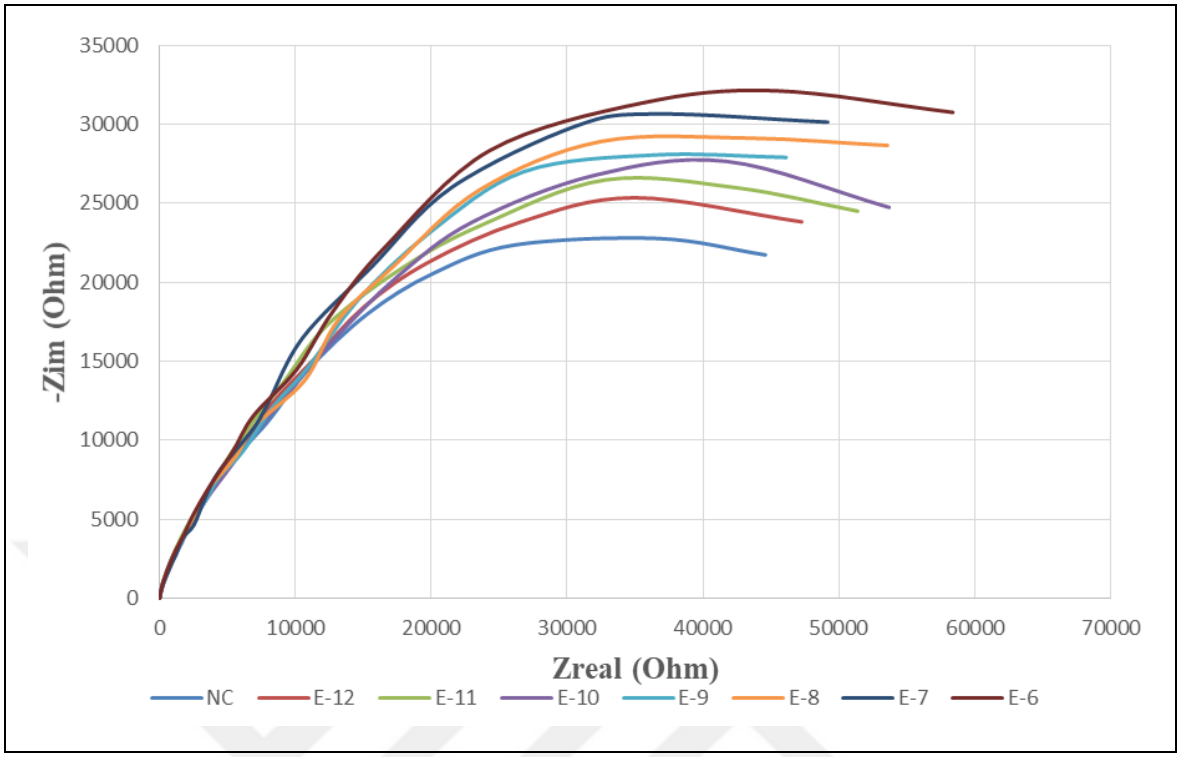

Figure 3.15. EIS response of PGE5-(TRIS-0.3M-Val-MIP) electrode.

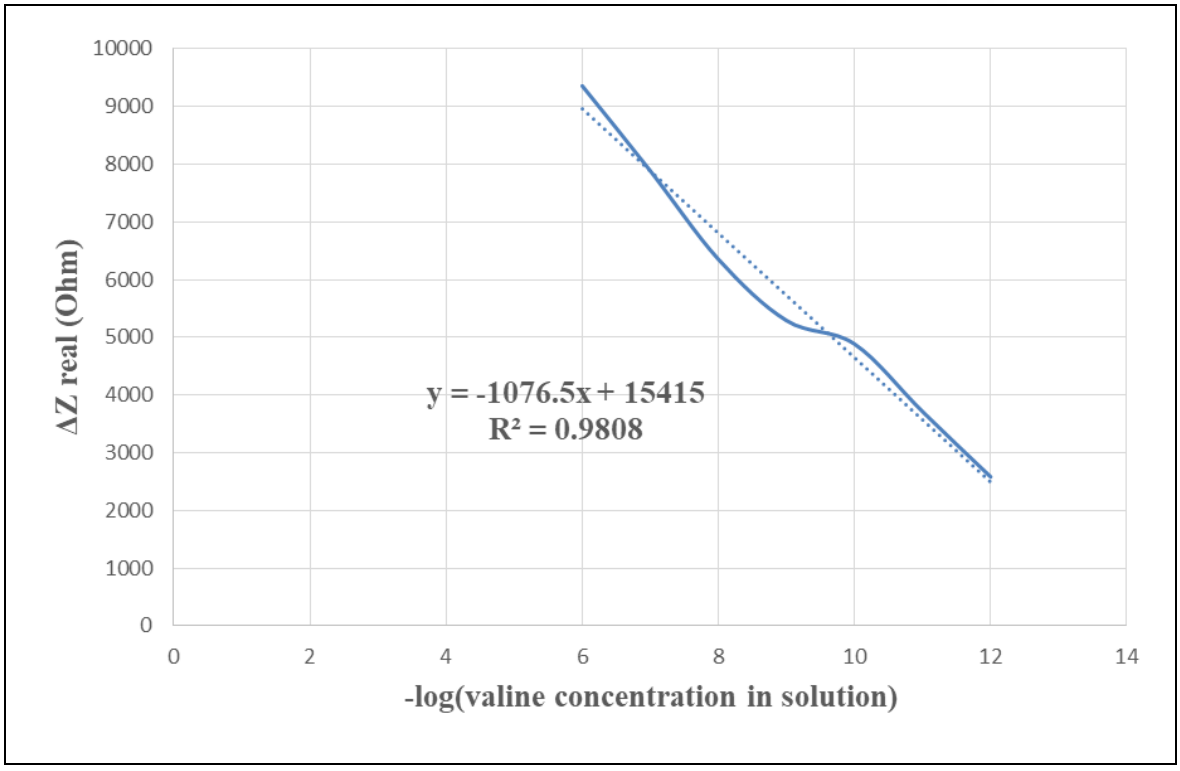

Figure 3.16. The regression curve of PGE5-(TRIS-0.3M-Val-MIP) electrode.

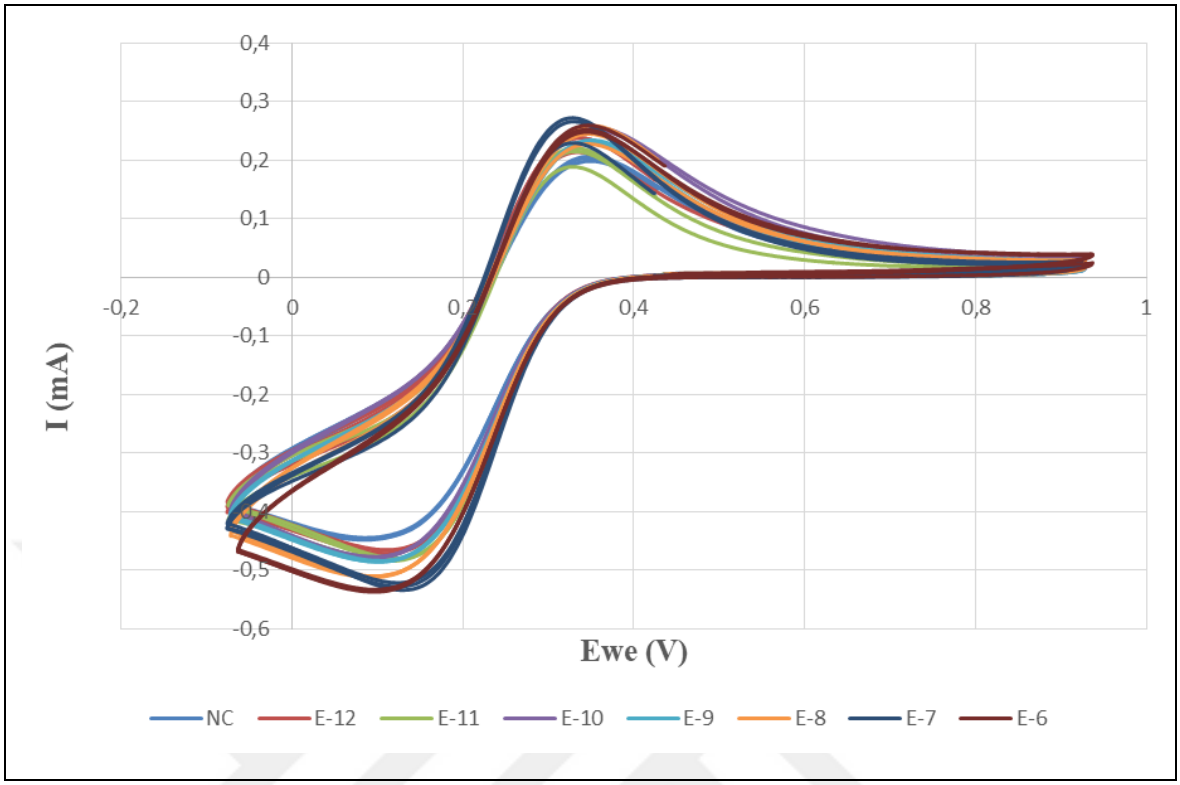

Figure 3.17. CV response of PGE5-(TRIS-0.3M-Val-MIP) electrode.

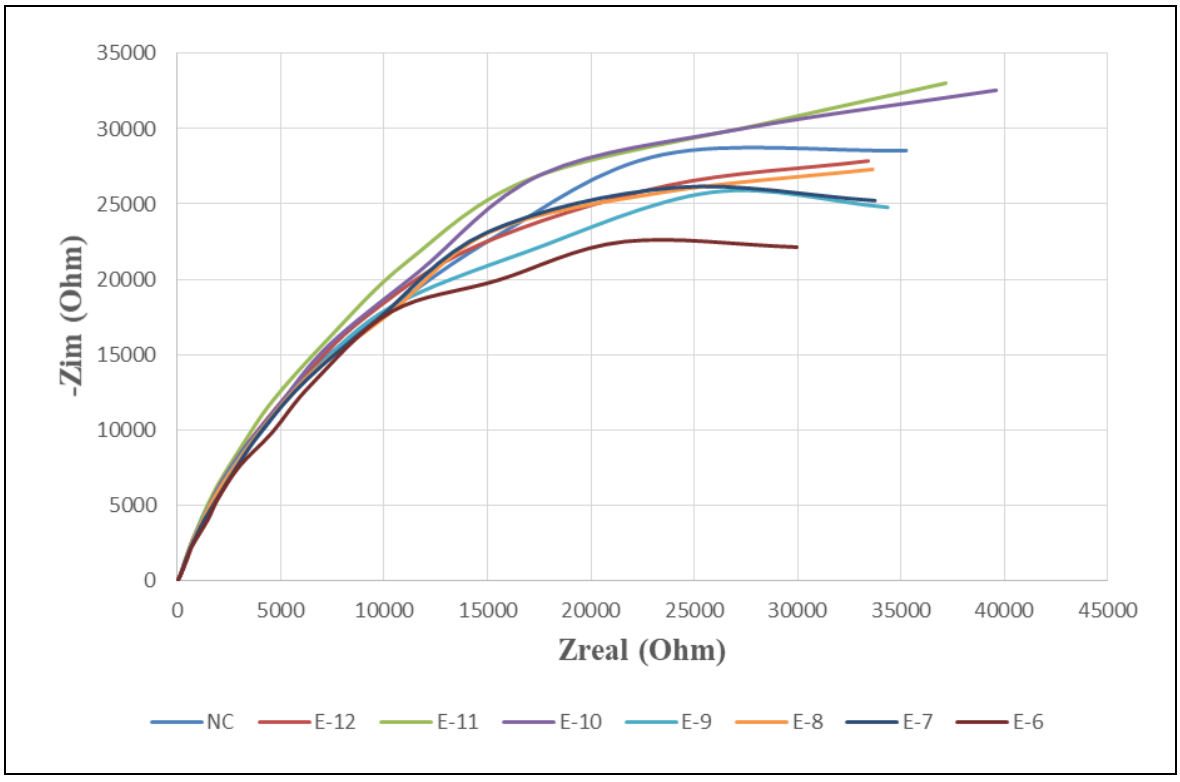

Figure 3.18. EIS response of PGE1-(TRIS-0.3M-Val-UMIP) electrode.

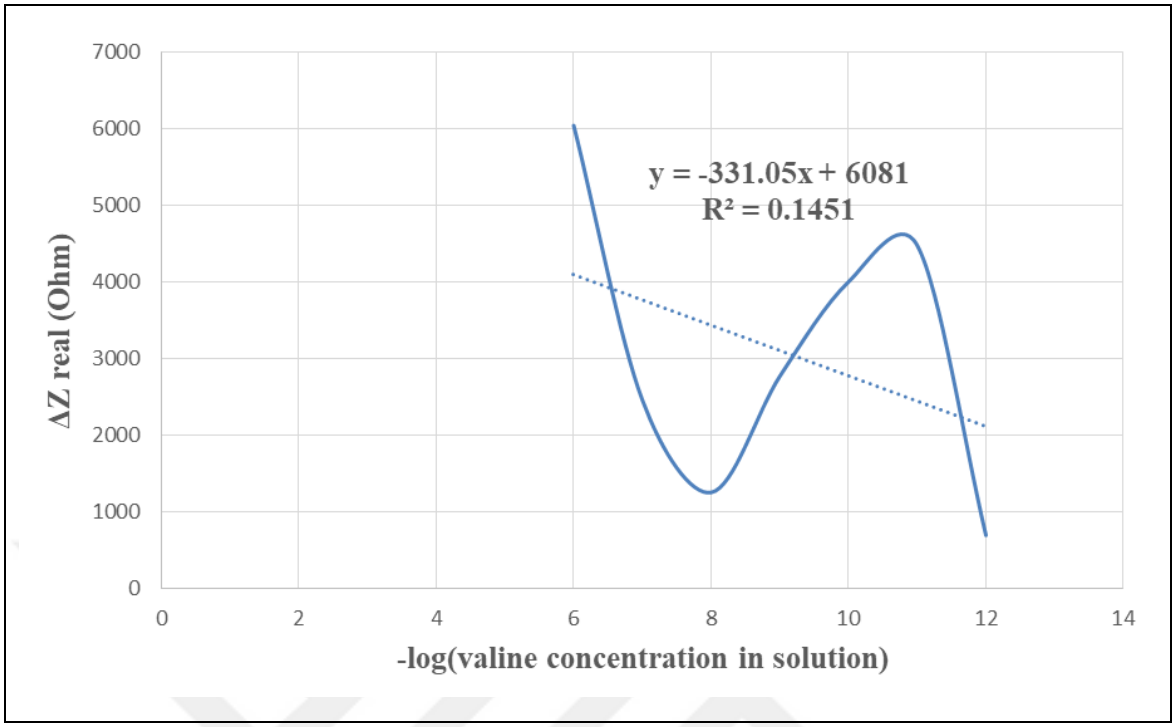

Figure 3.19. The regression curve of PGE1-(TRIS-0.3M-Val-UMIP) electrode.

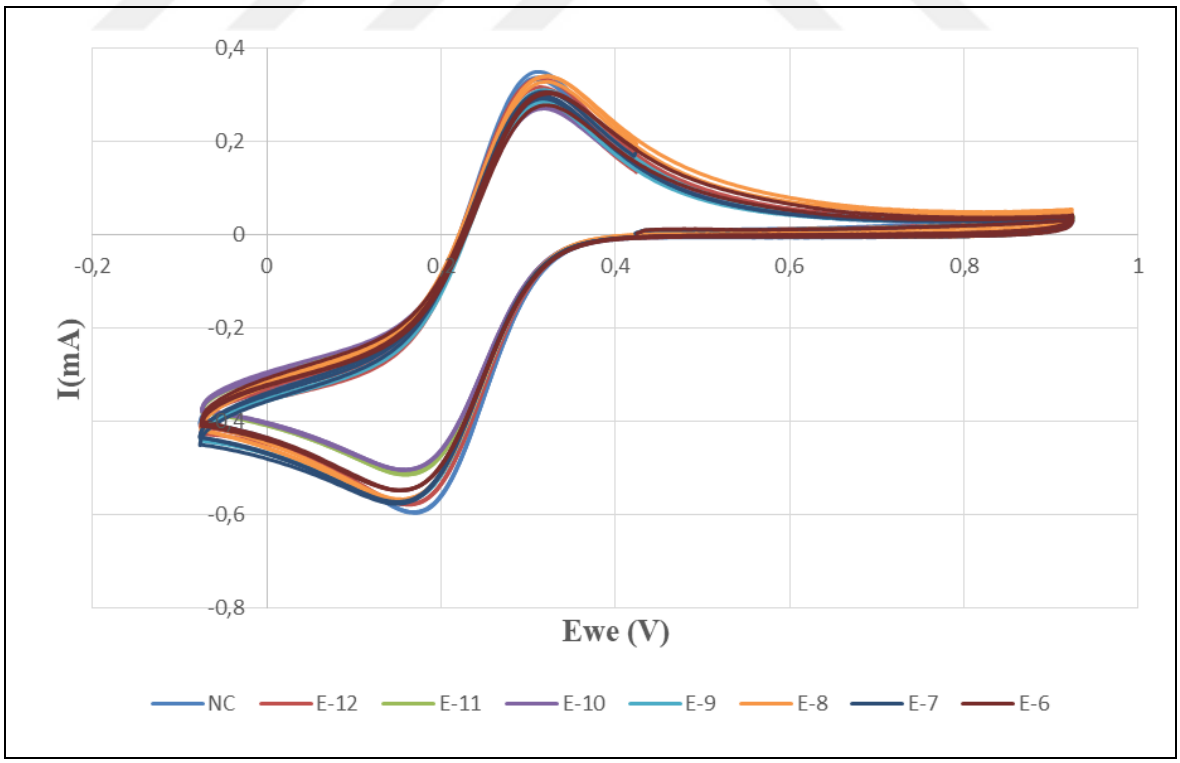

Figure 3.20. CV response of PGE1-(TRIS-0.3M-Val-UMIP) electrode.

It was thought that the hydrogel formulation could be further improved so that the valine concentrations could be better separated and detected. The UMIP version of this electrode was prepared as PGE2-(TRIS-0.3M-Val-UMIP) electrode with the same formulation. On these two electrodes, EIS and CV measurements were made at pH 5, 60 mV scan rate and 30 sec response time, in blank solution and with E-10, E-8 and E-6 M valine (Figures 3.21, 3.23-3.24, 3.26). The EIS response of the PGE6-(TRIS-0.3M-Val-MIP) electrode show that the increase in analyte concentration correlated with an increase in R_{ct} (Figure 3.21) with 97.39 percent success (Figure 3.22).

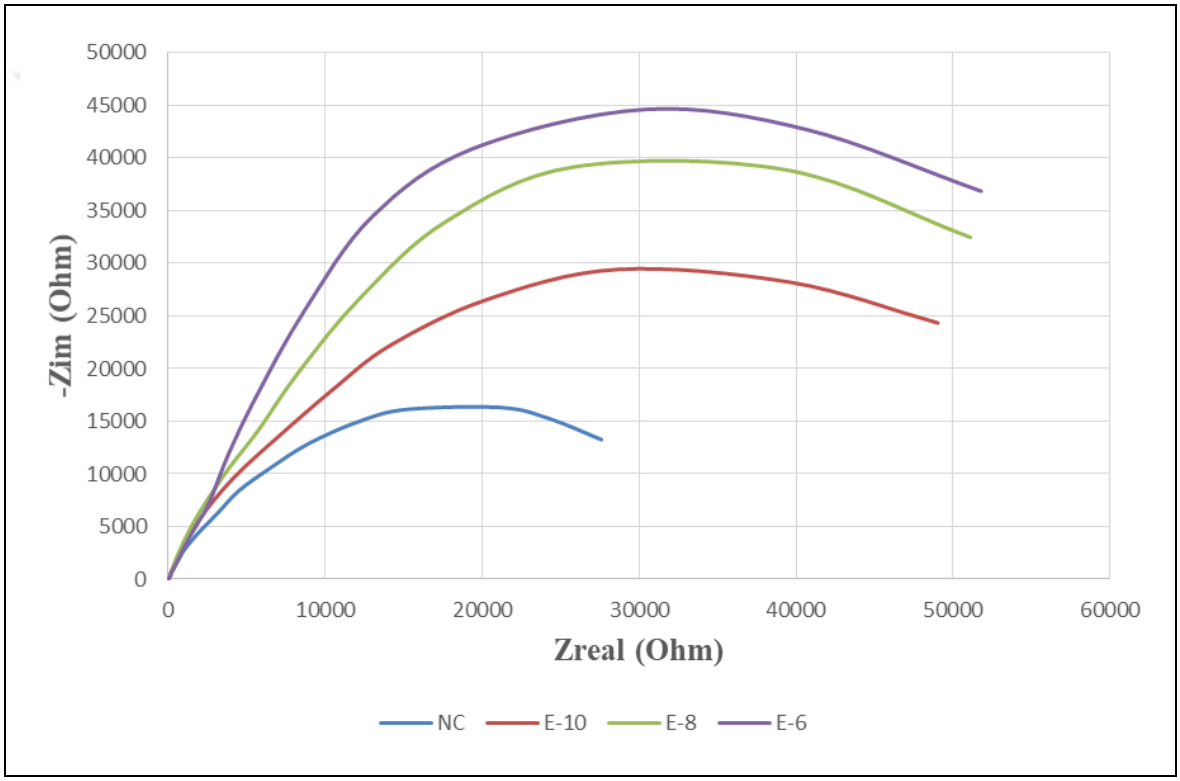

Figure 3.21. EIS response of PGE6-(TRIS-0.3M-Val-MIP) electrode.

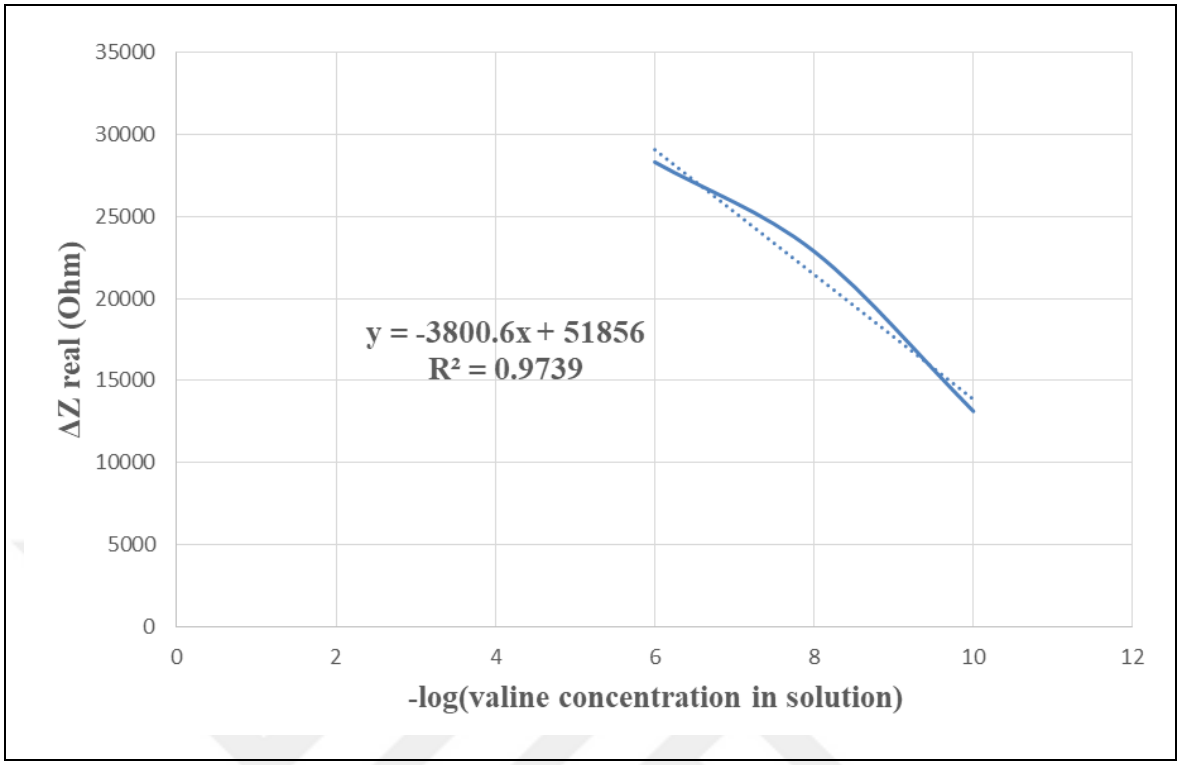

Figure 3.22. The regression curve of PGE6-(TRIS-0.3M-Val-MIP).

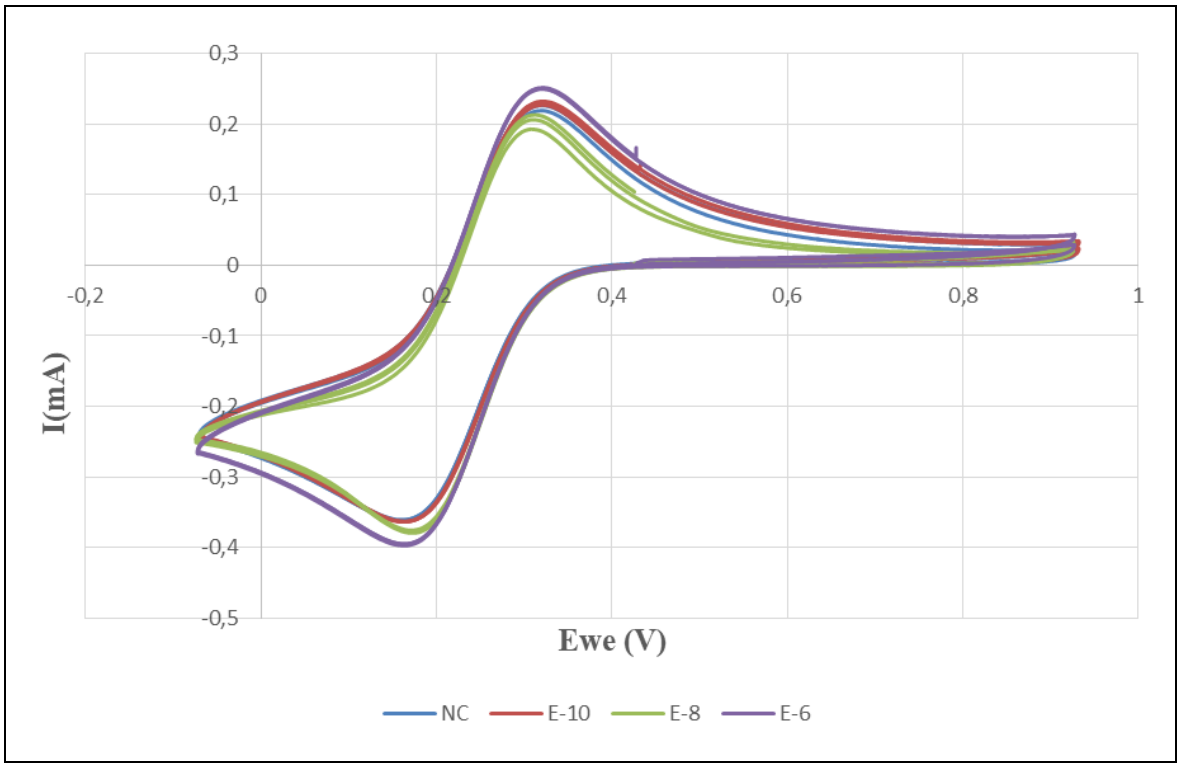

Figure 3.23. CV response of PGE6-(TRIS-0.3M-Val-MIP) electrode.

When the EIS and CV data of the PGE2-(TRIS-0.3M-Val-UMIP) electrode are examined, it is observed that as expected there is no valine attachment to the electrode surface (Figures 3.24, 3.26) and the electrode can detect valine with 17.2 percent success (Figure 3.25).

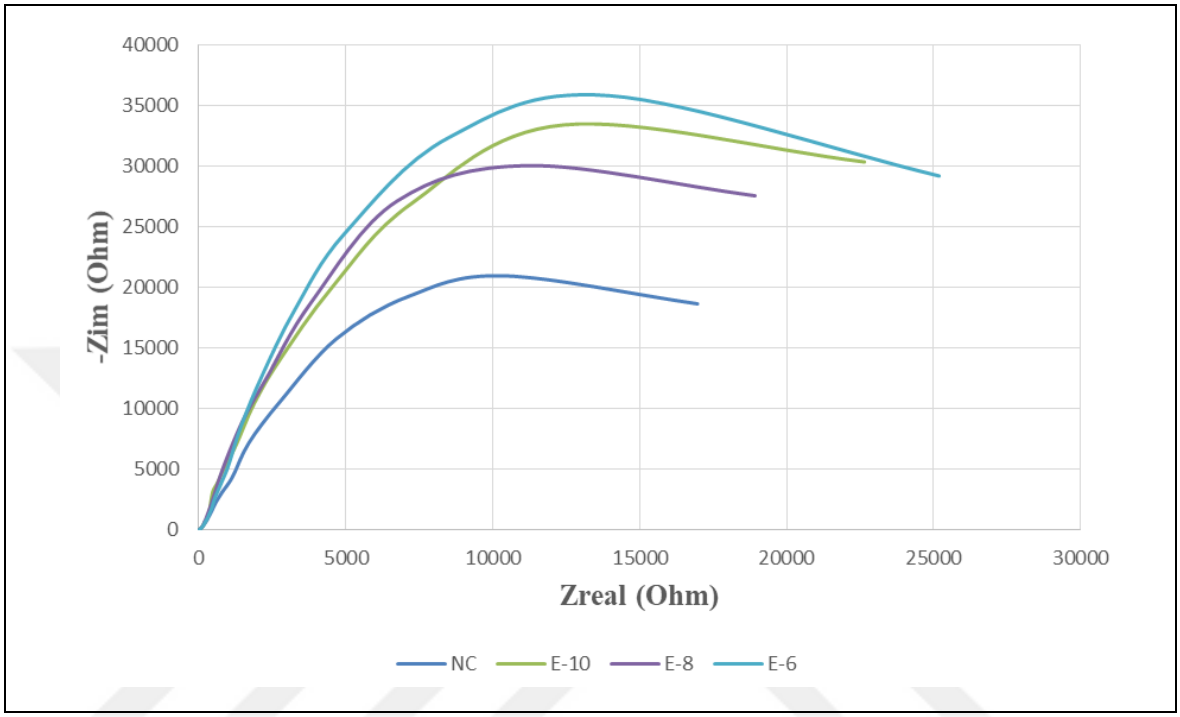

Figure 3.24. EIS response of PGE2-(TRIS-0.3M-Val-UMIP) electrode.

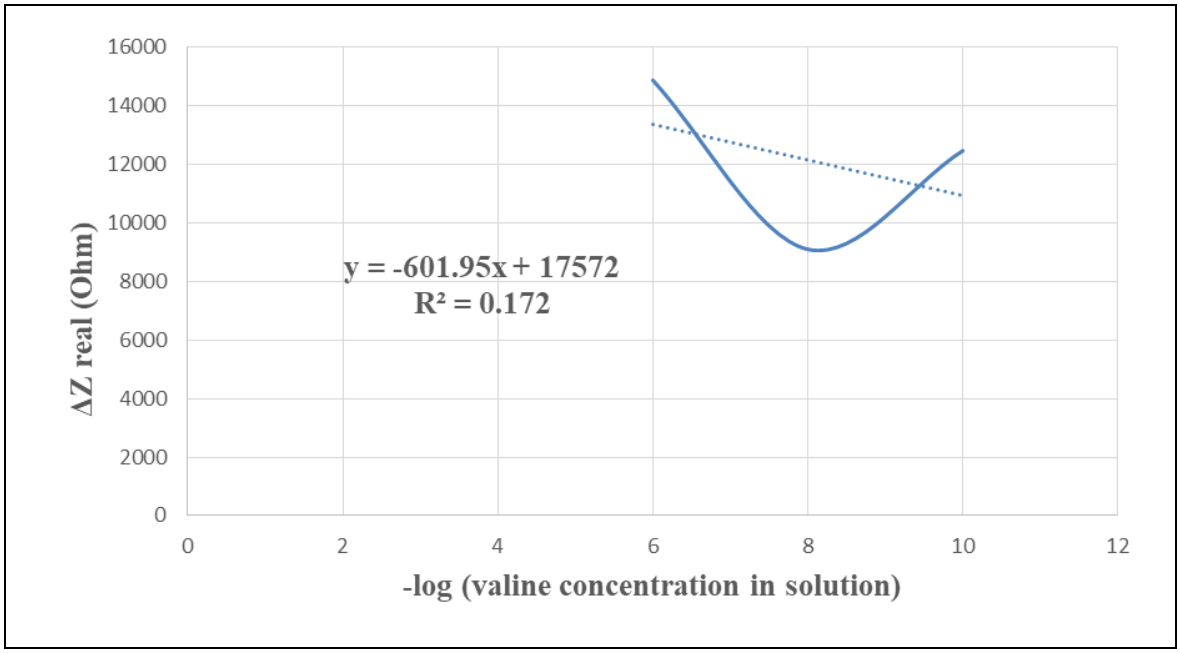

Figure 3.25. The regression curve of PGE2-(TRIS-0.3M-Val-UMIP) electrode.

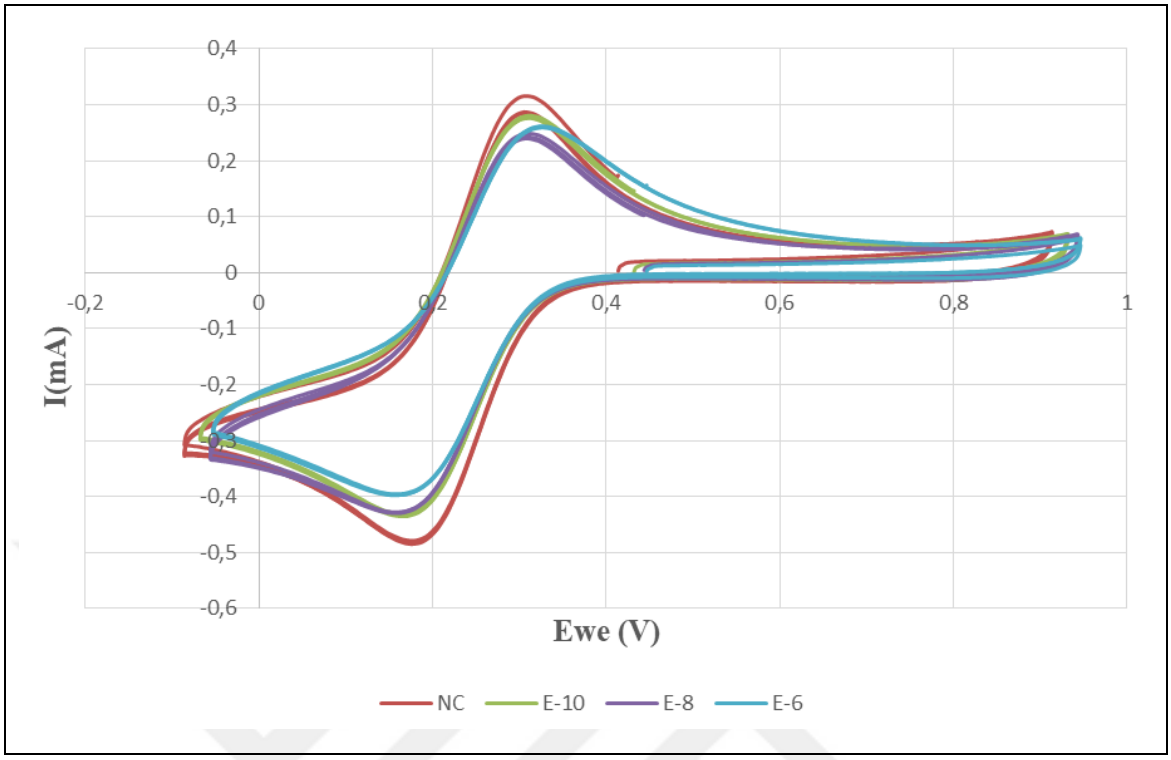

Figure 3.26. CV response of PGE2-(TRIS-0.3M-Val-UMIP) electrode.

Based on the above results, with the modification of hydrogel formulation, the R_{ct} could be detected. The UMIP version of this electrode was prepared as PGE3-(TRIS-0.3M-Val-UMIP), EIS and CV measurements were conducted at pH 5, 60 mV scan rate and 30 sec response time, in blank solution and at E-15 to E-6 M valine (Figures 3.30, 3.31, 3.32).

The graph in Figure 3.27 shows the behavior of the PGE7-(TRIS-0.3M-Val-MIP) electrode at varying solution concentrations. As a result of the graph obtained, it can be said that an electrode that can detect valine concentrations in the E-15 M to E-6 M range has been obtained. The valine molecules attached to the surface of the imprinted PGEs increase with the increase of the solution concentration and cause the inhibition of charge transfer. It is seen that with increasing valine concentration, the impedance of the electrode increases linearly and the R_{ct} values differ clearly, and the valine molecule can be detected very well in the E-15 and E-6 M range. The regression analysis using the changes in the impedance of the PGE7-(TRIS-0.3M-Val-MIP) electrode in different valine concontrations displayed a success rate of 96.72 percent (Figure 3.28).

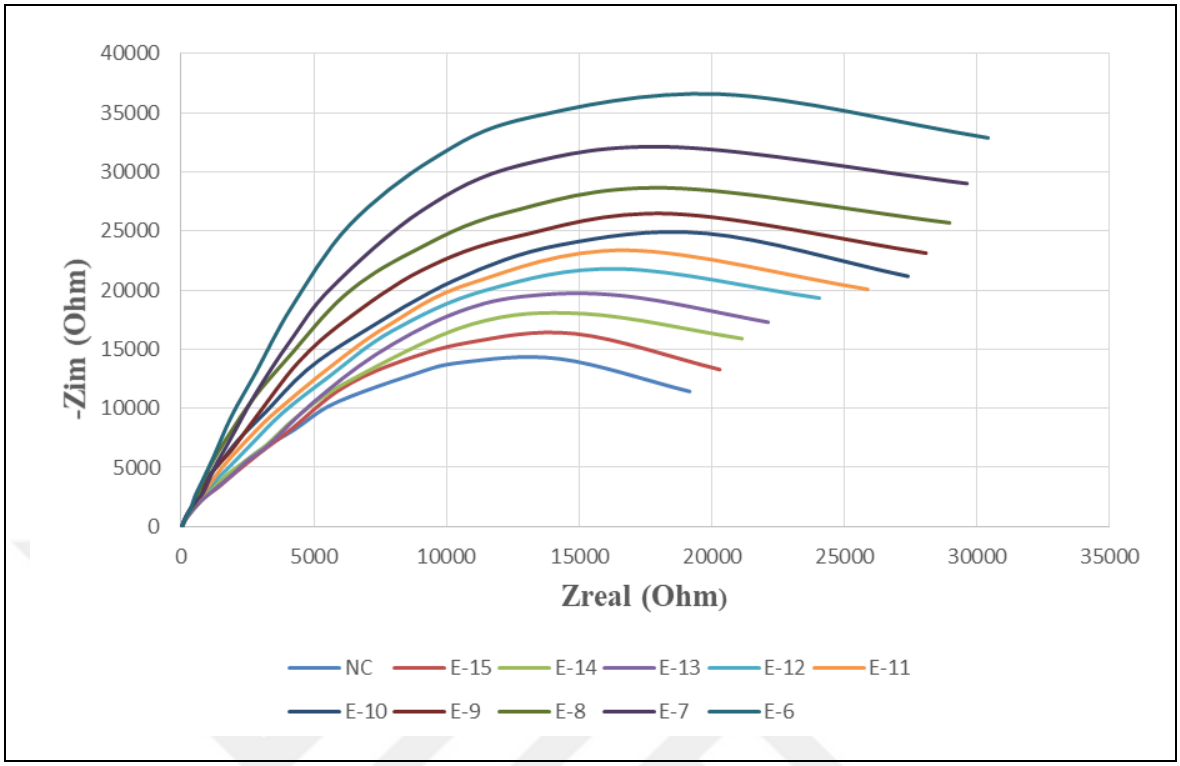

Figure 3.27. EIS response of PGE7-(TRIS-0.3M-Val-MIP) electrode.

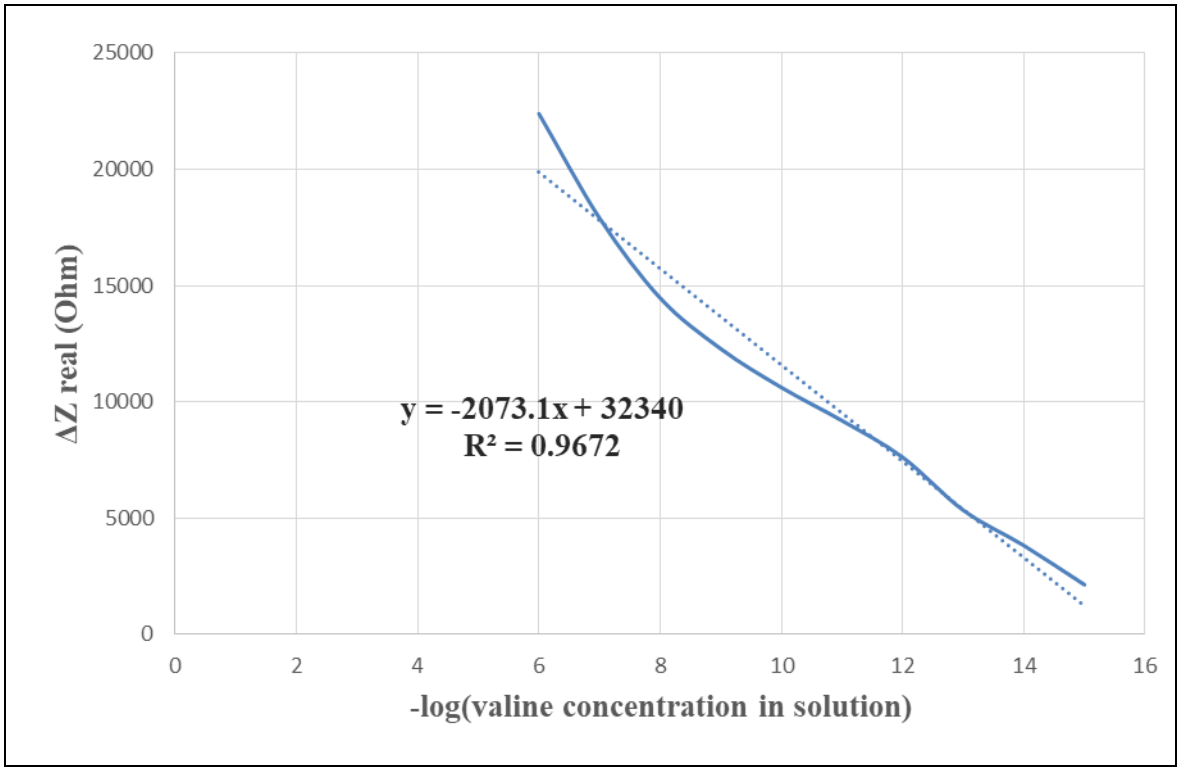

Figure 3.28. The curve of PGE7-(TRIS-0.3M-Val-MIP) electrode.

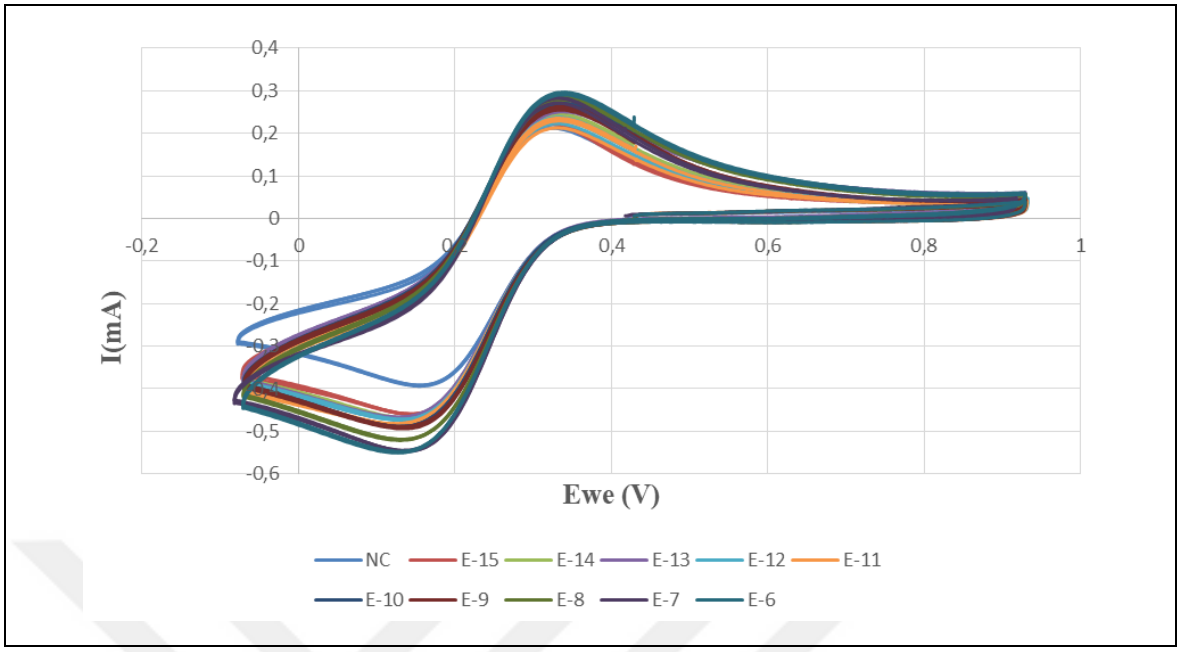

Figure 3.29. CV response of PGE7-(TRIS-0.3M-Val-MIP) electrode.

The EIS and CV response of PGE3-(TRIS-0.3M-Val-UMIP) electrode (Figures 3.30, 3.32) show that valine is not bound to the electrode surface, detecting valine with a success rate of only 29.31 percent (Figure 3.31).

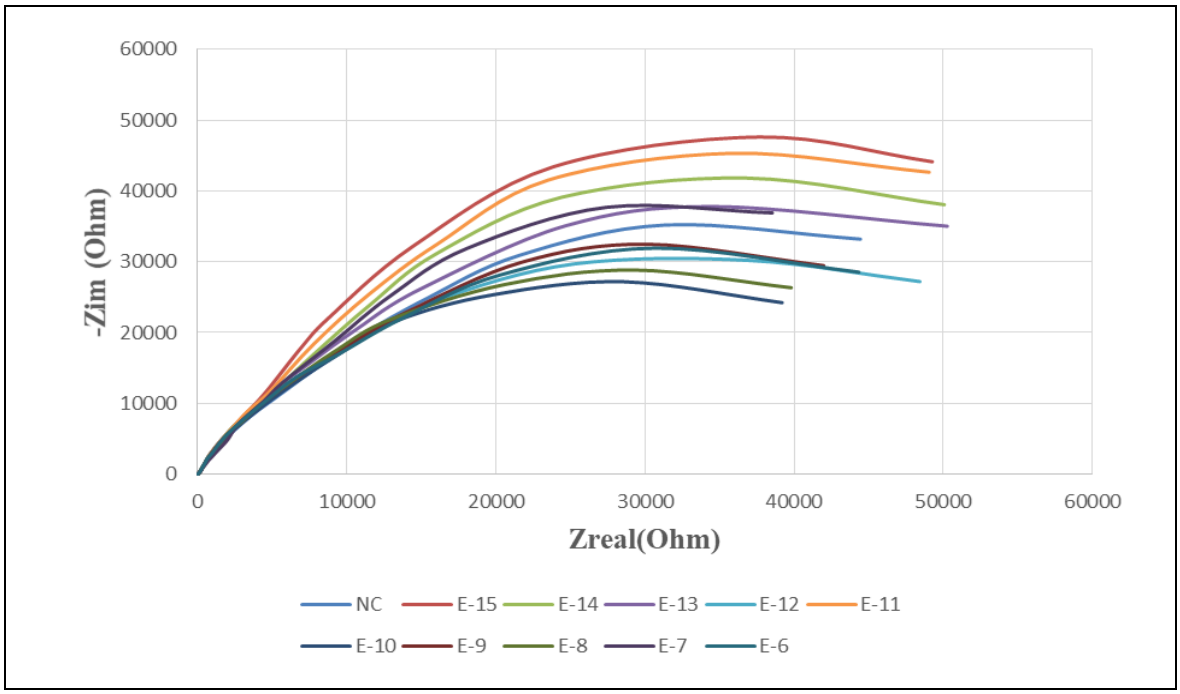

Figure 3.30. EIS response of PGE3-(TRIS-0.3M-Val-UMIP) electrode.

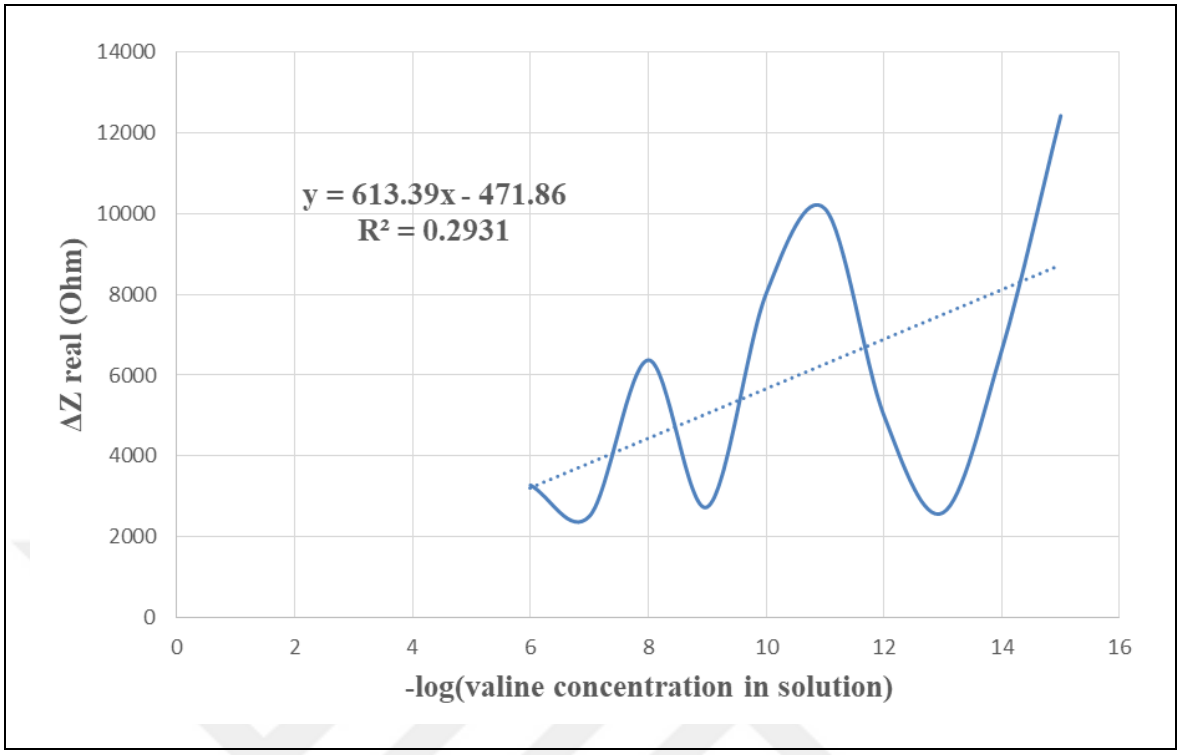

Figure 3.31. The regression curve of PGE3-(TRIS-0.3M-Val-UMIP) electrode.

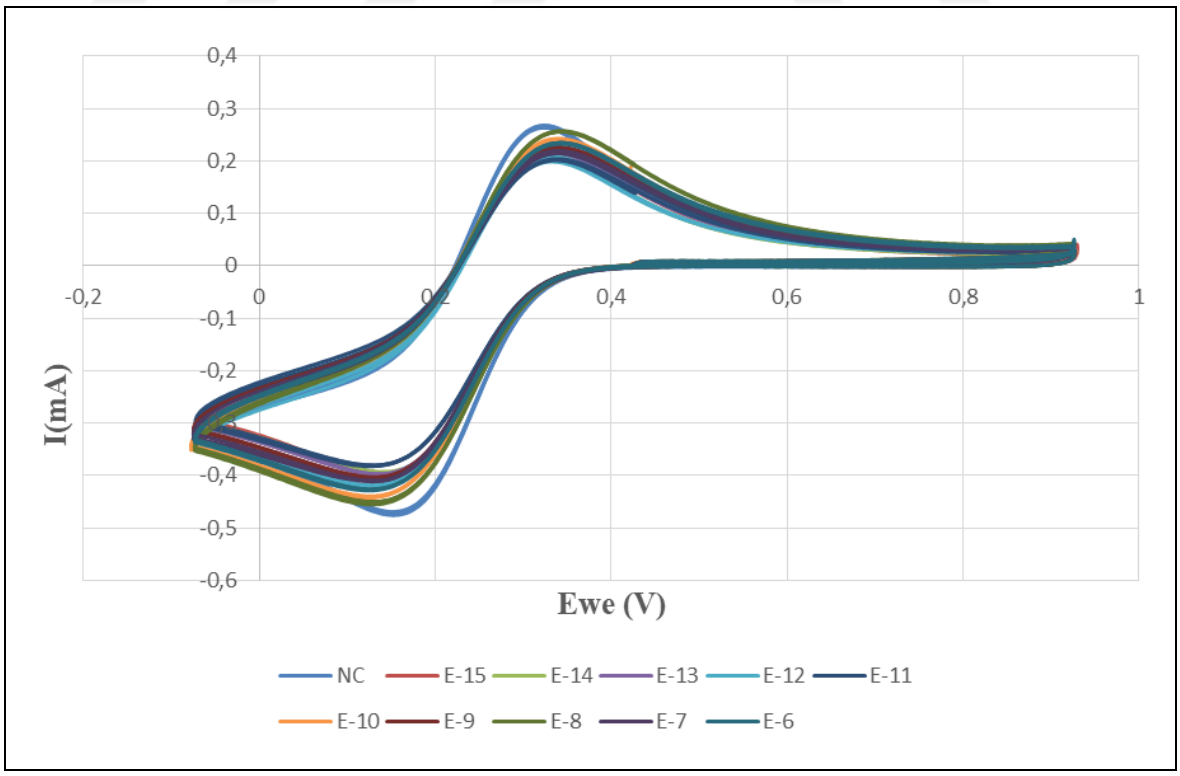

Figure 3.32. CV response of PGE3-(TRIS-0.3M-Val-UMIP) electrode.

When the data of PGE7-(TRIS-0.3M-Val-MIP) and PGE3-(TRIS-0.3M-Val-UMIP) electrodes are examined, in order to detect valine molecule with pencil graphite electrodes, it was decided to work with these hydrogel formulation in Rdx-PBS solution (pH5) at 60 mV/s scan rate and 30 seconds response time.

After the hydrogel modification on the PGE electrode was completed, the hydrogel formulation decided for valine on the main working electrode, the Au electrode, was imprinted molecularly as a 0.3 M valine concentration. EIS and CV analyzes were performed at scan rates ranging from 10 mV/s to 100 mV/s in 100 mL of Rdx-PBS (pH5) solutions containing 1 mL E-8 M valine with 30 seconds response time on the Au-0.3M-Val-MIP electrode. As can be seen in Figure 3.33 and 3.34, the scan rate was selected as 100 mV/s.

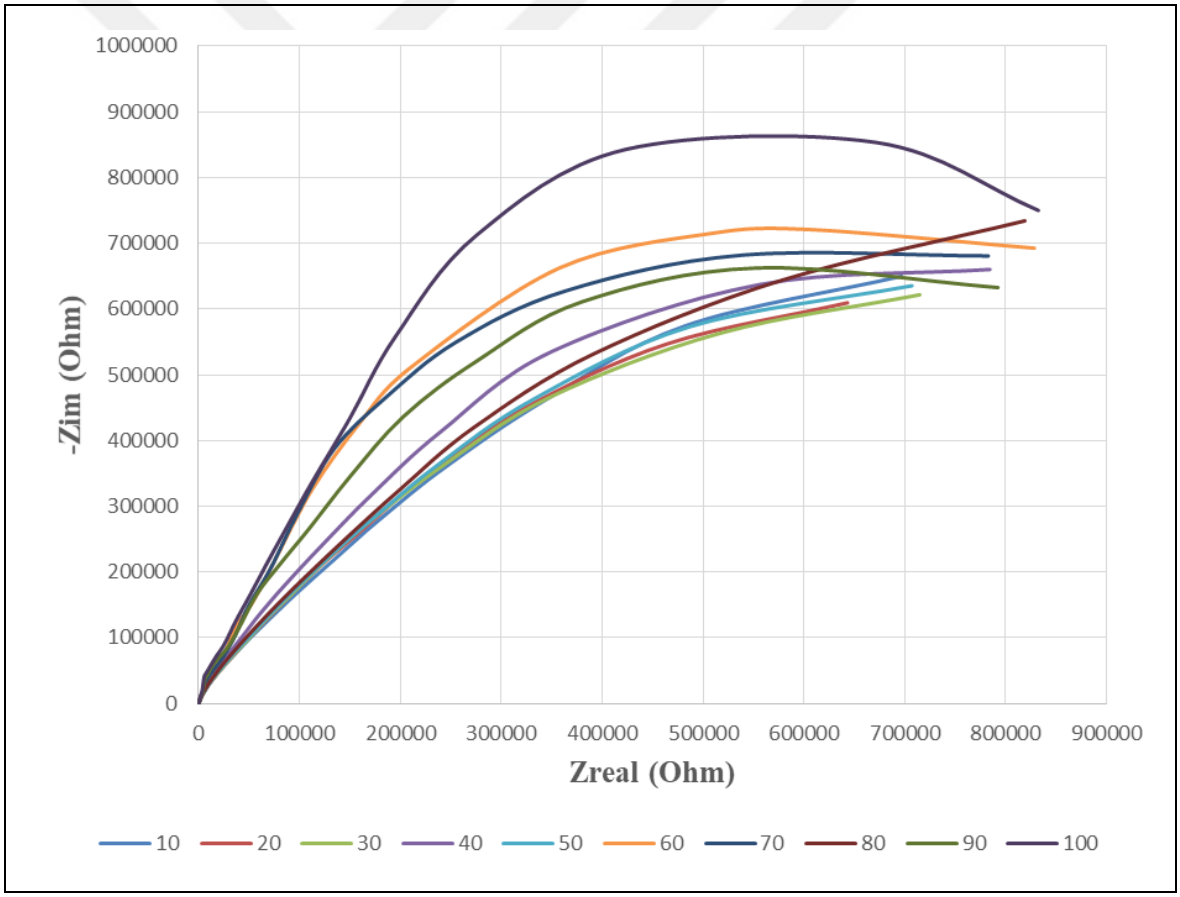

Figure 3.33. EIS response of Au-0.3M-Val-MIP electrode at pH 5 and different scan rates.

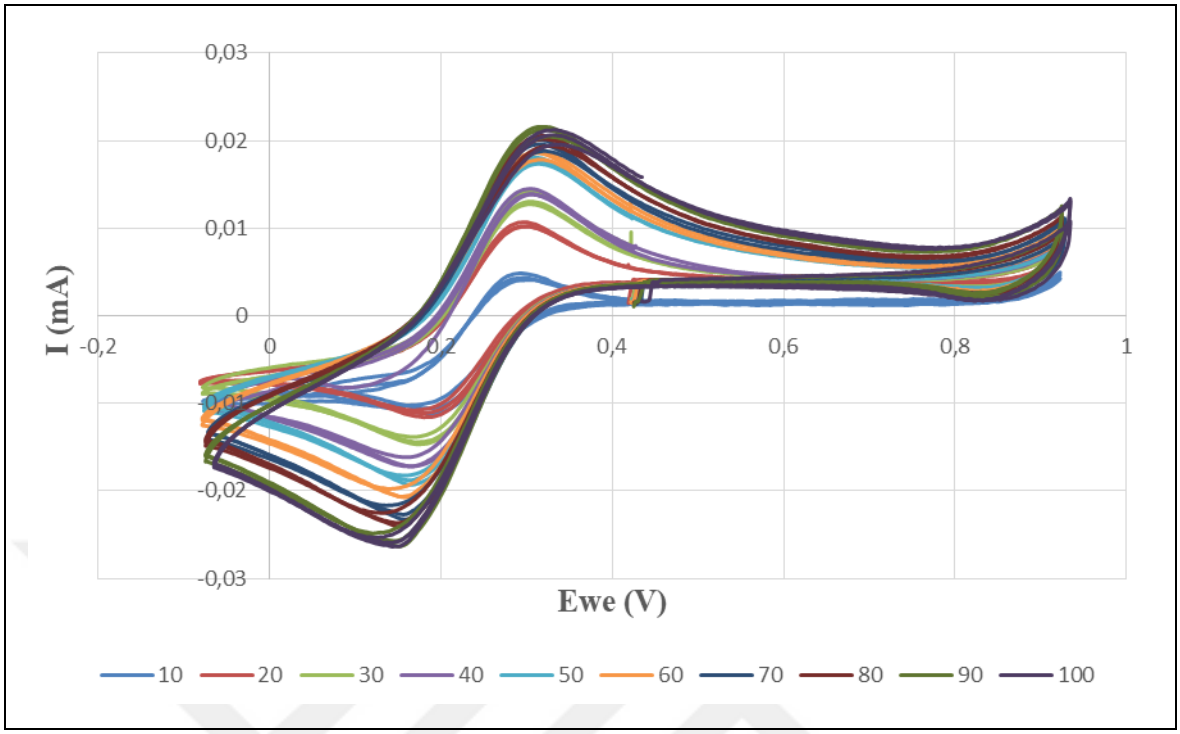

Figure 3.34. CV response of Au-0.3M-Val-MIP electrode at pH 5 and different scan rates.

As a result, it was decided to work with the hydrogel formulation determined at pH 5, 100 mV/s scan rate and 30 seconds response time in Rdx-PBS to determine the valine fixation limits of the Au electrode.

3.2. ANALYSIS OF ELECTRODES

3.2.1. Control Group

The CV plot obtained from electrochemical measurements provides information about electron transfer kinetics and results; the EIS graph gives data about the reaction characteristic of the electrode interface. Furthermore, the CV graph represents the change in electron transfer kinetics caused by reduction-oxidation reactions [77].

Au non-imprinting electrode was prepared as a control group (Au-NIP). The control group electrode was coated with hydrogel solution without valine. EIS and CV measurements were made at pH 5, 100 mV/s scan rate and 30 sec response time, in blank, followed by E-15, E-14, E-13, E-12, E-11, E-10, E-9, E-8, E-7 and E-6 M valine Rdx-PBS (Figures 3.35, 3.37).

The CV and EIS graphs of the NIP electrodes indicated and increase in cell potential, current amplitude and peak potential (Figure 3.35). Figure 3.36 displays regression curve with a success rate of 91.68 percent. However, the high success rate may be due to the non-specific binding of valine to the organic polymer. It is seen that there are two different linearities in the range of E-6/E-9 M and in the range of E-9/E-15 M (Figure 3.36).

According to the CV results, as the concentration increases, the solution conductivity increased (Figure 3.37). It is seen that the conductivity of the solution increases as the conductive substance valine is not connected to the electrode and remains in the solution.

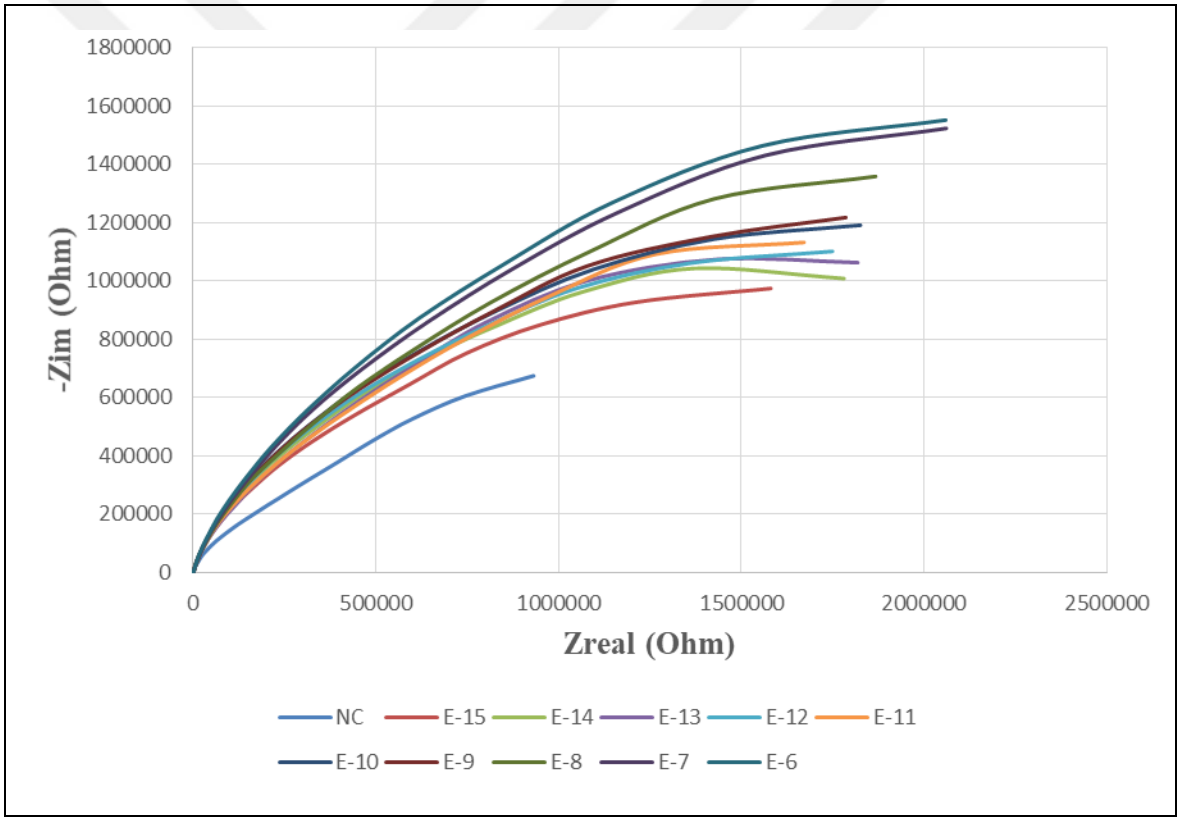

Figure 3.35. EIS response of Au-NIP electrode.

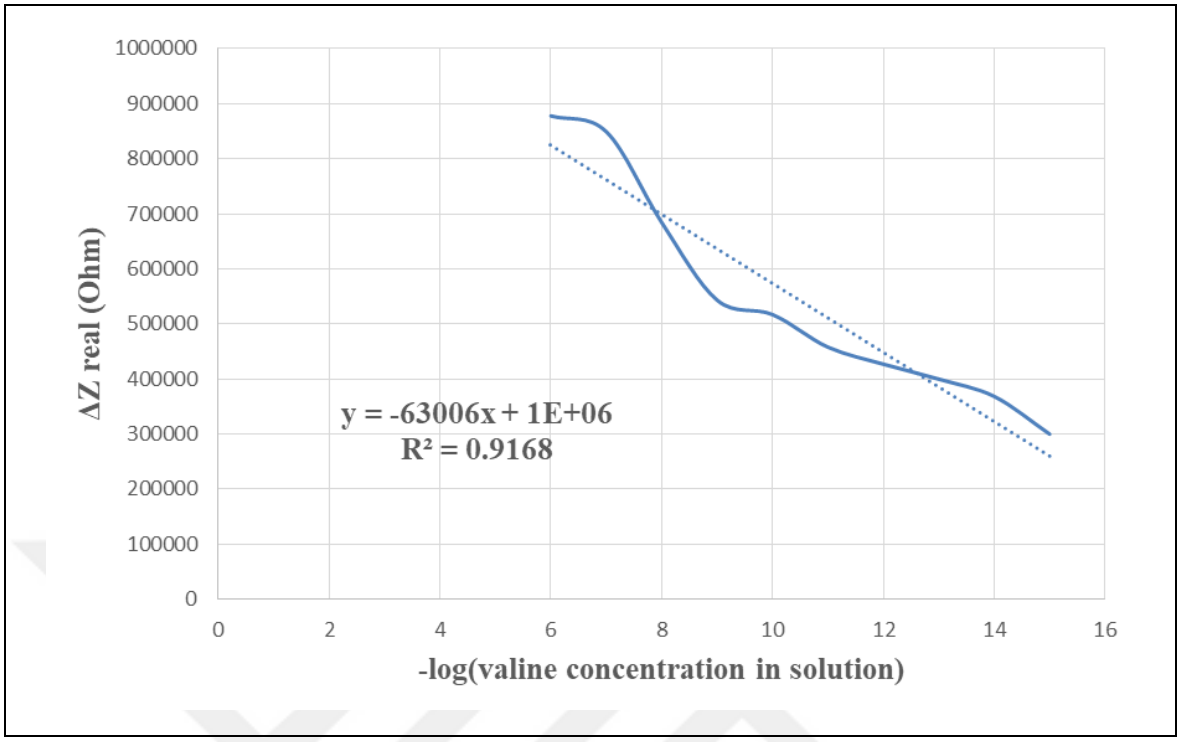

Figure 3.36. The regression curve of Au-NIP electrode.

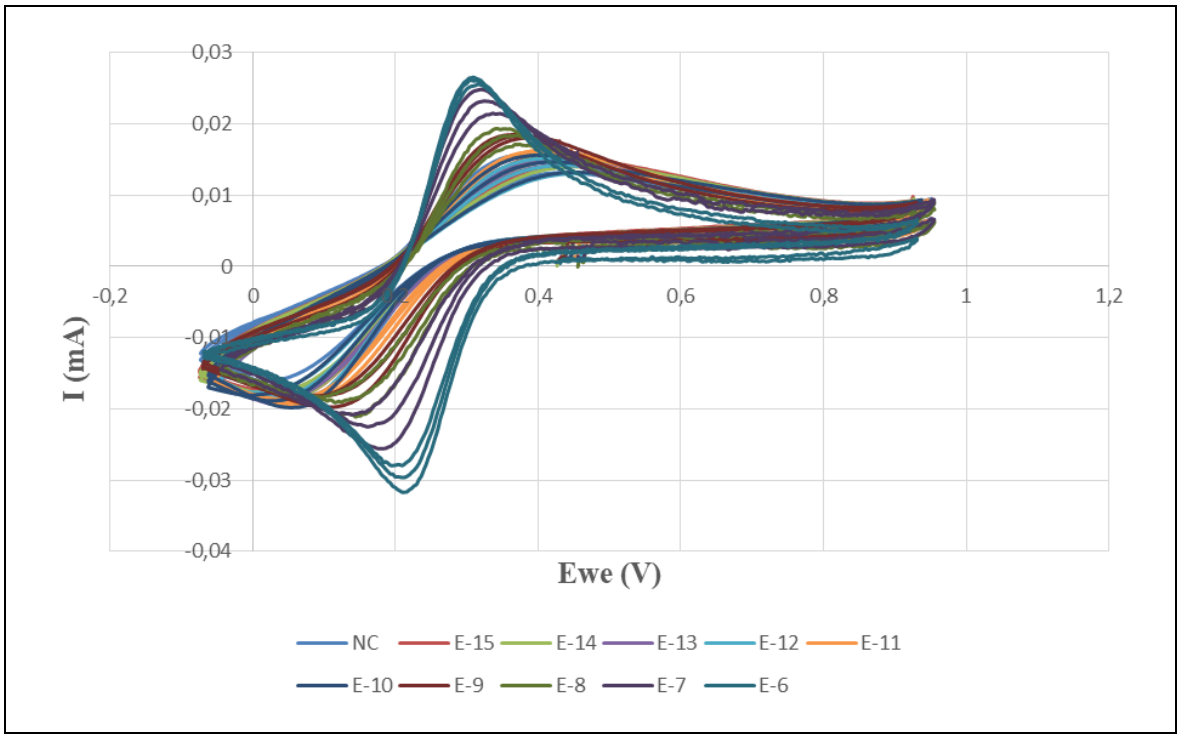

Figure 3.37. CV response of Au-NIP electrode.

3.2.2. Valine Molecular Imprinting Group (Val-MIP)

In this study, in order to evaluate the data of the electrodes forming the experimental group, 0.15 M, 0.2 M, 0.25 M, 0.275 M, 0.3 M, 0.325 M, 0.35 M, 0.4 M, 0.45 M and 0.5 M valine were imprinted on the electrodes (Figures 3.38, 3.44, 3.50, 3.56, 3.62, 3.68, 3.74, 3.80, 3.86, 3.92) with eighteen different electrodes as Au-0.15M-Val-MIP, Au-0.2 M-Val-MIP, Au-0.25M-Val-MIP, Au-0.275M-Val-MIP, Au-0.3M-Val-MIP, Au-0.325M-Val-MIP, Au-0.35M-Val-MIP, Au-0.4M-Val-MIP, Au-0.45M-Val-MIP and Au-0.5M-Val-MIP electrodes. The EIS graphs display that with increased number of valine receptors, increased number of valine molecules are bound to these receptors and hence increasing the impedance of Au electrode. The CV plots of the above given electrodes (Au-0.15M-Val-MIP, Au-0.2 M-Val-MIP, Au-0.25M-Val-MIP, Au-0.275M-Val-MIP, Au-0.3M-Val-MIP, Au-0.325M-Val-MIP, Au-0.35M-Val-MIP, Au-0.4M-Val-MIP, Au-0.45M-Val-MIP, and Au-0.5M-Val-MIP) are given in Figures 3.42, 3.48, 3.54, 3.60, 3.66, 3.72, 3.78, 3.84, 3.90 and 3.96. As seen in Figure 3.38, Au-0.15M-Val-MIP electrode can detect valine molecule with 0.74 percent success (Figure 3.39) in the range of E-18 M and E-6 M valine. It was found that the Au-0.15M-Val-MIP electrode could detect the range of valine concentrations of E-12 M and E-9 M with an success of 94.82 percent (Figure 3.40). With increasing valine concentration, anodic currents and cell potential remain constant, while cathodic currents increase (Figure 3.43).

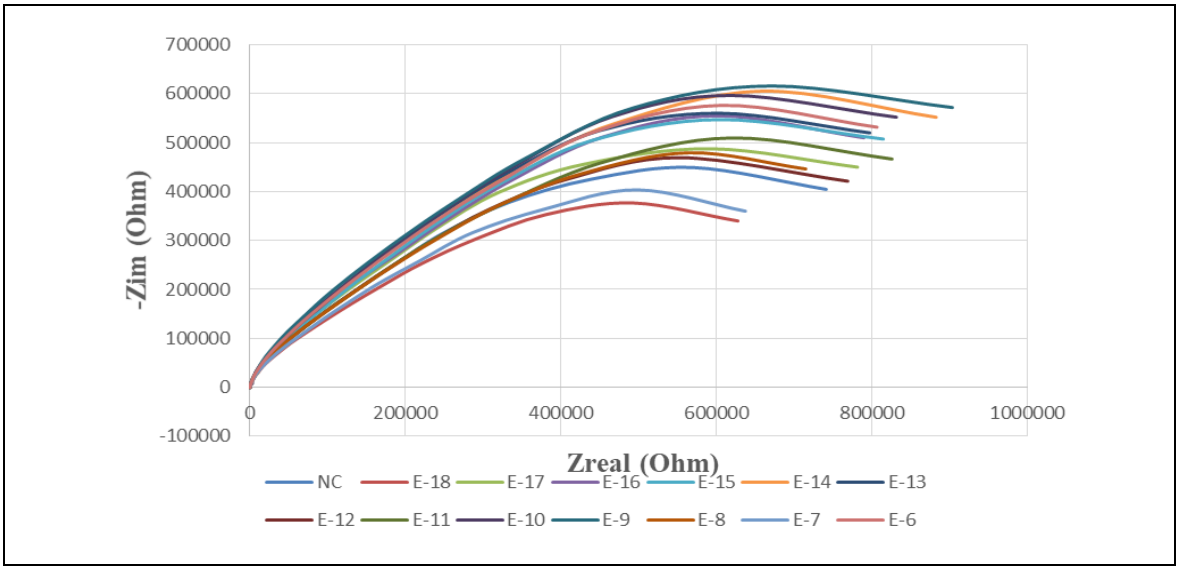

Figure 3.38. EIS response of Au-0.15M-Val-MIP electrode .

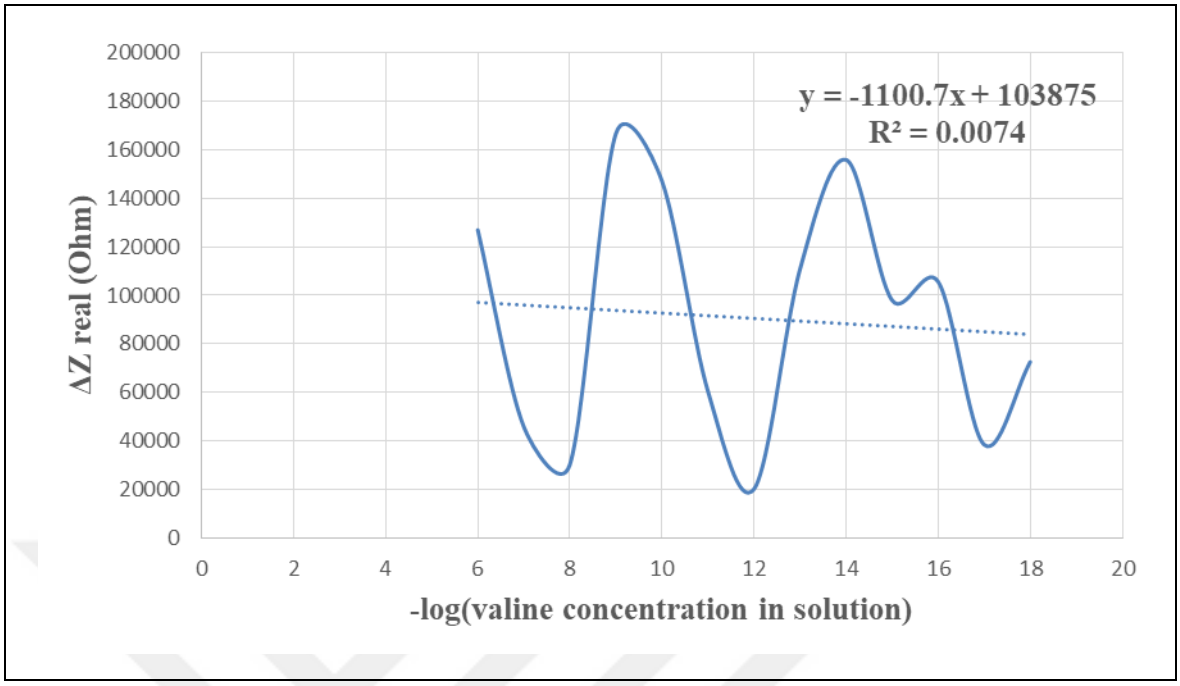

Figure 3.39. The regression curve of Au-0.15M-Val-MIP electrode.

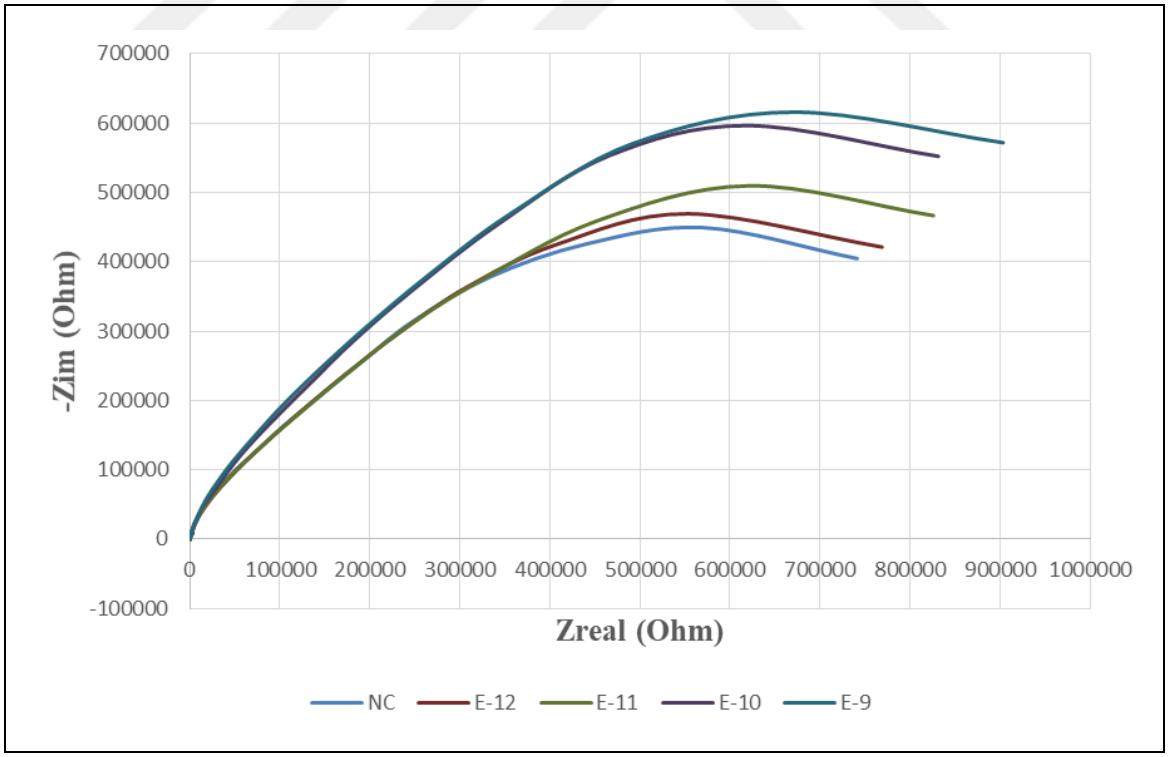

Figure 3.40. EIS response of the Au-0.15M-Val-MIP electrode.

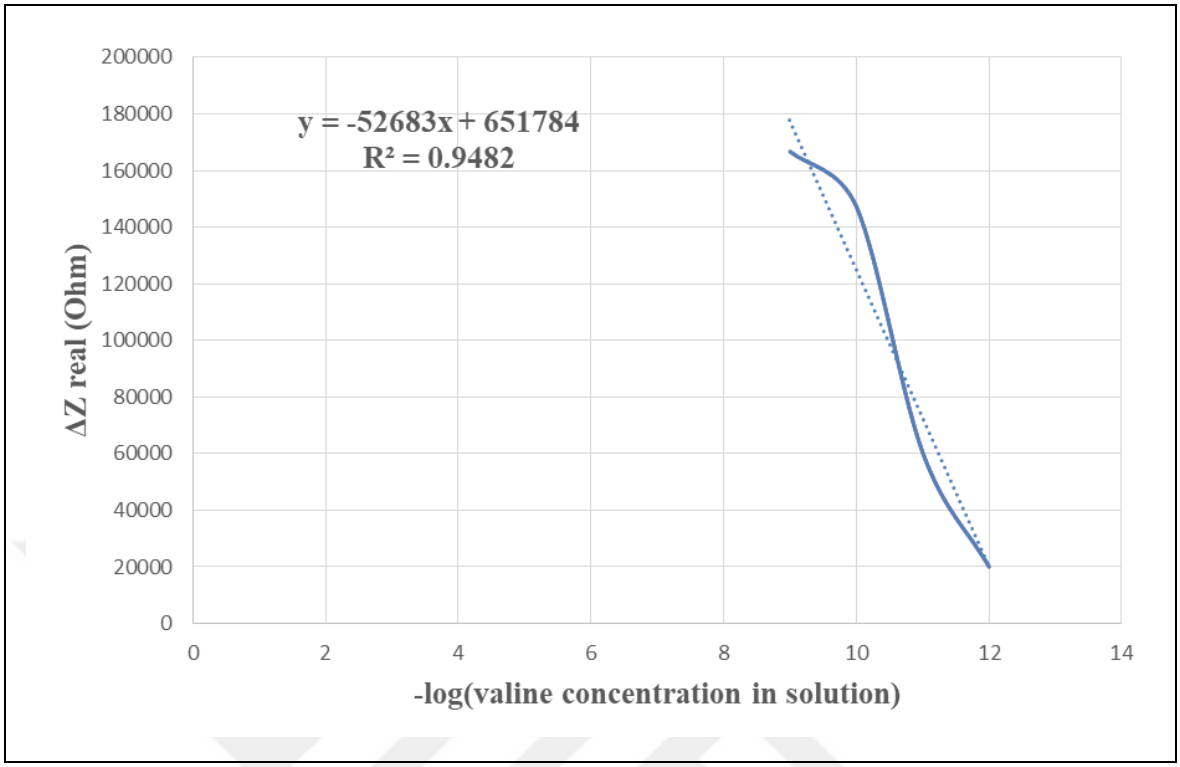

Figure 3.41. The regression curve of the Au-0.15M-Val-MIP electrode.

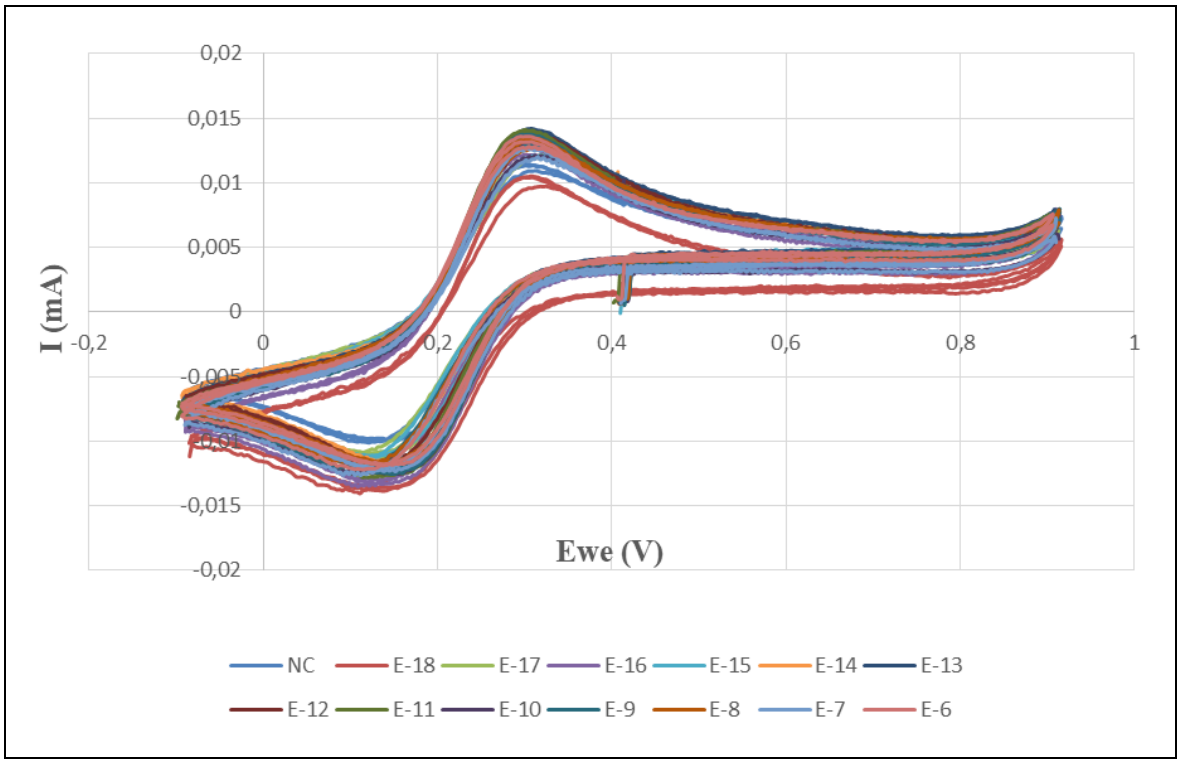

Figure 3.42. CV response of Au-0.15M-Val-MIP electrode.

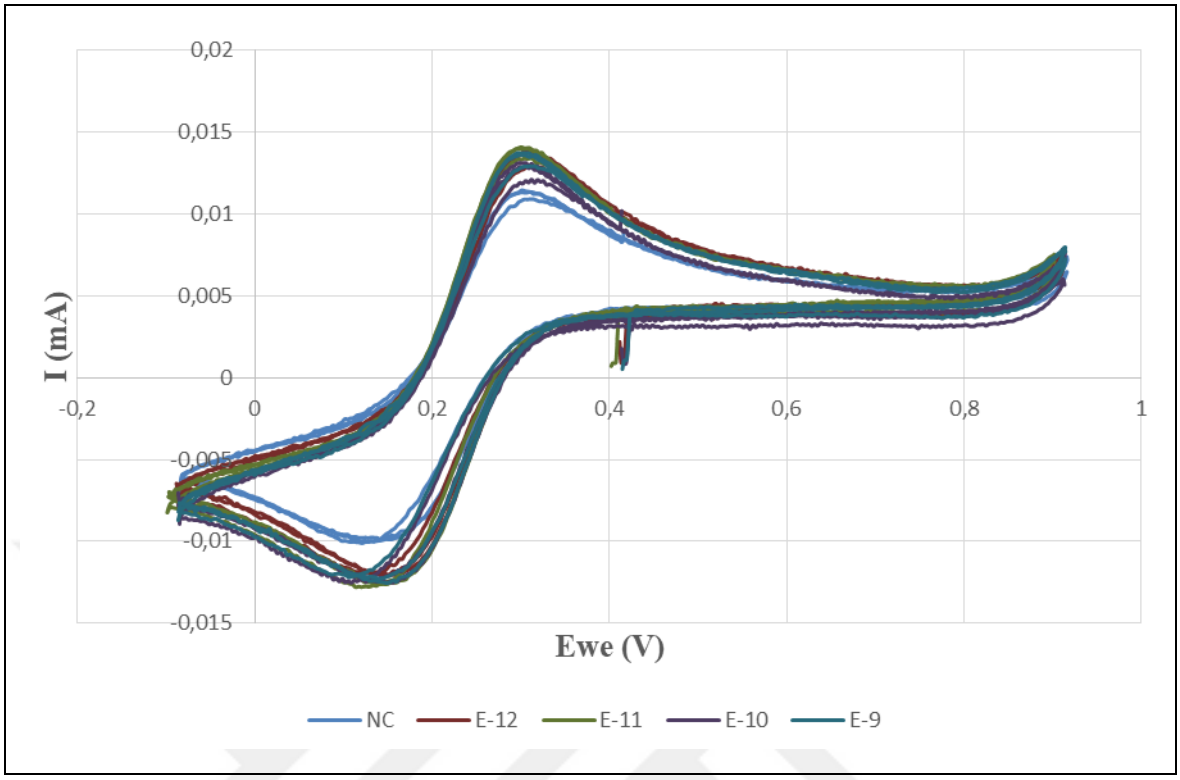

Figure 3.43. CV results of the Au-0.15M-Val-MIP electrode.

The Au-0.2M-Val-MIP electrode can detect valine molecules with 87.5 percent success (Figure 3.45) in the range of E-18 M and E-6 M valine (Figure 3.44). According to the regression curve (Figure 3.47), the Au-0.2M-Val-MIP electrode could detect the range of valine concentrations of E-13 M and E-7 M valine with a success rate of 98.76 percent (Figure 3.46). It is seen that with increasing valine concentration, anodic currents and cathodic currents increase (Figure 3.49).

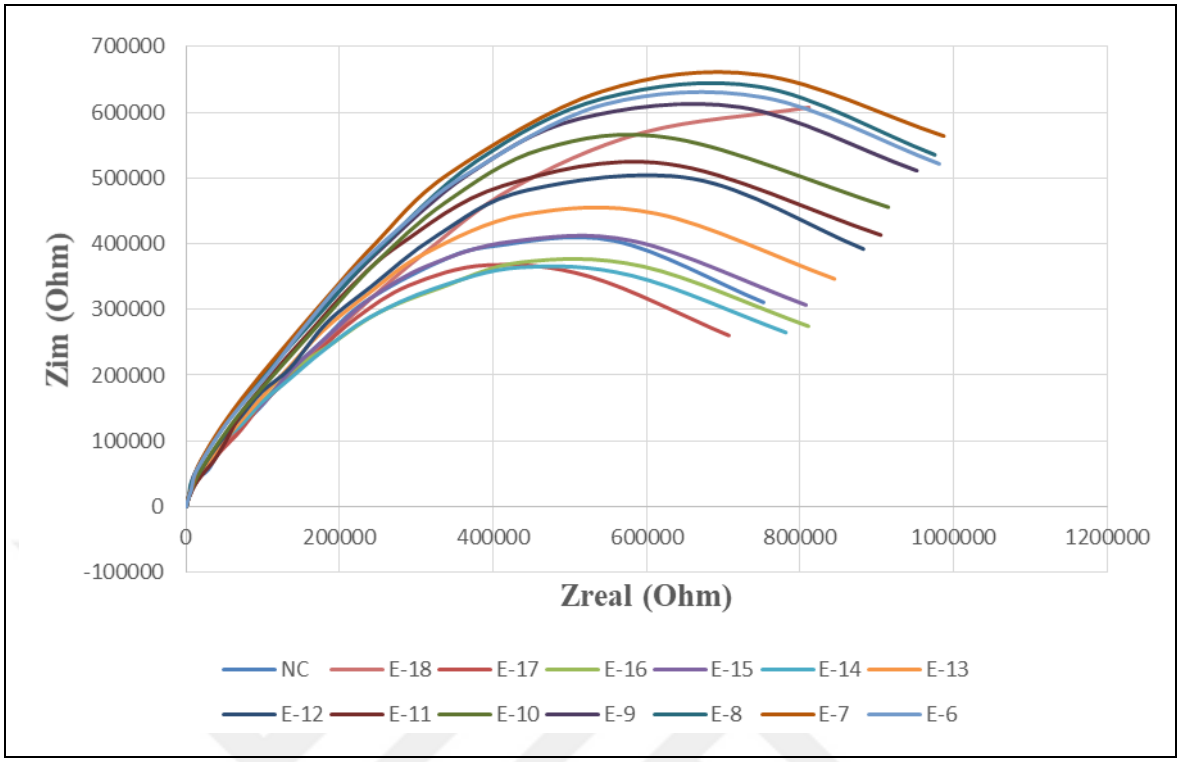

Figure 3.44. EIS response of Au-0.2M-Val-MIP electrode.

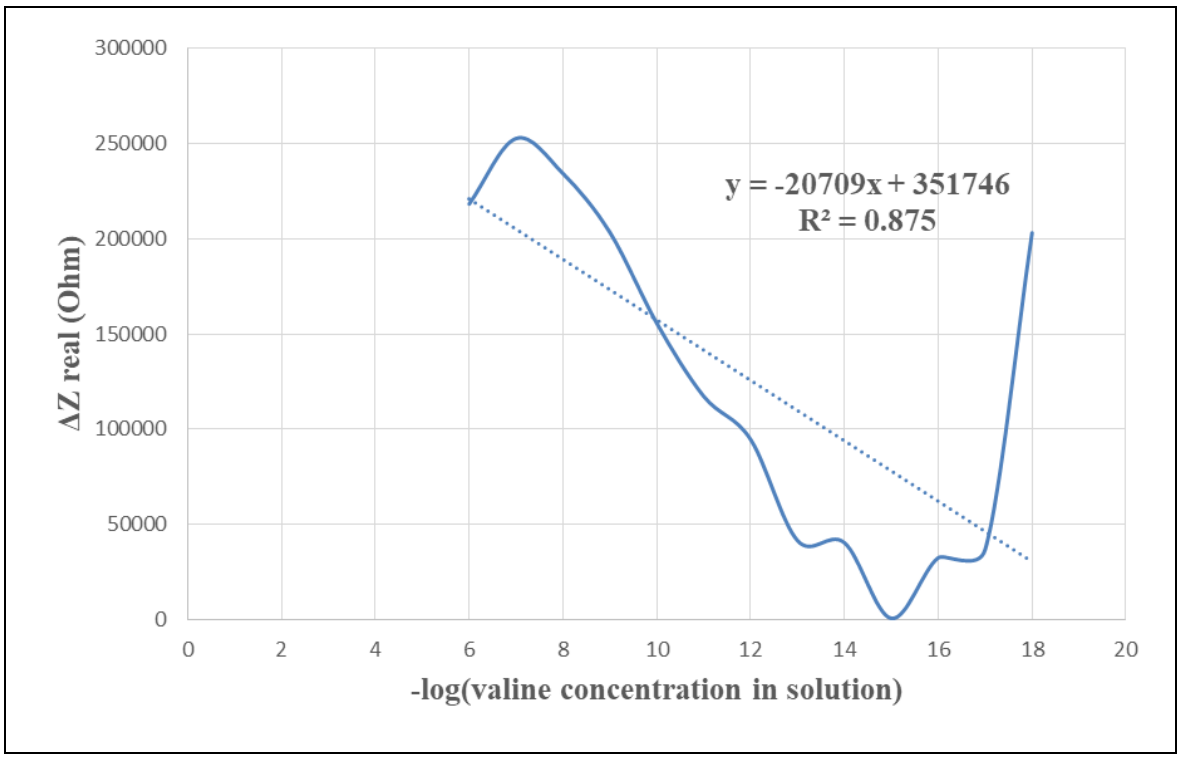

Figure 3.45. The regression curve of Au-0.2M-Val-MIP electrode.

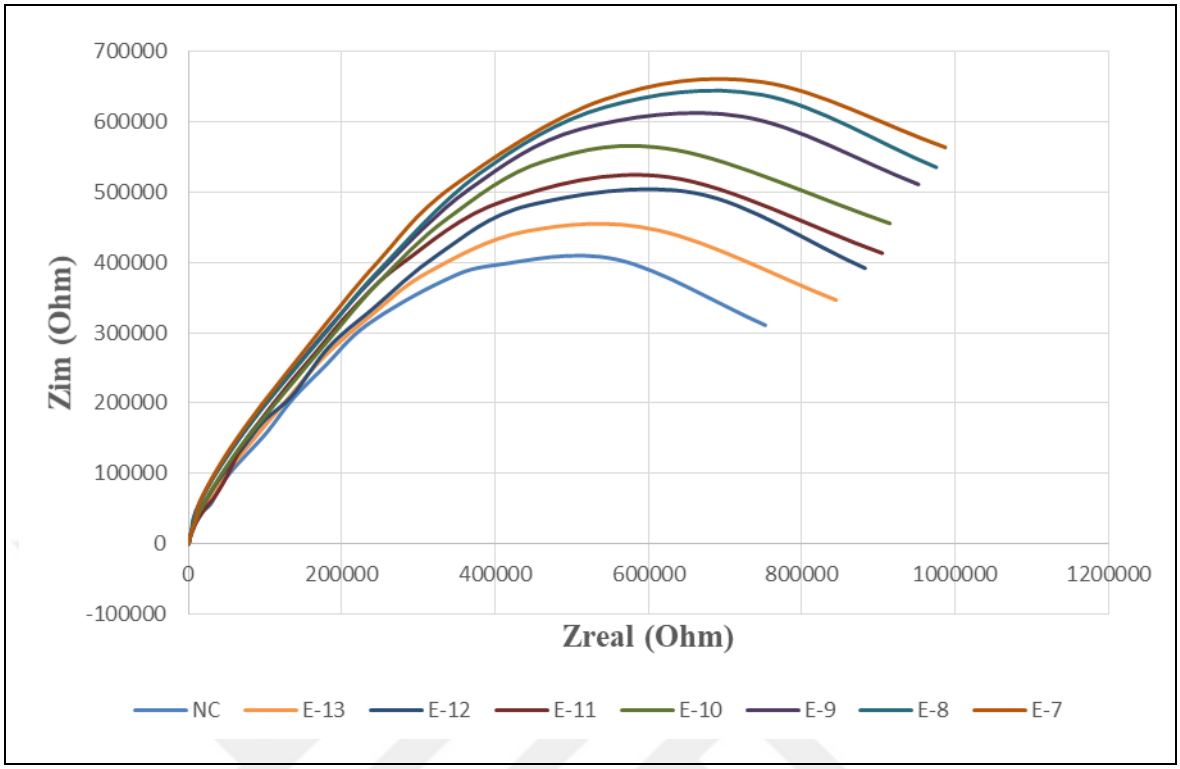

Figure 3.46. EIS response of the Au-0.2M-Val-MIP electrode.

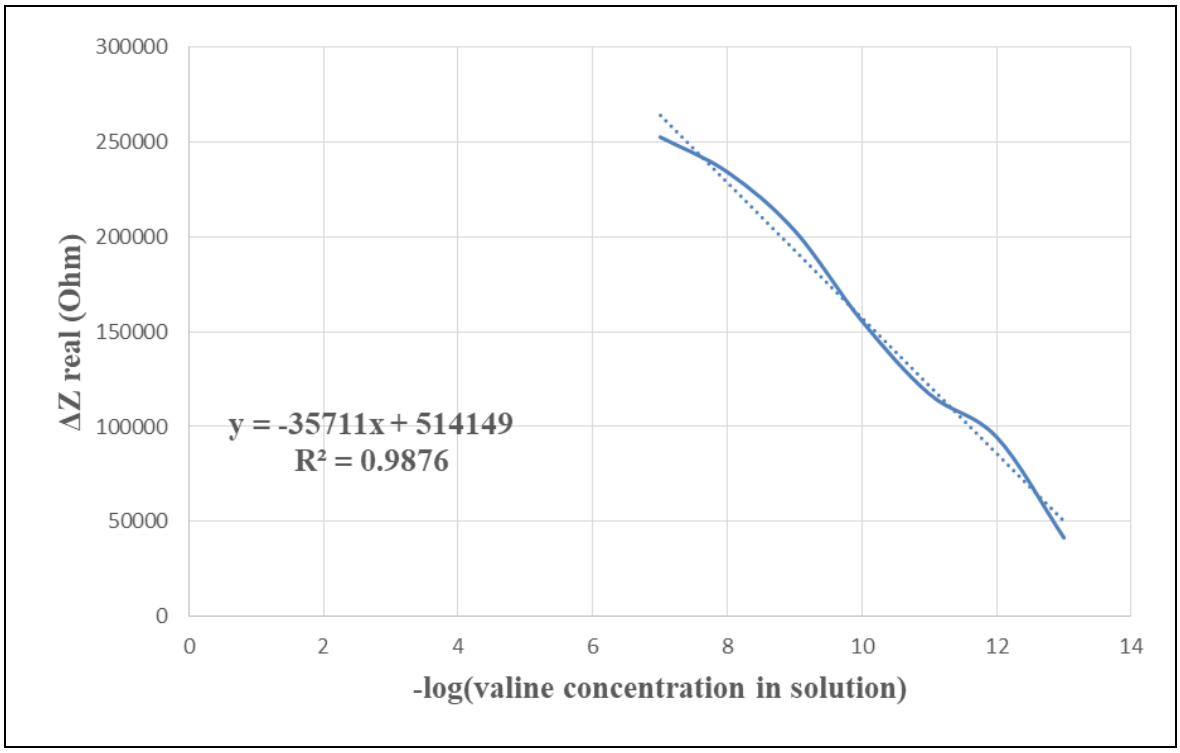

Figure 3.47. The regression curve of Au-0.2M-Val-MIP electrode.

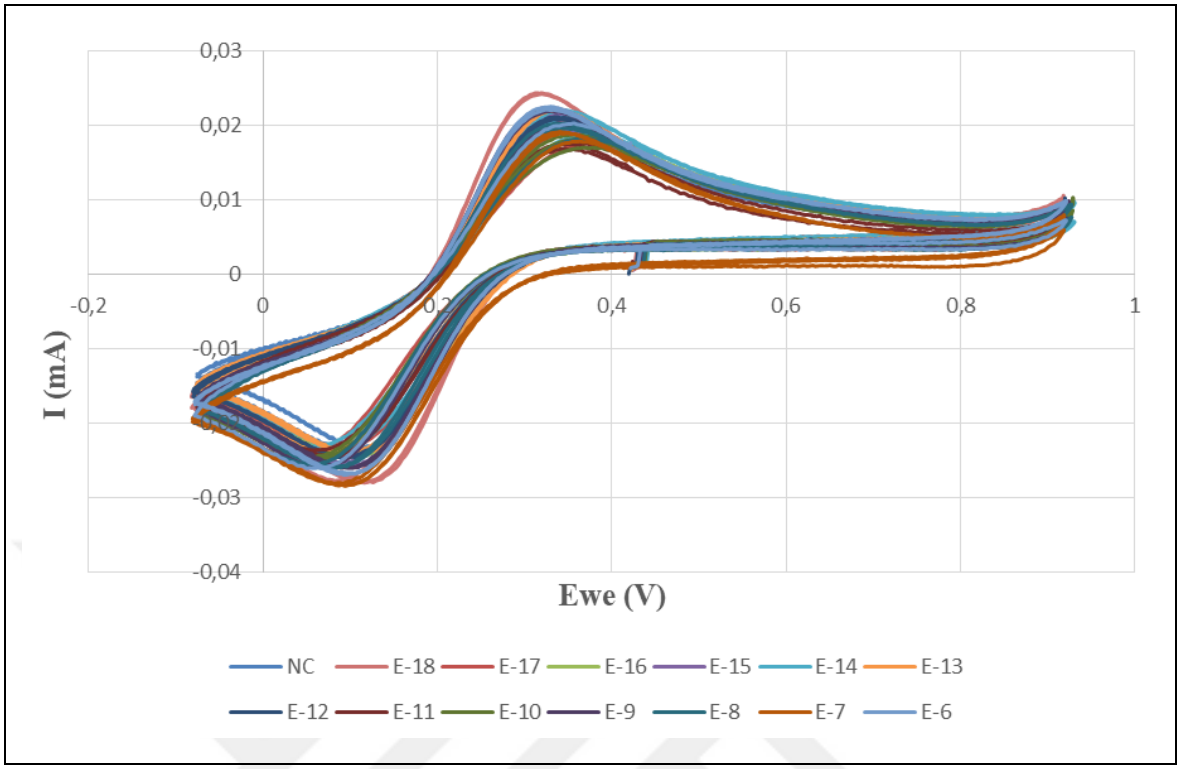

Figure 3.48. CV response of Au-0.2M-Val-MIP electrode.

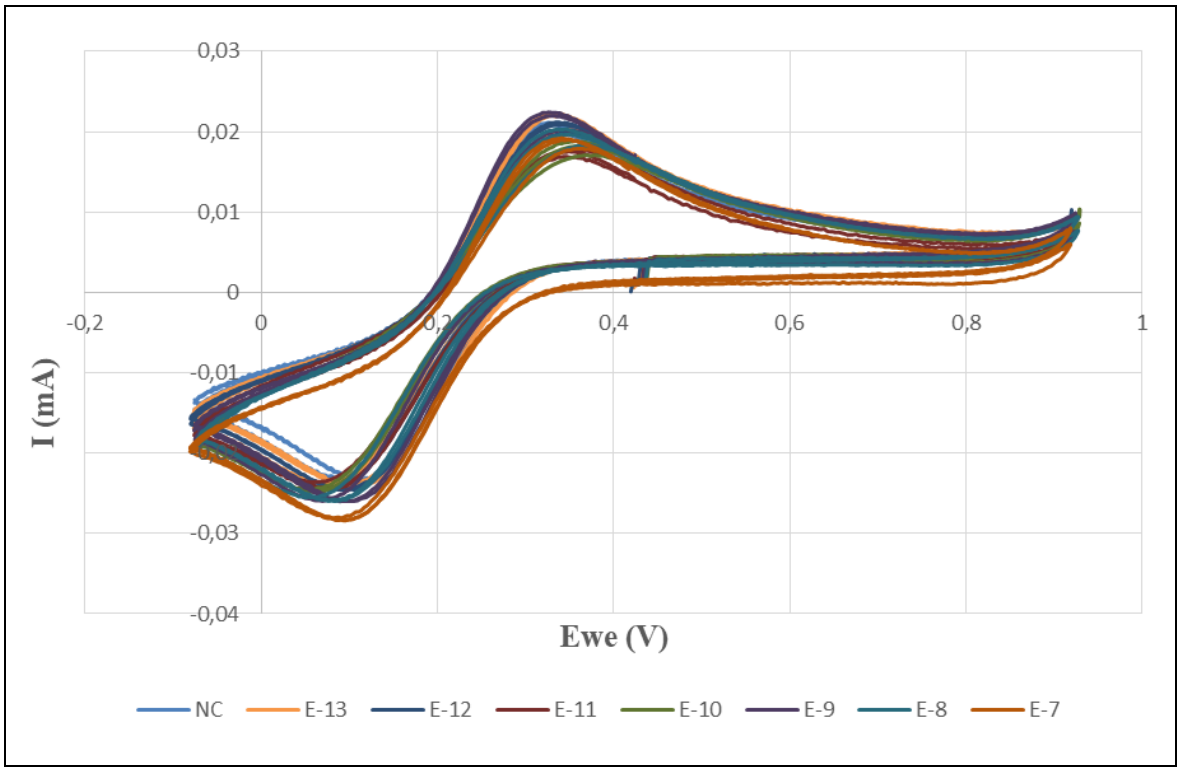

Figure 3.49. CV response of Au-0.2M-Val-MIP electrode.

The Au-0.25M-Val-MIP electrode can detect valine molecules with 39.57 percent success (Figure 3.51) in the range of E-18 M and E-6 M valine (Figure 3.50). According to the regression curve (Figure 3.53), the Au-0.25M-Val-MIP electrode could detect the E-13 M to E-7 M valine range with a success rate of 97.57 percent (Figure 3.52). It is seen that with increasing valine concentration, anodic currents and cathodic currents increase (Figure 3.55).

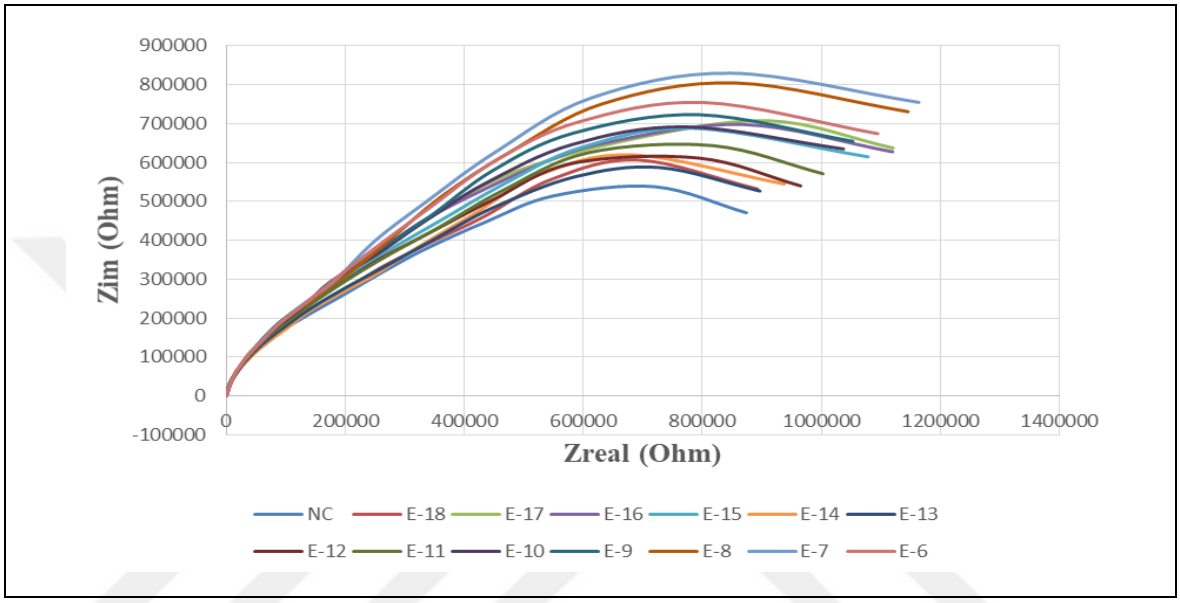

Figure 3.50. EIS response of Au-0.25M-Val-MIP electrode.

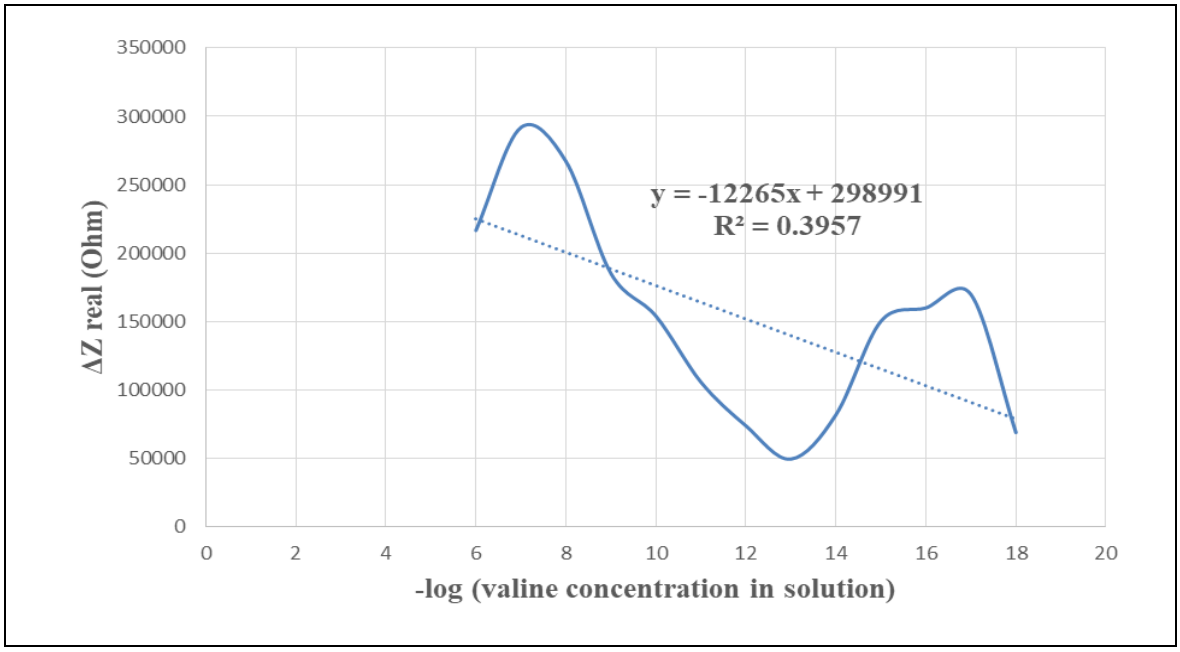

Figure 3.51. The regression curve of Au-0.25M-Val-MIP electrode.

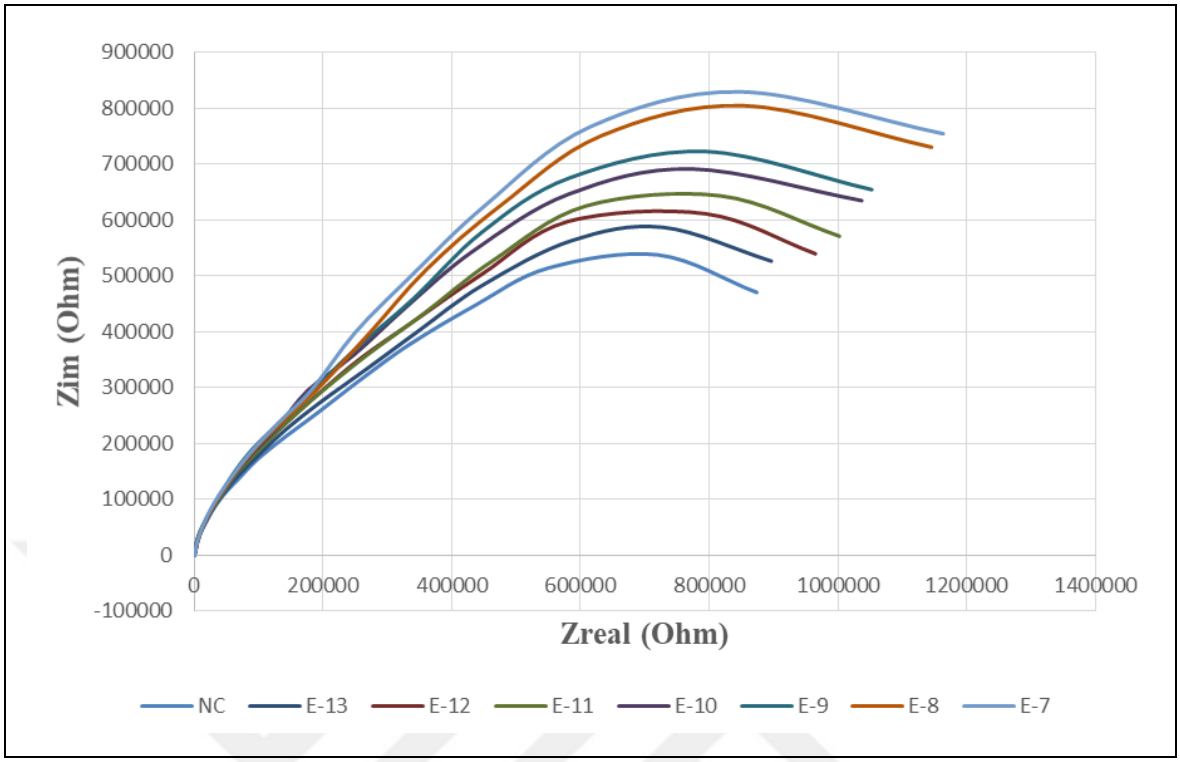

Figure 3.52. EIS response of Au-0.25M-Val-MIP electrode.

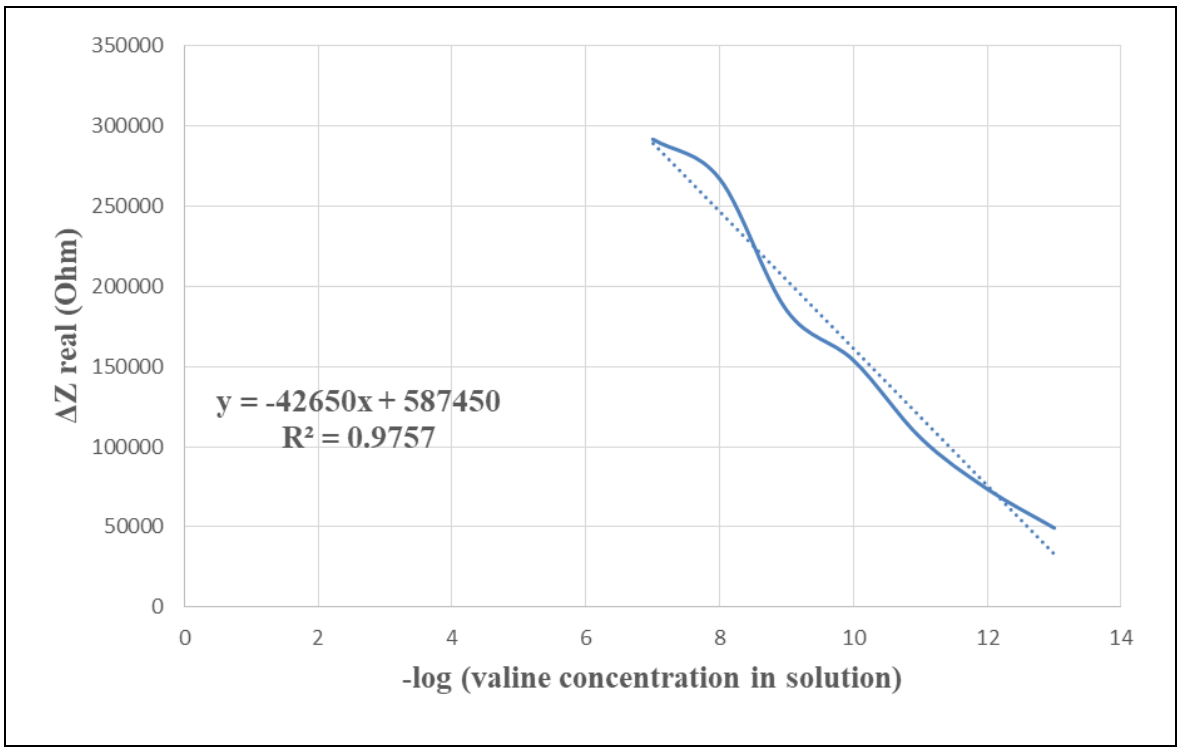

Figure 3.53. The regression curve of Au-0.25M-Val-MIP electrode.

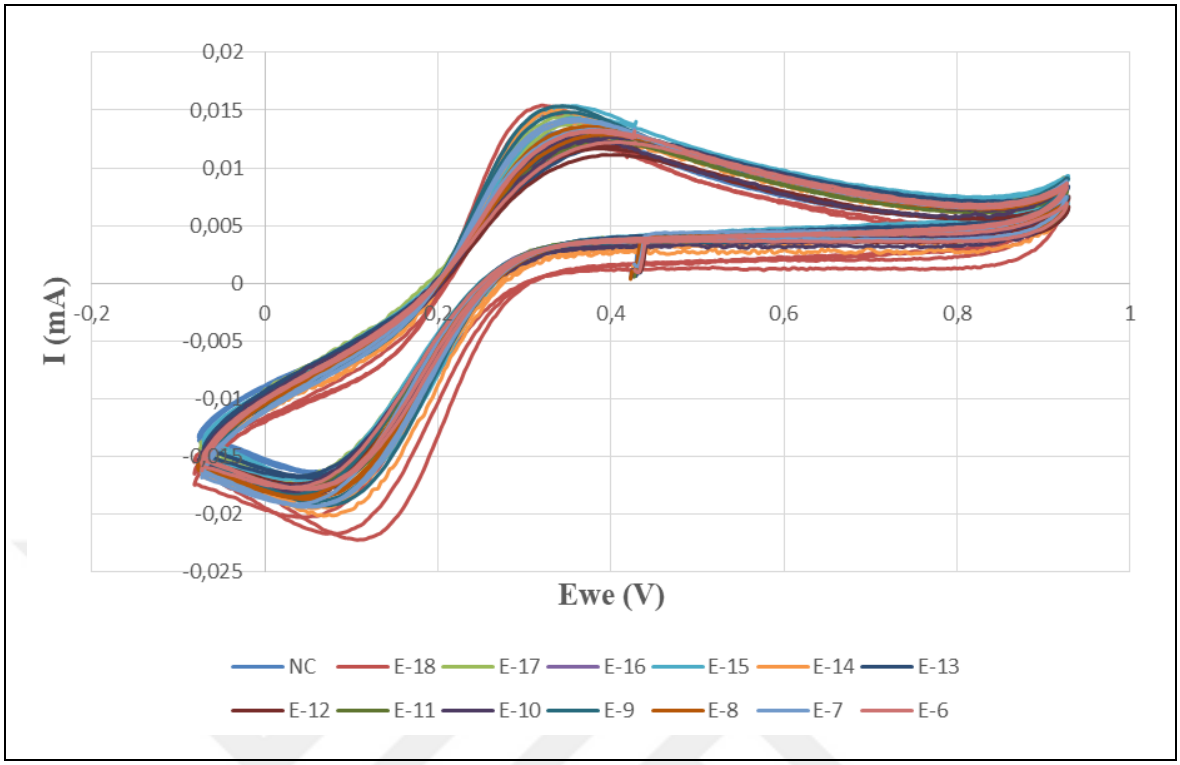

Figure 3.54. CV response of Au-0.25M-Val-MIP electrode.

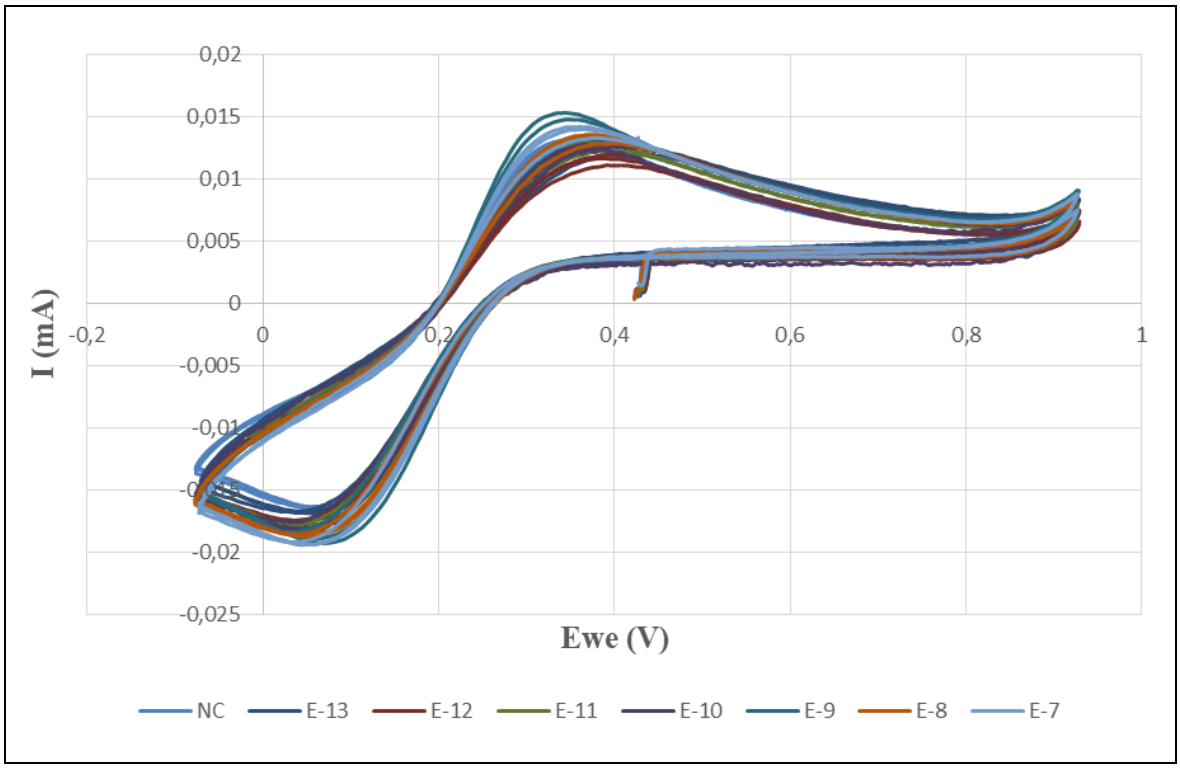

Figure 3.55. CV response of Au-0.25M-Val-MIP electrode.

Figure 3.56 shows that the Au-0.275M-Val-MIP electrode can detect valine molecules with a success rate of 28.16 percent (Figure 3.57) in the concentration range of E-18 M and E-6 M valine. The Au-0.275M-Val-MIP electrode successfully detected E-14 M and E-7 M valine with a success rate of 99.47 percent (Figure 3.59). Figure 3.72 shows the anodic and cathodic current increase with increasing valine concentration. The conductivity of the solution increases as the amount of valine in the solution increases, and the current increases as a result.

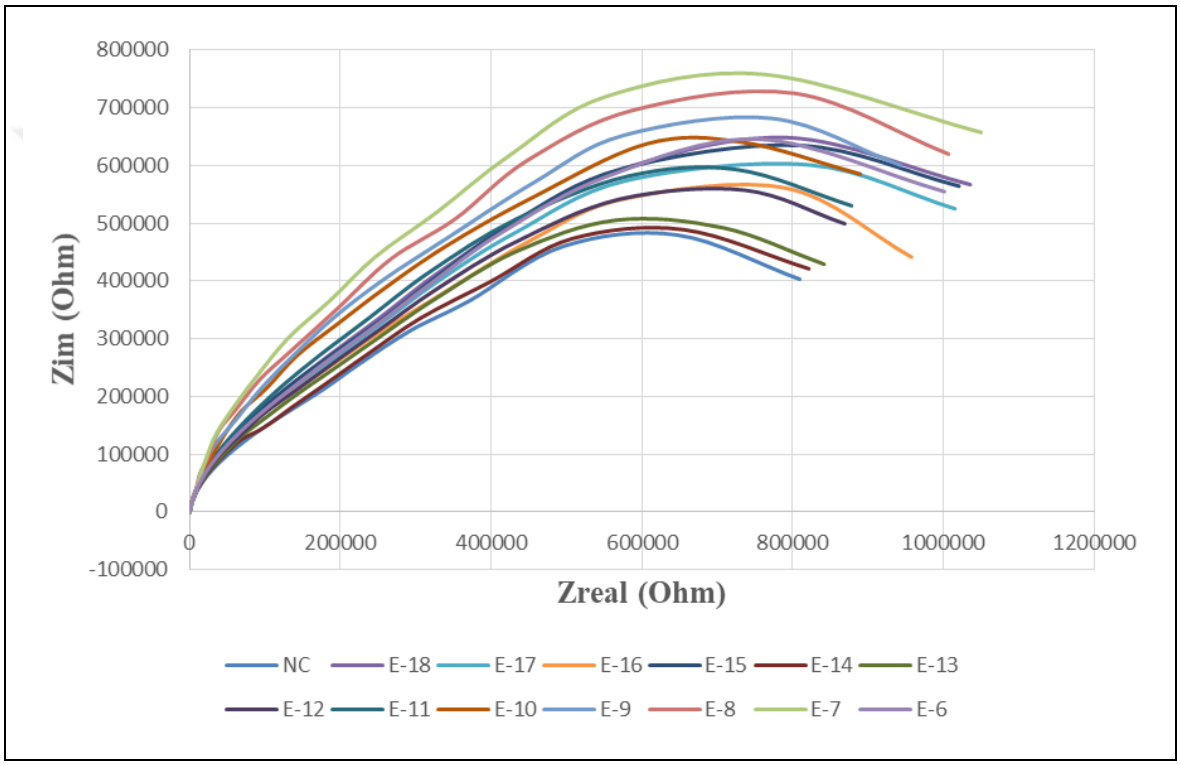

Figure 3.56. EIS response of Au-0.275M-Val-MIP electrode.

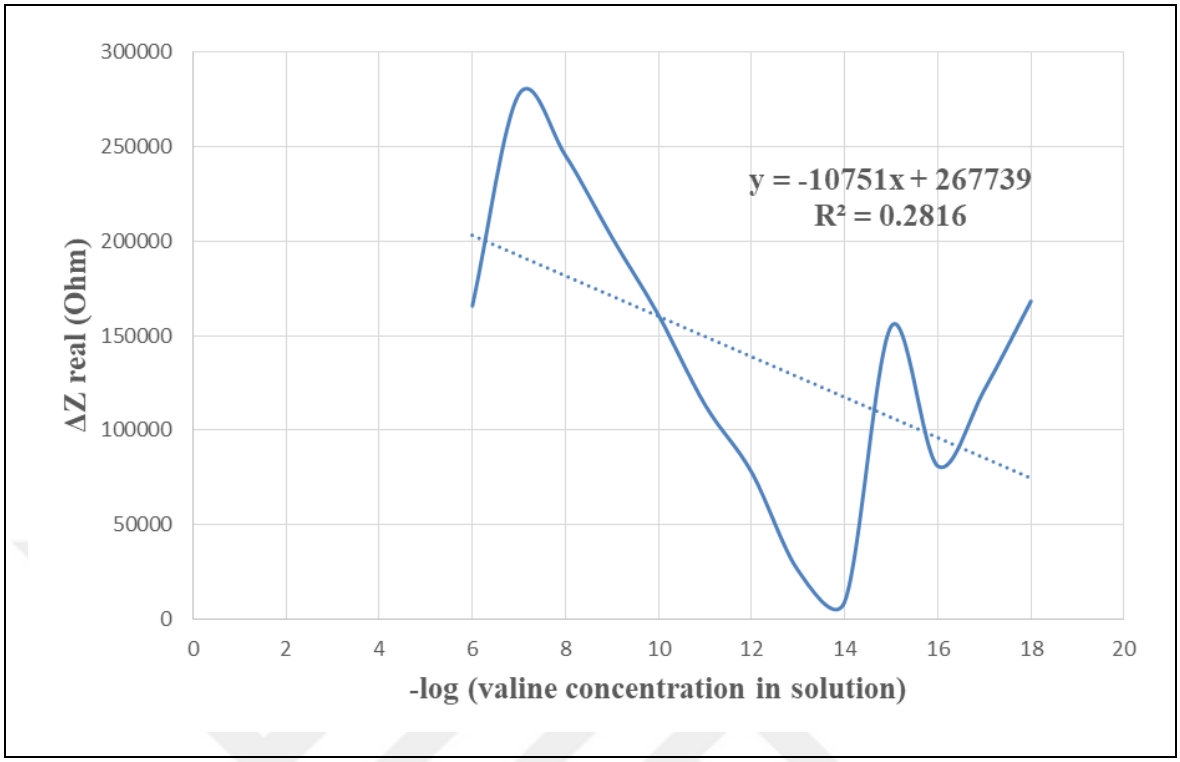

Figure 3.57. The regression curve of Au-0.275M-Val-MIP electrode.

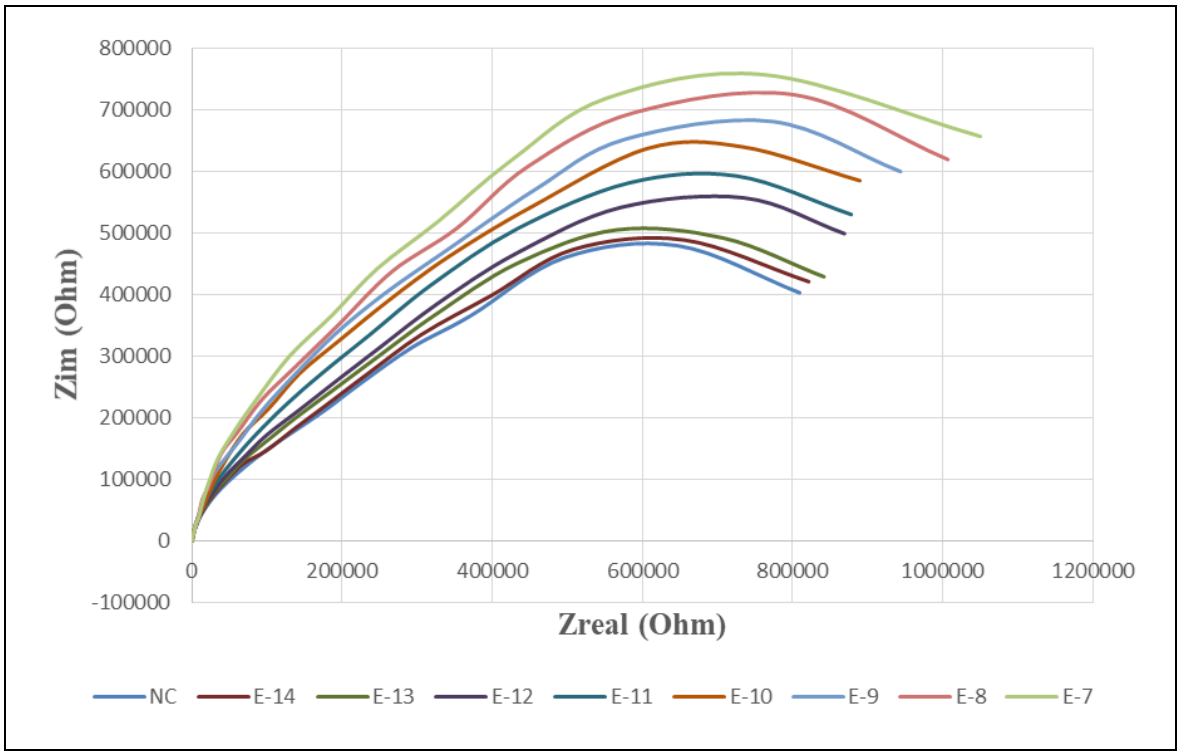

Figure 3.58. EIS response of Au-0.275M-Val-MIP electrode.

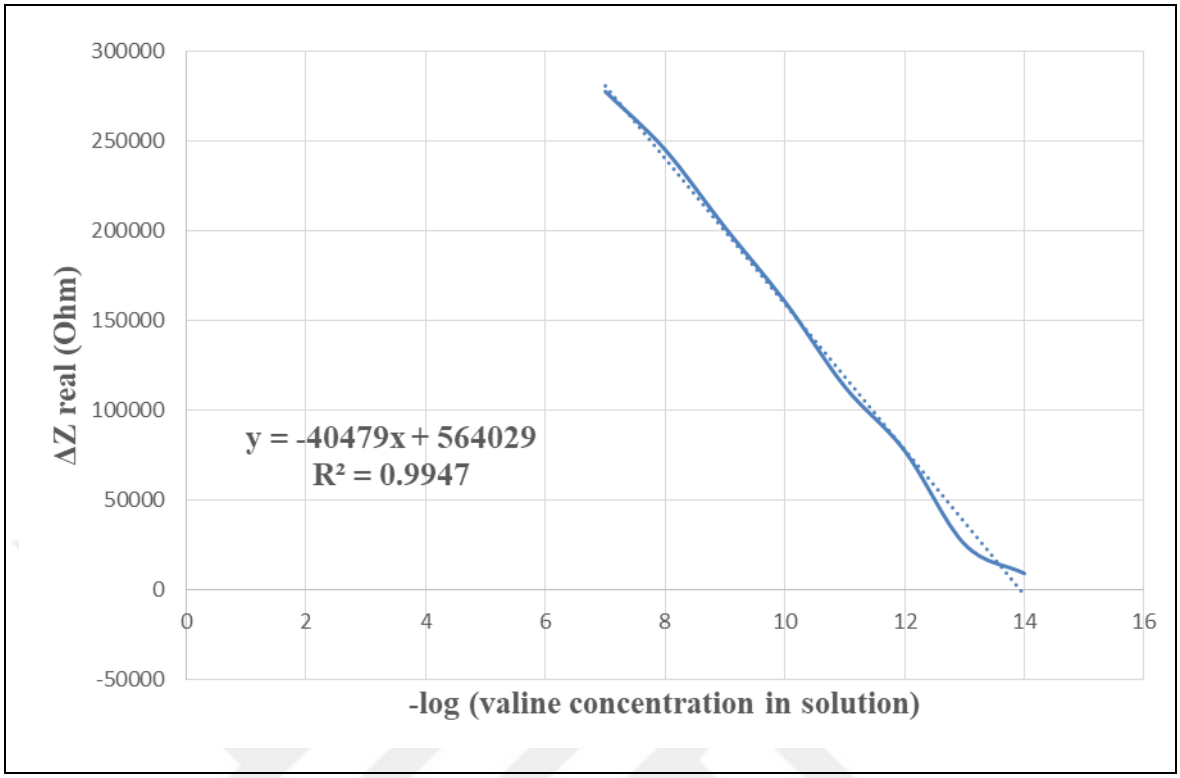

Figure 3.59. The regression curve of Au-0.275M-Val-MIP electrode.

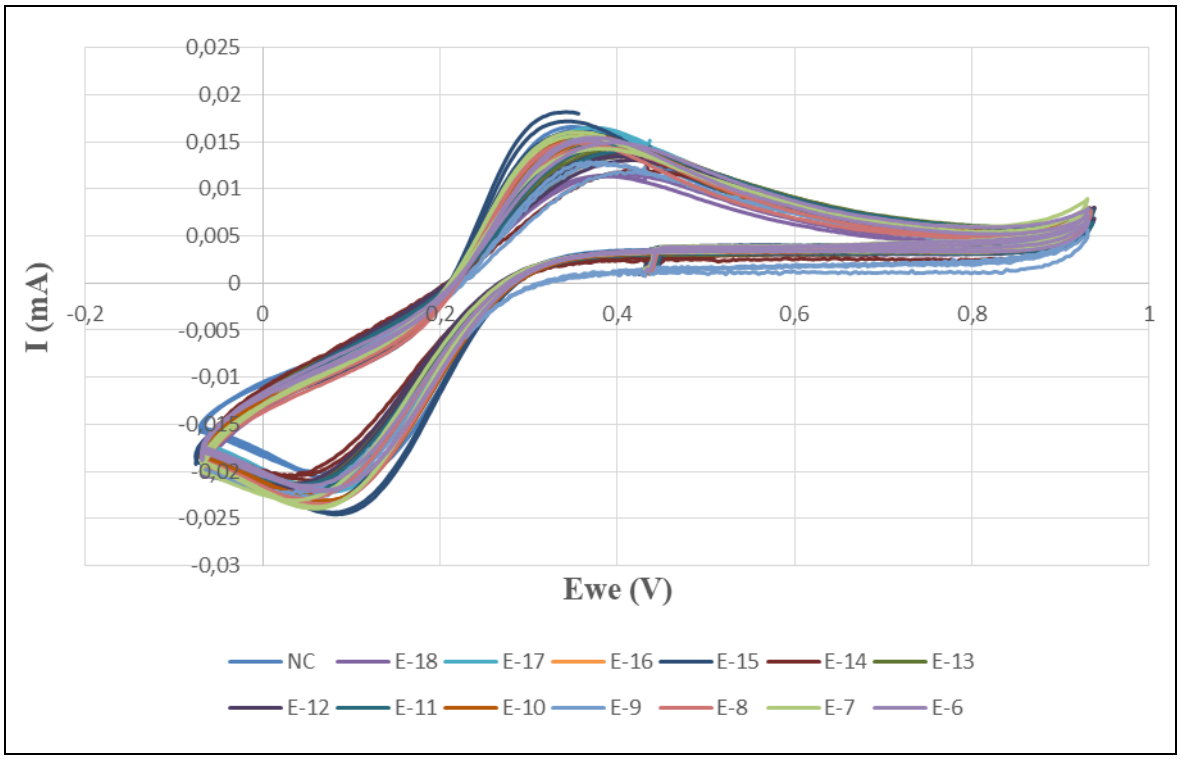

Figure 3.60. CV response of Au-0.275M-Val-MIP electrode.

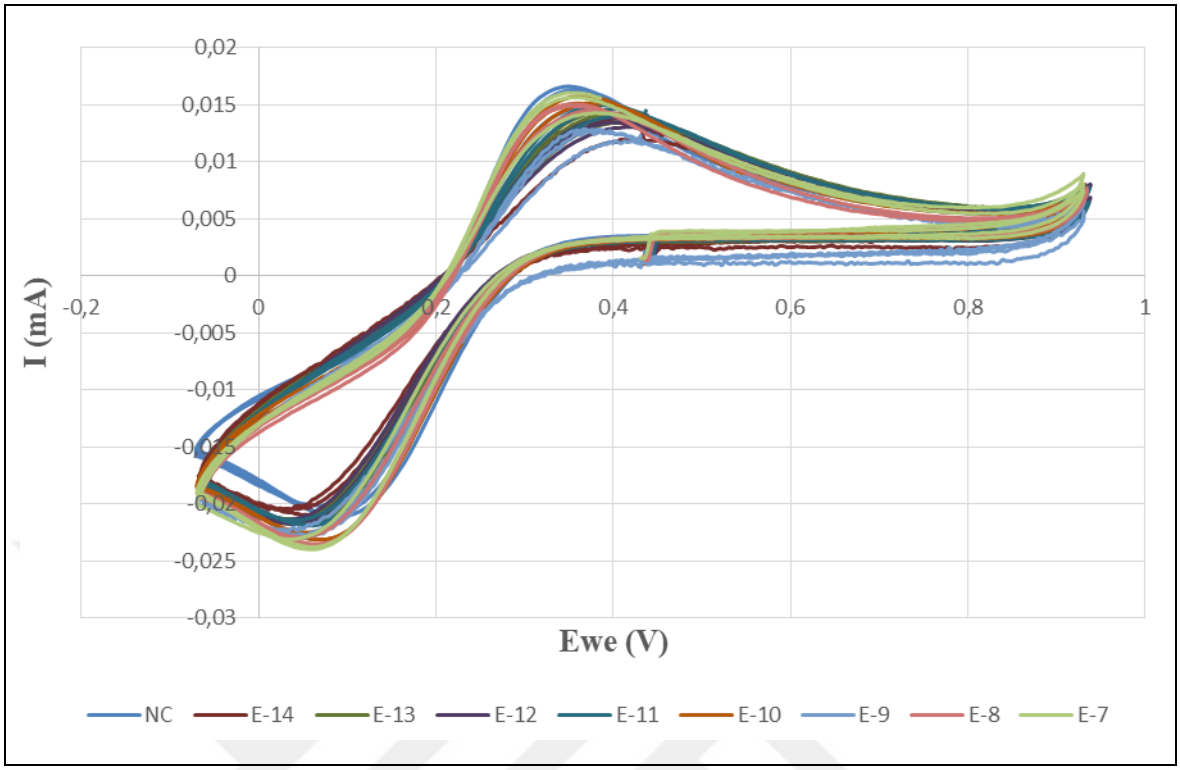

Figure 3.61. CV response of Au-0.275M-Val-MIP electrode.

Au-0.3M-Val-MIP electrode can detect valine molecules with 95.09 percent success (Figure 3.63) between concentrations of E-18 M and E-6 M valine (Figure 3.62). According to the regression curve (Figure 3.65), the Au-0.3M-Val-MIP electrode could detect the range of valine concentrations of E-15 and E-6 M with a success rate of 99.25 percent (Figure 3.64). Figure 3.67 shows that the anodic currents and cell potential remain constant while cathodic currents increase as the concentration of valine increases. The conductivity of the solution increases as the concentration of valine increases, and thus the current increases.

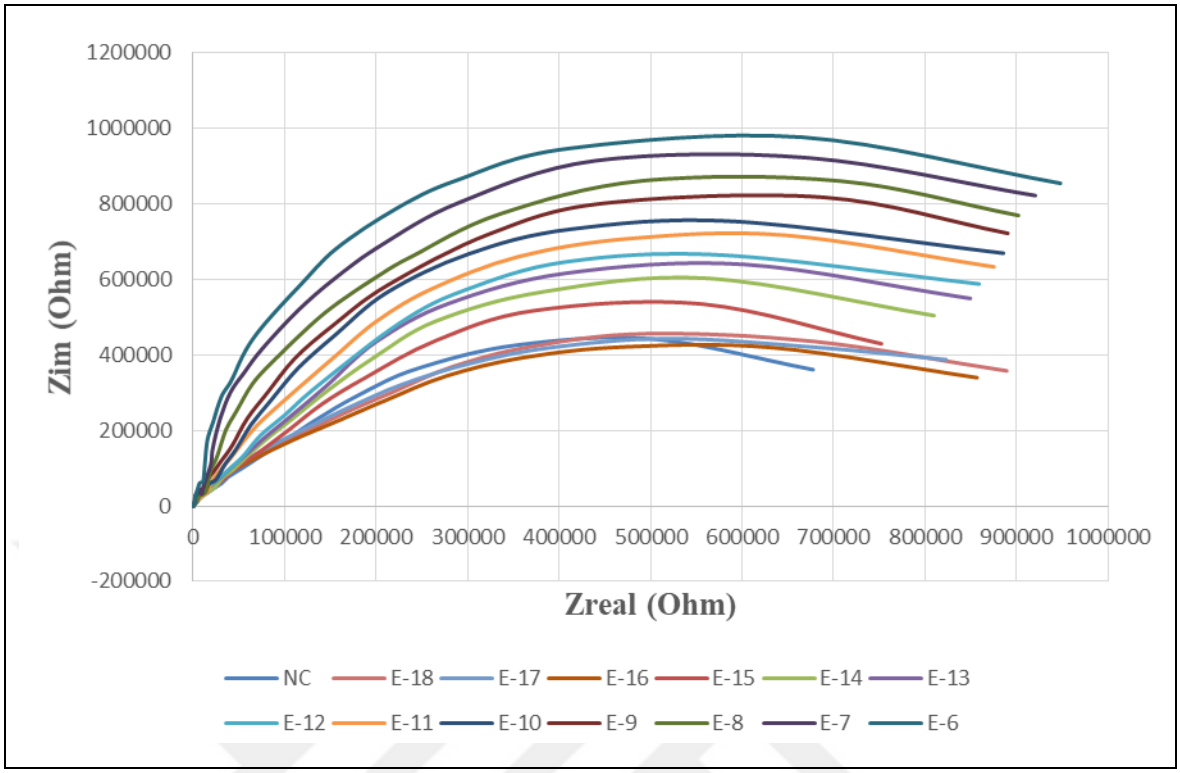

Figure 3.62. EIS response of Au-0.3M-Val-MIP electrode.

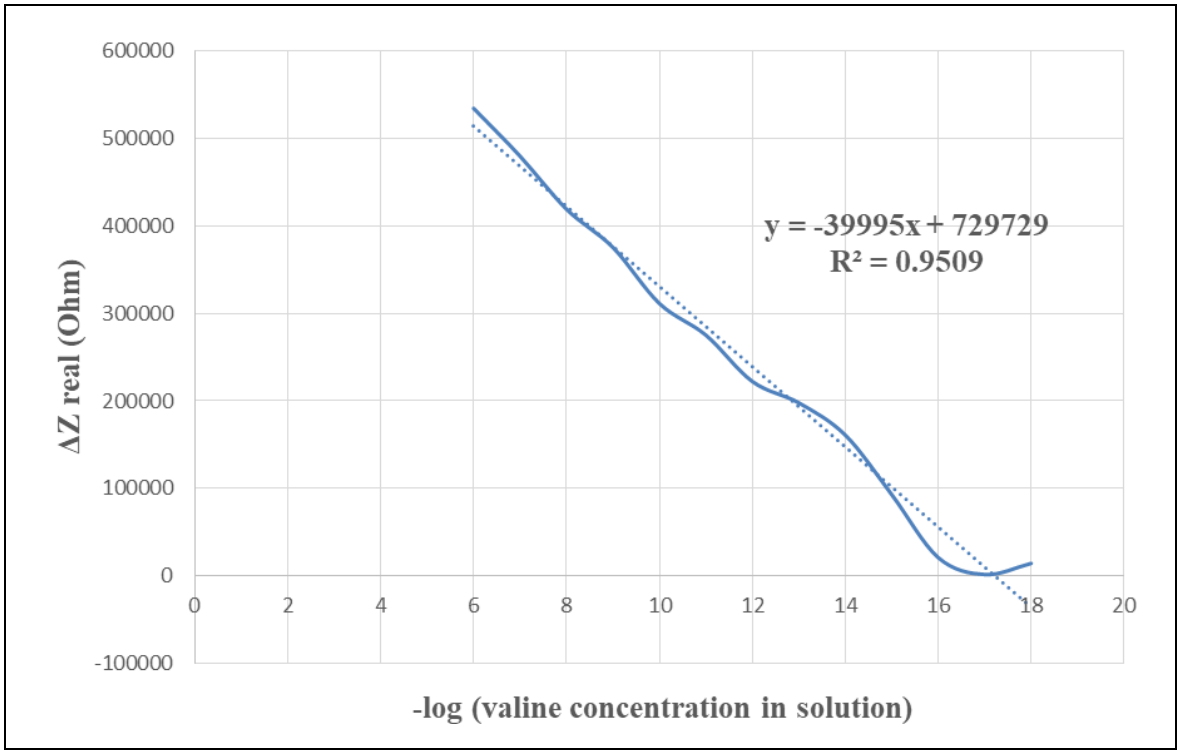

Figure 3.63. The regression curve of Au-0.3M-Val-MIP electrode.

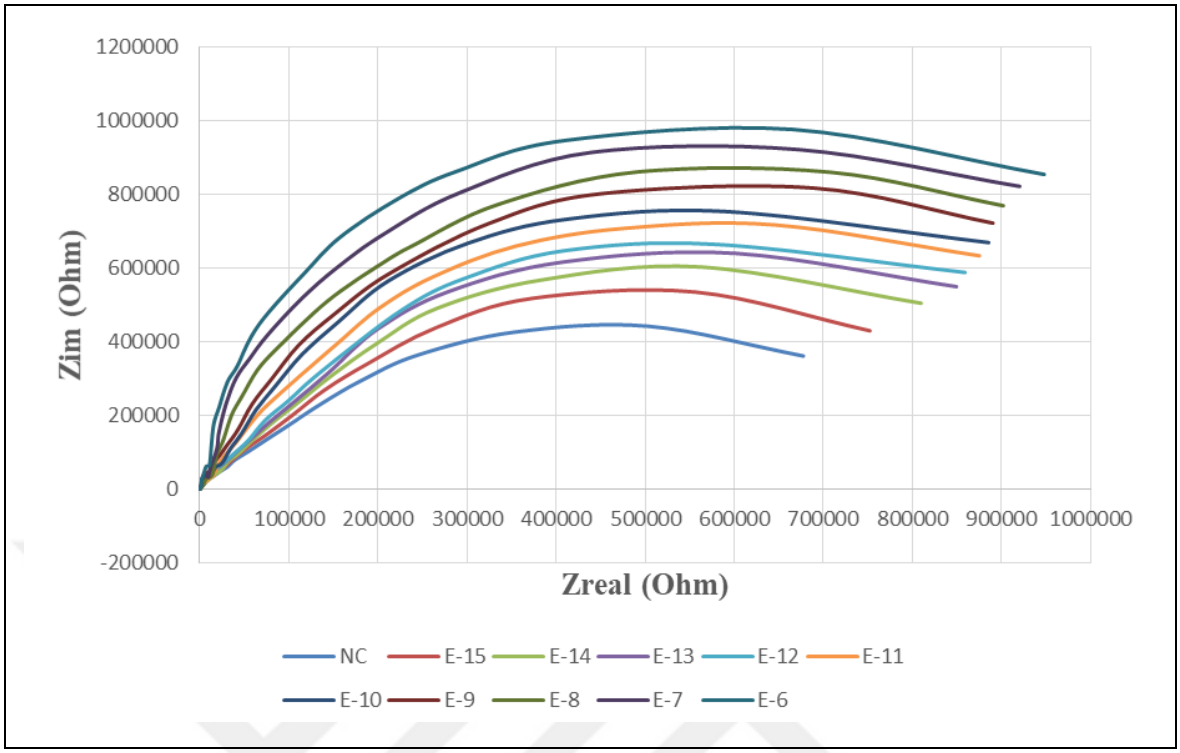

Figure 3.64. EIS response of Au-0.3M-Val-MIP electrode.

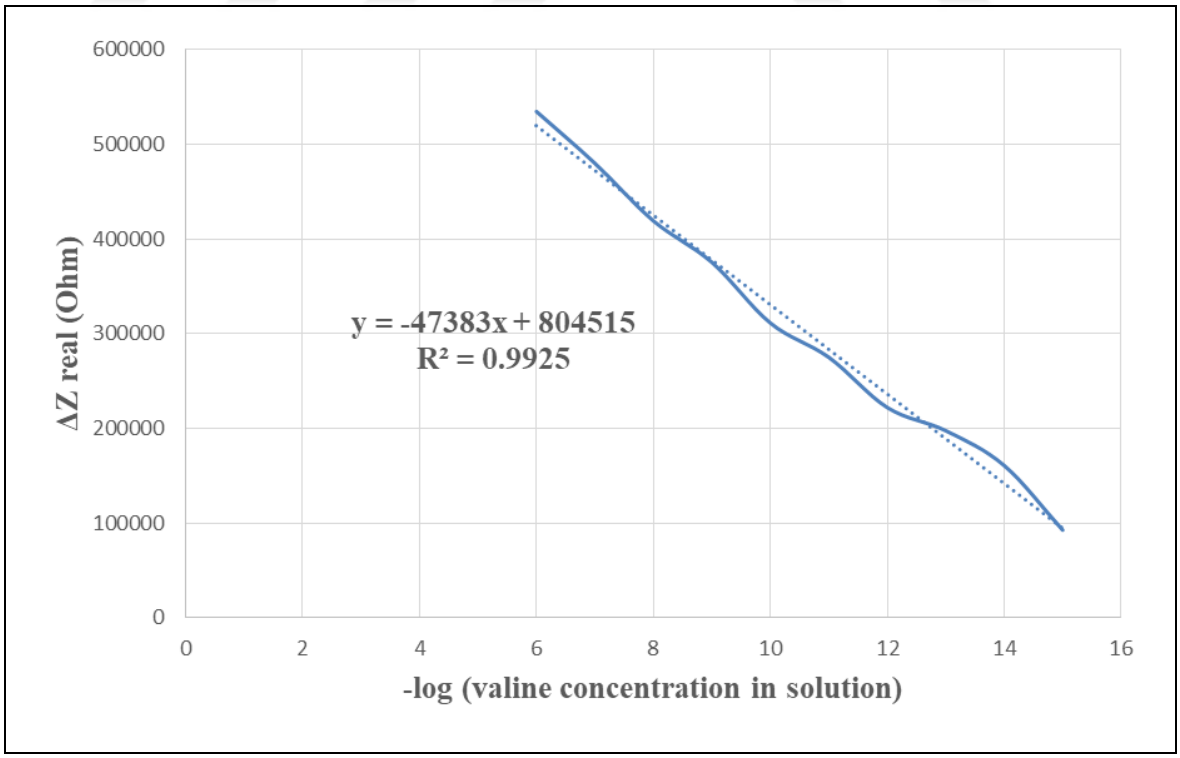

Figure 3.65. The regression curve of Au-0.3 M-Val-MIP electrode.

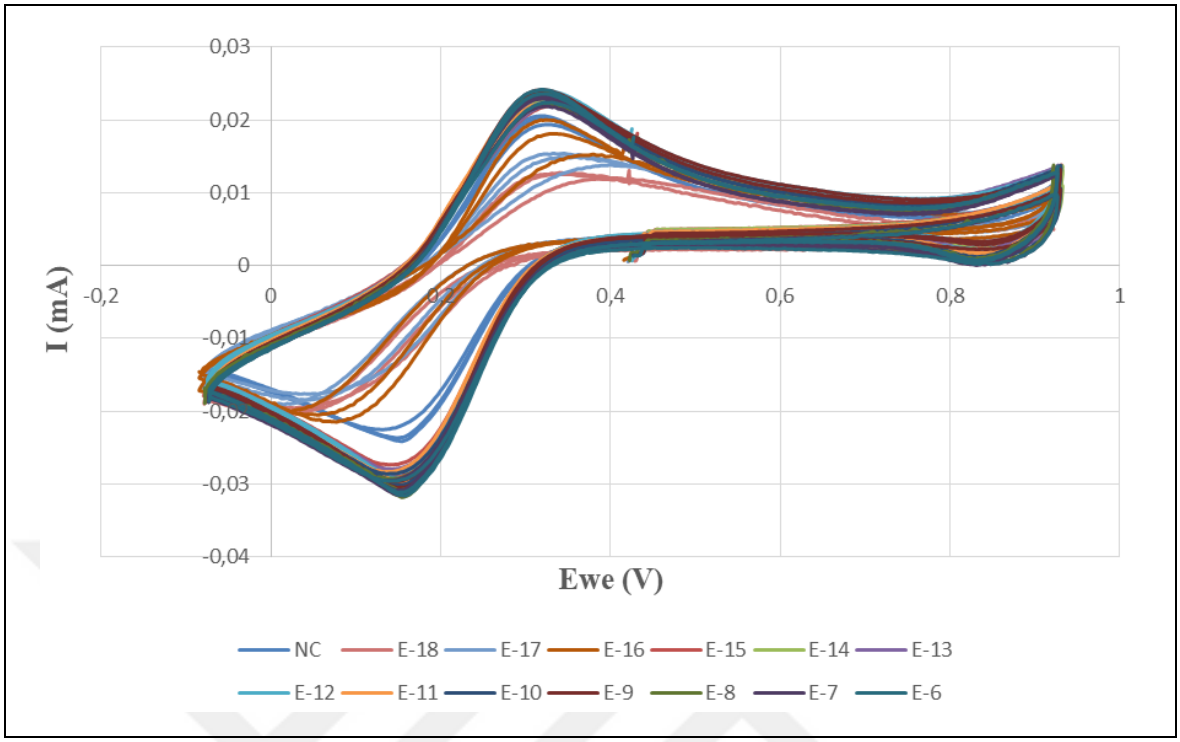

Figure 3.66. CV response of Au-0.3M-Val-MIP electrode.

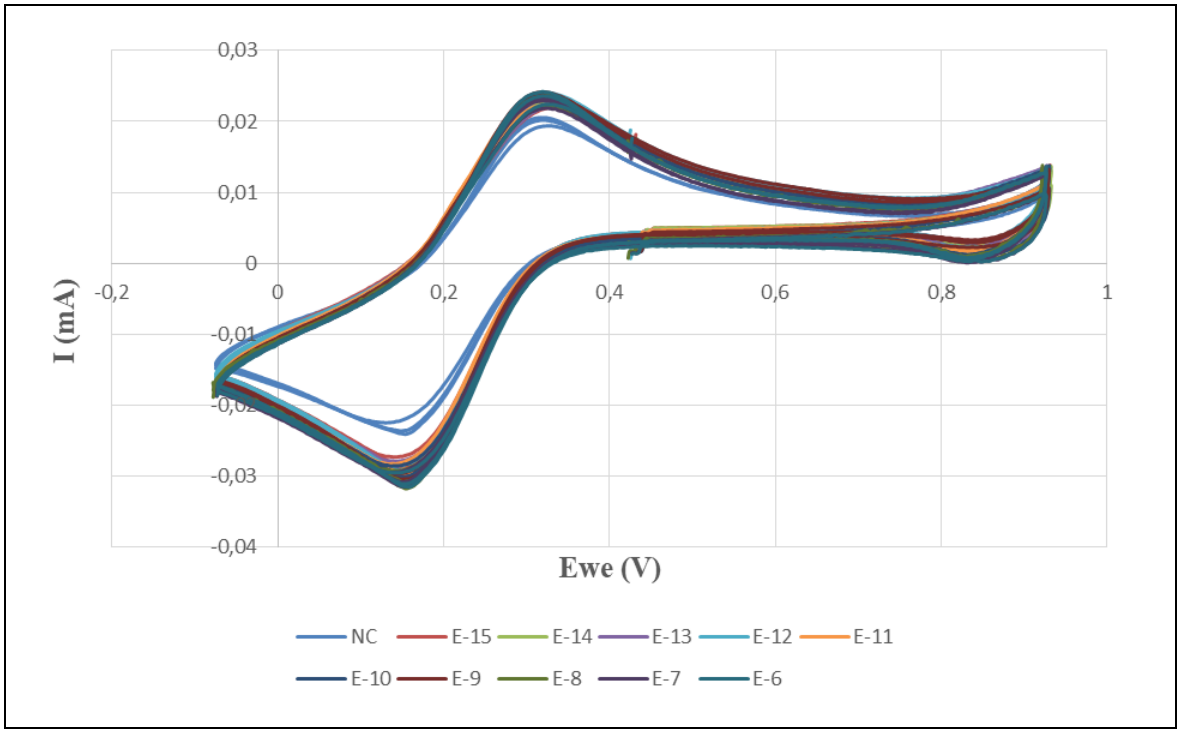

Figure 3.67. CV response of Au-0.3M-Val-MIP electrode.

Au-0.325M-Val-MIP electrode can detect valine molecules with 11.02 percent success (Figure 3.69) between concentrations of E-18 M and E-6 M valine (Figure 3.68). According to the regression curve (Figure 3.71), the Au-0.325M-Val-MIP electrode could detect the range of valine concentrations of E-14 M and E-6 M with a success rate of 97.97 percent (Figure 3.70). Anodic currents and cathodic currents data do not show a certain increase or decrease depending on the concentration (Figure 3.73).

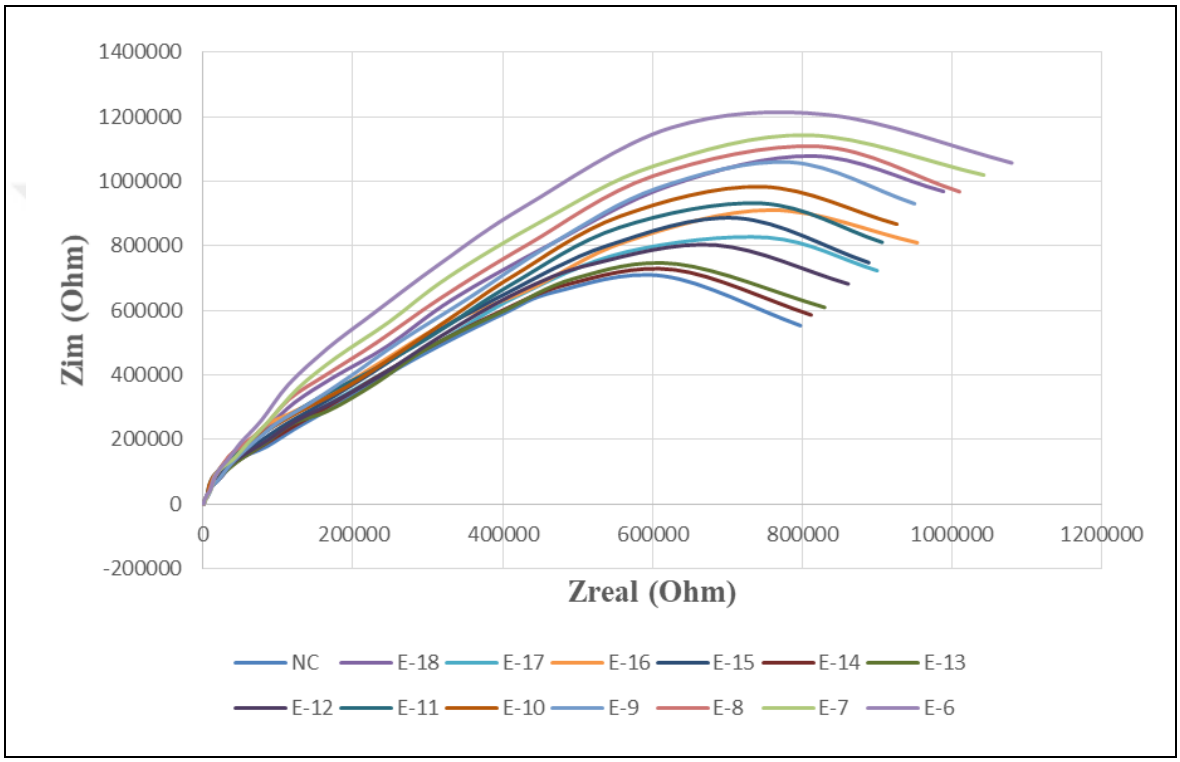

Figure 3.68. EIS response of Au-0.325M-Val-MIP electrode.

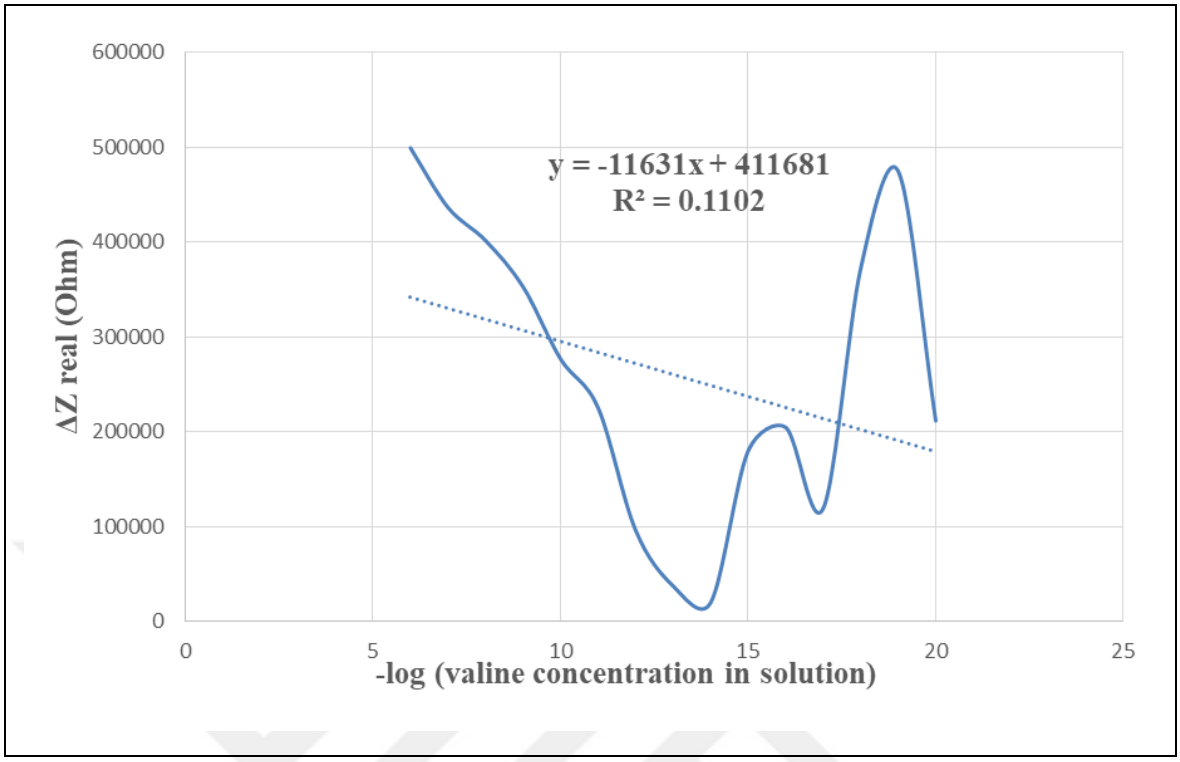

Figure 3.69. The regression curve of Au-0.325M-Val-MIP electrode.

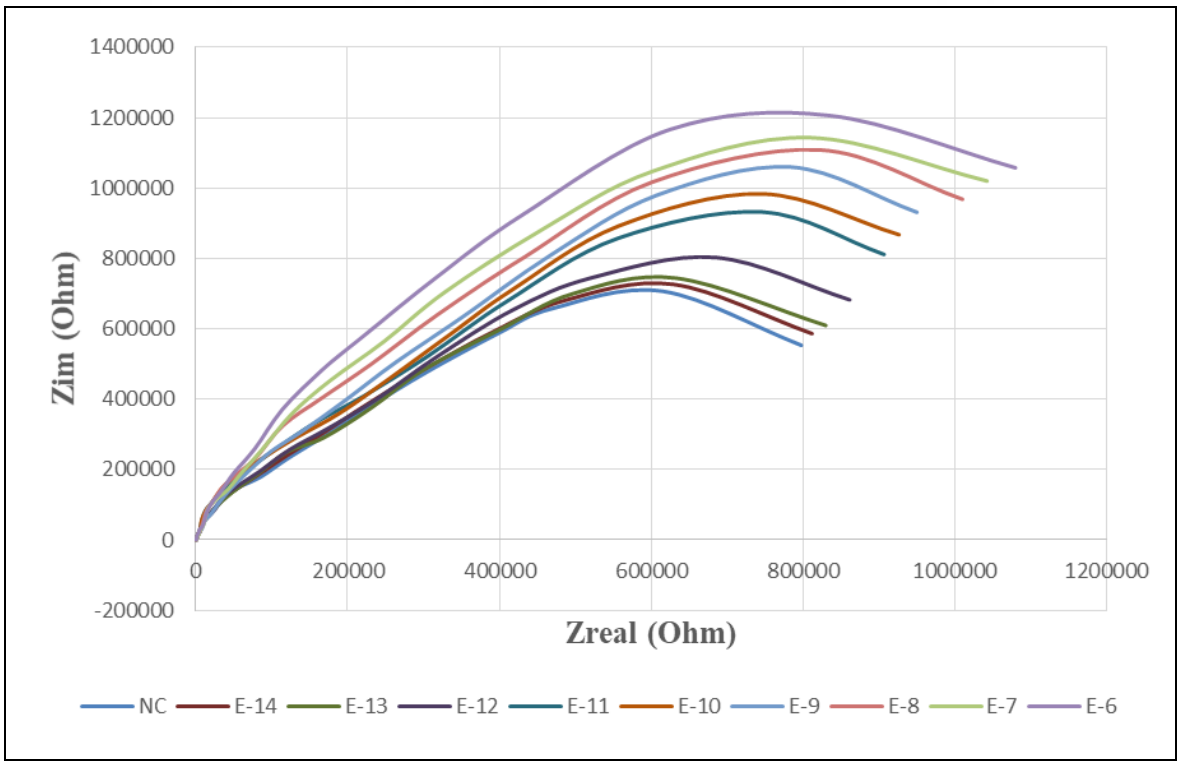

Figure 3.70. EIS response of Au-0.325M-Val-MIP electrode.

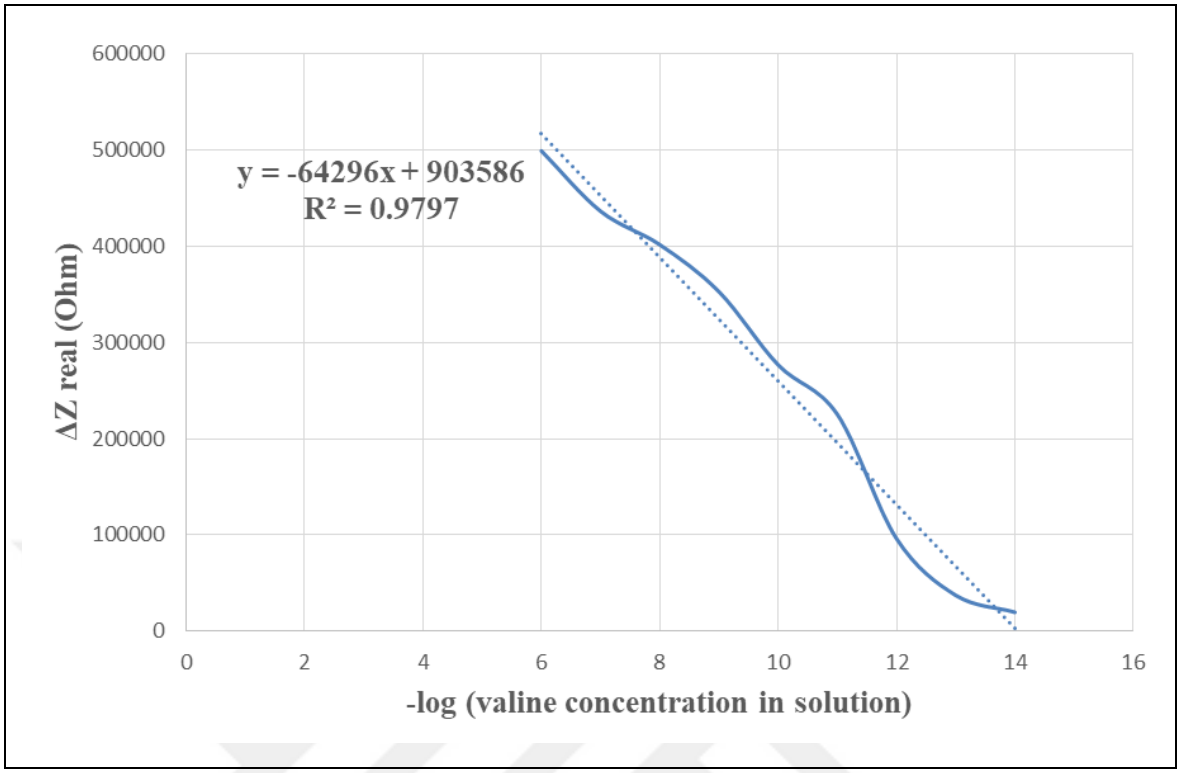

Figure 3.71. The regression curve of Au-0.325M-Val-MIP electrode.

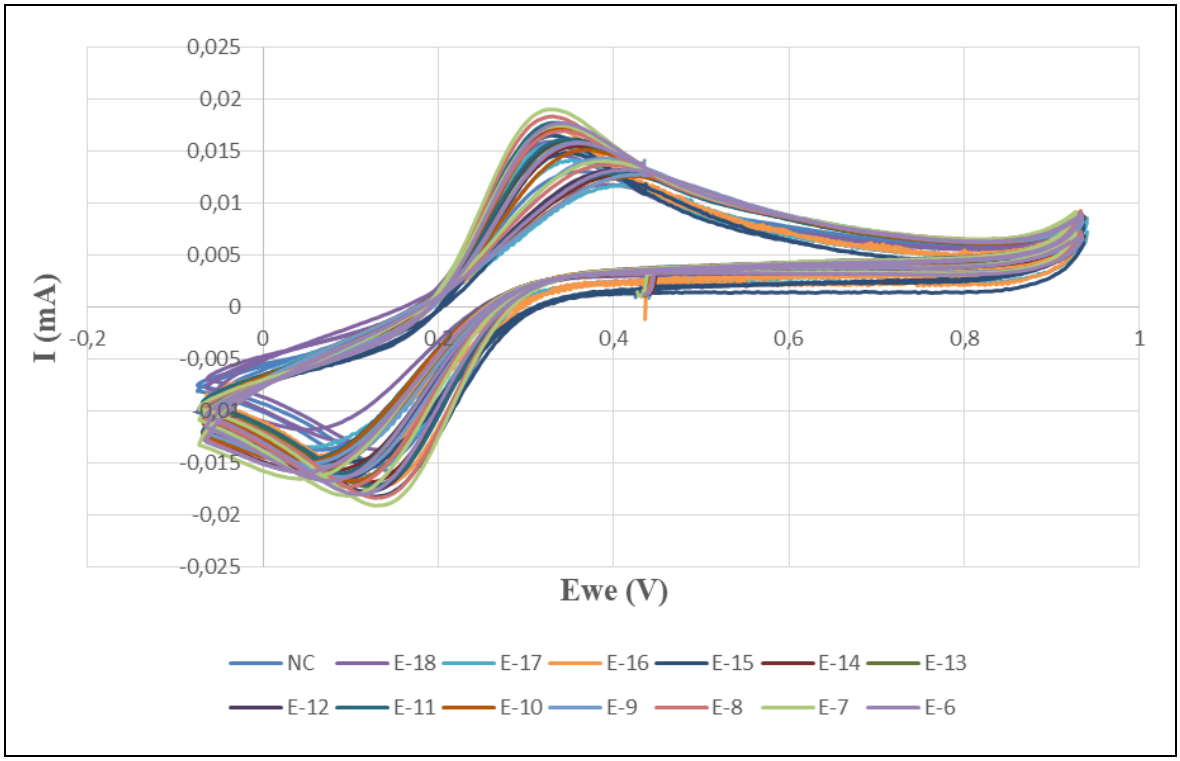

Figure 3.72. CV response of Au-0.325M-Val-MIP electrode.

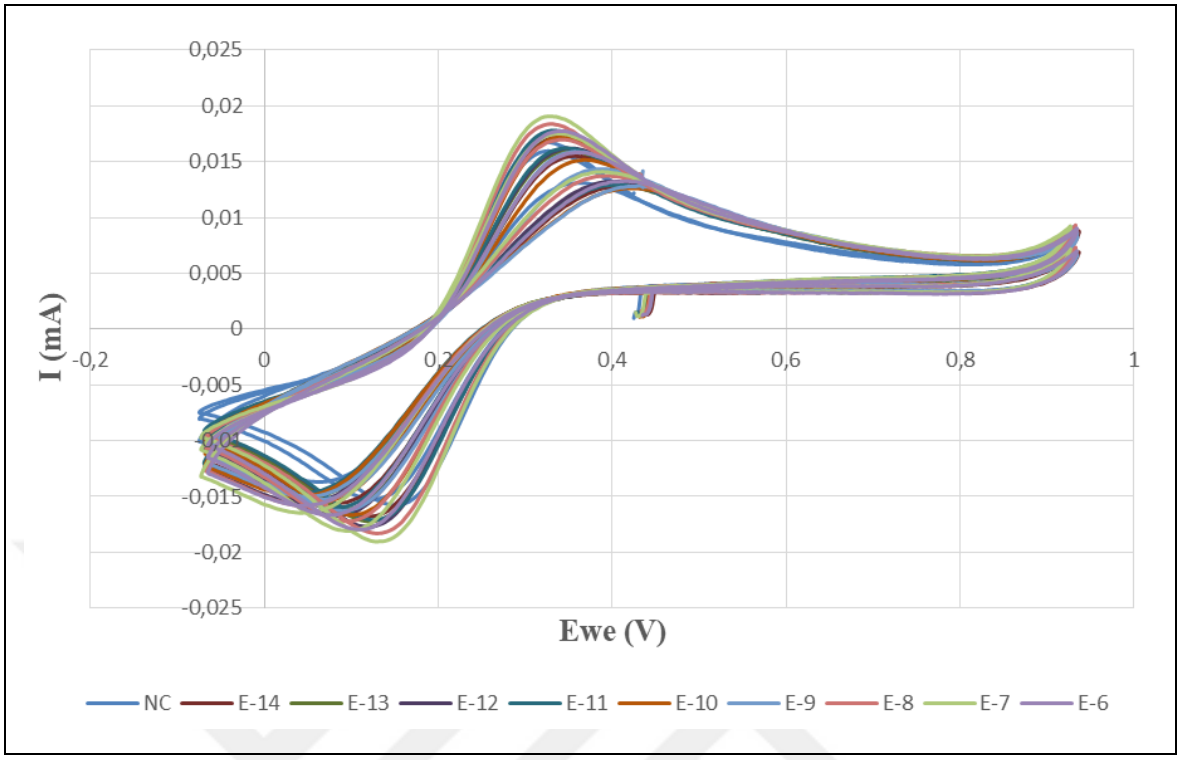

Figure 3.73. CV response of Au-0.325M-Val-MIP electrode.

Au-0.35M-Val-MIP electrode can detect valine molecules with 47.45 percent success (Figure 3.75) between concentrations of E-18 M and E-6 M valine (Figure 3.74). The regression curve (Figure 3.77) indicates that Au-0.35M-Val-MIP electrode could detect the range of valine concentrations of E-14 M and E-7 M with a success rate of 98.8 percent (Figure 3.76). As shown in Figure 3.79, anodic currents and cathodic currents data do not show a certain increase or decrease depending on the concentration.

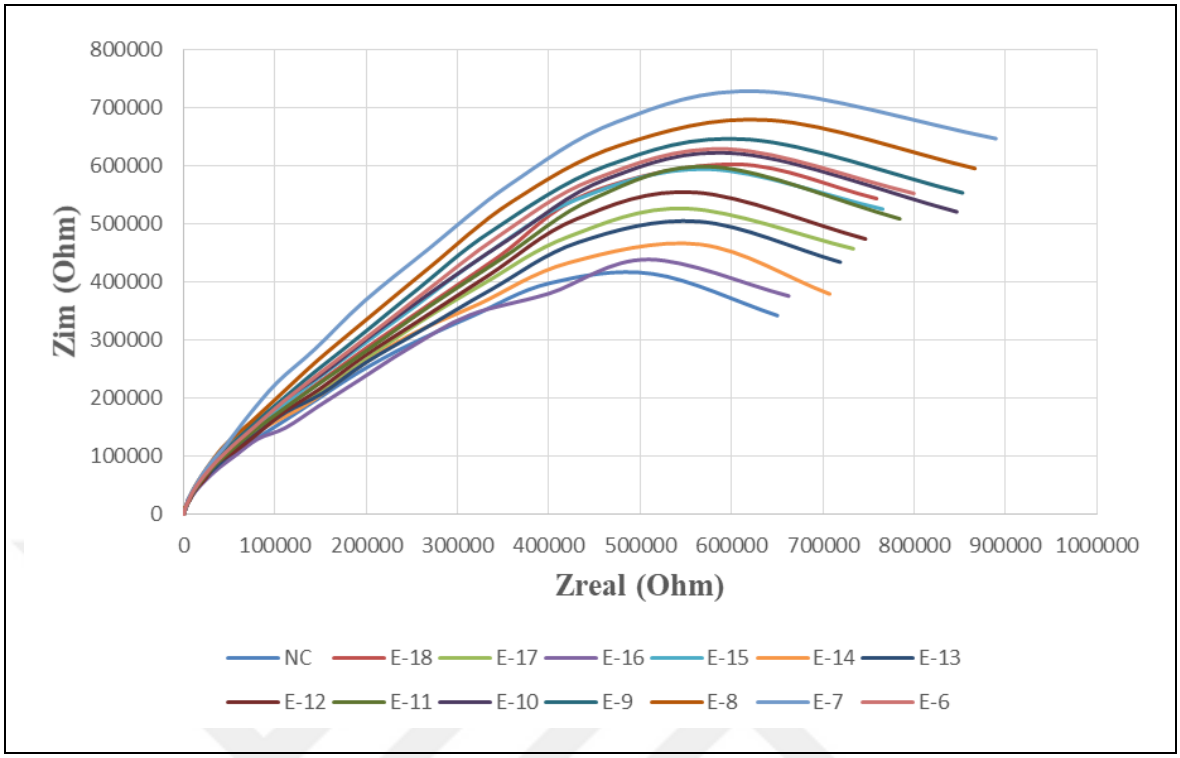

Figure 3.74. EIS response of Au-0.35M-Val-MIP electrode.

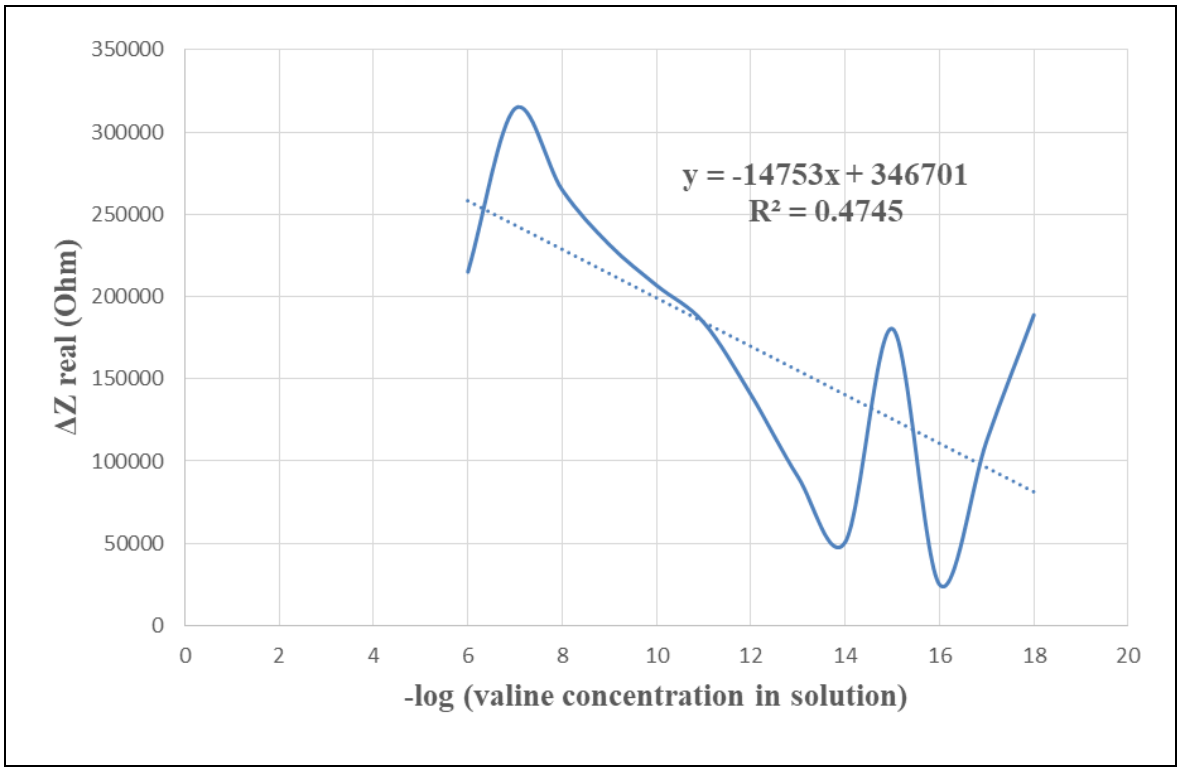

Figure 3.75. The regression curve of Au-0.35M-Val-MIP electrode.

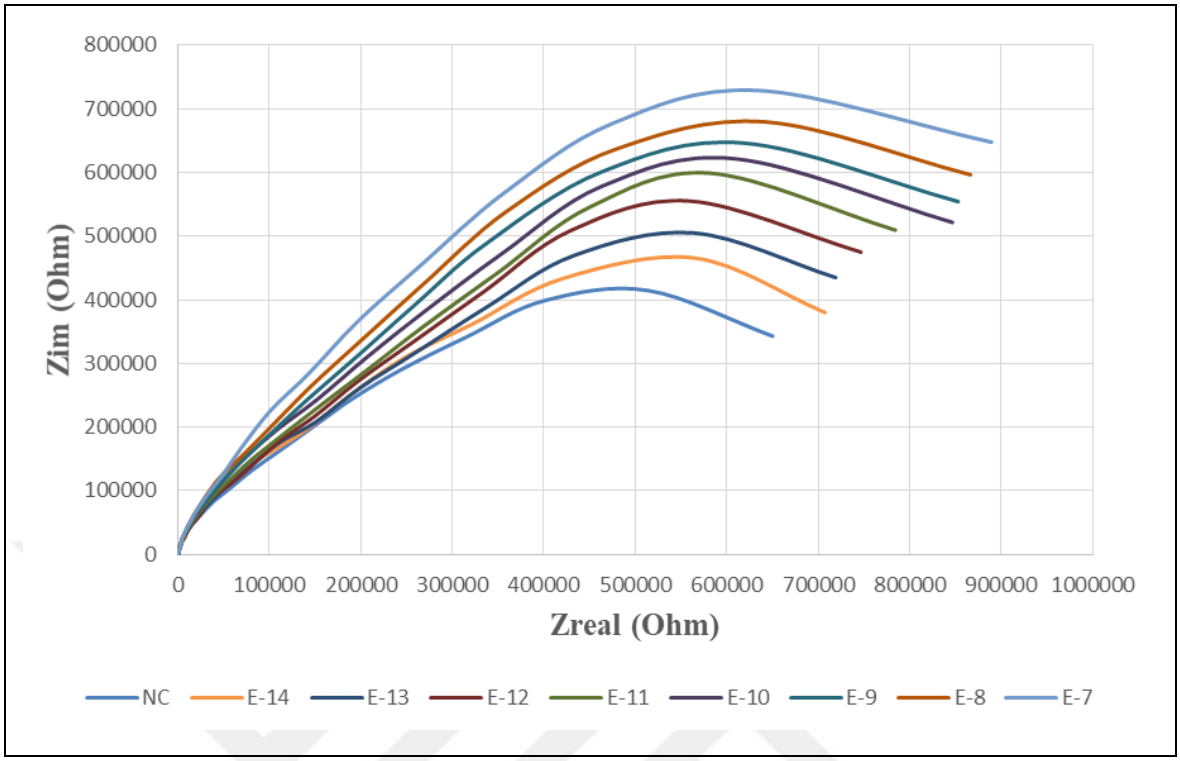

Figure 3.76. EIS response of Au-0.35M-Val-MIP electrode.

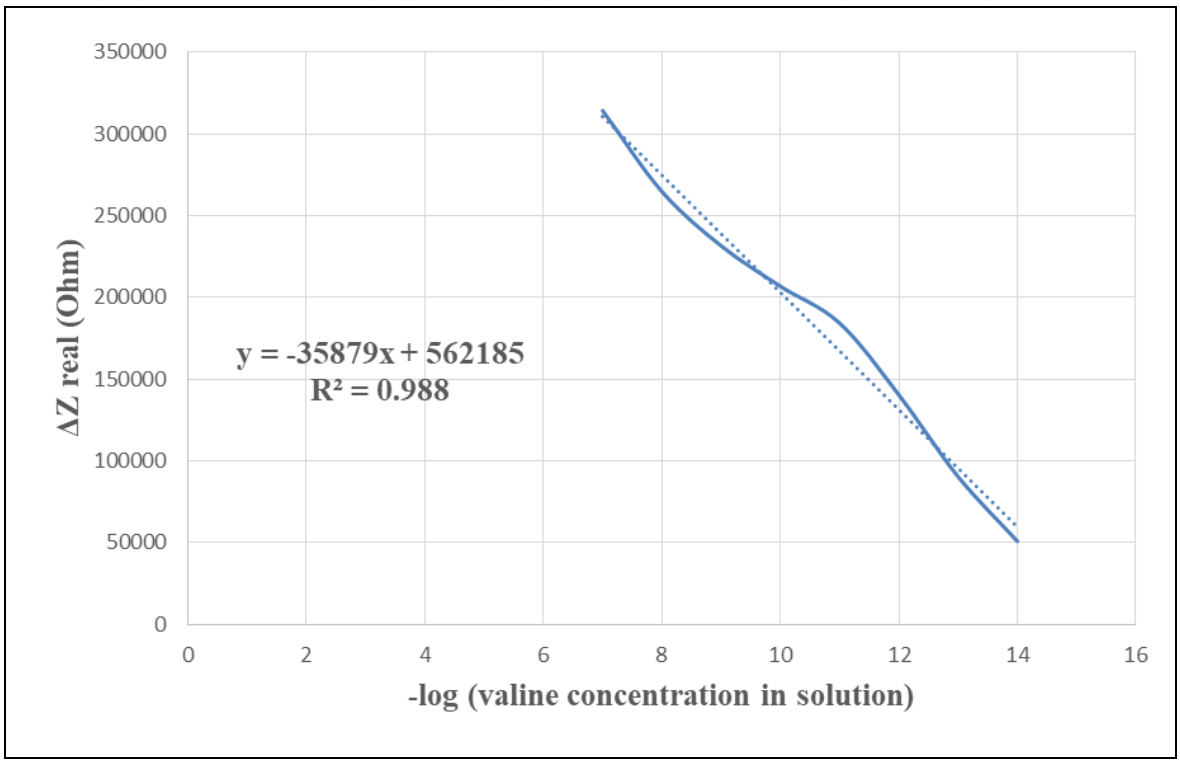

Figure 3.77. The regression curve of Au-0.35M-Val-MIP electrode.

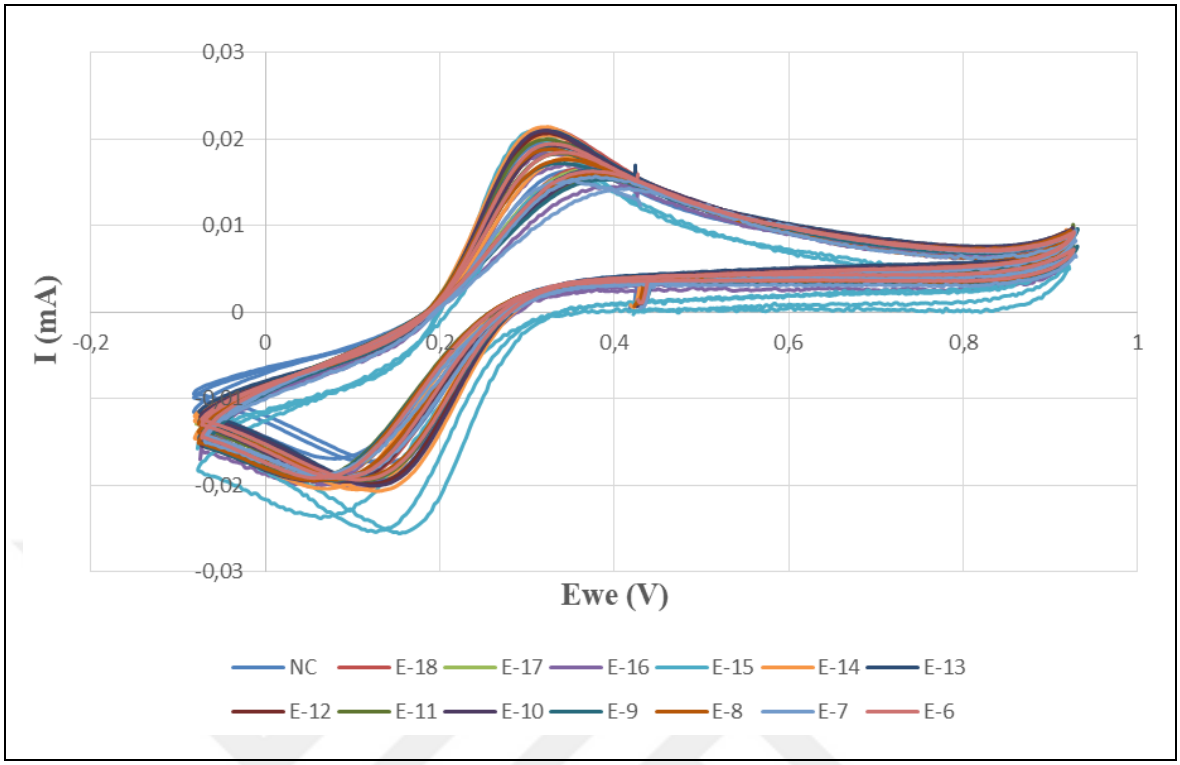

Figure 3.78. CV response of Au-0.35M-Val-MIP electrode.

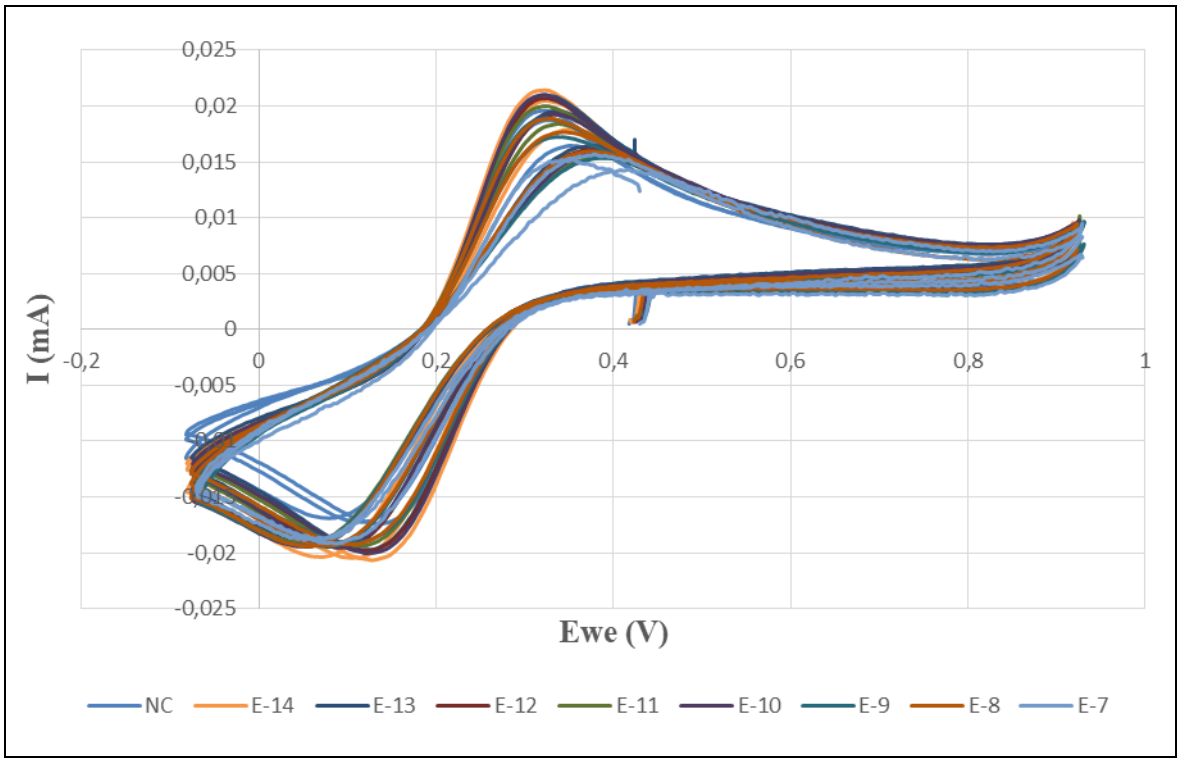

Figure 3.79. CV response of Au-0.35M-Val-MIP electrode.

Au-0.4M-Val-MIP electrode can detect valine molecules with 58.19 percent success (Figure 3.81) between concentrations of E-18 M and E-6 M valine (Figure 3.80). The regression curve (Figure 3.83) of Au-0.4M-Val-MIP electrode indicates detection of E-14 M and E-7 M valine with a success rate of 94.82 percent (Figure 3.82). As shown in Figure 3.85, while cathodic currents increase, anodic currents data does not show a certain increase or decrease depending on the concentration.

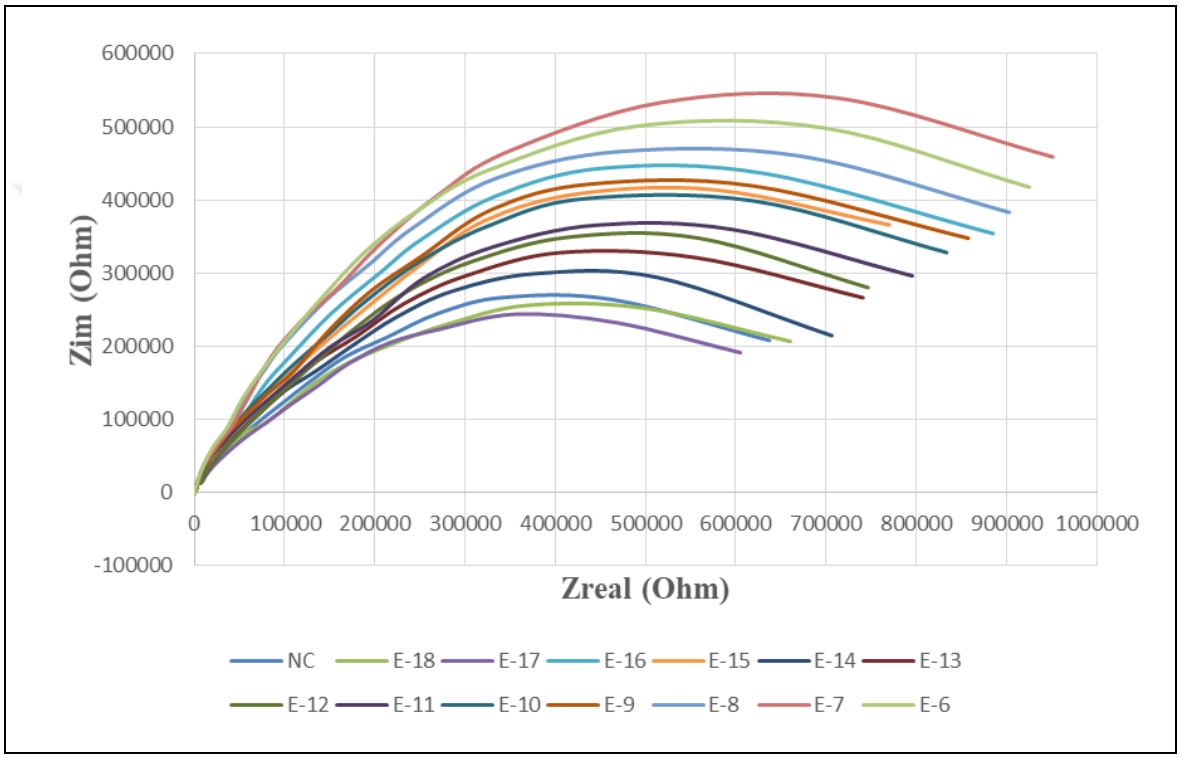

Figure 3.80. EIS response of Au-0.4M-Val-MIP electrode.

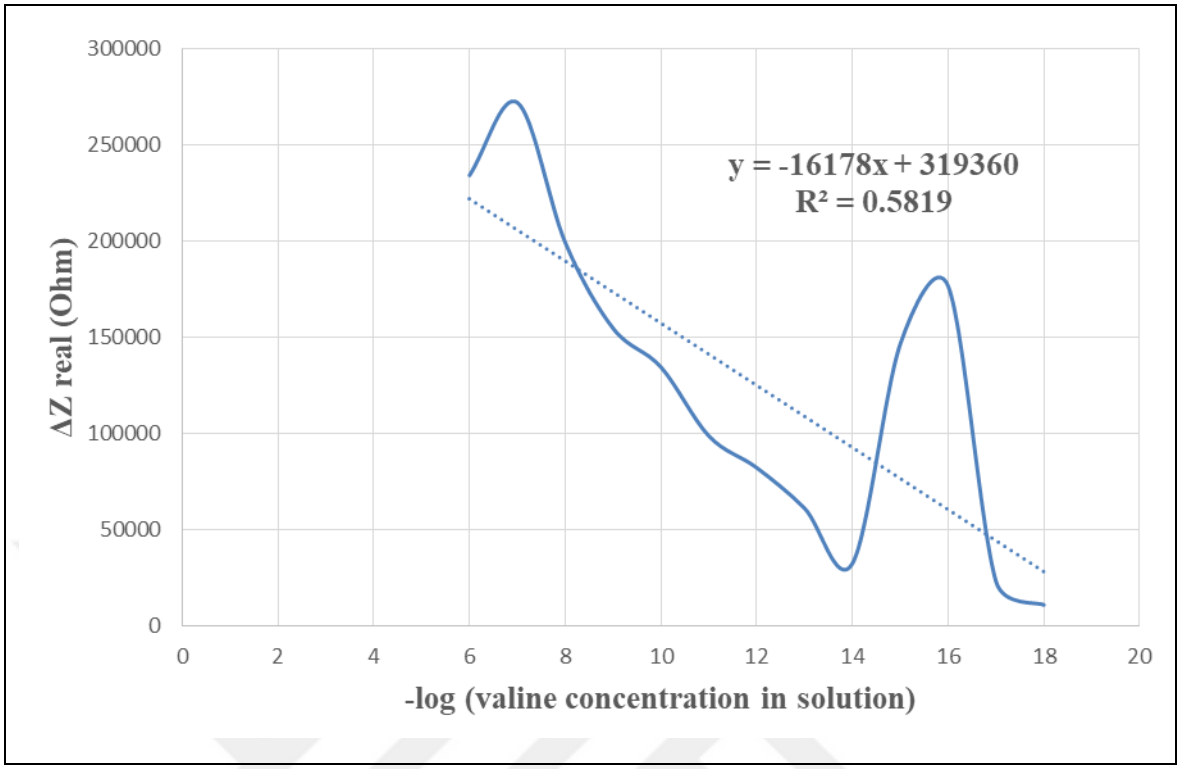

Figure 3.81. The regression curve of Au-0.4M-Val-MIP electrode.

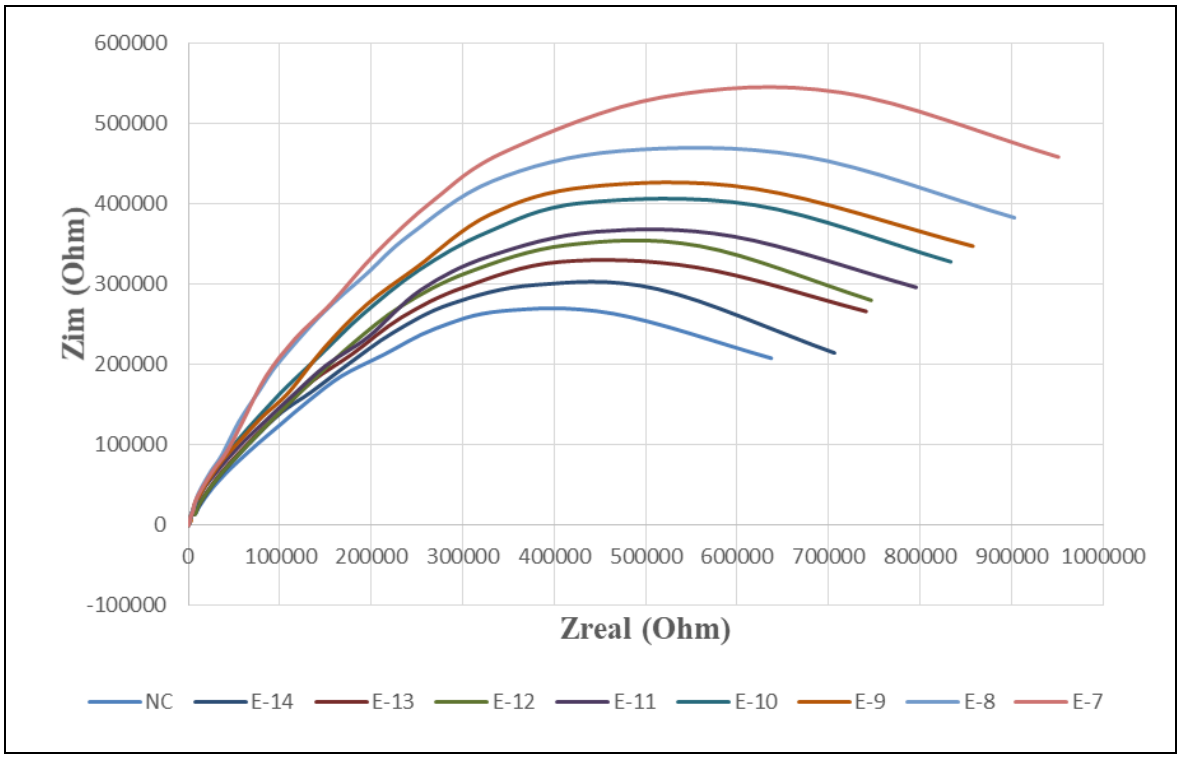

Figure 3.82. EIS response of Au-0.4M-Val-MIP electrode.

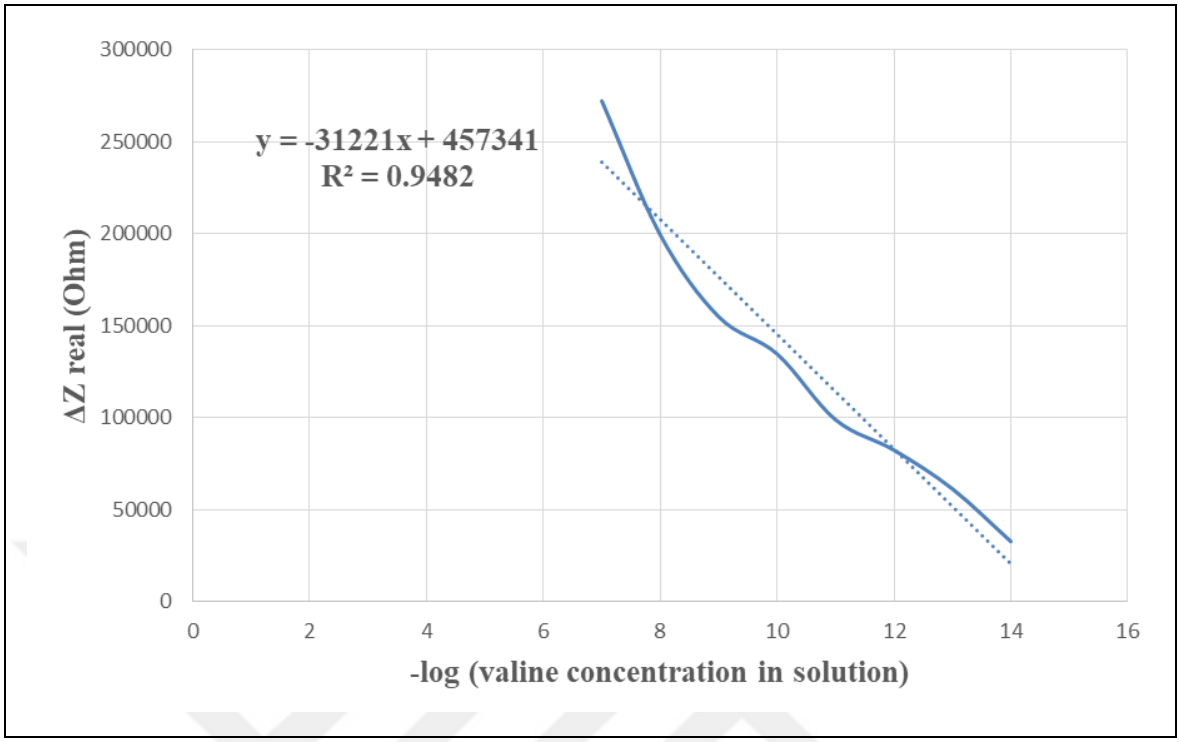

Figure 3.83. The regression curve of Au-0.4M-Val-MIP electrode.

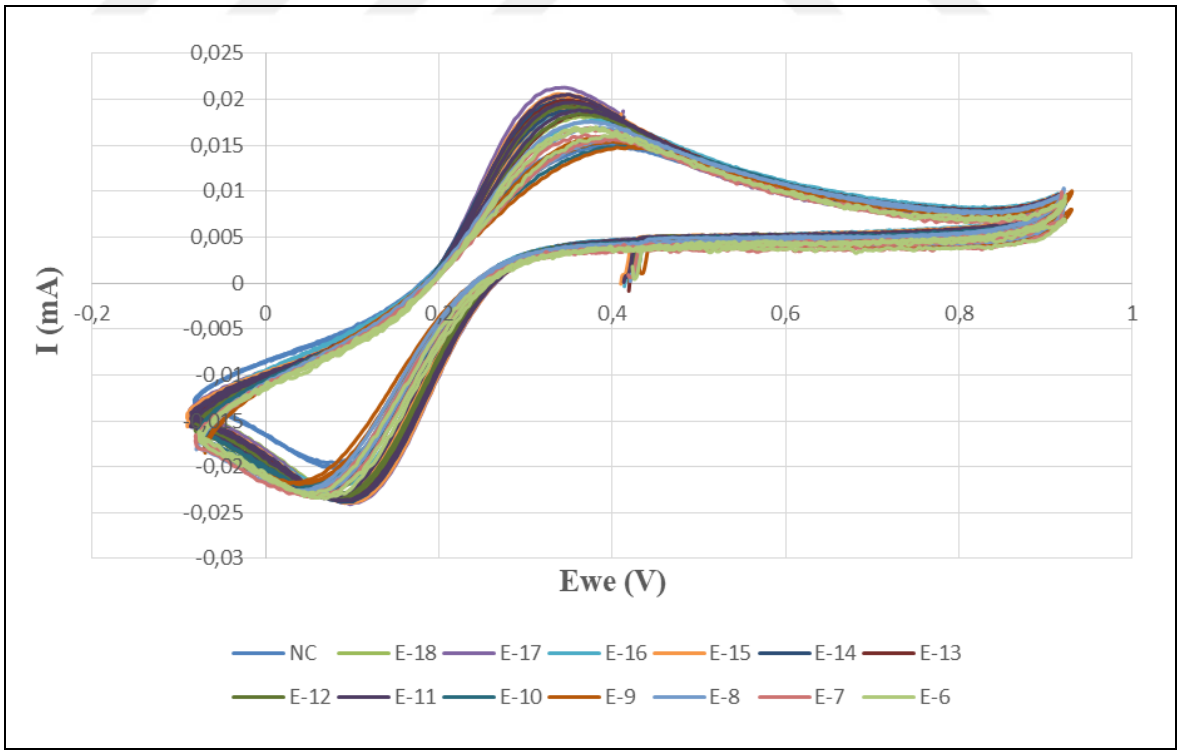

Figure 3.84. CV response of Au-0.4M-Val-MIP electrode.

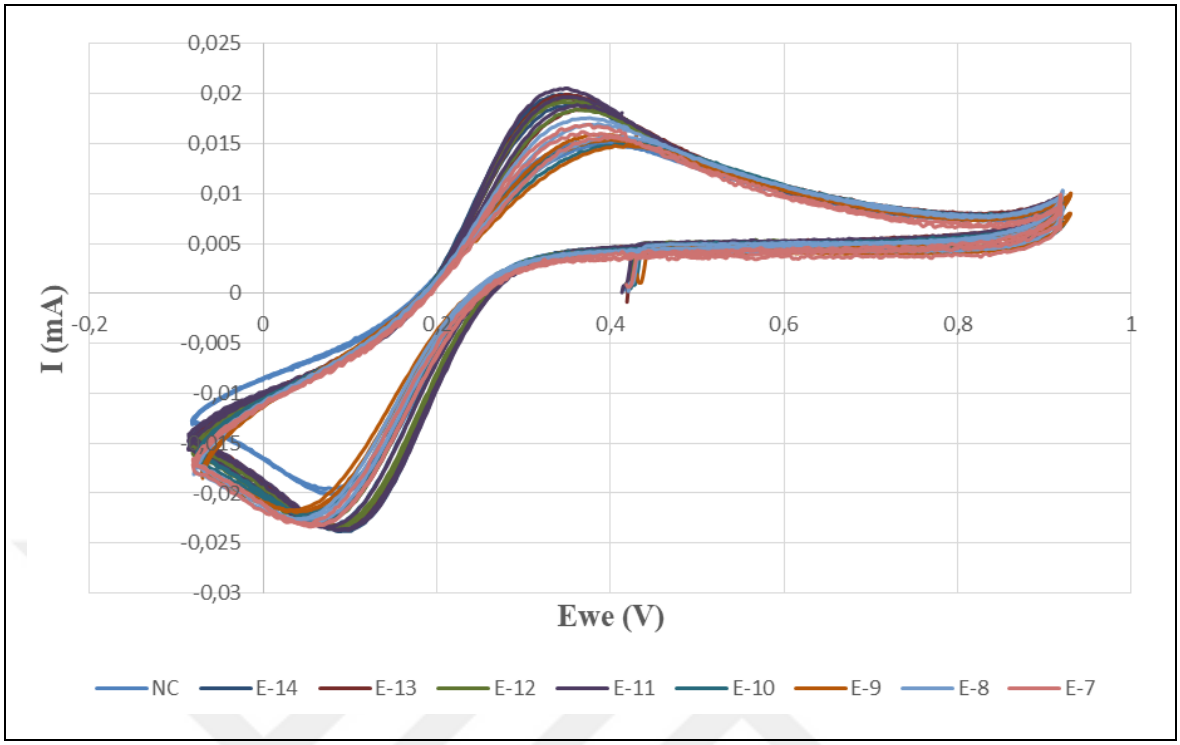

Figure 3.85. CV response of Au-0.4M-Val-MIP electrode.

Au-0.45M-Val-MIP electrode can detect valine molecules with 35.25 percent success (Figure 3.87) between concentrations of E-18 M and E-6 M valine (Figure 3.86). According to the regression curve (Figure 3.89), the Au-0.4M-Val-MIP electrode could detect E-12 M to E-7 M valine with a success rate of 94.52 percent (Figure 3.88). As shown in Figure 3.91, while anodic currents do not show a certain increase or decrease depending on the concentration, cathodic currents increase.

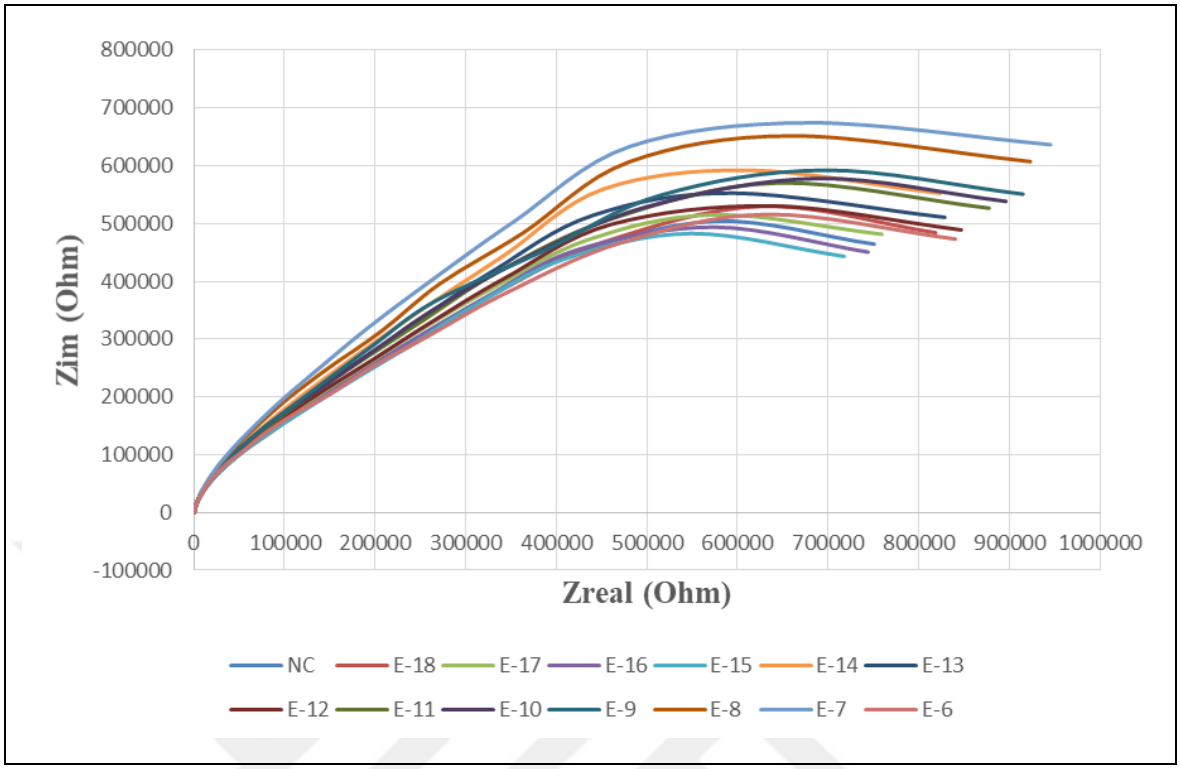

Figure 3.86. EIS response of Au-0.45M-Val-MIP electrode.

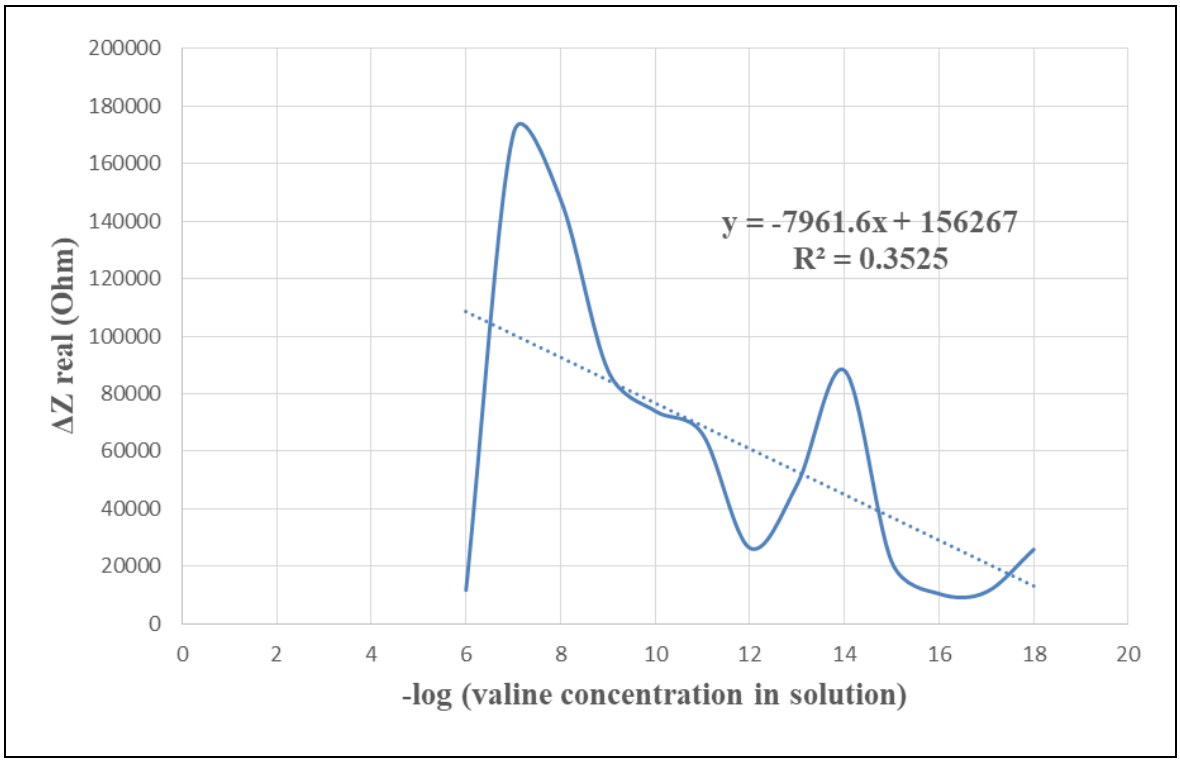

Figure 3.87. The regression curve of Au-0.45M-Val-MIP electrode.

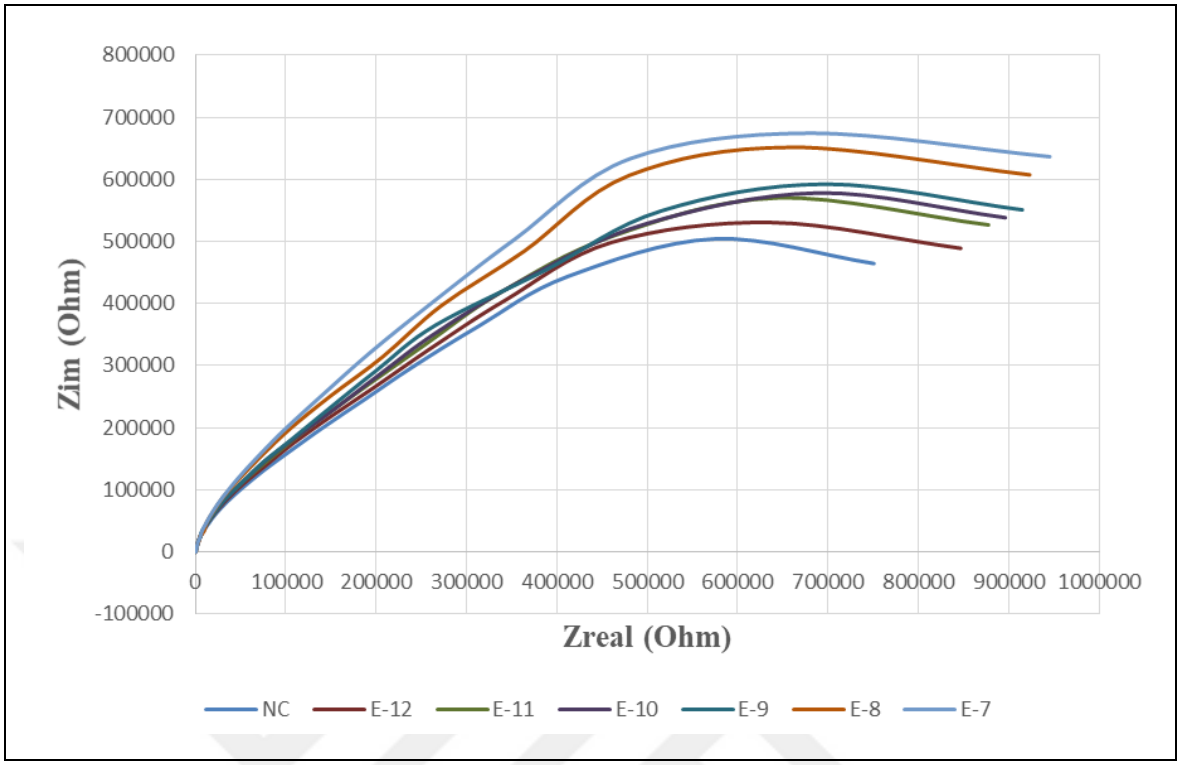

Figure 3.88. EIS response of Au-0.45M-Val-MIP electrode.

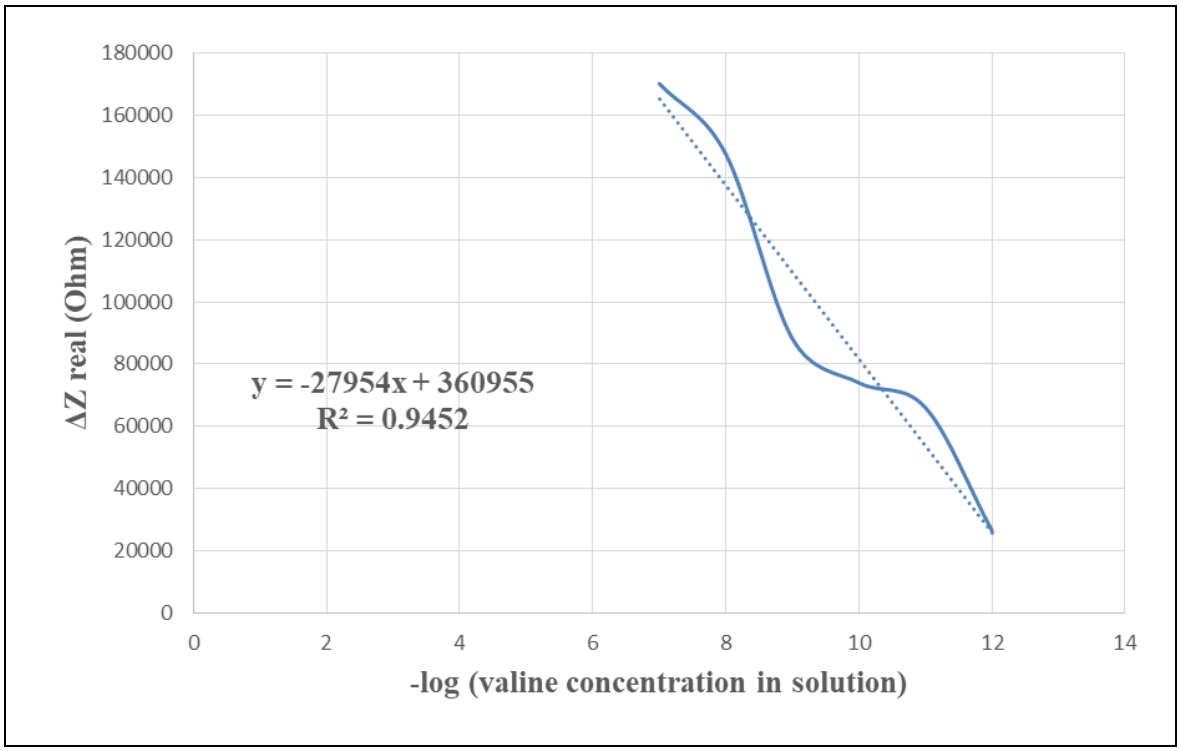

Figure 3.89. The regression curve of Au-0.45M-Val-MIP electrode.

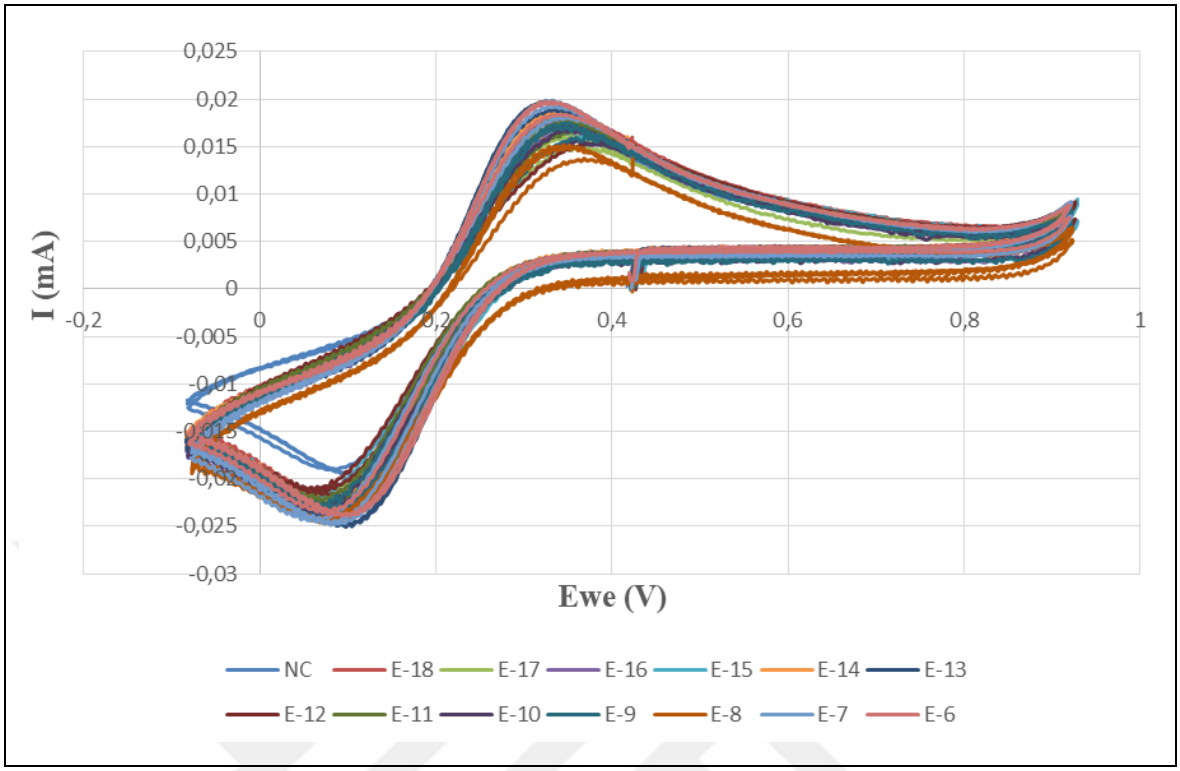

Figure 3.90. CV response of Au-0.45M-Val-MIP electrode.

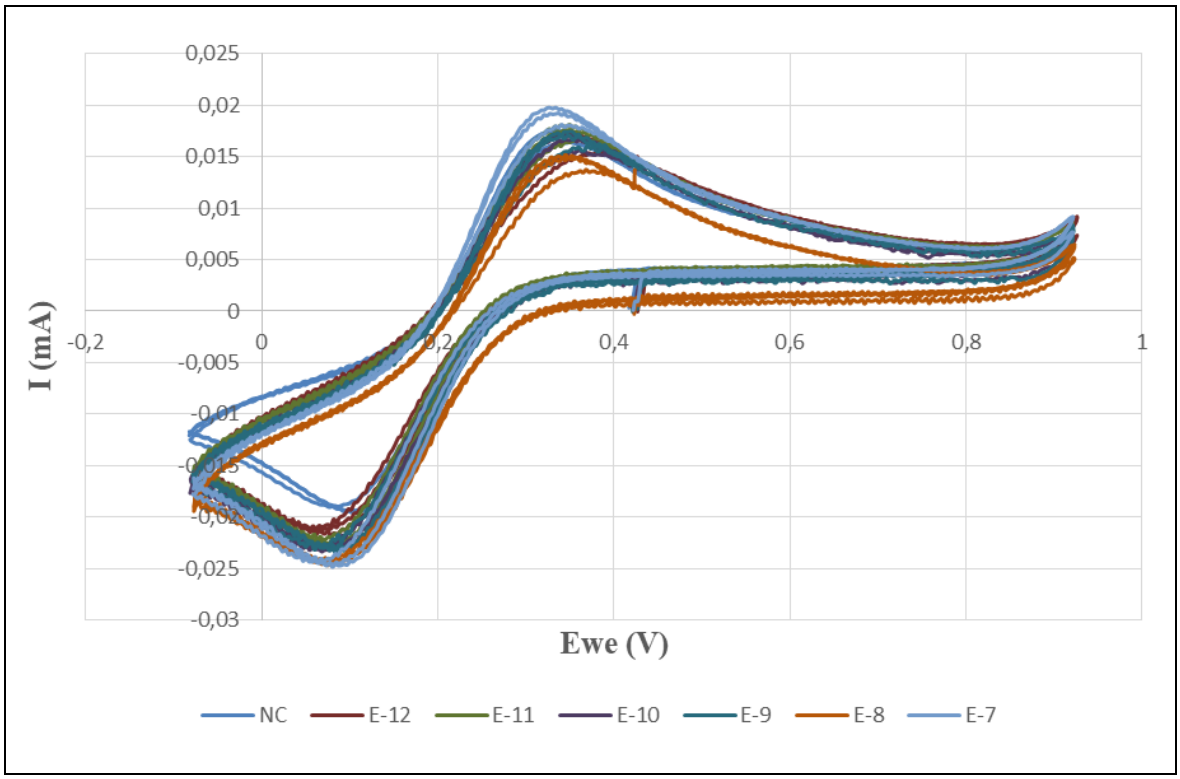

Figure 3.91. CV response of the Au-0.45M-Val-MIP electrode.

Au-0.5M-Val-MIP electrode can detect valine molecules with 8.4 percent success (Figure 3.93) between E-18 M and E-6 M valine (Figure 3.92). According to the regression curve (Figure 3.95), the Au-0.5M-Val-MIP electrode could detect E-12 M and E-8 M valine with a success rate of 94.52 percent (Figure 3.94). As shown in Figure 3.97, while anodic currents data does not show a certain increase or decrease depending on the concentration, cathodic currents increase.

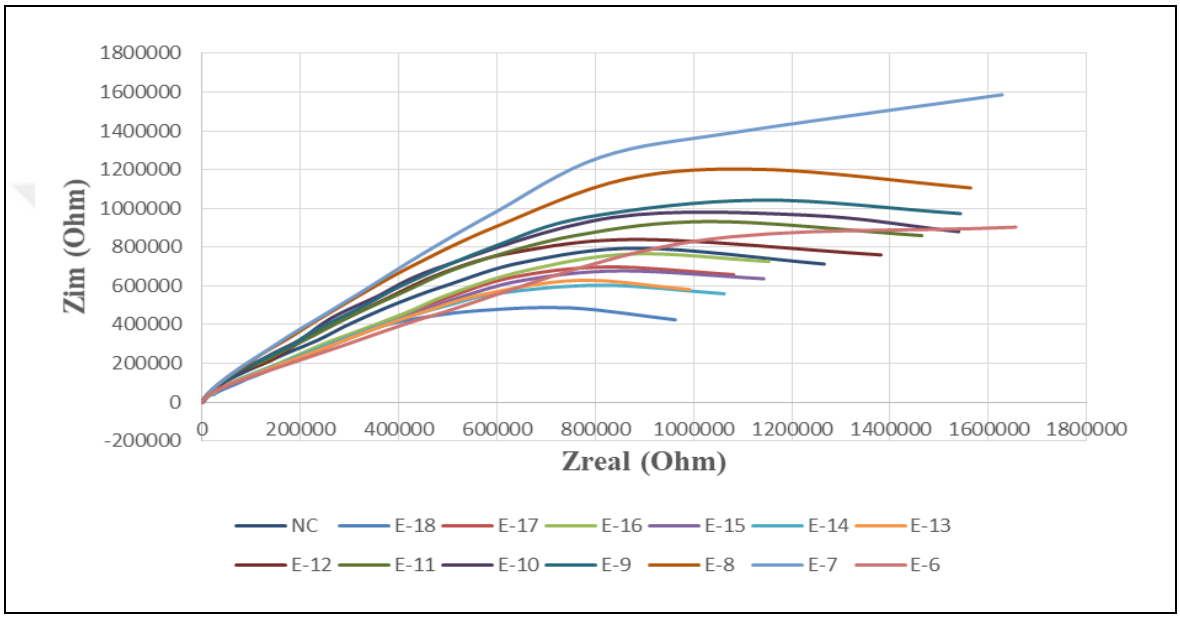

Figure 3.92. EIS response of Au-0.5M-Val-MIP electrode.

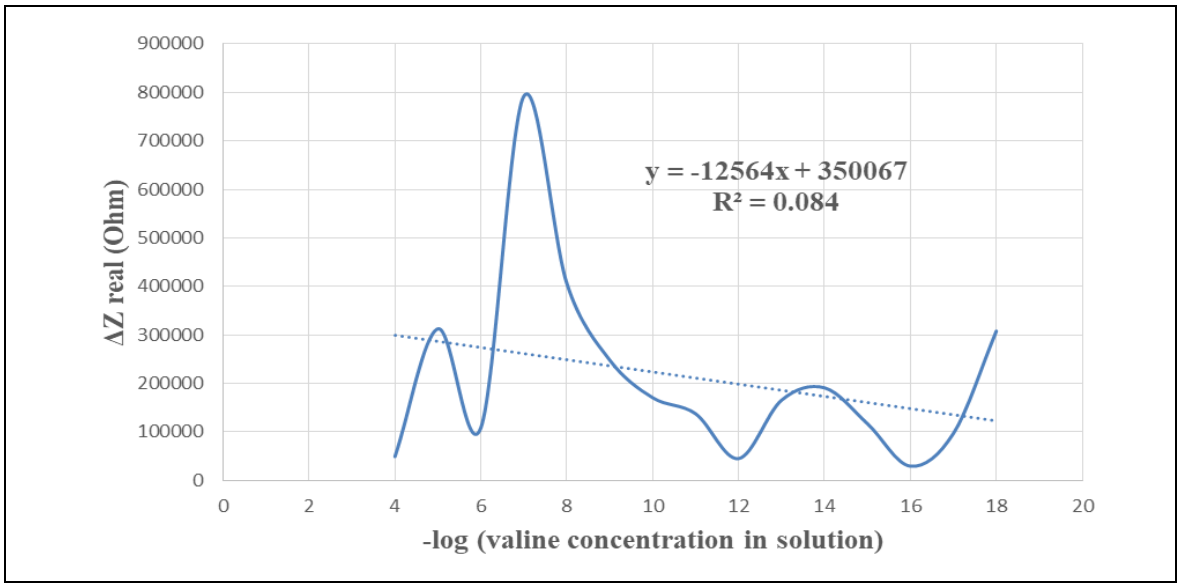

Figure 3.93. The regression curve of Au-0.5M-Val-MIP electrode.

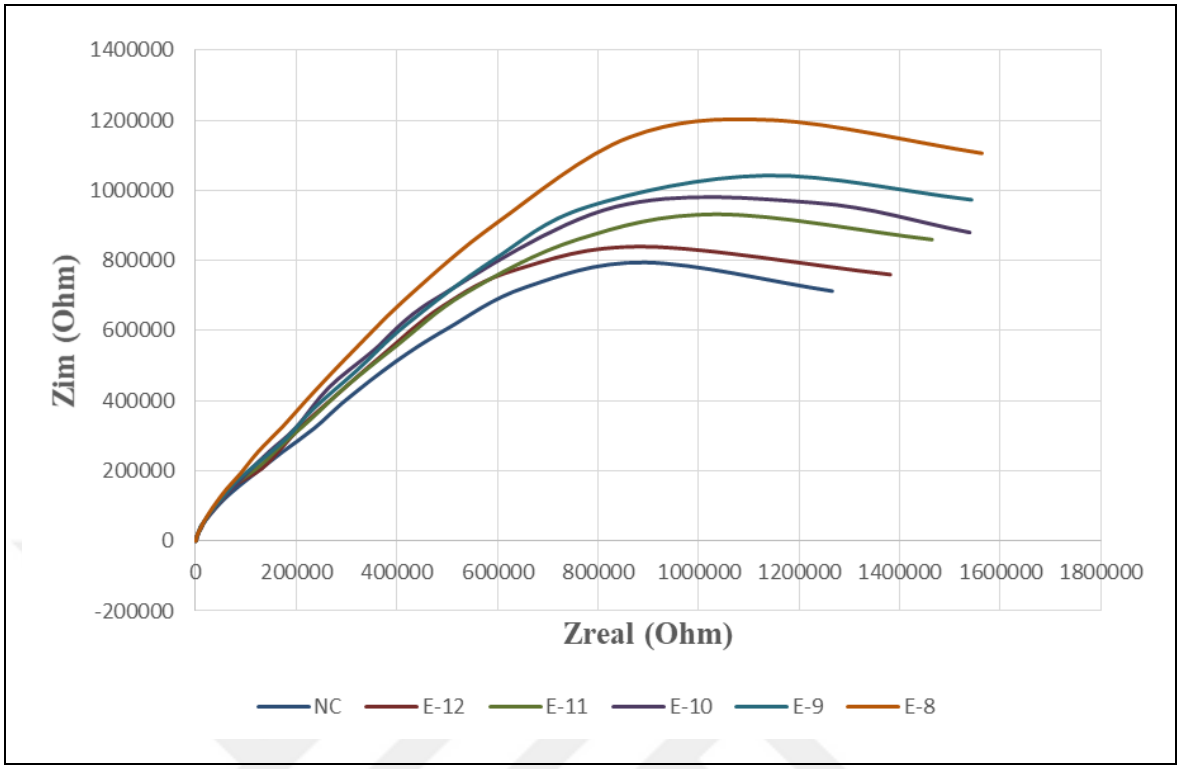

Figure 3.94. EIS response of Au-0.5M-Val-MIP electrode.

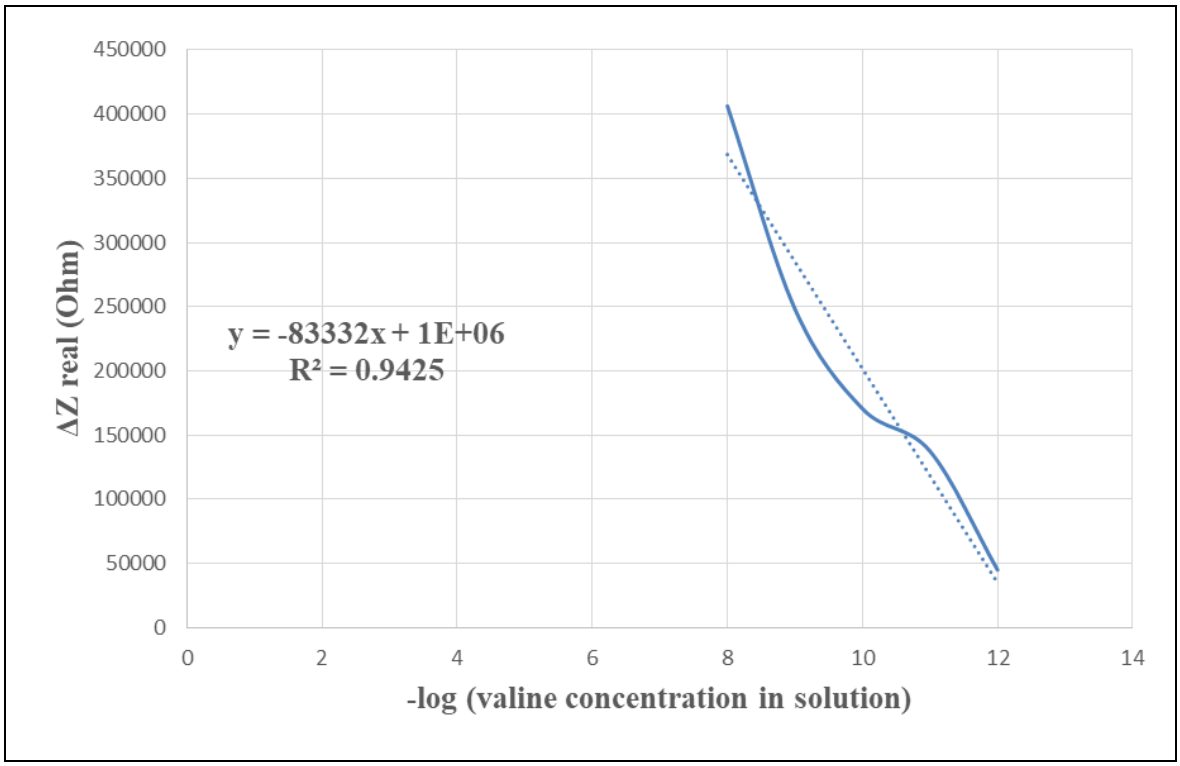

Figure 3.95. The regression curve of Au-0.5M-Val-MIP electrode.

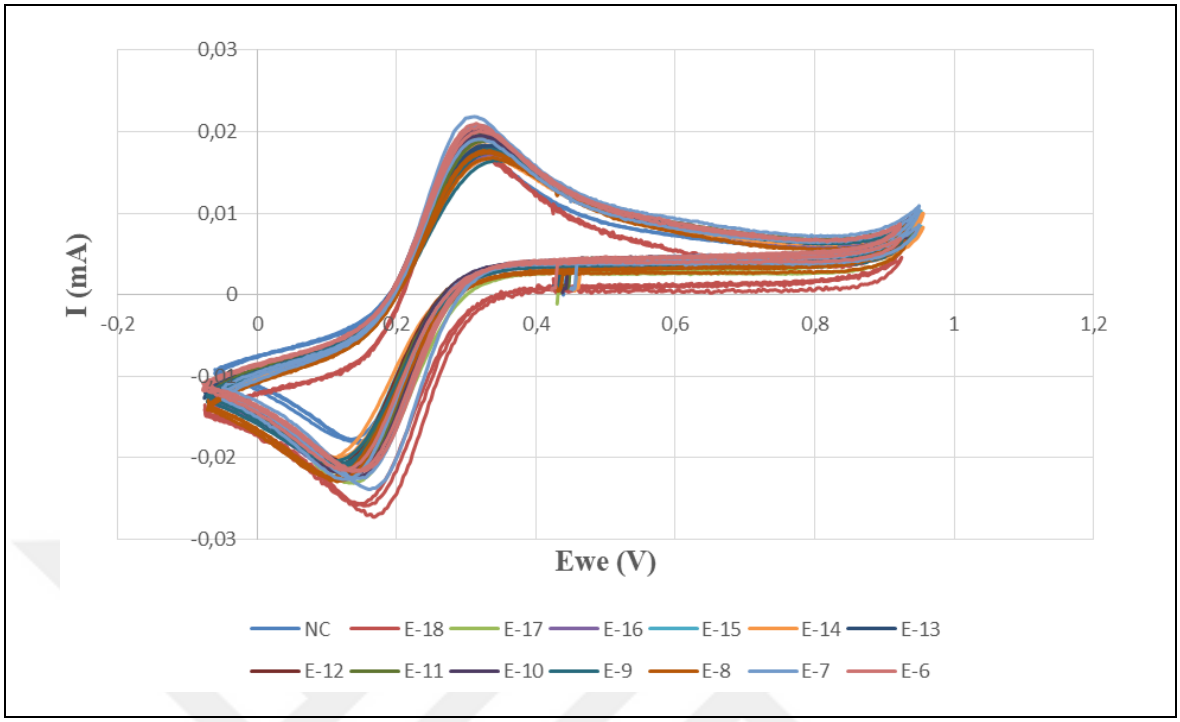

Figure 3.96. CV response of Au-0.5M-Val-MIP electrode.

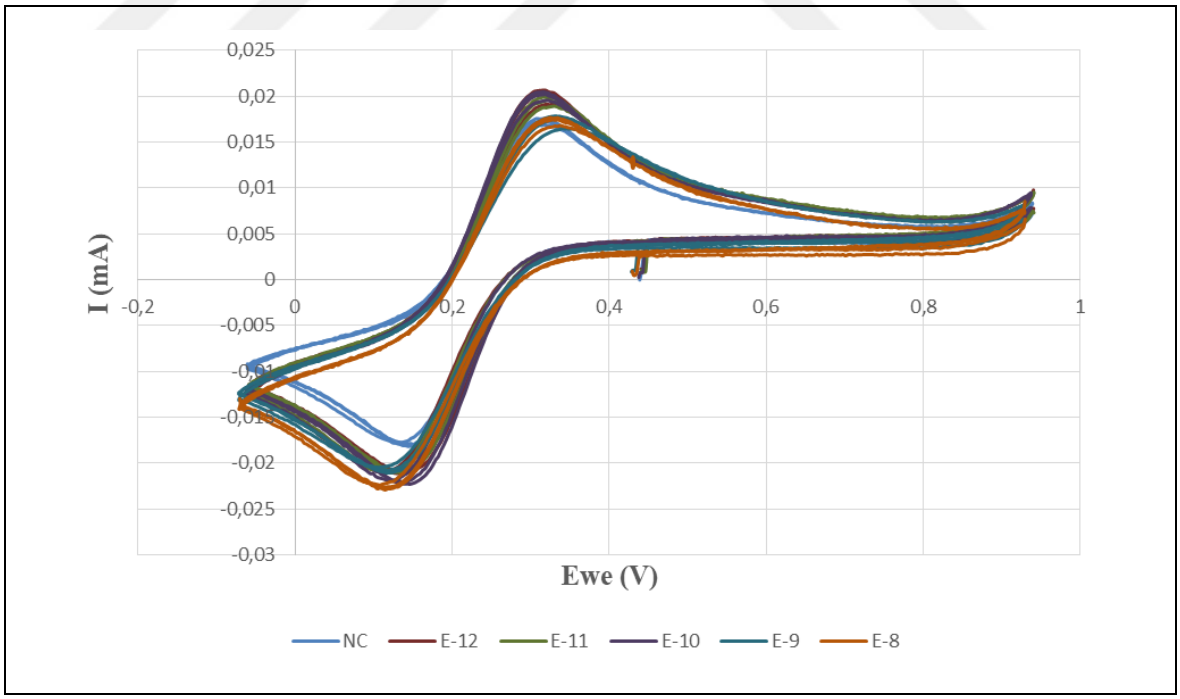

Figure 3.97. CV response of Au-0.5M-Val-MIP electrode.

According to the above given EIS and CV data, the concentration of valine imprinted on the electrode affects the binding property of valine. Depending on the molarity of the imprinted

molecule, the detection range of the electrode to valine and the success of separating the concentrations in the impedance responses vary. It is seen that the Au-0.3M-Val-MIP electrode can detect the molecule in the widest range with its E-15 M and E-6 M valine detection range as shown in Table 3.1, and the best divergence of EIS curves. When Au-0.3M-Val-MIP electrode is chosen as the optimum point, it is revealed that there is aggregation in solutions with high valine concentration and separation in solutions with low concentration in the EIS graphs of electrodes imprinted with a concentration less than 0.3 M. On the EIS graphs, decomposition in solutions with high valine concentration and aggregation in solutions with low valine concentration were observed on electrodes imprinted with a concentration higher than 0.3 M. Further studies were continued with the Au-0.3M-Val-MIP electrode. Limit of detection and quantification are defined as lowest analyte concentration that reliably detected and quantified. LOQ may be equivalent to LOD or it could be at much higher concentration. LOQ was calculated as 7.18E-15 M and LOD was calculated as 9.76E-17 M using equations 2.1 and 2.2 as shown in Table 3.2.

Table 3.1. Detection range in Rdx-PBS solution containing different valine concentrations between E-18 M and E-6 M of Au-MIP group.

Electrode	Valine Detection Range (M)
Au-0.15M-Val-MIP	E-12 / E-9
Au-0.2M-Val-MIP	E-13 / E-7
Au-0.25M-Val-MIP	E-13 / E-7
Au-0.275M-Val-MIP	E-14 / E-7
Au-0.3M-Val-MIP	E-15 / E-6
Au-0.325M-Val-MIP	E-14 / E-6
Au-0.35M-Val-MIP	E-14 / E-7
Au-0.4M-Val-MIP	E-14 / E-7
Au-0.45M-Val-MIP	E-12 / E-7
Au-0.5M-Val-MIP	E-12 / E-8

Table 3.2. Features of concentration versus current graph obtained with Au-0.3M-Val-MIP electrode.

Regression equation	y = 2E-05x-16.93
Determination coefficient (R^2)	0.9925
Linearity range (M)	7.16E-15 - 7.16E-6
LOQ (M)	7.18E-15
LOD (M)	9.76E-17

3.2.3. Valine Unremoved Molecular Imprinting Group (Val-UMIP)

In this group, in order to evaluate the data of the unremoved molecular imprinting electrodes, 0.15 M, 0.2 M, 0.25 M, 0.275 M, 0.3 M, 0.325 M, 0.35 M, 0.4 M, 0.45 M and 0.5 M were first selected for the valine concentration to be printed on the electrodes. After molecular imprinting, valine was not removed with HCl and distilled water.

Figures 3.98, 3.104, 3.110, 3.116, 3.122, 3.125, 3.131, 3.137, 3.143 and 3.149 in solution with different valine concentrations, respectively, EIS plots from Au-0.15M-Val-UMIP, Au-0.2 M-Val-UMIP, Au-0.25M-Val-UMIP, Au-0.275M-Val-UMIP, Au-0.3M-Val-UMIP, Au-0.325M-Val-UMIP, Au-0.35M-Val-UMIP, Au-0.4M-Val-UMIP, Au-0.45M-Val-UMIP and Au-0.5M-Val-UMIP electrodes are shown.

In the Au-UMIP group, the EIS and CV measurements of the electrodes were made in Rdx-PBS solutions containing valine concentrations in the range of E-15 M and E-6 M. This range was preferred because the range in which the electrodes detect the most valine molecules in the Au-MIP group was chosen as E-15/E-6 M for the Au-0.3M-Val-MIP electrode. The successes of detecting valine in the E-15/E-6 M range of each electrode and in the concentration range that the MIP state can detect were shown with regression curves. Since the valine molecule is not removed after the molecular imprinting process, valine-specific voids formed on the polymer have reached the saturation level. The graphs below show that the electrodes in this group cannot detect different valine concentrations in the Rdx-PBS solution.

Figures 3.102, 3.108, 3.114, 3.120, 3.124, 3.129, 3.135, 3.141, 3.147 and 3.153 in solution with different valine concentrations, respectively, CV plots from Au-0.15M-Val-UMIP, Au-0.2 M-Val-UMIP, Au-0.25M-Val-UMIP, Au-0.275M-Val-UMIP, Au-0.3M-Val-UMIP, Au-0.325M-Val-UMIP, Au-0.35M-Val-UMIP, Au-0.4M-Val-UMIP, Au-0.45M-Val-UMIP, and Au-0.5M-Val-UMIP electrodes are shown. These graphs show the change in current versus changing voltage in the range of -500/+500 mV.

Au-0.15M-Val-UMIP electrode detected valine molecule with 1.76 percent success in E-15/E-6 M range and with 13.44 percent success in E-12 Mto E-9 M range (Figures 3.99 and 3.101). There was no regular increase or decrease in the anodic and cathodic currents in the CV curves due to increasing valine concentration (Figure 103).

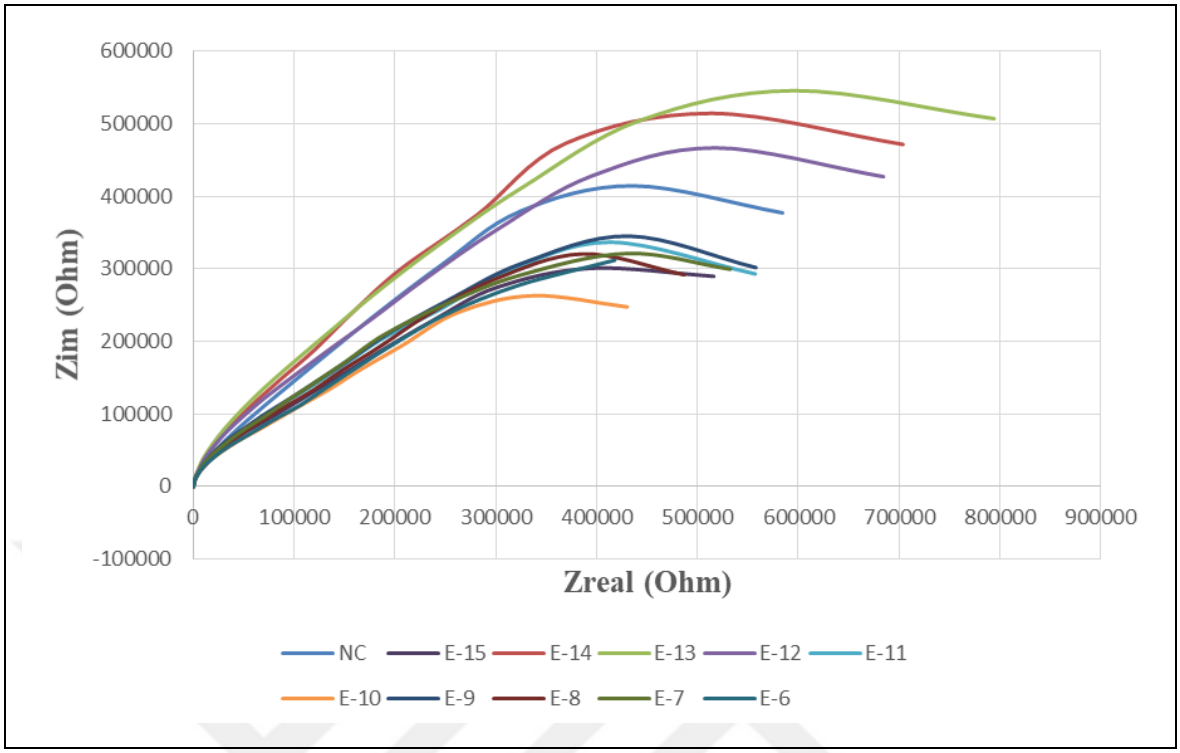

Figure 3.98. EIS response of Au-0.15M-Val-UMIP electrode.

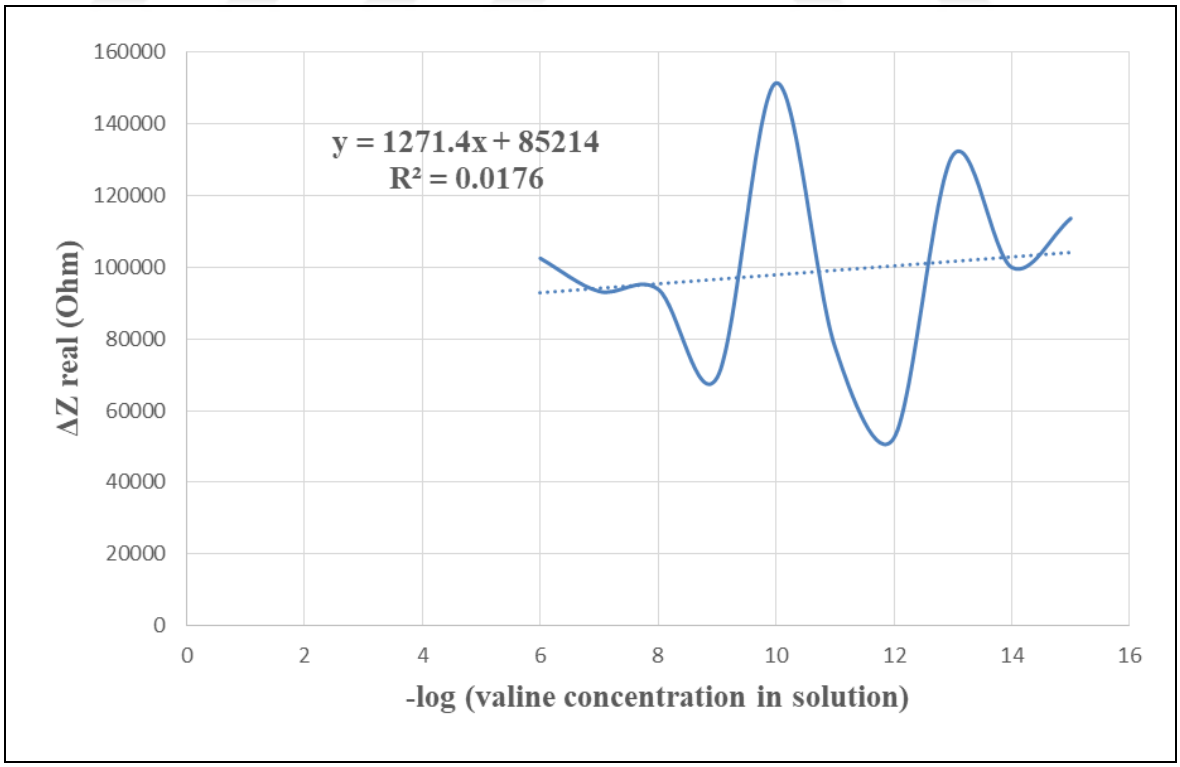

Figure 3.99. The regression curve of Au-0.15M-Val-UMIP electrode.

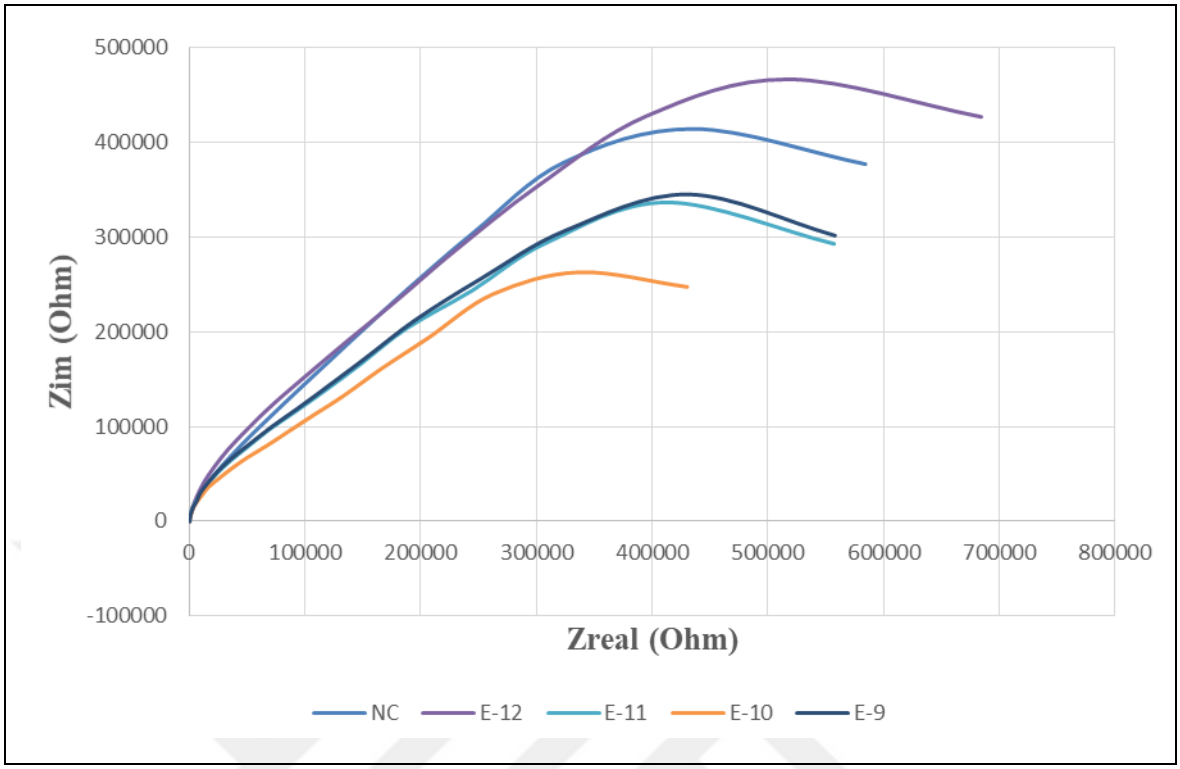

Figure 3.100. EIS response of Au-0.15M-Val-UMIP electrode.

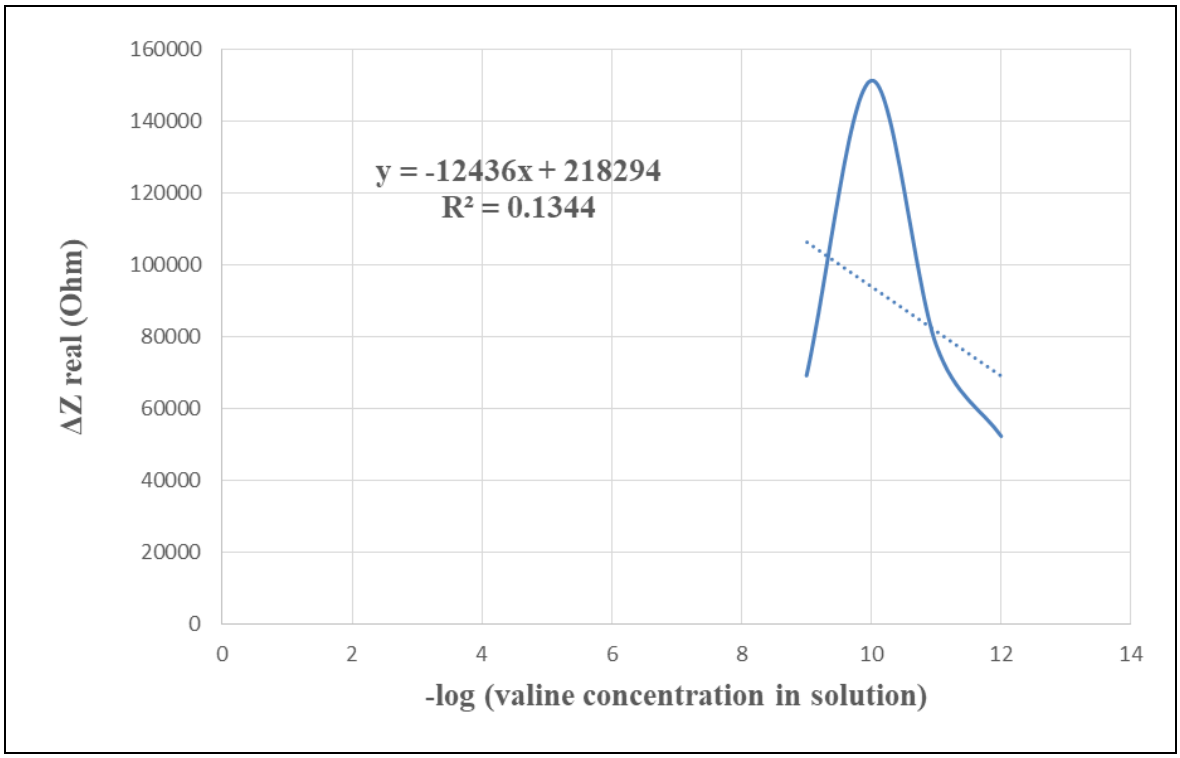

Figure 3.101. The regression curve of Au-0.15M-Val-UMIP electrode.

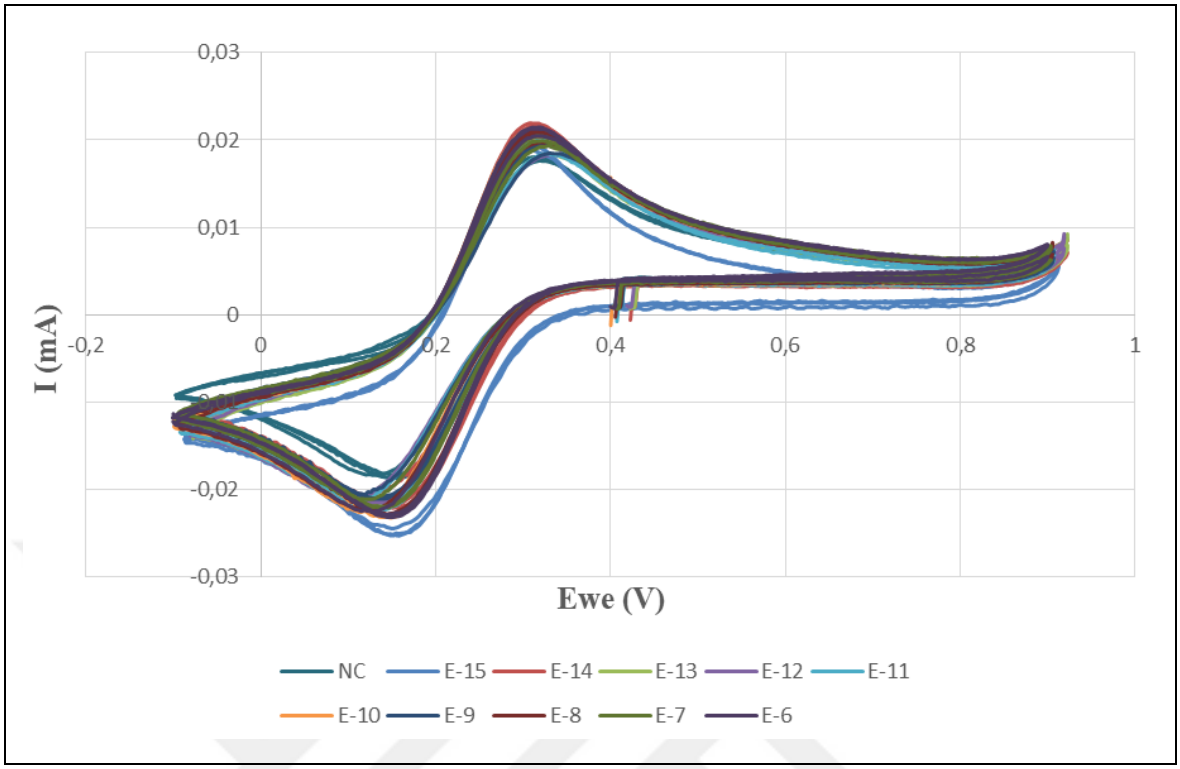

Figure 3.102. CV response of Au-0.15M-Val-UMIP electrode.

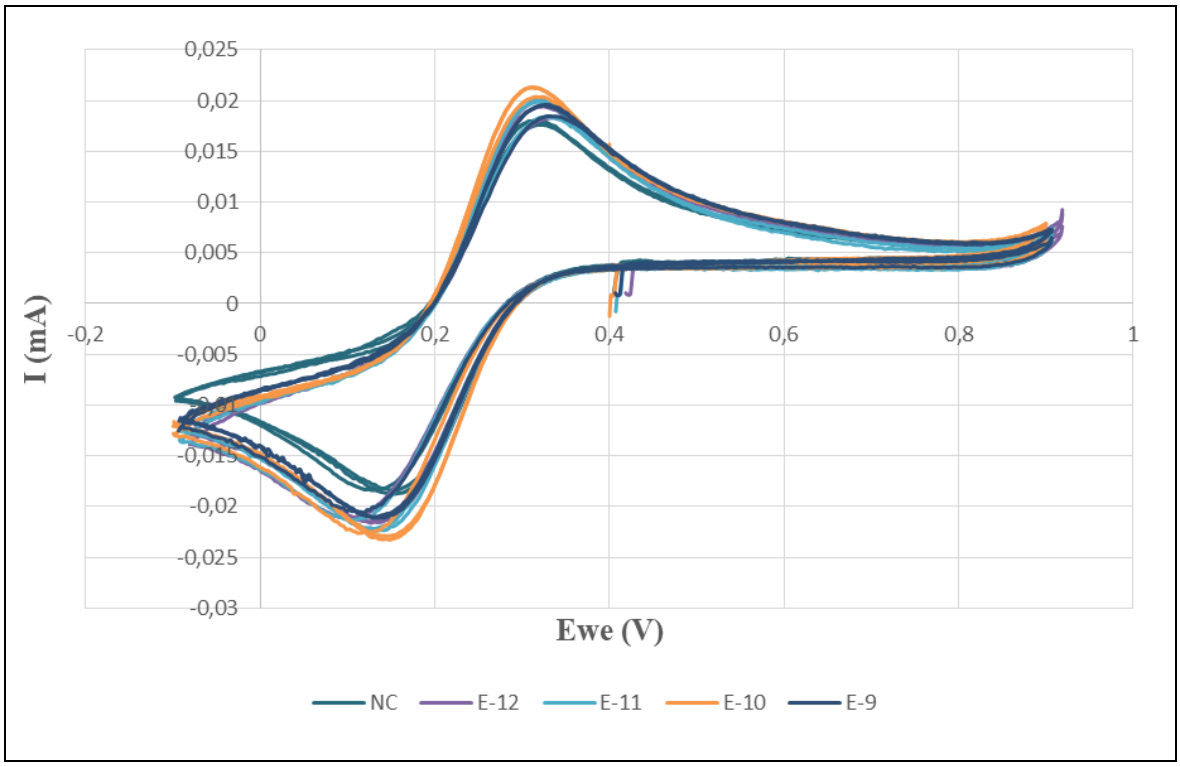

Figure 3.103. CV response of the Au-0.15M-Val-UMIP electrode.

Au-0.2M-Val-UMIP electrode regression curves (Figure 3.105, 3.107) with 15.64 percent success in the E-15 M to E-6 M range and 0.12 percent in the E-13 M to E-7 M range detected the valine molecule. These ratios show that the valine molecule could not be detected correctly. There was no regular increase or decrease in the anodic and cathodic currents in the CV curves due to increasing valine concentration (Figures 3.108 - 3.109).

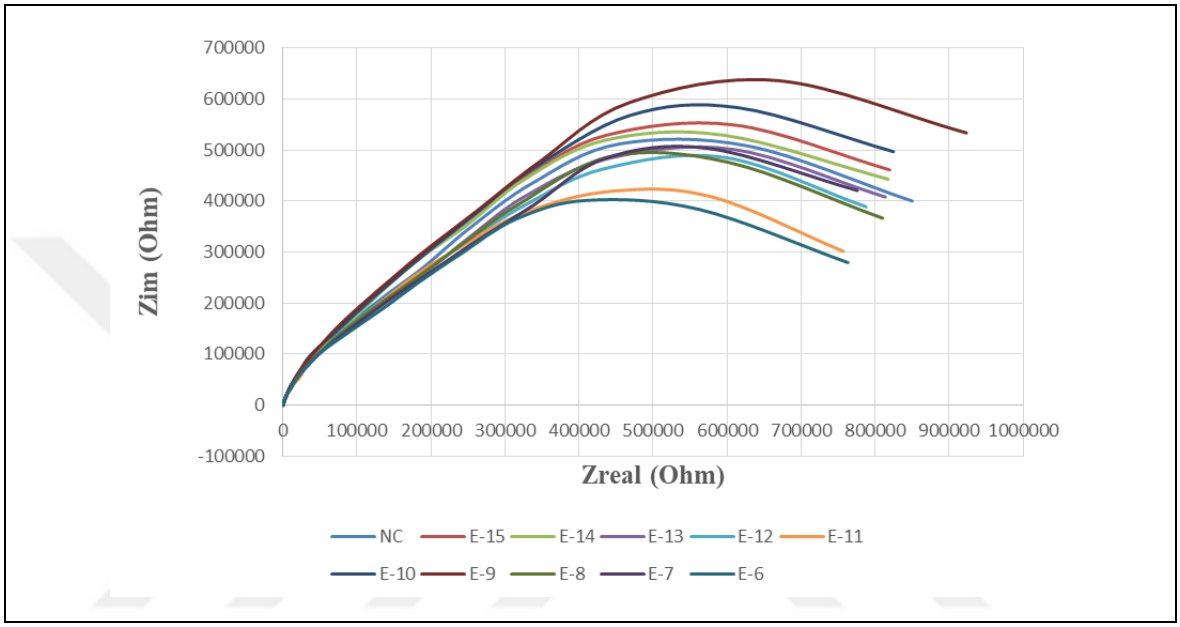

Figure 3.104. EIS response of Au-0.2M-Val-UMIP electrode.

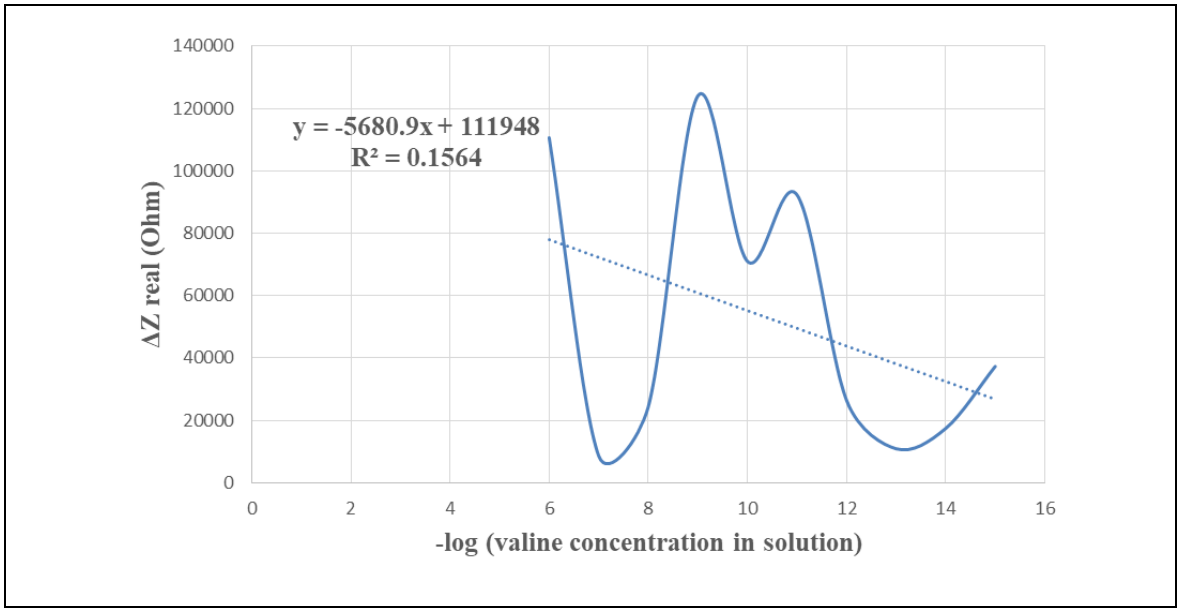

Figure 3.105. The regression curve of Au-0.2M-Val-UMIP electrode.

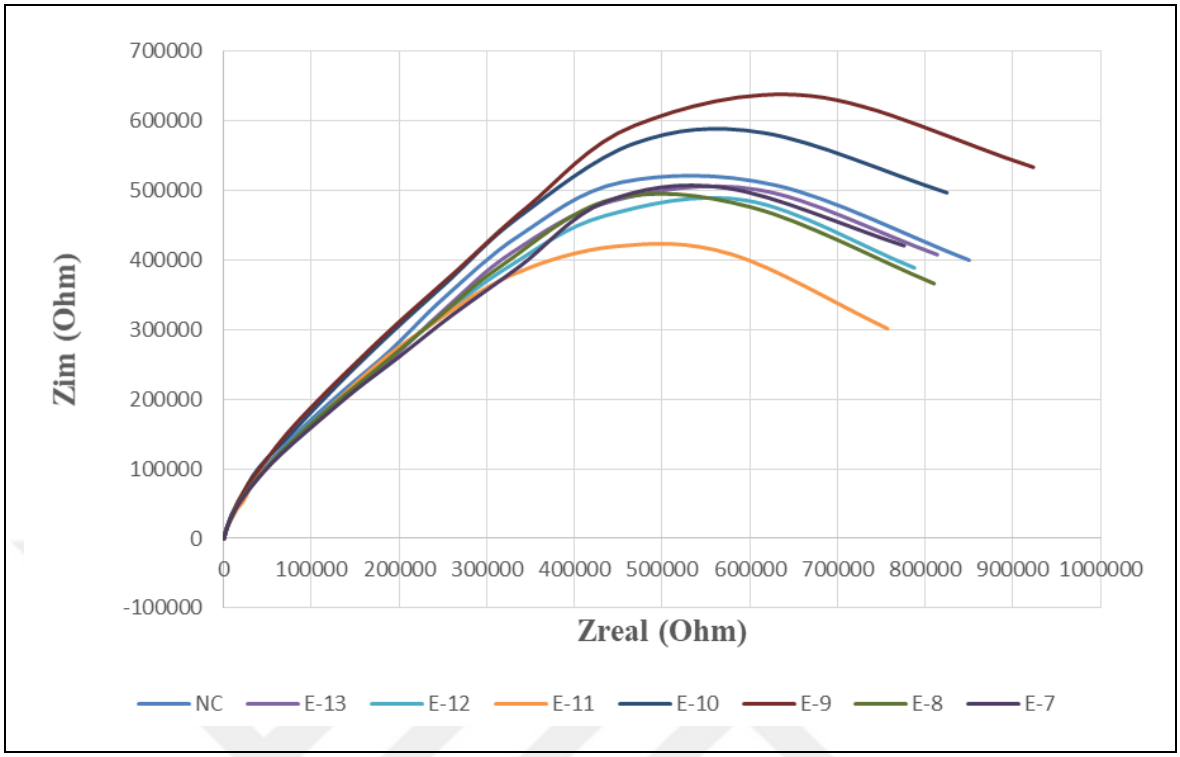

Figure 3.106. EIS response of the Au-0.2M-Val-UMIP electrode.

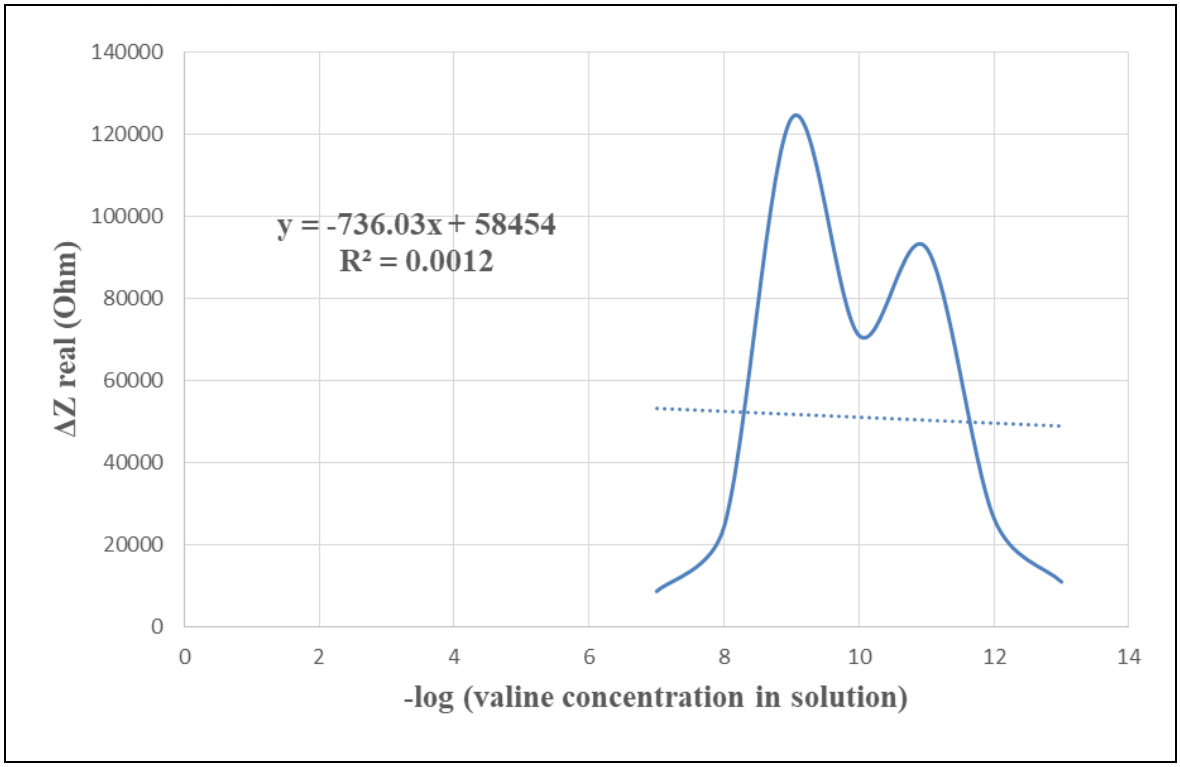

Figure 3.107. The regression curve of Au-0.2M-Val-UMIP electrode.

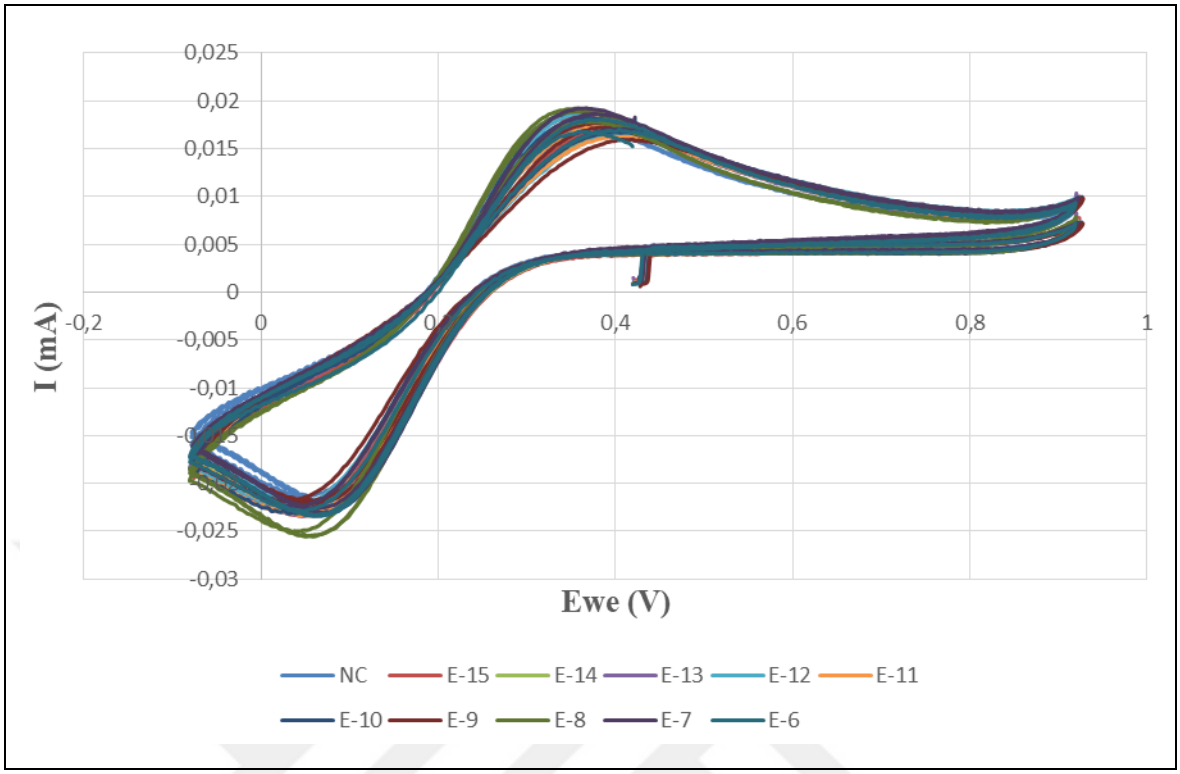

Figure 3.108. CV response of Au-0.2M-Val-UMIP electrode.

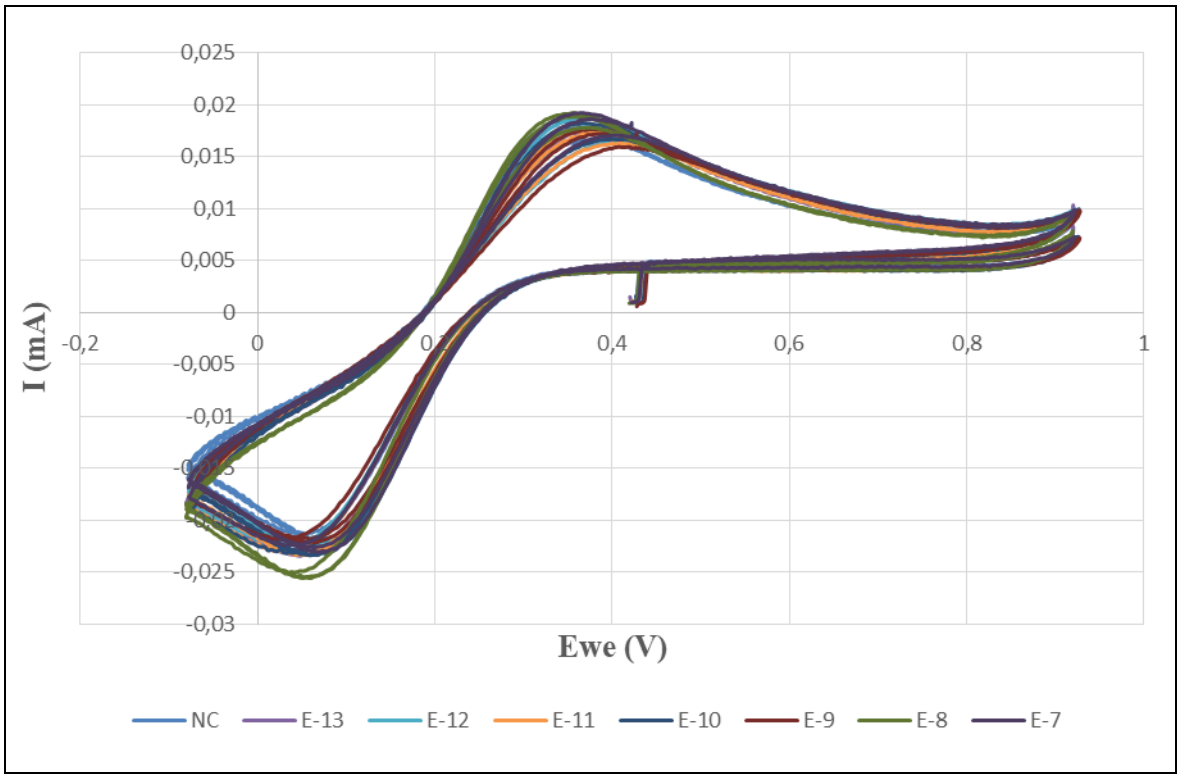

Figure 3.109. CV response of the Au-0.2M-Val-UMIP electrode.

The Au-0.25M-Val-UMIP electrode was insufficient to detected the valine molecule, with a 18.46 percent success rate in the E-15 M to E-6 M range and 22.93 percent in the E-13 M to E-7 M range (Figures 3.111, 3.113). The CV curves did not indicate a variation in anodic and cathodic currents (Figures 3.114 and 3.115).

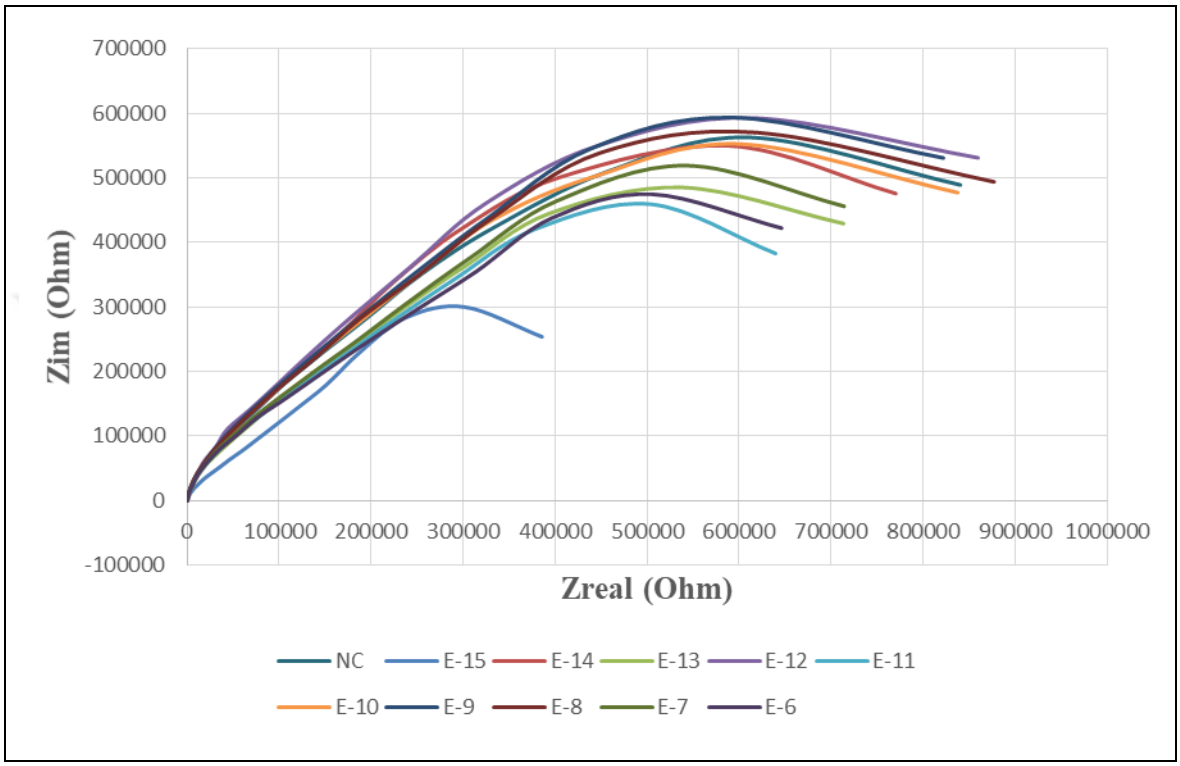

Figure 3.110. EIS response of Au-0.25M-Val-UMIP electrode.

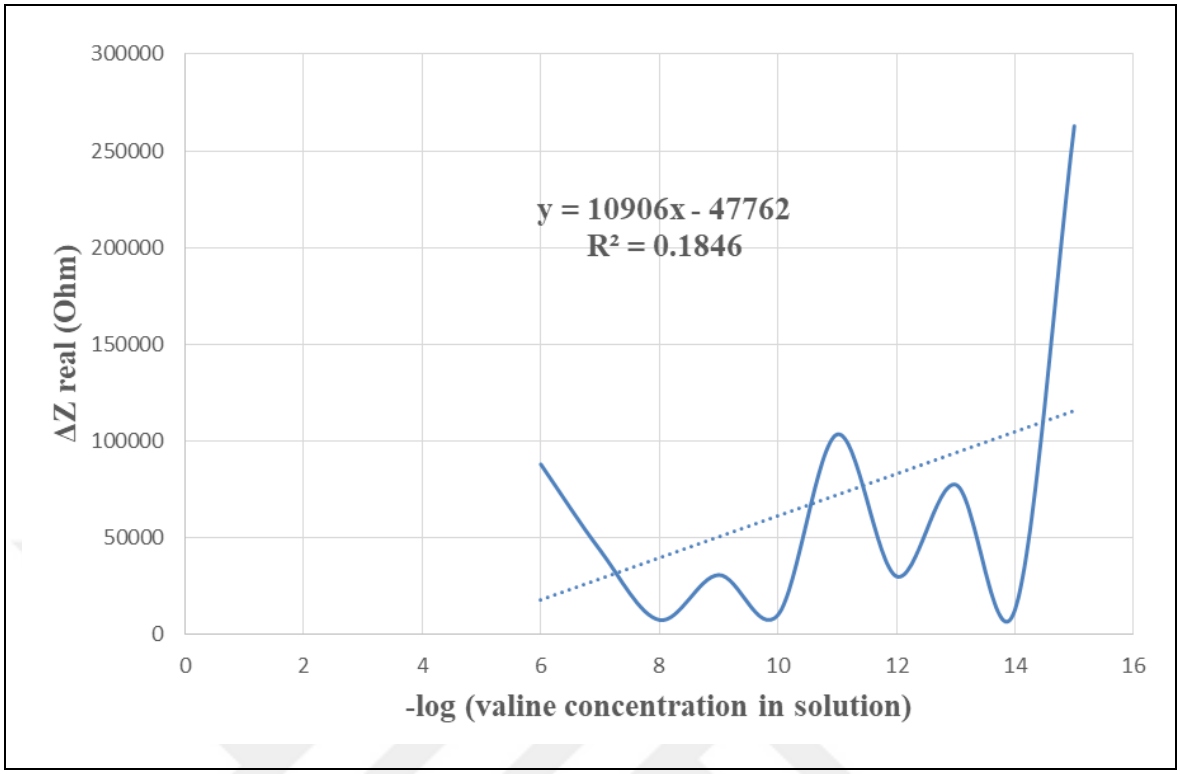

Figure 3.111. The regression curve of Au-0.25M-Val-UMIP electrode.

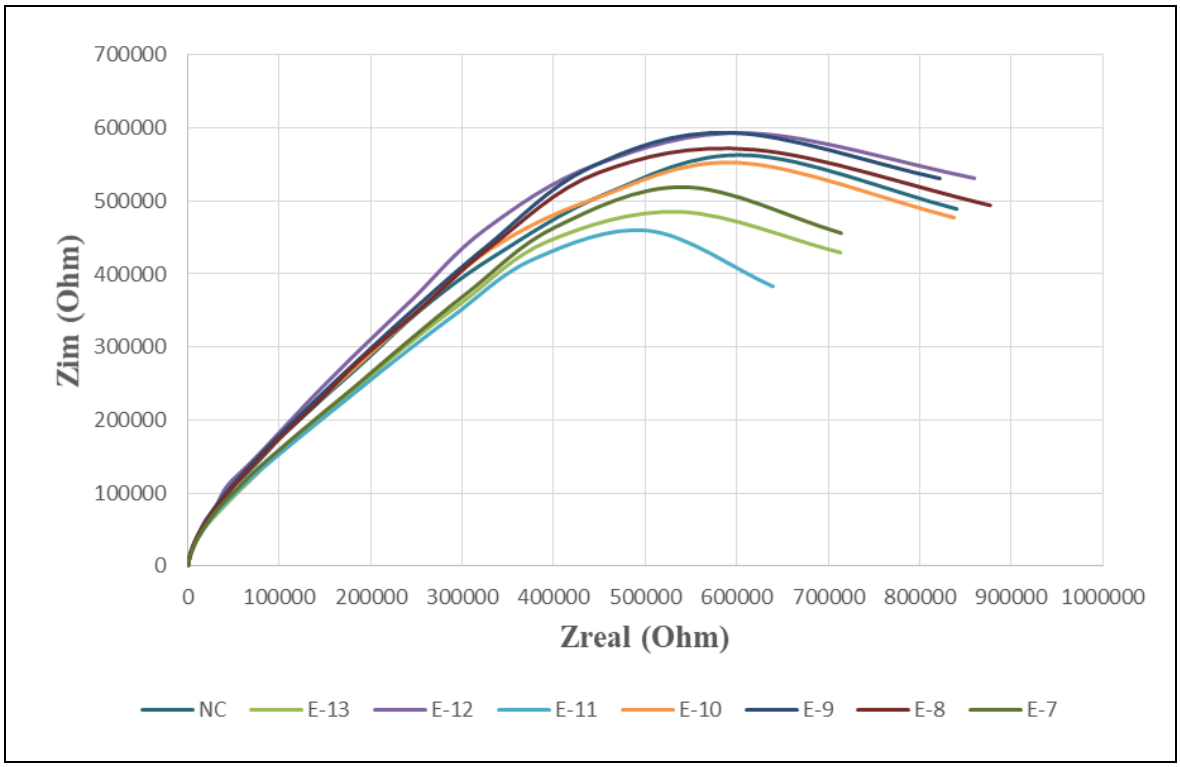

Figure 3.112. EIS response of the Au-0.25M-Val-UMIP electrode.

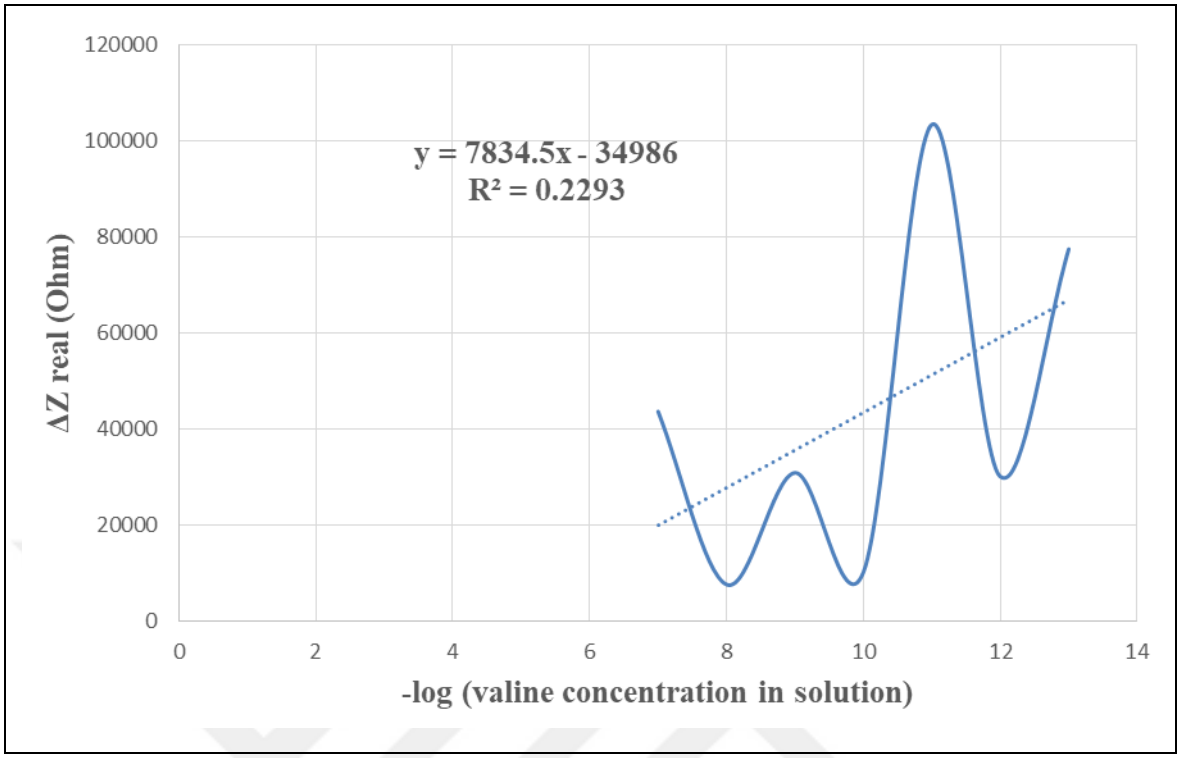

Figure 3.113. The regression curve of Au-0.25M-Val-UMIP electrode.

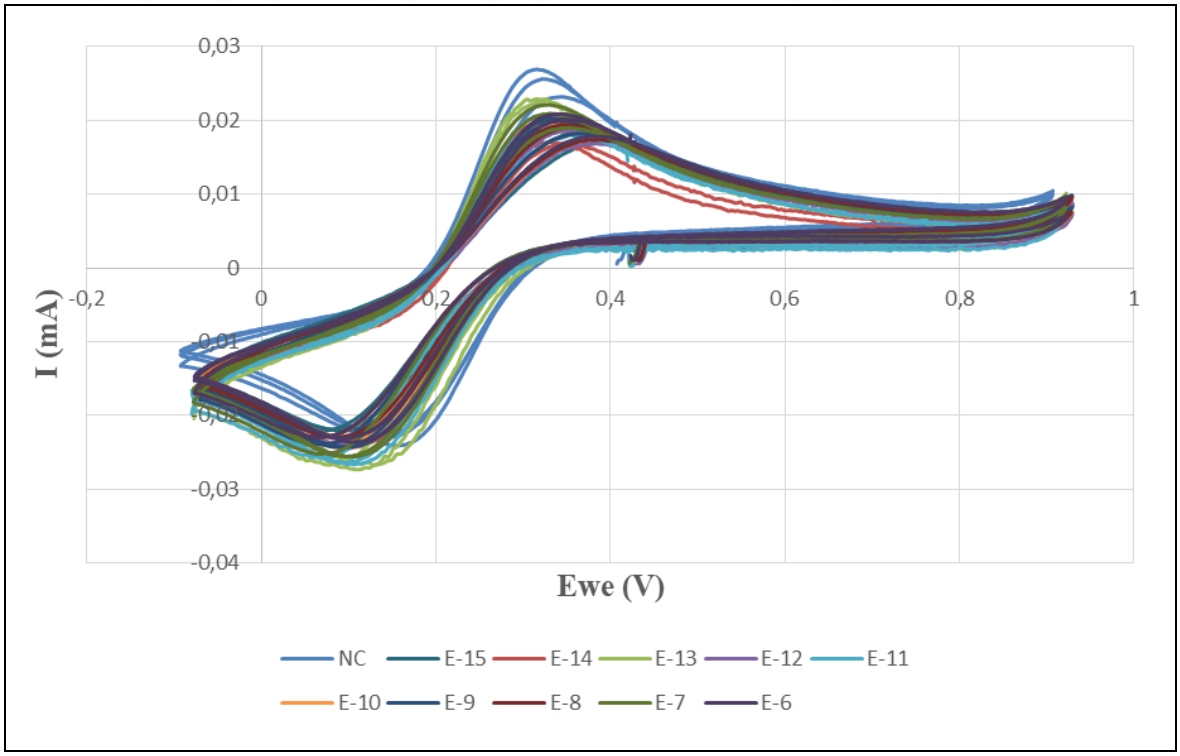

Figure 3.114. CV response of Au-0.25M-Val-UMIP electrode.

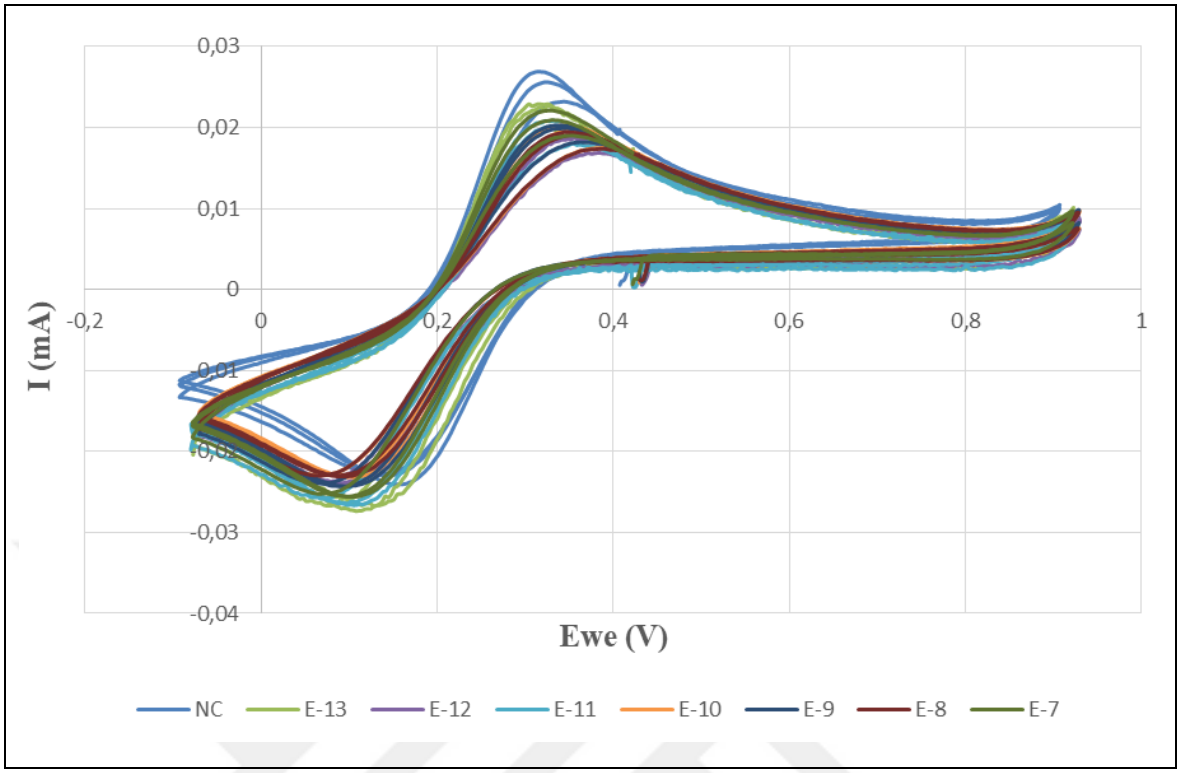

Figure 3.115. CV response of the Au-0.25M-Val-UMIP electrode.

The Au-0.275M-Val-UMIP electrode was insufficient to detect the valine molecule, with a 13.51 percent success rate in the E-15 M to E-6 M range and 0.01 percent in the E-14 M to E-7 M range (Figures 3.117, 3.119). The CV curves did not indicate a variation in anodic and cathodic currents (Figures 3.120 and 3.121).

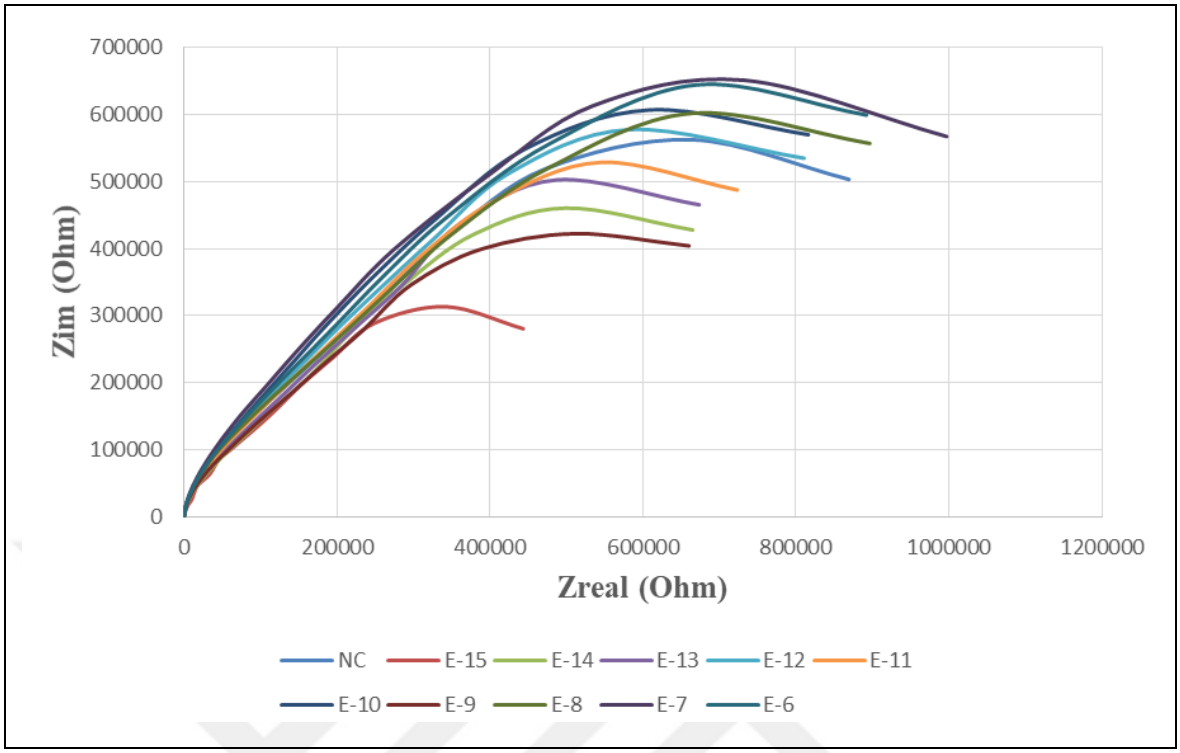

Figure 3.116. EIS response of Au-0.275M-Val-UMIP electrode.

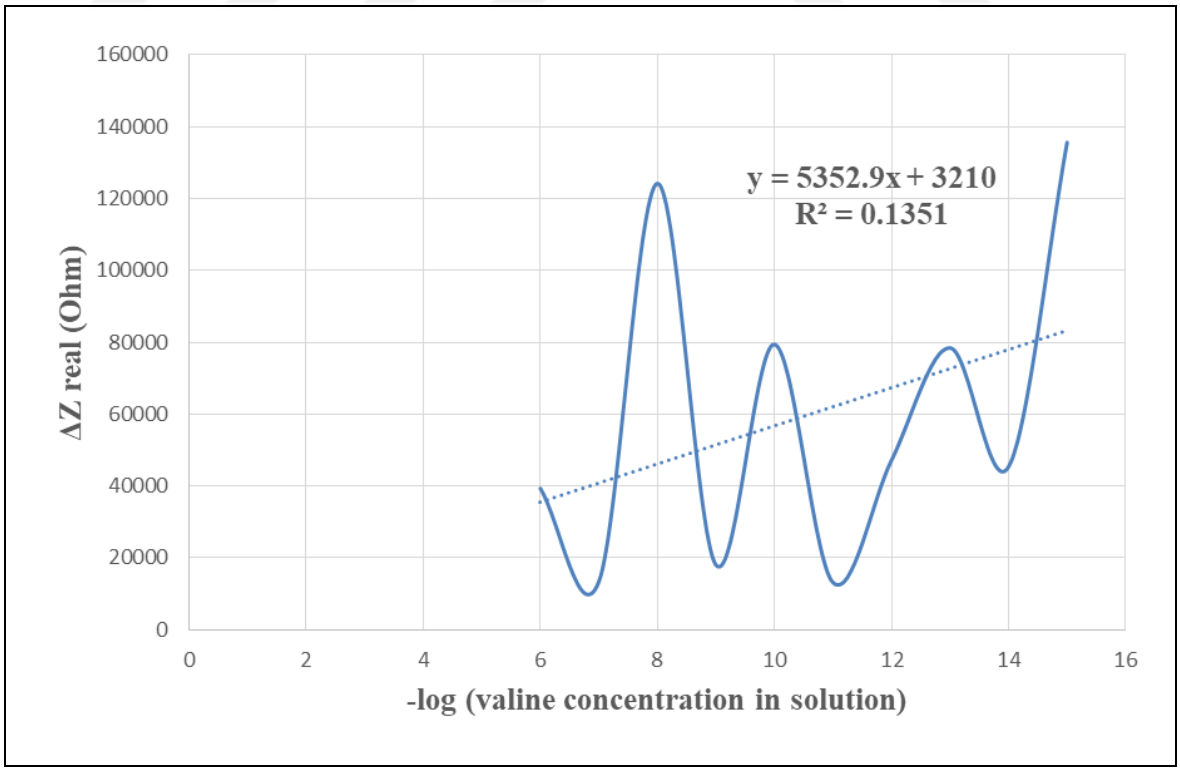

Figure 3.117. The regression curve of Au-0.275M-Val-UMIP electrode.

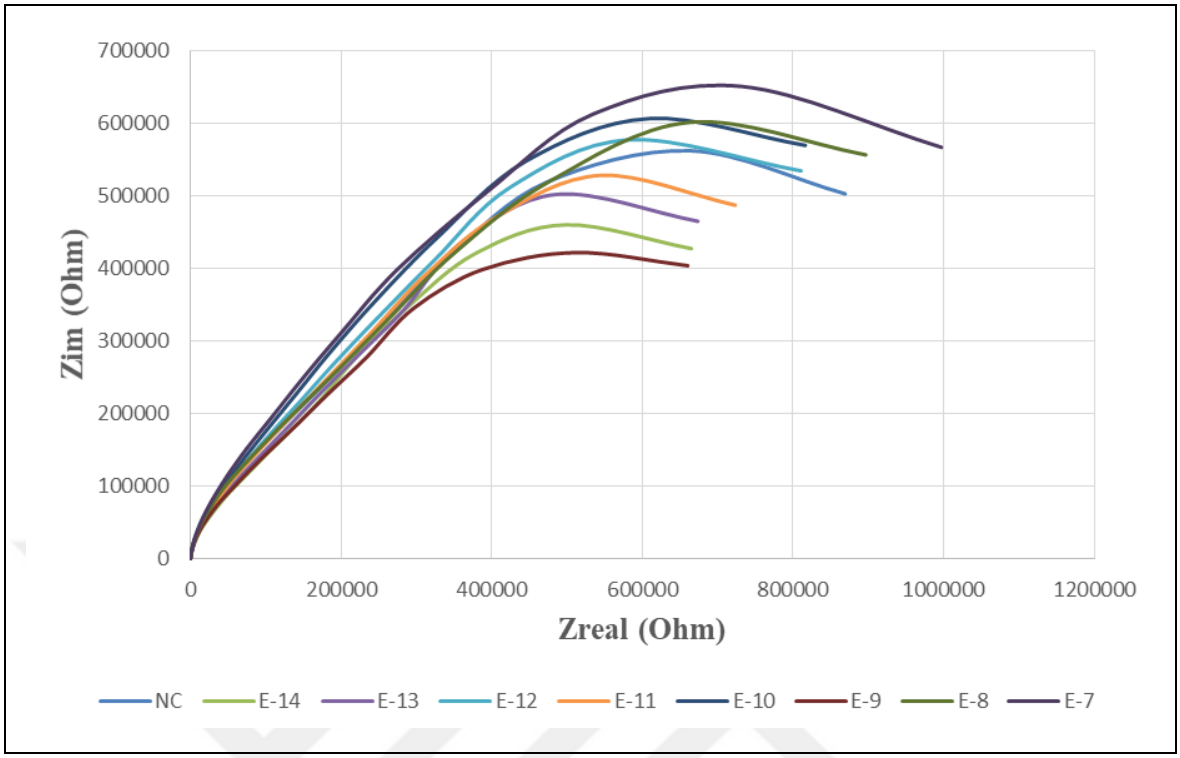

Figure 3.118. EIS response of Au-0.275M-Val-UMIP electrode.

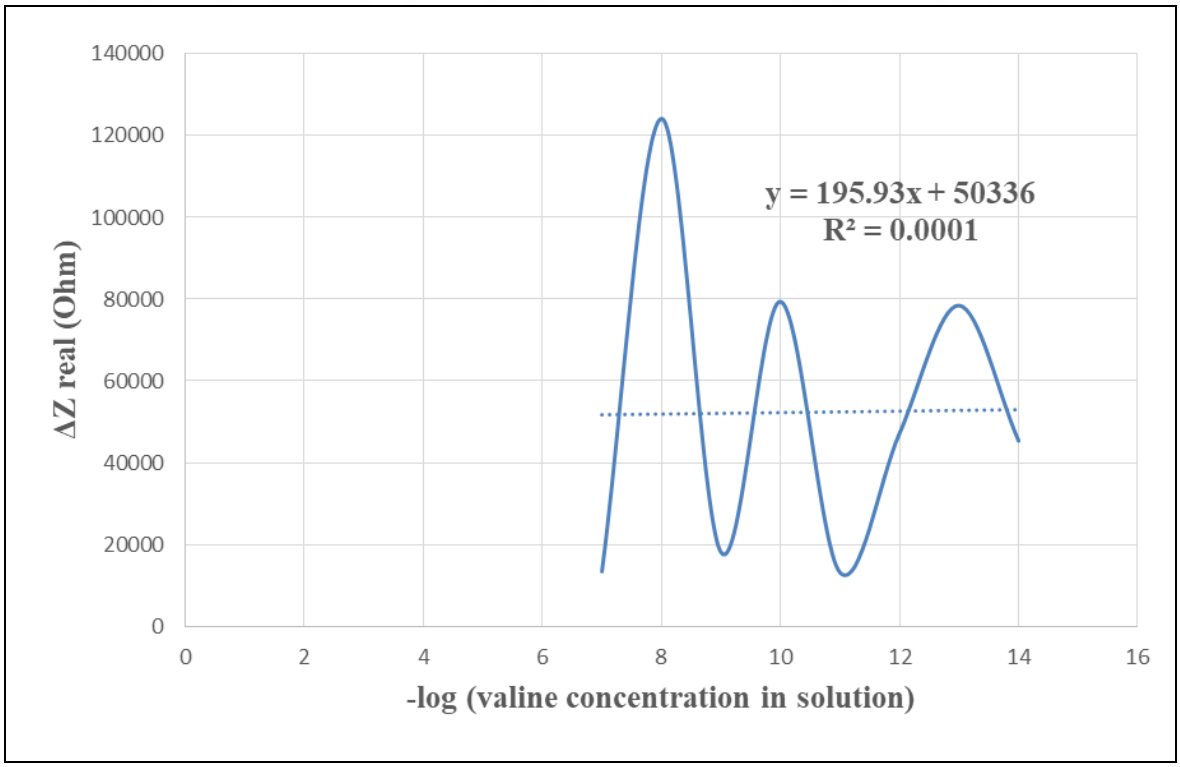

Figure 3.119. The regression curve of Au-0.275M-Val-UMIP electrode.

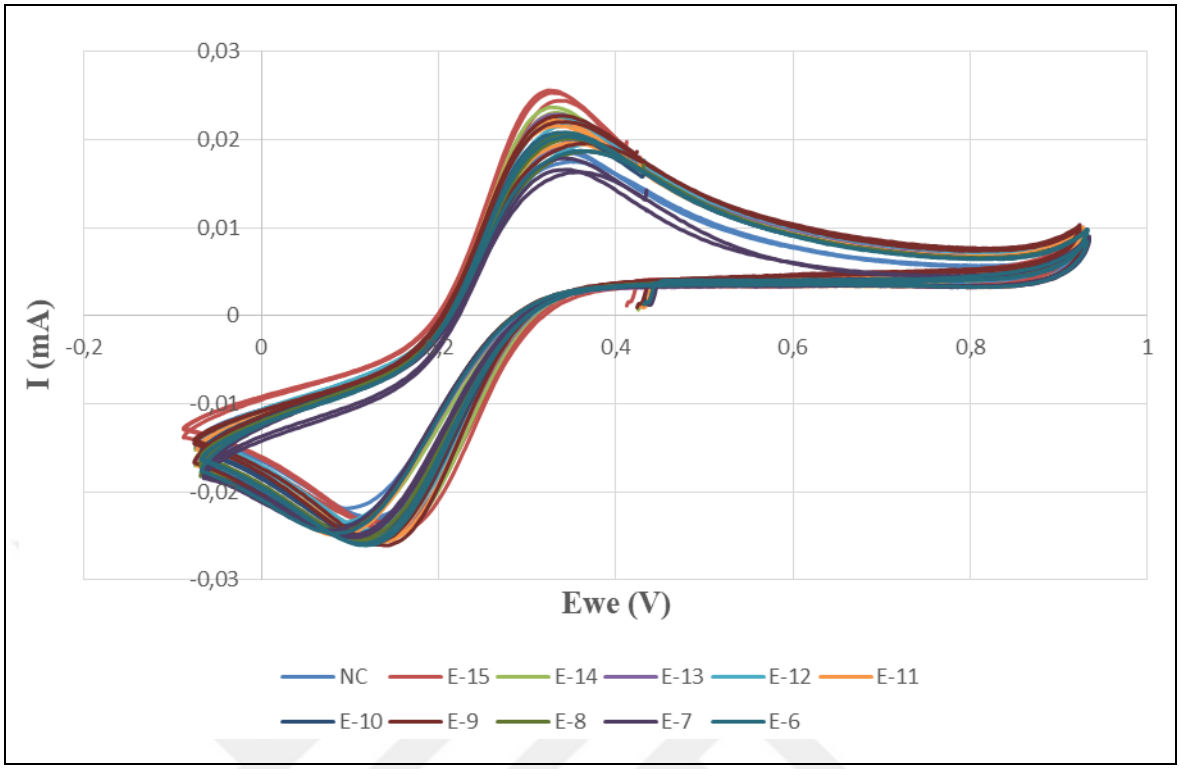

Figure 3.120. CV response of Au-0.275M-Val-UMIP electrode.

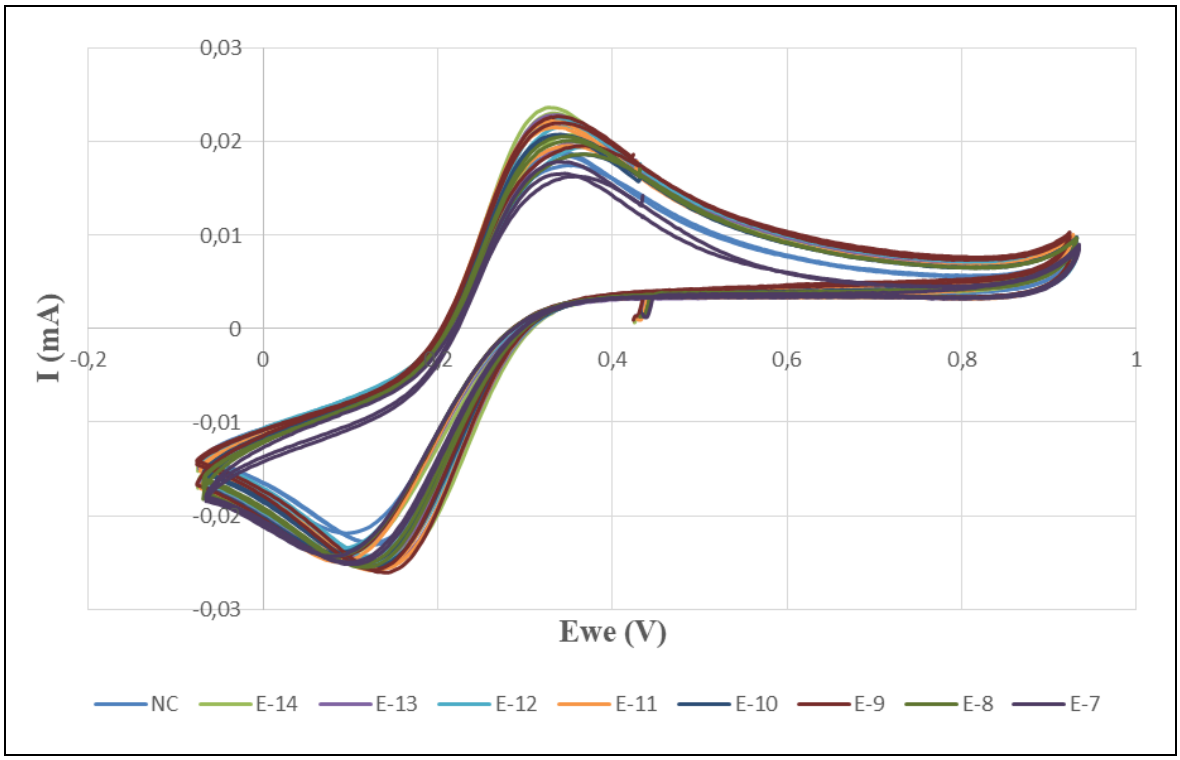

Figure 3.121. CV response of the Au-0.275M-Val-UMIP electrode.

The Au-0.3M-Val-UMIP electrode was insufficient to detected the valine molecule, with a 0.07 percent success rate in the E-15 M to E-6 M range (Figure 3.123). The CV curves did not indicate a variation in anodic and cathodic currents (Figure 3.124).

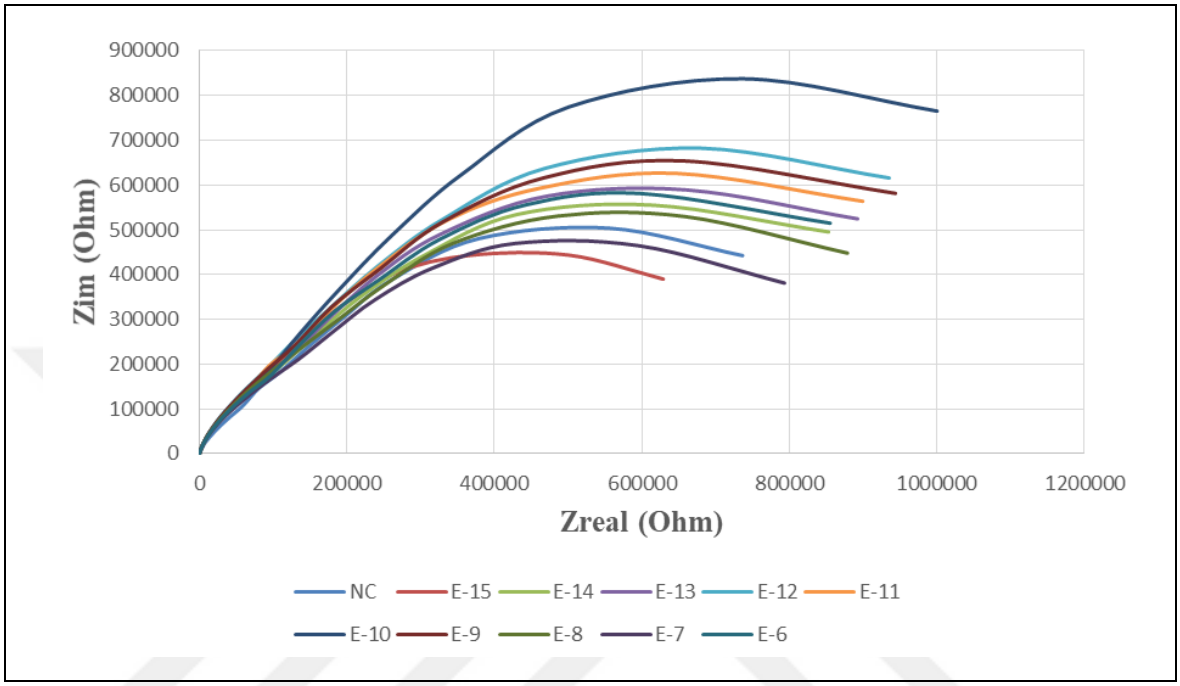

Figure 3.122. EIS response of Au-0.3M-Val-UMIP electrode.

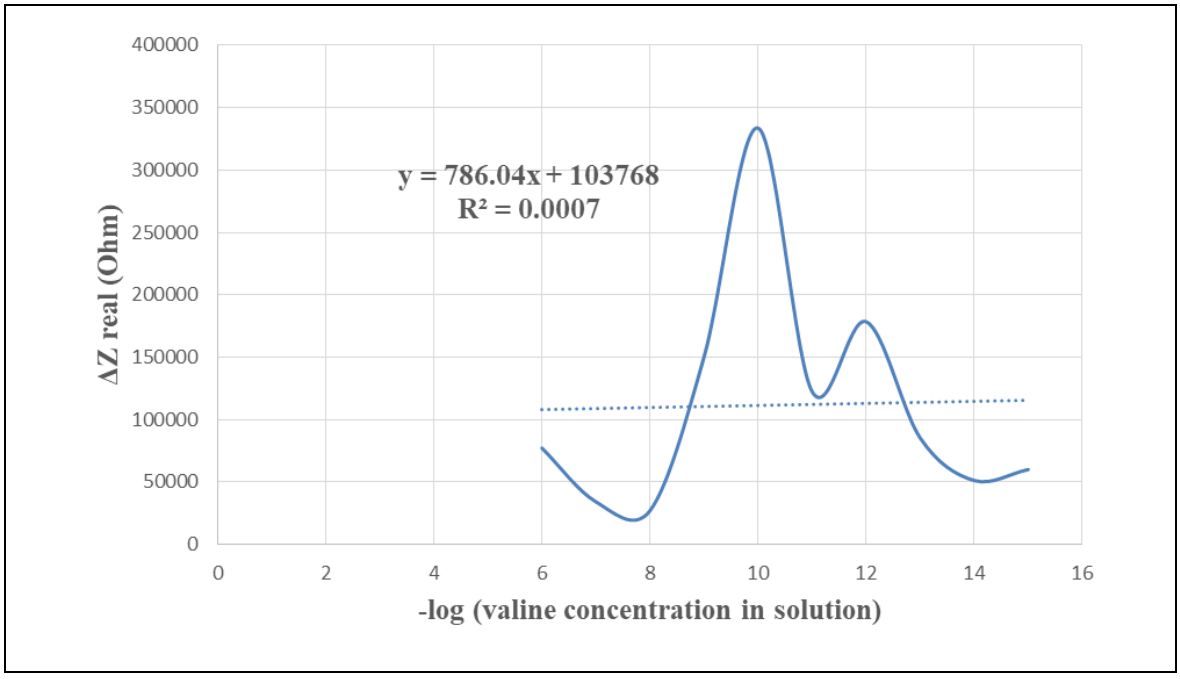

Figure 3.123. The regression curve of Au-0.3M-Val-UMIP electrode.

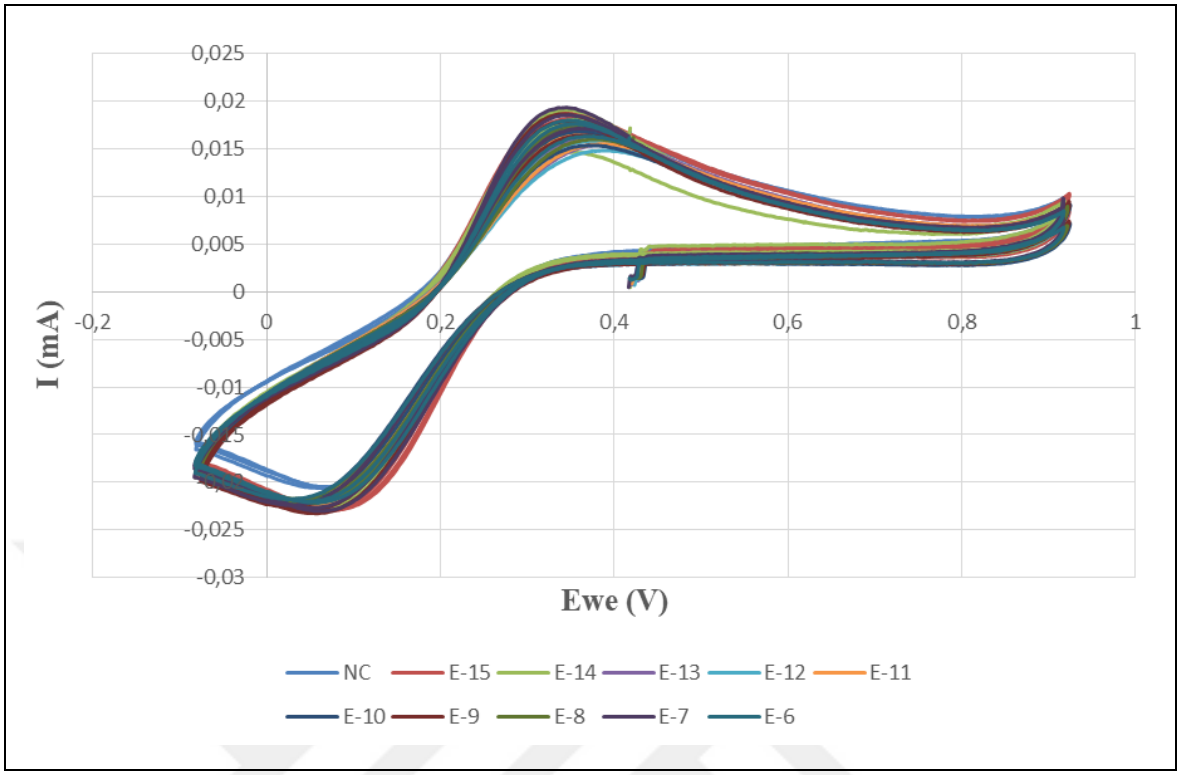

Figure 3.124. CV response of Au-0.3M-Val-UMIP electrode.

The Au-0.325M-Val-UMIP electrode was insufficient to detected the valine molecule, with a 0.96 percent success rate in the E-15 M to E-6 M range and 7.53 percent in the E-14 M to E-6 M range (Figures 3.125-3.128). The CV curves did not indicate a variation in anodic and cathodic currents (Figures 3.129, 3.130).

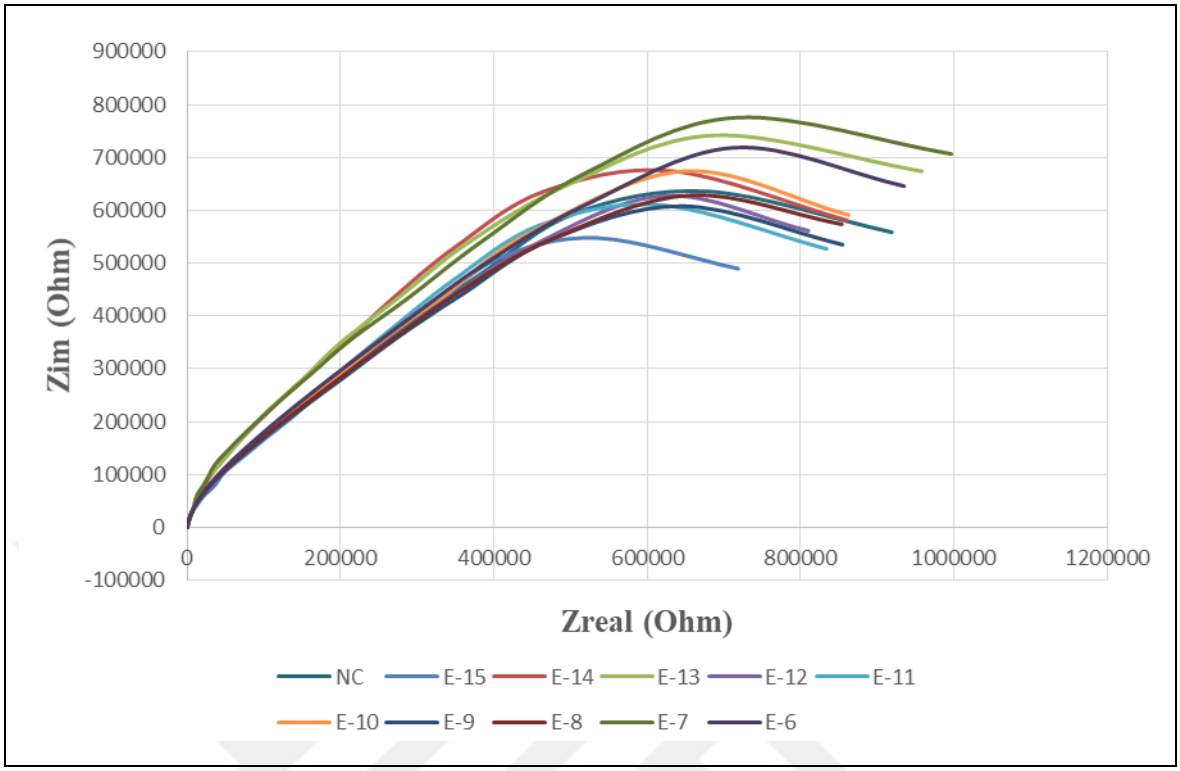

Figure 3.125. EIS response of Au-0.325M-Val-UMIP electrode.

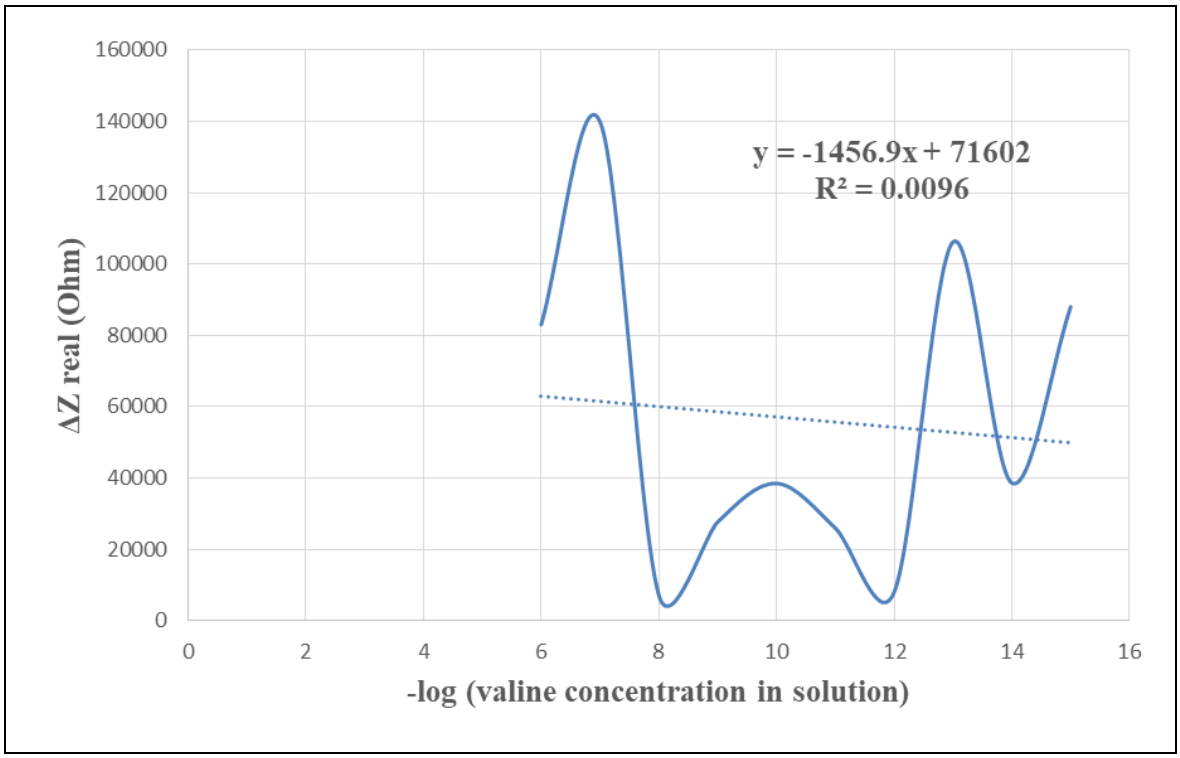

Figure 3.126. The regression curve of Au-0.325M-Val-UMIP electrode.

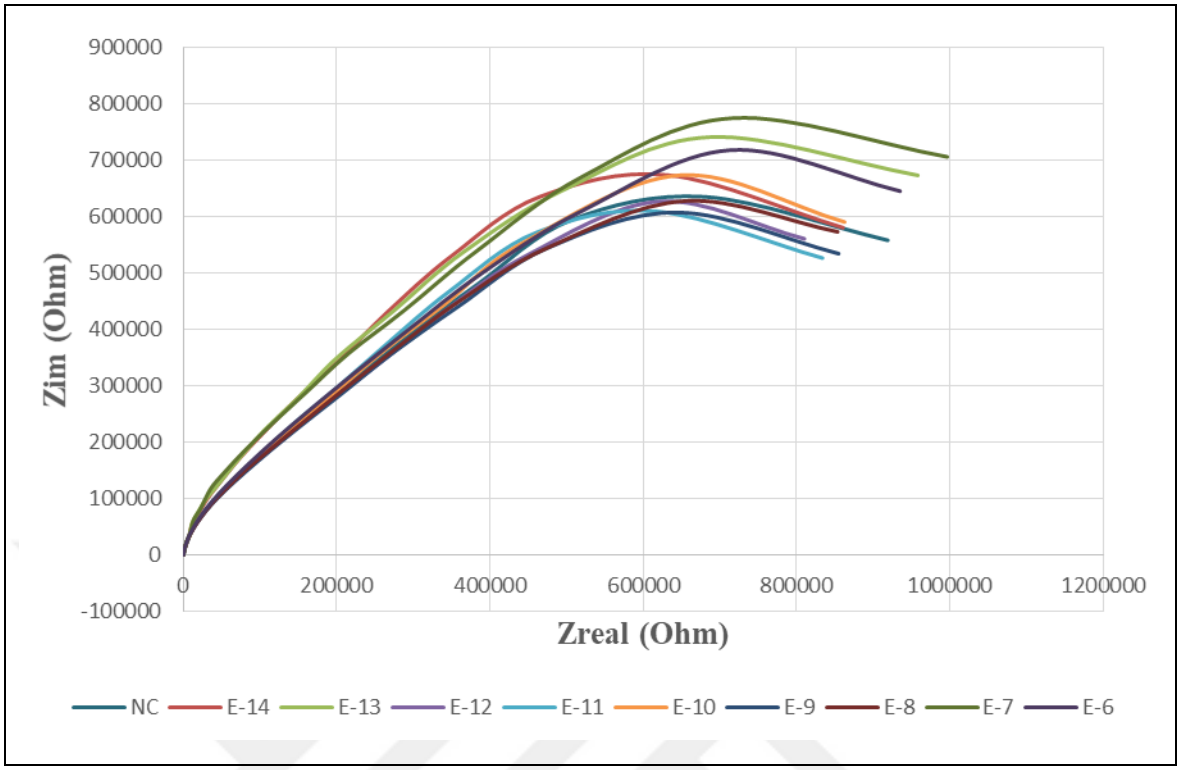

Figure 3.127. EIS response of the Au-0.325M-Val-UMIP electrode.

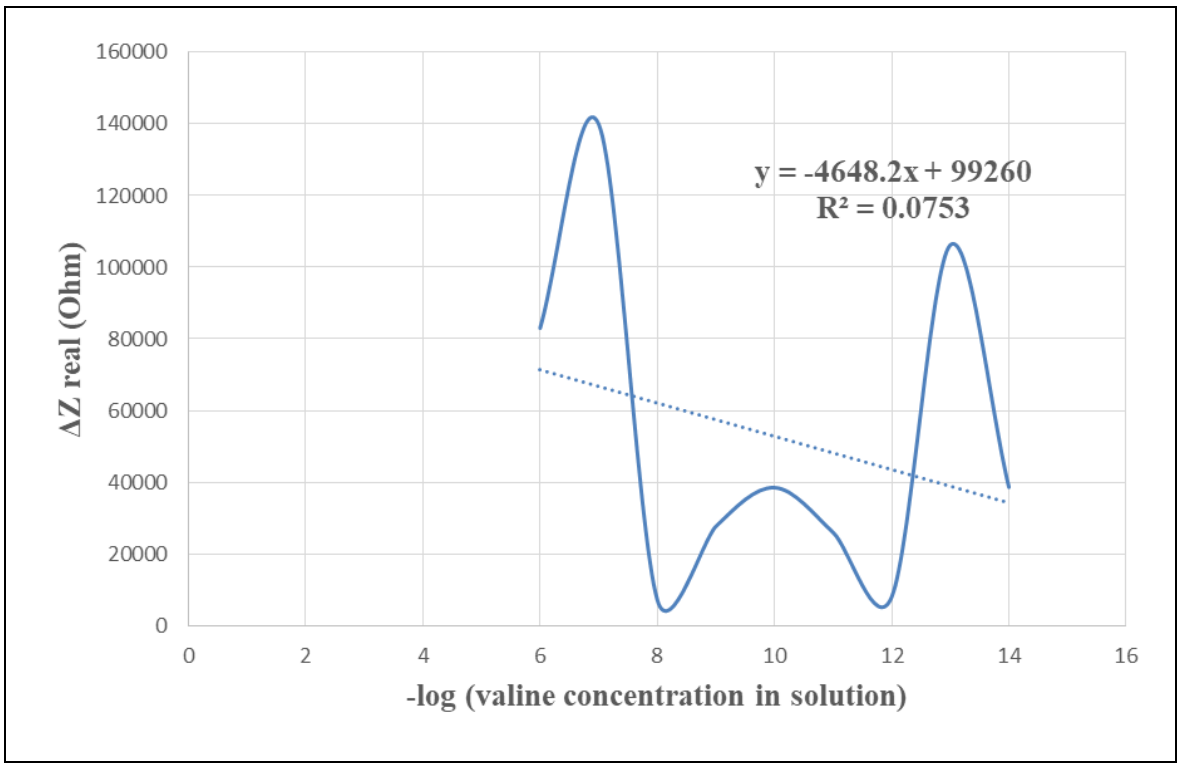

Figure 3.128. The regression curve of Au-0.325M-Val-UMIP electrode.

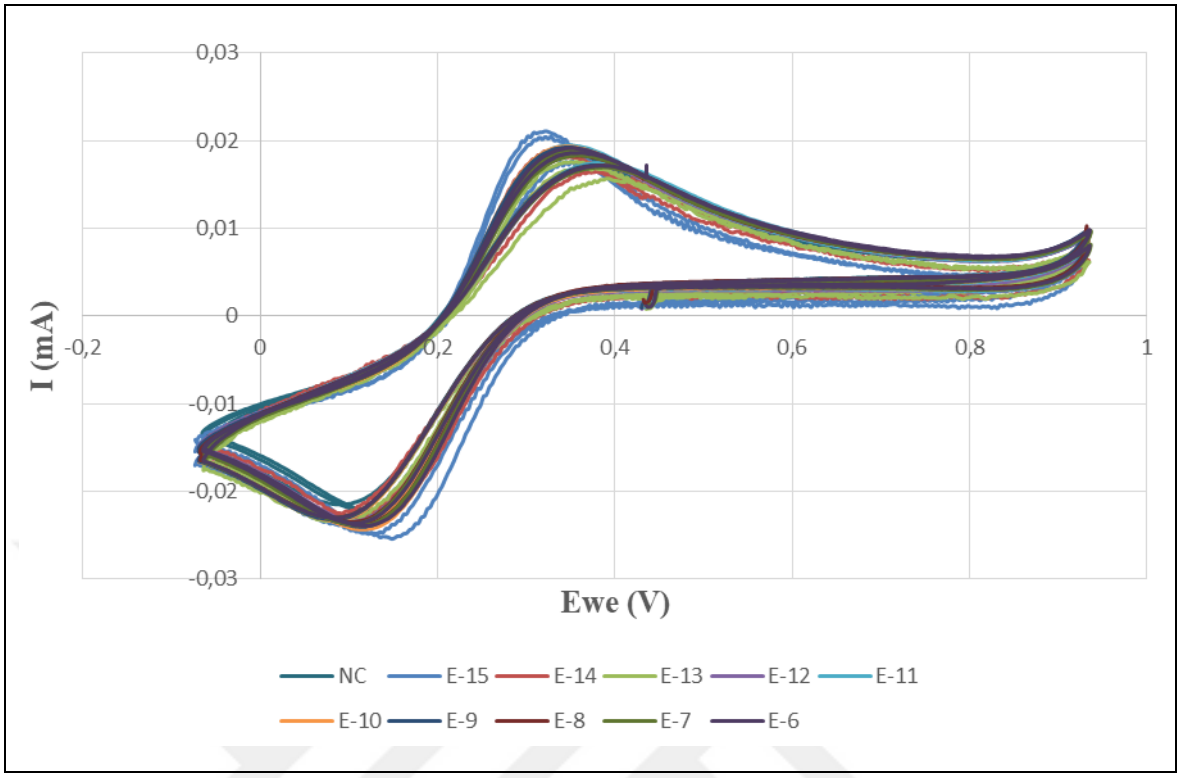

Figure 3.129. CV response of Au-0.325M-Val-UMIP electrode.

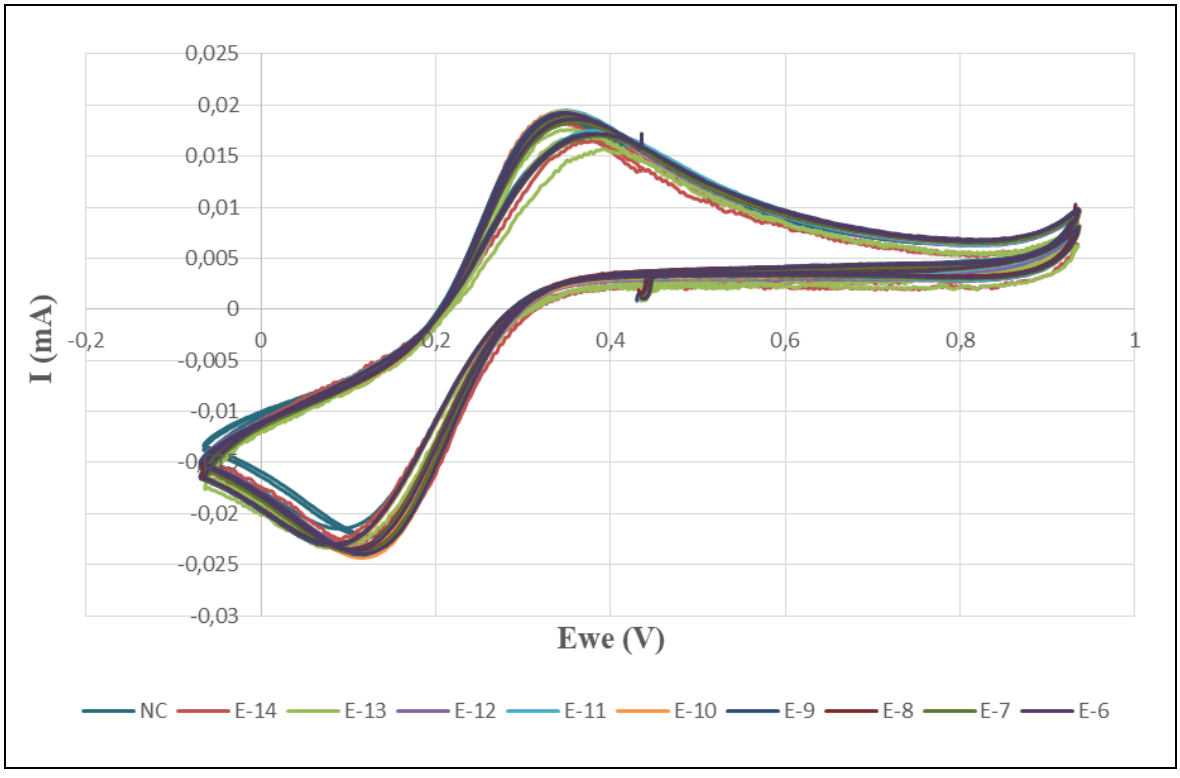

Figure 3.130. CV response of the Au-0.325M-Val-UMIP electrode.

The Au-0.35M-Val-UMIP electrode was insufficient to detected the valine molecule, with a 13.51 percent success rate in the E-15 M to E-6 M range and 0.01 percent in the E-14 M to E-7 M range (Figures 3.131-3.134). The CV curves did not indicate a variation in anodic and cathodic currents (Figures 3.135, 3.136).

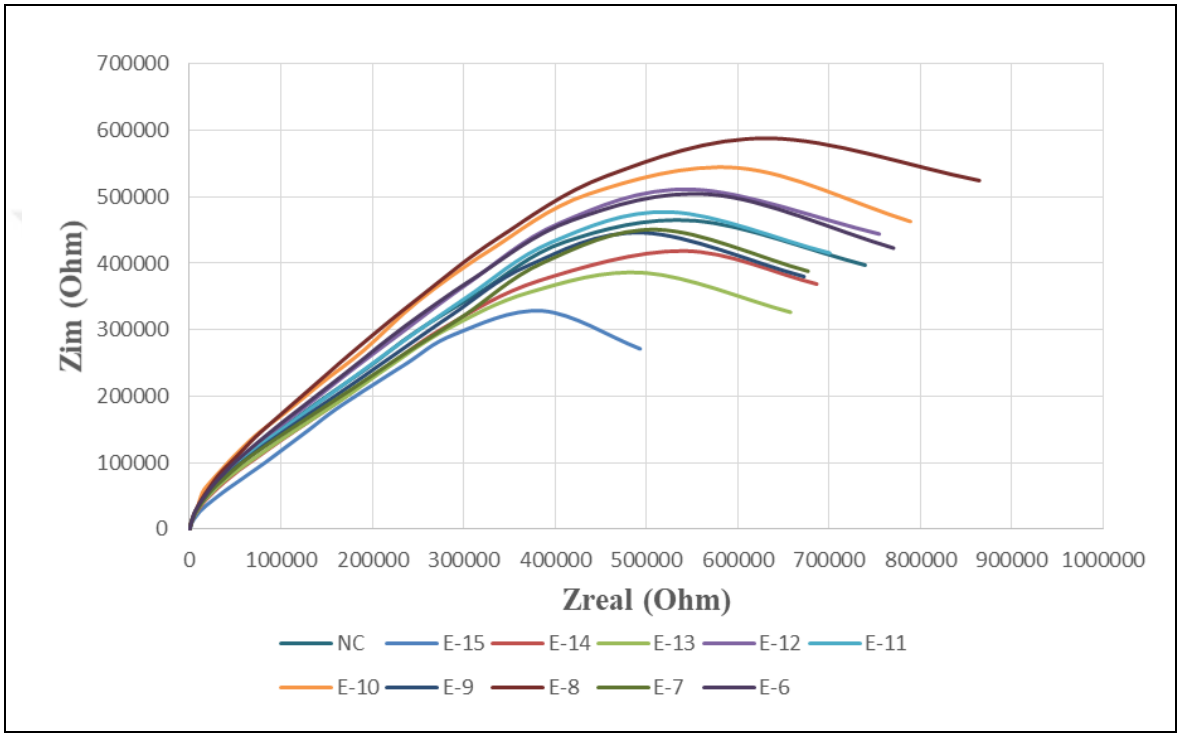

Figure 3.131. EIS response of Au-0.35M-Val-UMIP electrode.

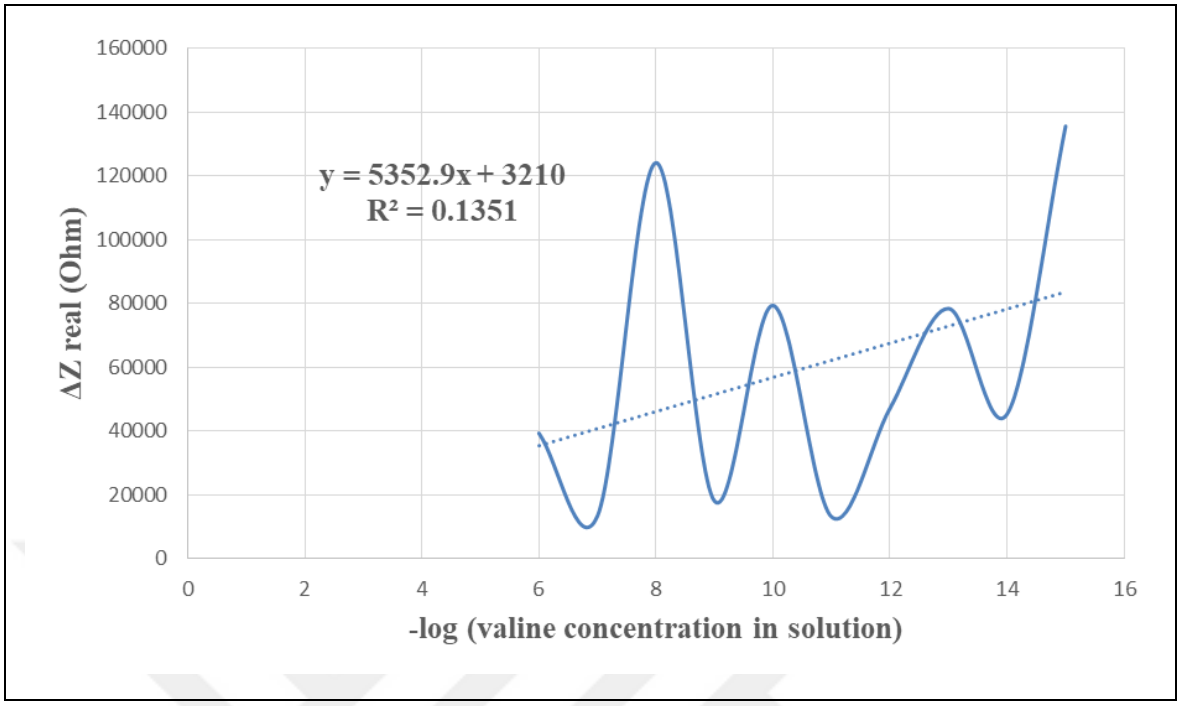

Figure 3.132. The regression curve of Au-0.35M-Val-UMIP electrode.

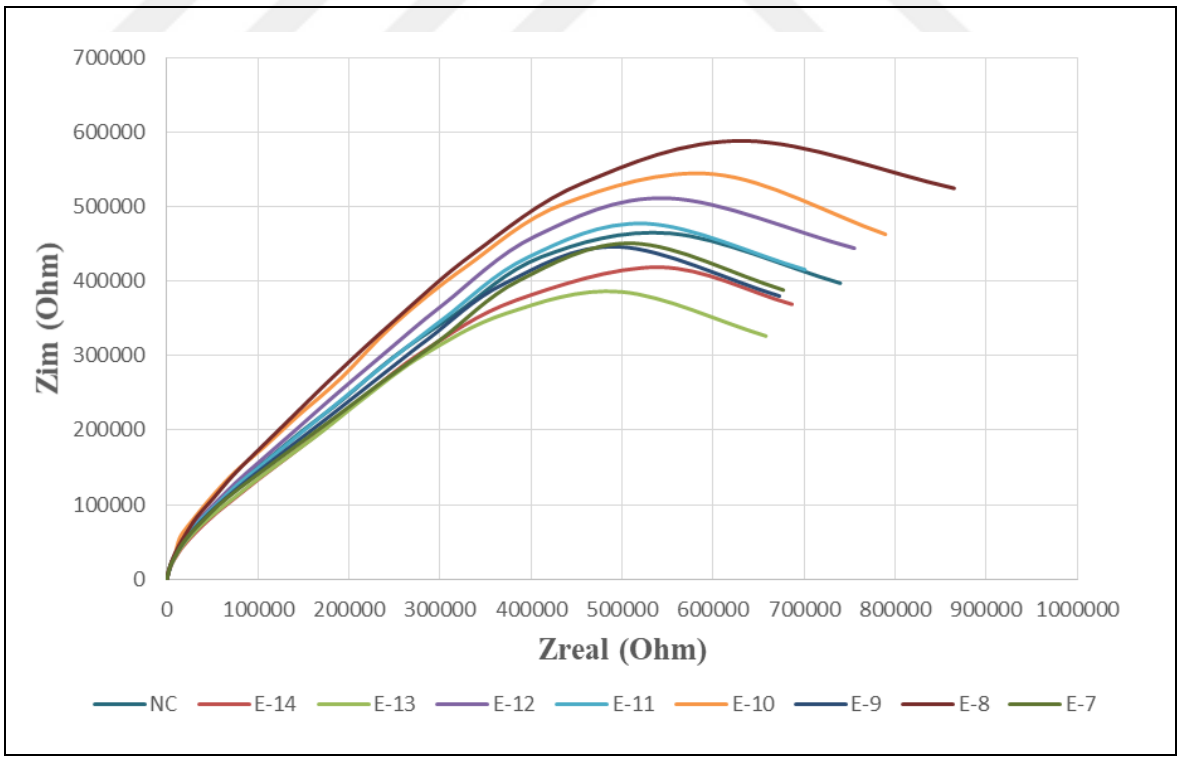

Figure 3.133. EIS response of the Au-0.35M-Val-UMIP electrode.

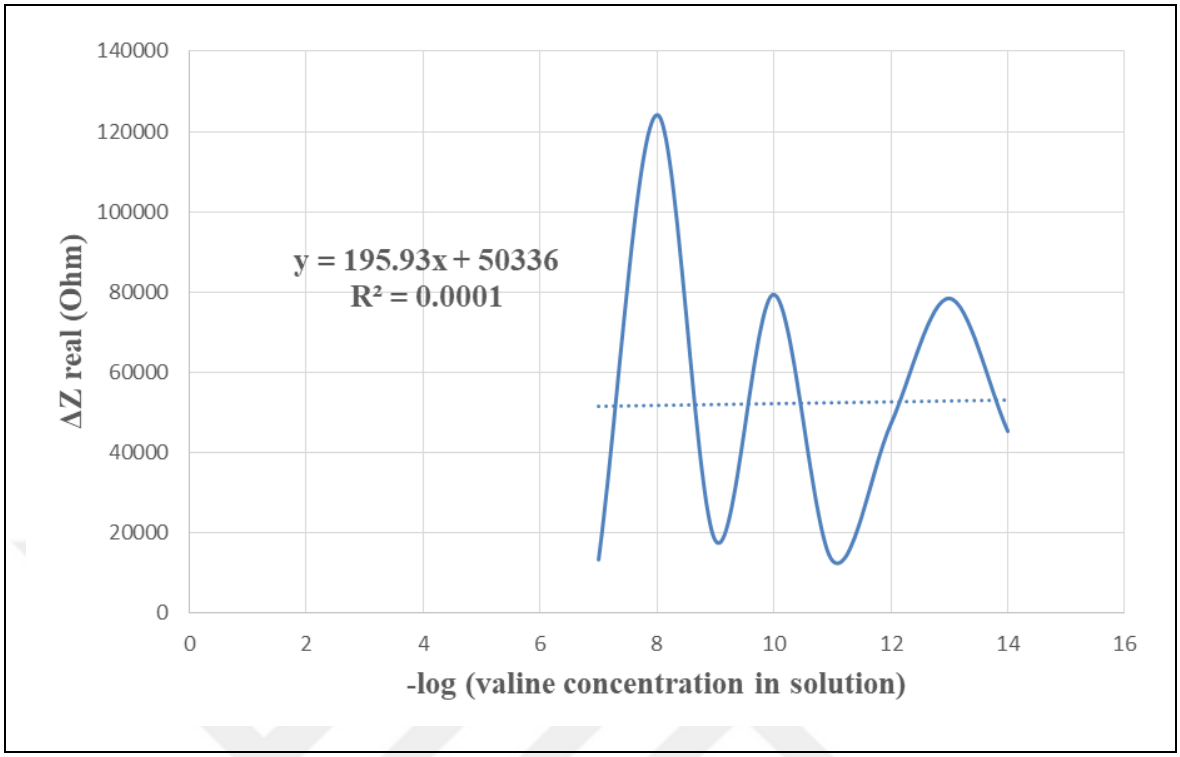

Figure 3.134. The regression curve of Au-0.35M-Val-UMIP electrode.

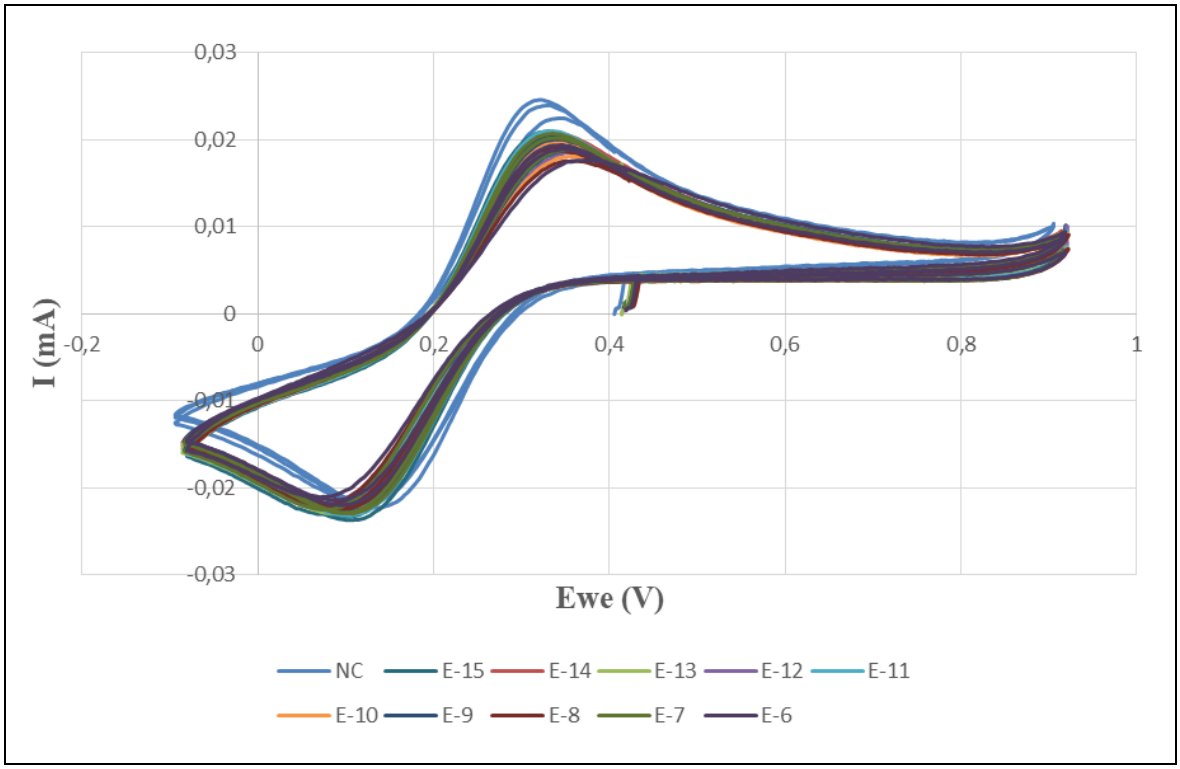

Figure 3.135. CV response of Au-0.35M-Val-UMIP electrode.

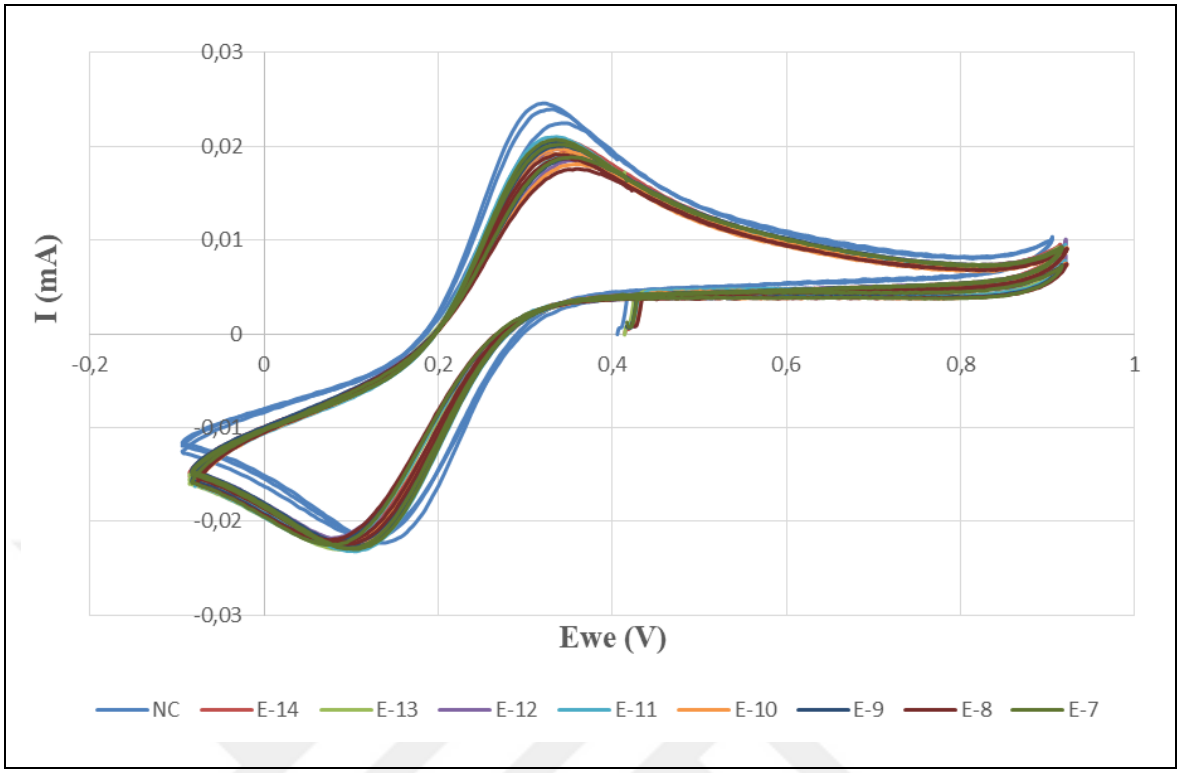

Figure 3.136. CV response of the Au-0.35M-Val-UMIP electrode.

The Au-0.4M-Val-UMIP electrode was insufficient to detected the valine molecule, with a 1.59 percent success rate in the E-15 M to E-6 M range and 15.39 percent in the E-14 M to E-7 M range (Figures 3.137-3.140). The CV curves did not indicate a variation in anodic and cathodic currents (Figures 3.141, 3.142).

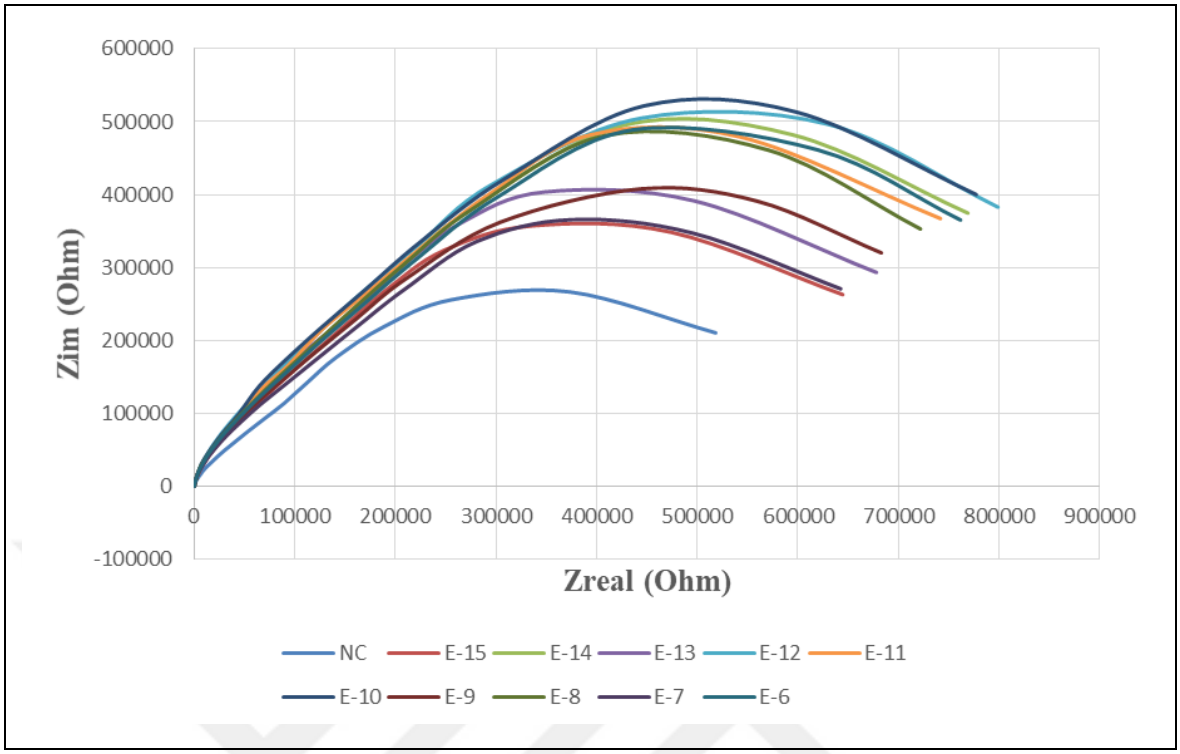

Figure 3.137. EIS response of Au-0.4M-Val-UMIP electrode.

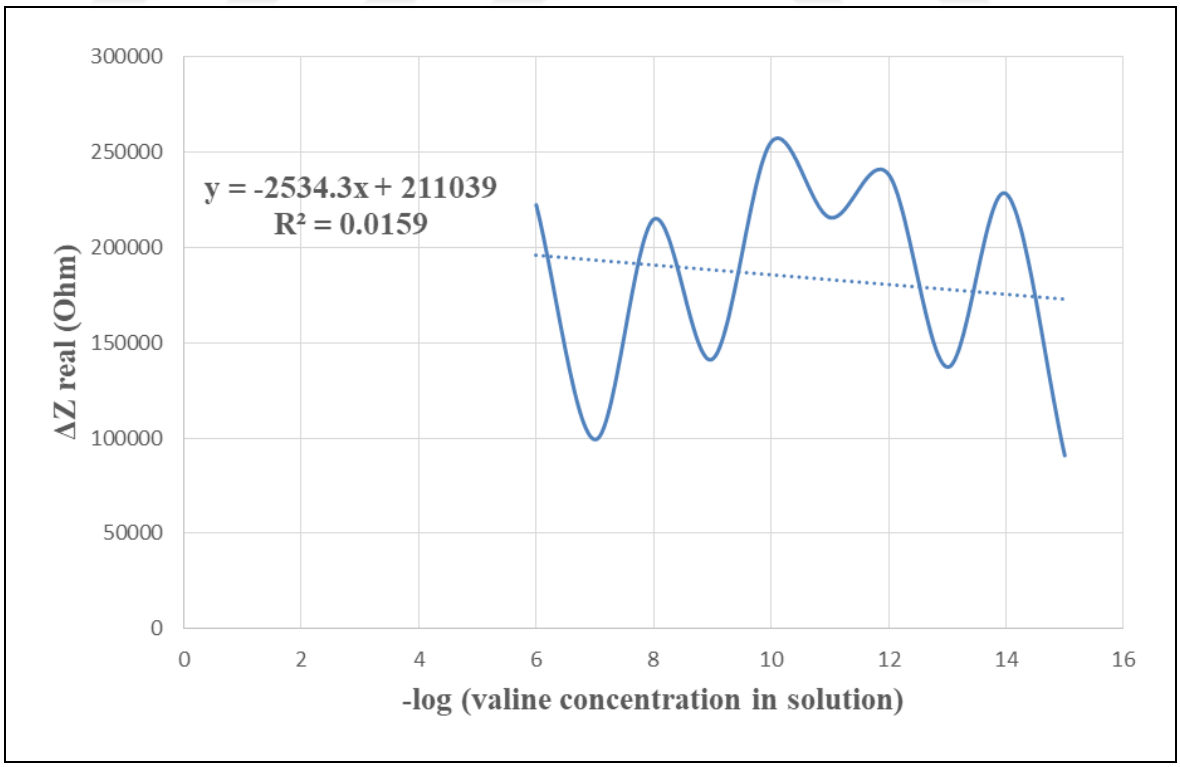

Figure 3.138. The regression curve of Au-0.4M-Val-UMIP electrode.

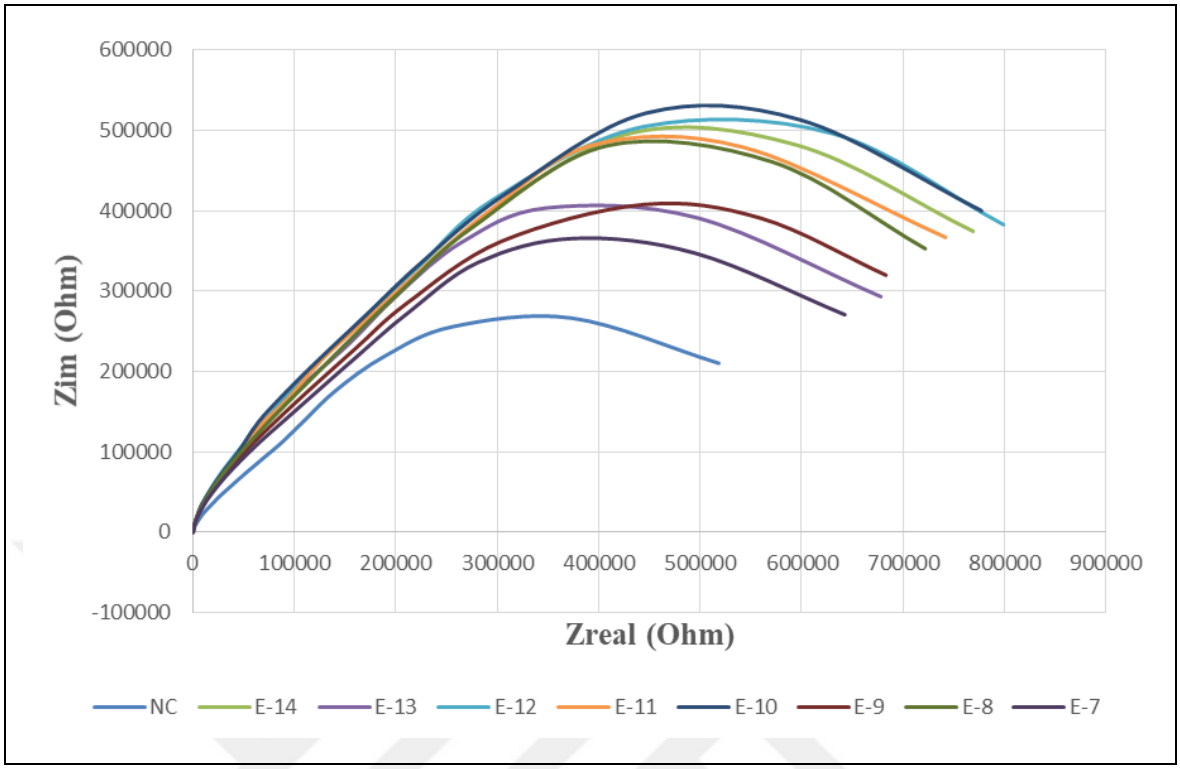

Figure 3.139. EIS response of the Au-0.4M-Val-UMIP electrode.

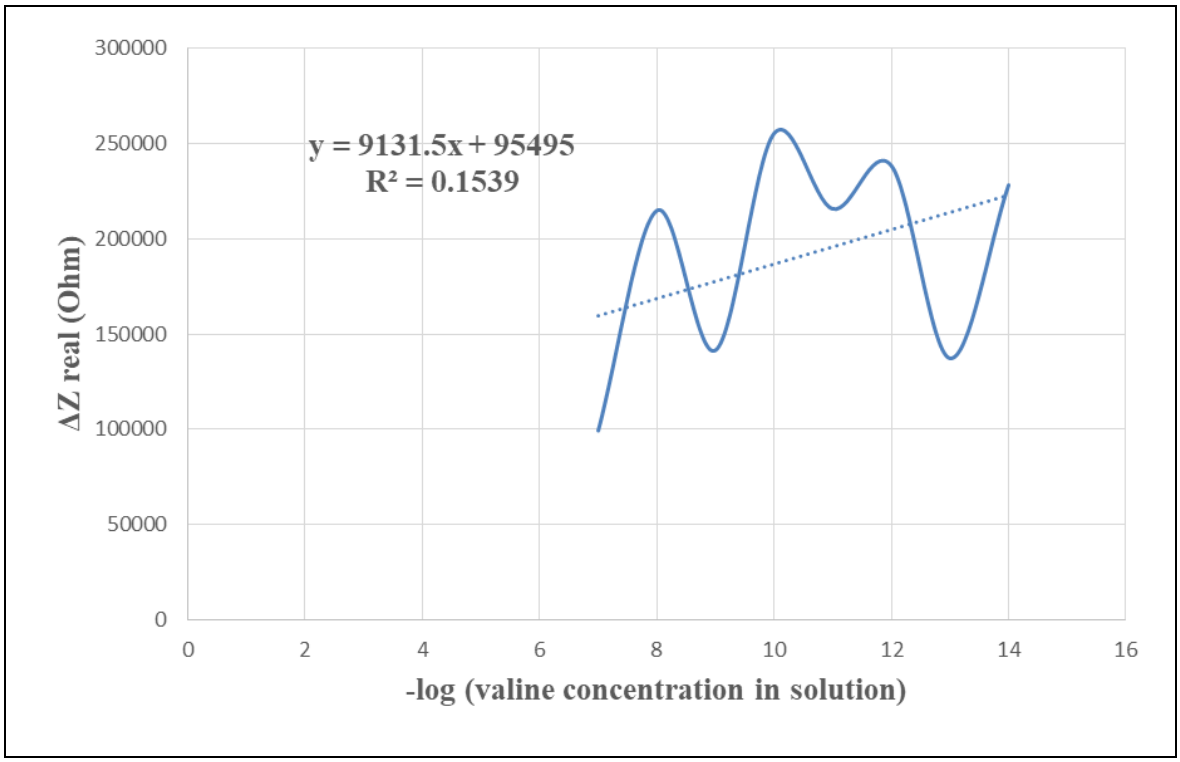

Figure 3.140. The regression curve of Au-0.4M-Val-UMIP electrode.

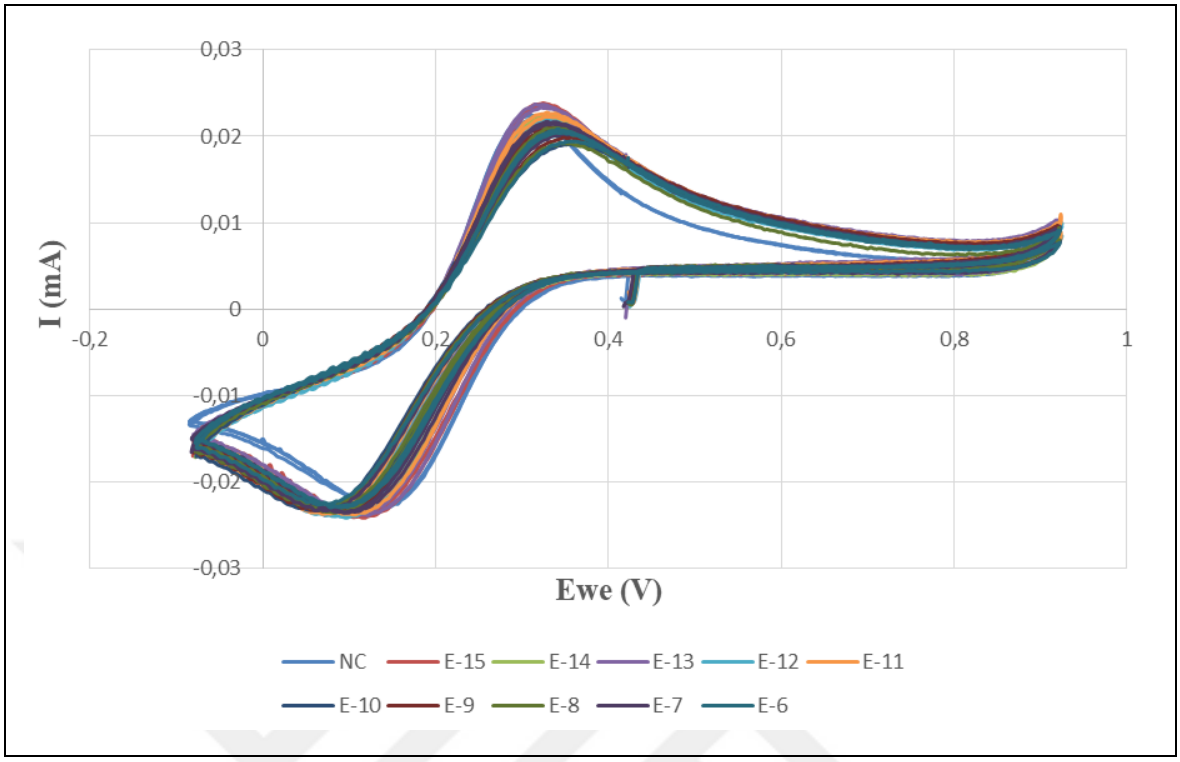

Figure 3.141. CV response of Au-0.4M-Val-UMIP electrode.

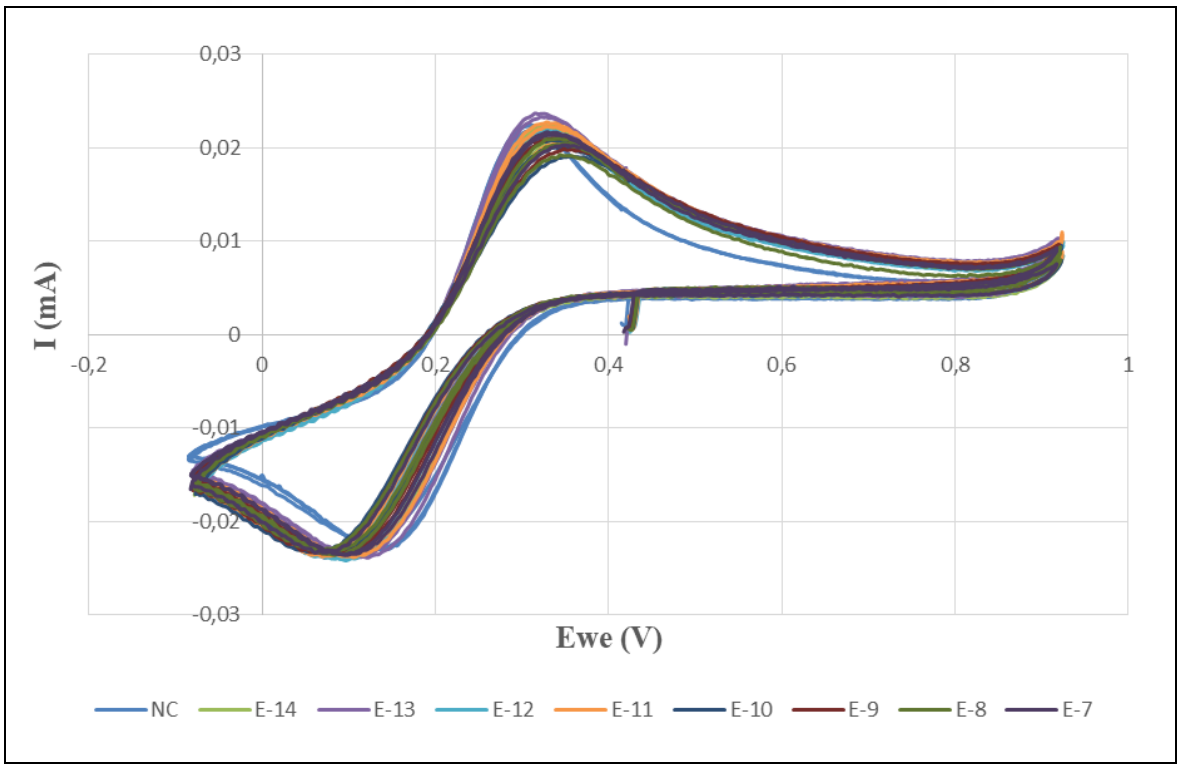

Figure 3.142. CV response of the Au-0.4M-Val-UMIP electrode.

The Au-0.45M-Val-UMIP electrode was insufficient to detected the valine molecule, with a 4.33 percent success rate in the E-15 M to E-6 M range and 45.87 percent in the E-12 M to E-7 M range (Figures 3.143-3.146). The CV curves did not indicate a variation in anodic and cathodic currents (Figures 3.147, 3.148).

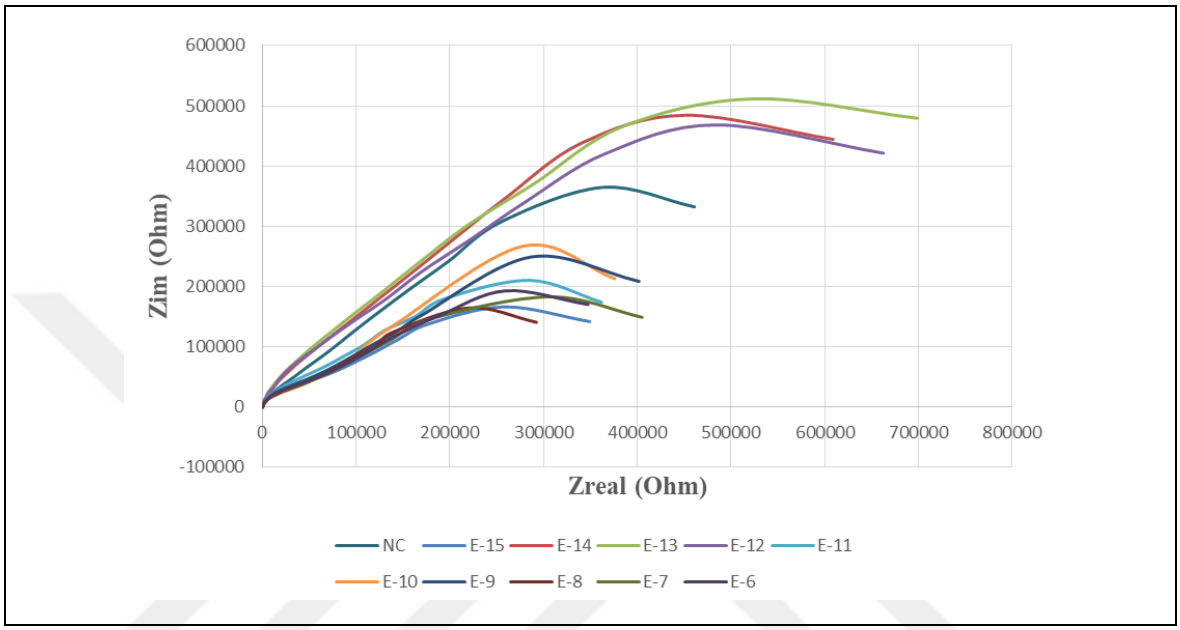

Figure 3.143. EIS response of Au-0.45M-Val-UMIP electrode.

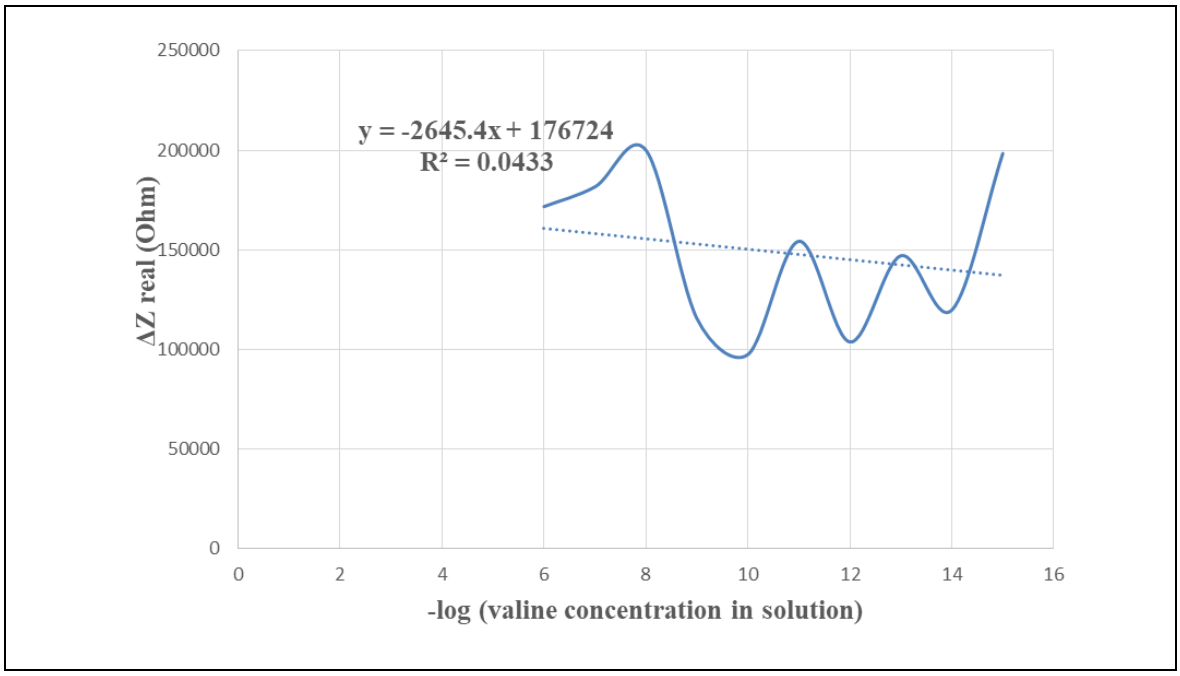

Figure 3.144. The regression curve of Au-0.45M-Val-UMIP electrode.

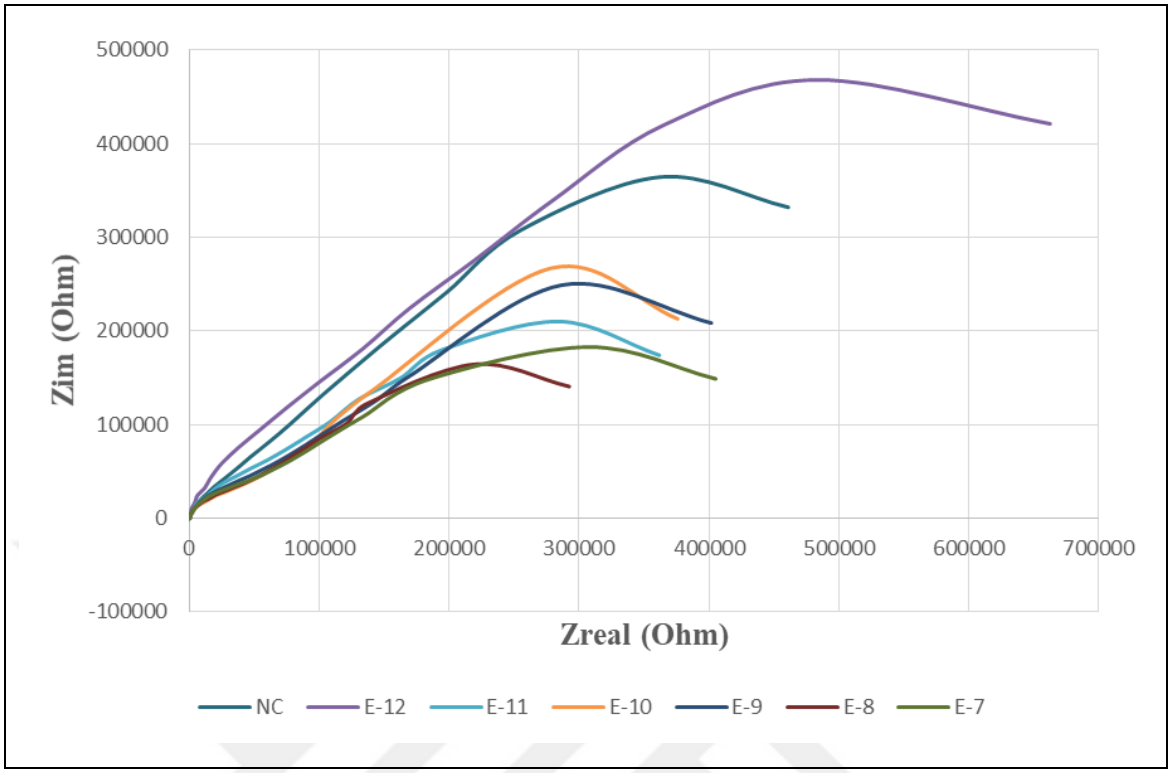

Figure 3.145. EIS response of the Au-0.45M-Val-UMIP electrode.

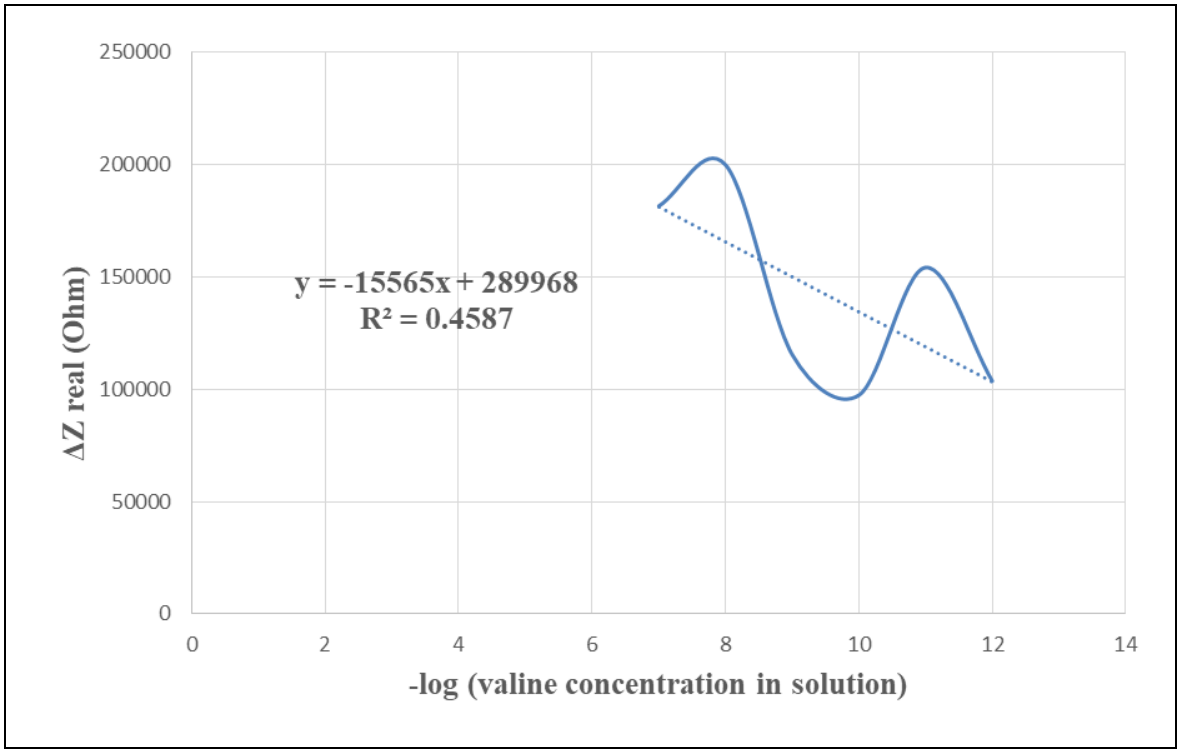

Figure 3.146. The regression curve of Au-0.45M-Val-UMIP electrode.

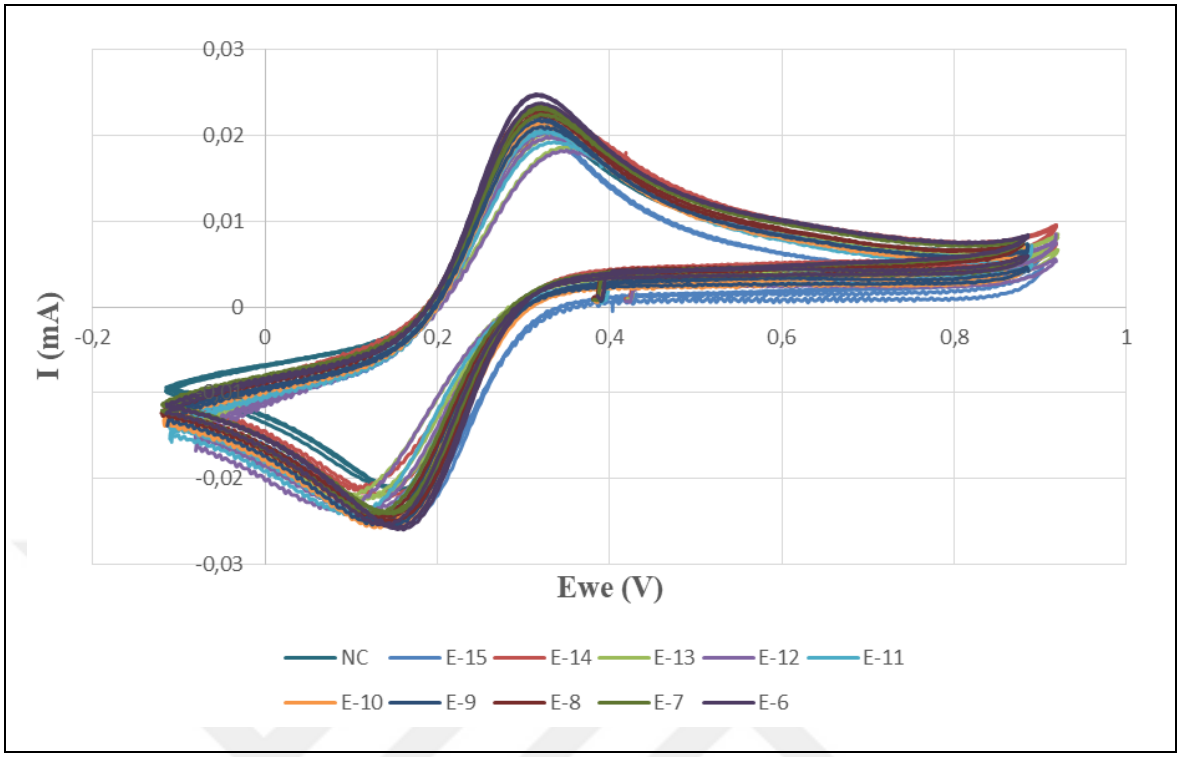

Figure 3.147. CV response of Au-0.45M-Val-UMIP electrode.

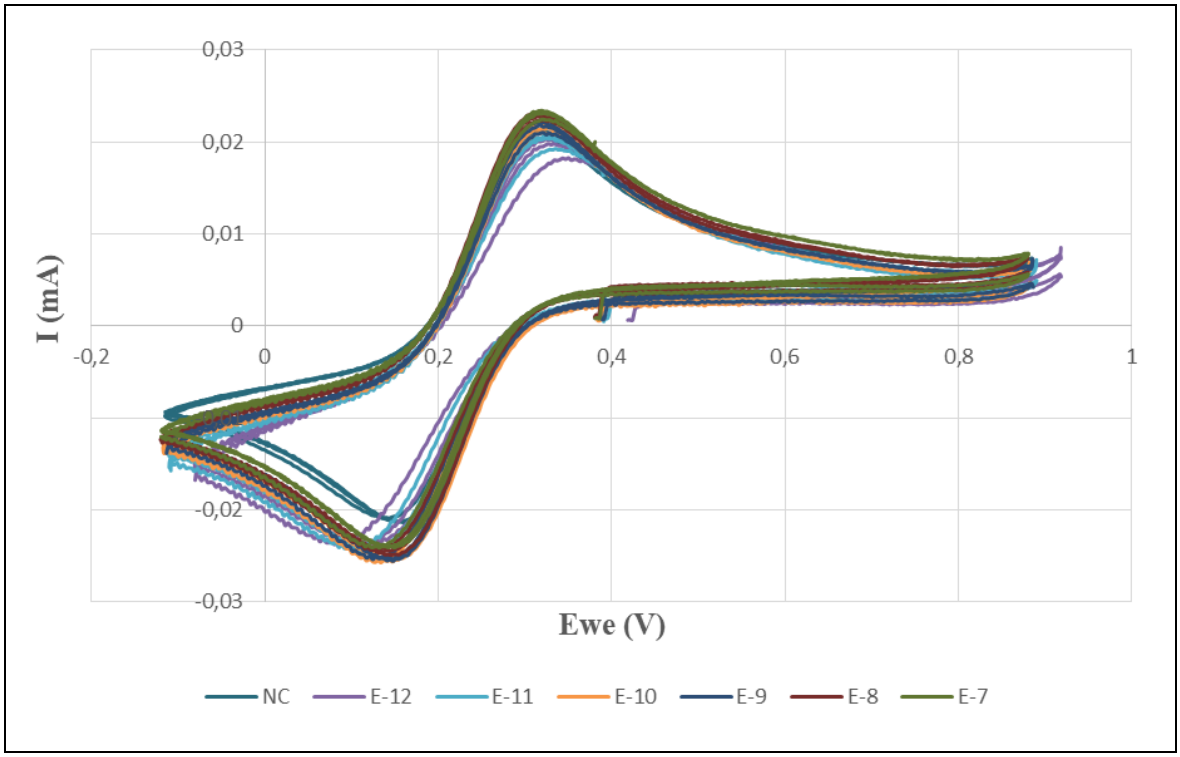

Figure 3.148. CV response of the Au-0.45M-Val-UMIP electrode.

The Au-0.5M-Val-UMIP electrode was insufficient to detected the valine molecule, with a 7.25 percent success rate in the E-15 to E-6 M range and 53.19 percent in the E-12 to E-8 M range (Figures 3.149-3.152). The CV curves did not indicate a variation in anodic and cathodic currents (Figures 3.153, 3.154).

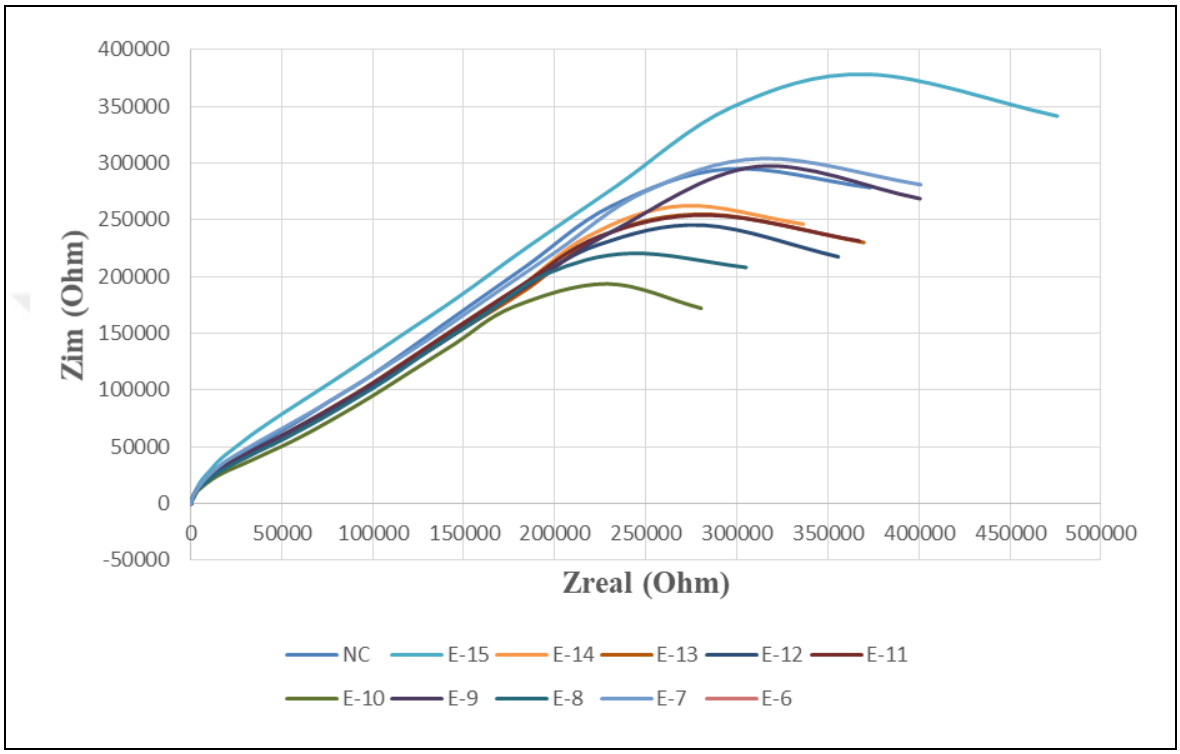

Figure 3.149. EIS response of Au-0.5M-Val-UMIP electrode.

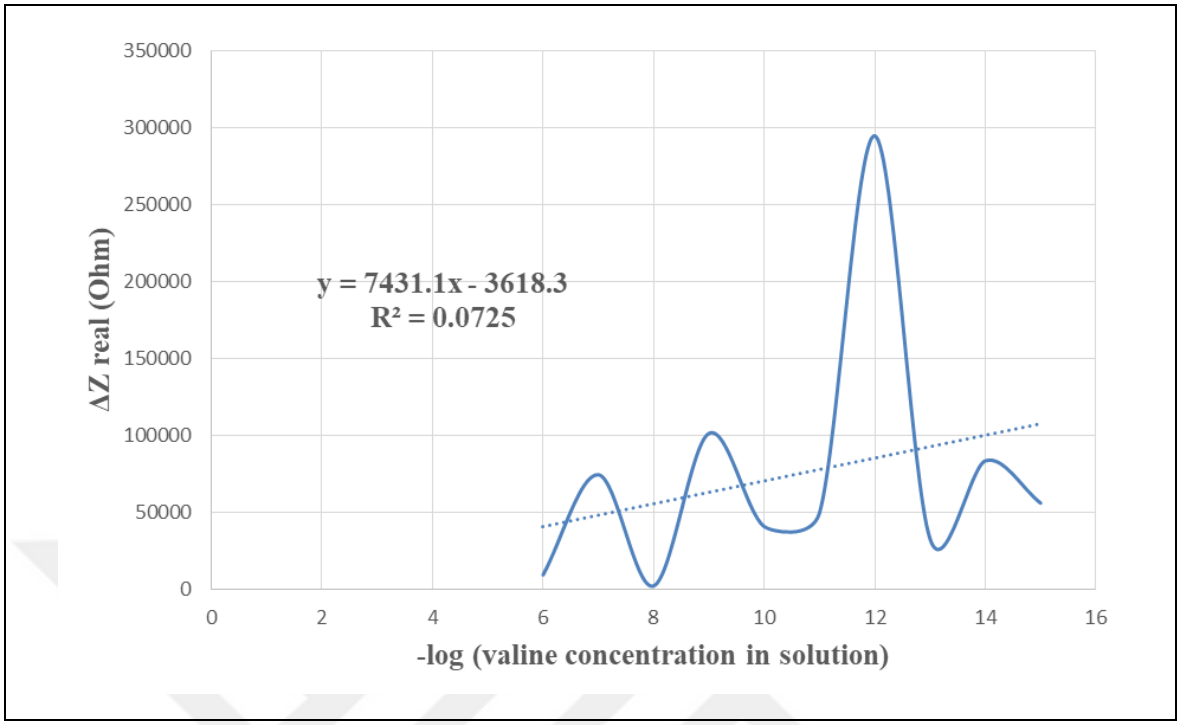

Figure 3.150. The regression curve of Au-0.5M-Val-UMIP electrode.

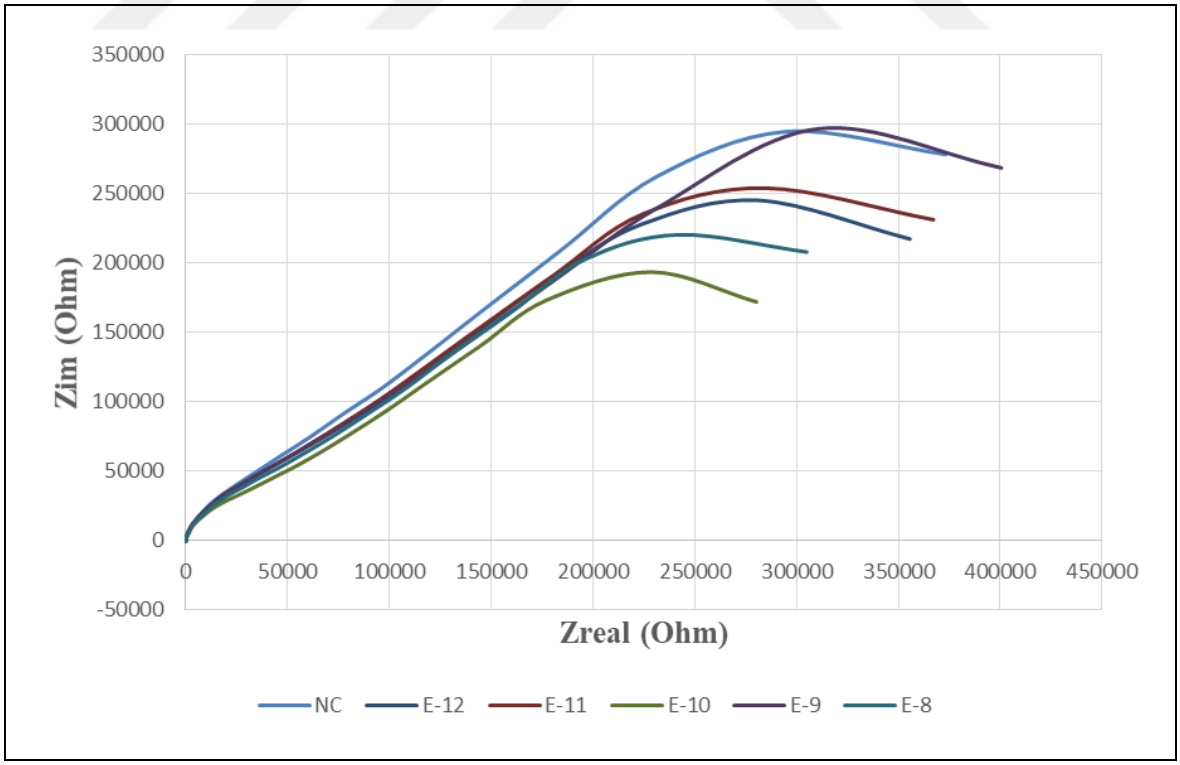

Figure 3.151. EIS response of the Au-0.5M-Val-UMIP electrode.

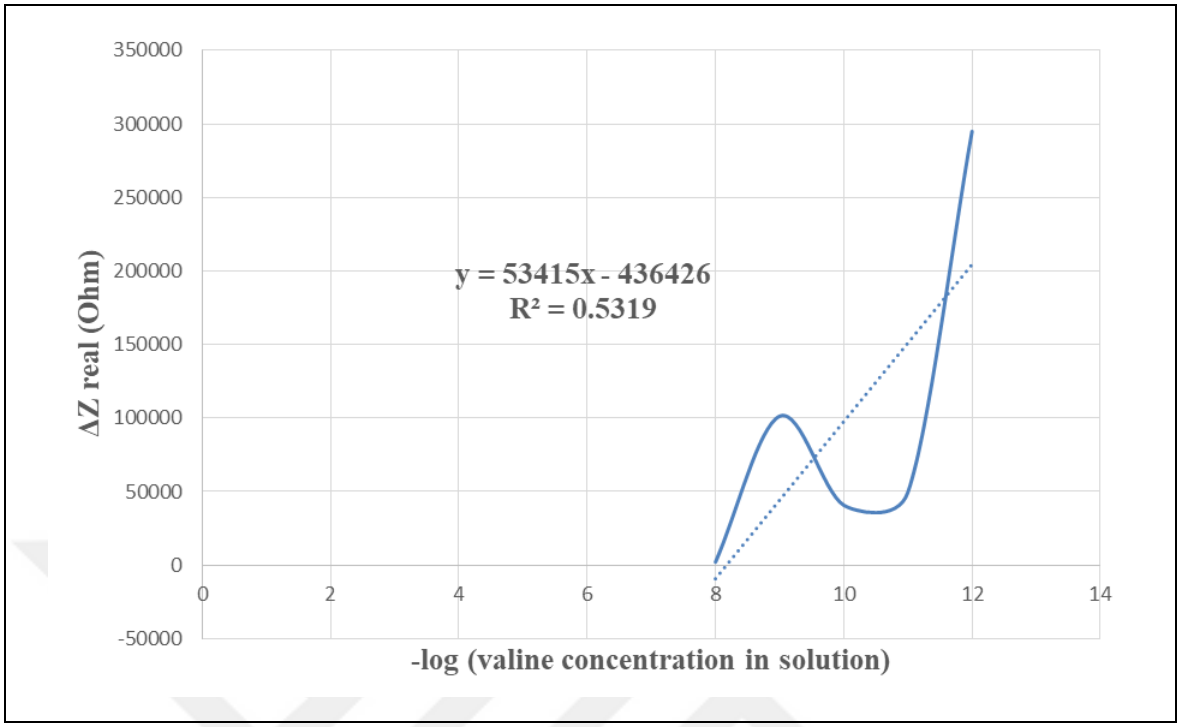

Figure 3.152. The regression curve of Au-0.5M-Val-UMIP electrode.

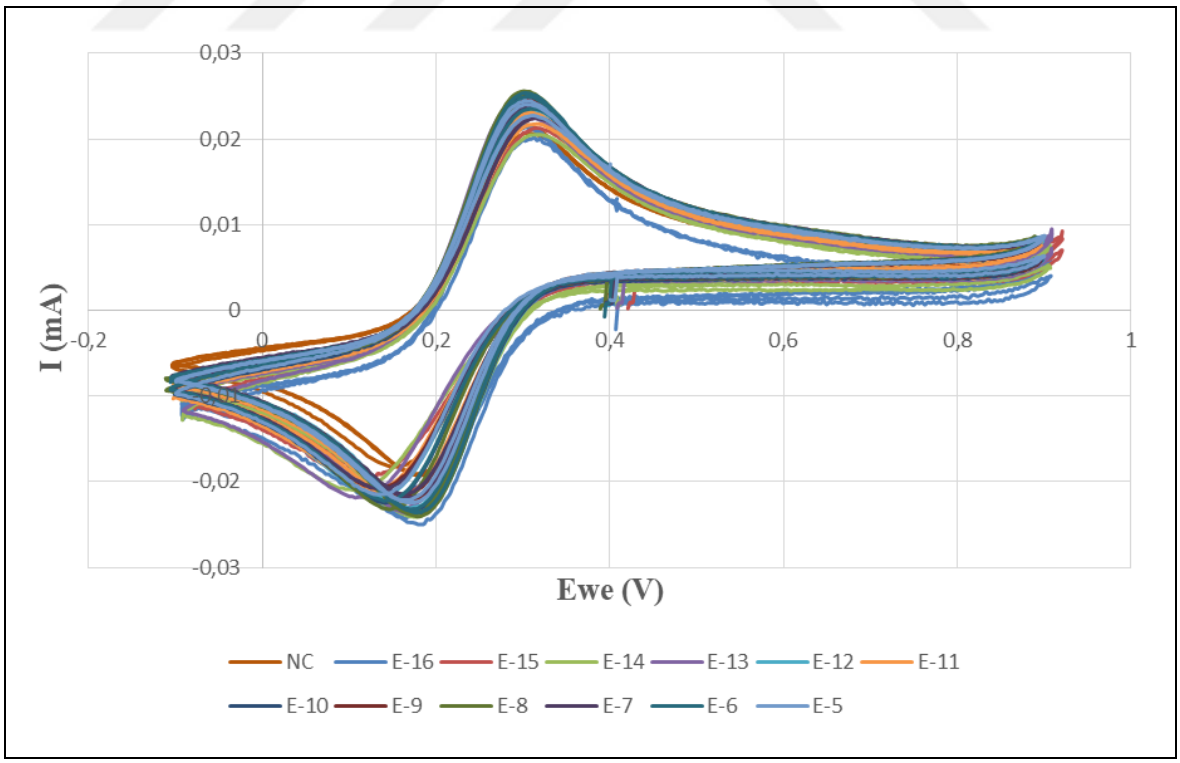

Figure 3.153. CV response of Au-0.5M-Val-UMIP electrode.

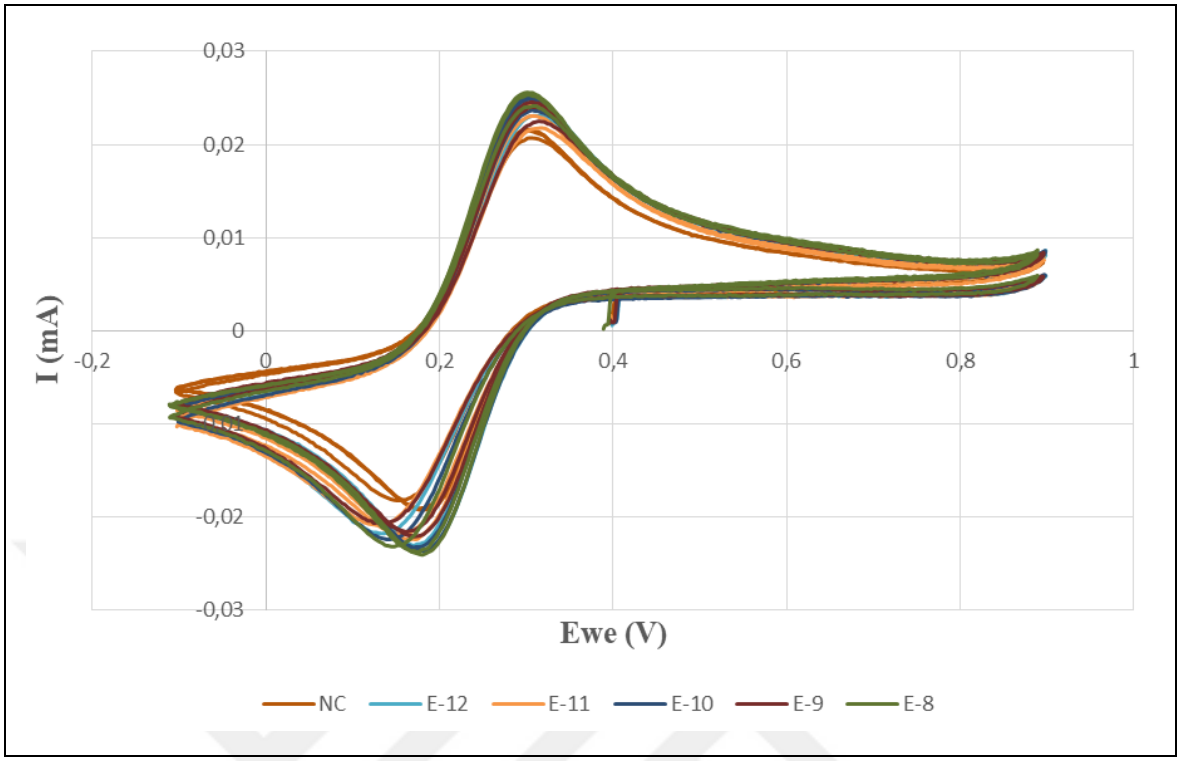

Figure 3.154. CV response of the Au-0.5M-Val-UMIP electrode.

3.3. REPRODUCIBILITY, PRECISION, STABILITY

Consistency within and between groups was examined to determine precision of the findings. Reliability refers to the repeatability or consistency of the measurement process in a measurement mechanism. The measurements taken are expected to be stable over time.

Anodic peak currents and corresponding anodic peak voltage values were found for each electrode as shown in Tables 3.3, 3.4, 3.5 and 3.6.

Table 3.3. Anodic peak current and anodic peak voltage values of electrodes.

Intra day	Electrode	1 st hour		2 nd hour		3 rd hour	
		Anodic current (mA)	Anodic voltage (V)	Anodic current (mA)	Anodic voltage (V)	Anodic current (mA)	Anodic voltage (V)
MIP	PGE-1	0.424050	0.331694	0.421790	0.334065	0.4313958	0.333743
	PGE-2	0.367811	0.326078	0.389933	0.325752	0.4033830	0.322080
	PGE-3	0.395170	0.324933	0.390497	0.327087	0.3857503	0.328411
	PGE-4	0.332799	0.337761	0.335222	0.339420	0.3330750	0.337787
	PGE-5	0.377362	0.335769	0.362534	0.334132	0.3579053	0.332792

	PGE-6	0.424942	0.327199	0.434407	0.323770	0.4539380	0.323473
UMIP	PGE-7	0.553566	0.325795	0.575905	0.321773	0.5862724	0.321446
	PGE-8	0.587927	0.325265	0.594608	0.321133	0.5881218	0.317110
	PGE-9	0.469173	0.331114	0.460677	0.324166	0.4531312	0.322437
	PGE-10	0.449011	0.321120	0.453223	0.315437	0.4460641	0.312747
	PGE-11	0.427092	0.323110	0.437753	0.317800	0.4255953	0.315128
	PGE-12	0.505353	0.322796	0.501488	0.322789	0.4933550	0.321788
NIP	PGE-13	0.491276	0.342871	0.471402	0.338910	0.4606160	0.338578
	PGE-14	0.439341	0.334766	0.419722	0.331317	0.4026304	0.332351
	PGE-15	0.505266	0.333441	0.509591	0.334011	0.4883829	0.333675
	PGE-16	0.508934	0.330127	0.480027	0.327374	0.4548552	0.327709
	PGE-17	0.579001	0.337693	0.554089	0.339359	0.5408117	0.334029
	PGE-18	0.556479	0.321036	0.514289	0.318381	0.4899834	0.320067

Table 3.4. Peak anodic current (Ip_a-mA) and peak anodic voltage (Ep_a-V) values of MIP electrodes.

MIP		PGE-1	PGE-2	PGE-3	PGE-4	PGE-5	PGE-6
Day 1	Ip_a	0.4089407	0.3478010	0.2966416	0.3263889	0.3665241	0.37152957
	Ep_a	0.3321993	0.3301058	0.3504380	0.3311981	0.3288320	0.34571731
Day 4	Ip_a	0.4081392	0.4256628	0.3439507	0.3611454	0.3952936	0.30605188
	Ep_a	0.3403731	0.3377154	0.3461460	0.3334094	0.3337984	0.34372061
Day 7	Ip_a	0.3406077	0.3797690	0.2732275	0.4128365	0.4540254	0.32545976
	Ep_a	0.3279375	0.3398182	0.3457608	0.3323867	0.3413096	0.34803691
Day 10	Ip_a	0.3354126	0.3773254	0.2872356	0.4169027	0.4695491	0.32651124
	Ep_a	0.3306342	0.3369938	0.3433909	0.3389927	0.3433404	0.34568893
Day 13	Ip_a	0.3469902	0.3416014	0.2913625	0.4246686	0.4262946	0.33395588
	Ep_a	0.3323483	0.3363555	0.3453806	0.3417198	0.3440364	0.34635421
Day 16	Ip_a	0.3747387	0.4246780	0.3258322	0.4220990	0.4246499	0.32988524
	Ep_a	0.3375882	0.3360749	0.3476116	0.3350181	0.3296378	0.34437975
Day 19	Ip_a	0.3544216	0.4179592	0.3317544	0.4242242	0.4414513	0.33902426
	Ep_a	0.3430554	0.3377470	0.3517116	0.3350161	0.3327127	0.34403821
Day 22	Ip_a	0.3706355	0.3986793	0.3409632	0.3939947	0.4460531	0.33274358
	Ep_a	0.3383857	0.3367534	0.3490625	0.3390180	0.3313709	0.34668219

Day 45	Ip_a	0.3727746	0.3837167	0.3008339	0.3346221	0.3752533	0.31329538
	Ep_a	0.3353146	0.3379816	0.3466284	0.3326754	0.3307542	0.34039884

Table 3.5. Peak anodic current (Ip_a-mA) and peak anodic voltage (Ep_a-V) values of UMIP electrodes.

UMIP		PGE-7	PGE-8	PGE-9	PGE-10	PGE-11	PGE-12
Day 1	Ip_a	0.5621707	0.4437909	0.5215064	0.4562559	0.3959200	0.47046045
	Ep_a	0.3237449	0.3231695	0.3254133	0.3270363	0.3207575	0.32353252
Day 4	Ip_a	0.5952803	0.4553259	0.5827317	0.5205158	0.4667991	0.45849106
	Ep_a	0.3261688	0.3314181	0.3307956	0.3306891	0.3254663	0.32705333
Day 7	Ip_a	0.6184842	0.4697999	0.5800888	0.5150096	0.4763858	0.45589432
	Ep_a	0.3300174	0.3273705	0.3257138	0.3284080	0.3257368	0.32771030
Day 10	Ip_a	0.5685482	0.4054562	0.4775815	0.4438375	0.4479145	0.41889229
	Ep_a	0.3240570	0.3255455	0.3311153	0.3282130	0.3285325	0.32473349
Day 13	Ip_a	0.5783843	0.4101855	0.4666601	0.4555474	0.4468235	0.43132979
	Ep_a	0.3254226	0.3284133	0.3280401	0.3301074	0.3270801	0.32508316
Day 16	Ip_a	0.4590150	0.4171956	0.4804888	0.4322748	0.4643042	0.44454357
	Ep_a	0.3293377	0.3270184	0.3223688	0.3306072	0.3293336	0.33095184
Day 19	Ip_a	0.4592277	0.3926754	0.4936769	0.4321462	0.4700821	0.44121687
	Ep_a	0.3286841	0.3273342	0.3209776	0.3313446	0.3310219	0.32569974
Day 22	Ip_a	0.4663803	0.3840666	0.5100064	0.4427874	0.4787480	0.44934195
	Ep_a	0.3353360	0.3280518	0.3243348	0.3277097	0.3273198	0.32635113
Day 45	Ip_a	0.4958313	0.4501094	0.5185765	0.4812254	0.4371178	0.45598539
	Ep_a	0.3296159	0.3287249	0.3250944	0.3336260	0.3240846	0.32704949

Table 3.6. Peak anodic current (Ip_a-mA) and peak anodic voltage (Ep_a-V) values of NIP electrodes.

NIP		PGE-13	PGE-14	PGE-15	PGE-16	PGE-17	PGE-18
Day 1	Ip_a	0.4894885	0.4192540	0.4722164	0.4018216	0.4221075	0.40846906
	Ep_a	0.3311978	0.3327404	0.3254252	0.3311991	0.3240840	0.33042919
Day 4	Ip_a	0.3925898	0.3676220	0.4912317	0.4897185	0.4625534	0.41873599
	Ep_a	0.3351482	0.3300426	0.3263798	0.3318092	0.3313460	0.33382323
Day 7	Ip_a	0.4040703	0.3740476	0.5076747	0.4931569	0.4627487	0.41845710
	Ep_a	0.3350568	0.3338160	0.3254003	0.3293640	0.3313561	0.33305209
Day 10	Ip_a	0.4104158	0.3873480	0.4217125	0.4285600	0.3595884	0.36238001
	Ep_a	0.3240551	0.3395271	0.3242210	0.3294291	0.3275296	0.32875639
Day 13	Ip_a	0.4352089	0.3956858	0.4254304	0.4195662	0.3579937	0.35214004
	Ep_a	0.3300867	0.3447562	0.3247501	0.3283933	0.3317826	0.32608830
Day 16	Ip_a	0.3881299	0.3676421	0.4614228	0.4184563	0.4706310	0.45742625
	Ep_a	0.3379640	0.3480675	0.3413083	0.3317224	0.3320055	0.33659699
Day 19	Ip_a	0.3935246	0.3743778	0.4630637	0.4216151	0.4636611	0.45517313
	Ep_a	0.3389841	0.3503963	0.3413856	0.3330661	0.3320212	0.33733031
Day 22	Ip_a	0.3825340	0.3795635	0.4696570	0.4316145	0.4690687	0.45312502
	Ep_a	0.3413503	0.3527144	0.3427221	0.3300504	0.3333568	0.33897441
Day 45	Ip_a	0.4041475	0.2856747	0.4381279	0.4026545	0.4011578	0.39699410
	Ep_a	0.3229870	0.3356193	0.3267180	0.3334090	0.3369219	0.33660513

Table 3.7. Intra-day average, standard deviation and %RSD values of the electrodes.

Between hours	Electrodes	Average	Standard deviation	%RSD
MIP	PGE-1	0.425745565	0.00502203	1.179584811
	PGE-2	0.387042883	0.017960972	4.640563747
	PGE-3	0.390472766	0.004710088	1.206252697
	PGE-4	0.33369883	0.001326643	0.397557007
	PGE-5	0.365934063	0.010164054	2.777564454

	PGE-6	0.437762601	0.014786258	3.377688612
UMIP	PGE-7	0.571914768	0.016714303	2.922516384
	PGE-8	0.590219266	0.003802497	0.644251673
	PGE-9	0.460993986	0.008025874	1.74099315
	PGE-10	0.449432971	0.00359825	0.800619967
	PGE-11	0.43014706	0.006629619	1.541244741
	PGE-12	0.500065757	0.006124574	1.224753697
NIP	PGE-13	0.474431726	0.01555314	3.278267378
	PGE-14	0.420564906	0.018370035	4.36794281
	PGE-15	0.501080309	0.011206831	2.236533952
	PGE-16	0.481272434	0.027061112	5.622826052
	PGE-17	0.557967748	0.019388194	3.474787582
	PGE-18	0.520250965	0.033646661	6.4673904

Table 3.8. Intra-day average, standard deviation and %RSD values of different electrodes.

Between electrodes	Hour	Average	Standard deviation	%RSD
MIP	1 st hour	0.387022641	0.035434194	9.155586787
	2 nd hour	0.38906442	0.036694959	9.431589584
	3 rd hour	0.394241293	0.045080898	11.43484946
UMIP	1 st hour	0.498687461	0.062425181	12.51789664
	2 nd hour	0.503942768	0.066678874	13.23143786
	3 rd hour	0.498756675	0.071951488	14.42617051
NIP	1 st hour	0.513383498	0.049436168	9.629481397
	2 nd hour	0.491520572	0.045720073	9.301761922
	3 rd hour	0.472879973	0.045951902	9.717455717

Average, standard deviation and percent relative standard deviation (RSD percent) values calculated according to different hours and according to the same hour for the intra-day measurements are shown in Tables 3.7 and 3.8.

Table 3.9. The p values of intra-day t-test results between different electrodes of the same group.

Within group	1 st hour	2 nd hour	3 rd hour
p-MIP	0.608229447	0.498326374	0.555030455
p-UMIP	0.145078121	0.159156827	0.148610799
p-NIP	0.073184738	0.217912537	0.276761538

According to the t-test results at the same time between different electrodes of the same group, it is understood that there is no significant difference in the results of the MIP, UMIP and NIP groups within themselves. Each group seems to be consistent within itself as shown in Table 3.9.

According to the intra-day t-test results between different hours of the electrodes of the same group, it seems that there is no significant difference when the same measurement is made at different times for each group (MIP, UMIP and NIP) as shown in Table 3.10.

Table 3.10. The p values in the intra-day t-test results between the measurements at different hours of the electrodes of the same group.

Between groups	1^{st} – 2^{nd} hours	1^{st} – 3^{rd} hours	2^{nd} – 3^{rd} hours
p-MIP	0.923834536	0.764127469	0.831697186
p-UMIP	0.890721293	0.998614932	0.899532331
p-NUP	0.44490602	0.172325635	0.497266419

The significance value is used to determine homogeneity between groups. If this value is greater than 0.05, it indicates that homogeneity is achieved. But the variance difference is not measured at this point. Although homogeneity seems to be a prerequisite, one-way ANOVA test can be conducted even if it is not homogeneous. According to Table 3.11, it can be said that the significance value is greater than 0.05 and the homogeneity of the variances is ensured.

Table 3.11. Test of homogeneity of variances.

Levene statistics	df1	df2	Significance values
3.118	2	51	0.053 *

Table 3.12. ANOVA test result of electrodes.

ANOVA	Sum of squares	df	Mean square	F	Significance values
Between groups	0.136	2	0.068	26.931	1.04E-8 *
Within groups	0.129	51	0.003	-	-
Total	0.266	53	-	-	-

The point where the actual variance difference is measured is the significance value obtained from the ANOVA test. If the significance value is less than 0.05, it can be said that there is a significant difference between the groups. But if this value is not less than 0.05, there is no significant difference between the groups. According to the result of this test, if there is a

significant difference between the groups, 'Post Hoc' tests can be started. According to the ANOVA test result (Table 3.12), the significance value is much lower than 0.05 and there is a significant difference between groups. It has been concluded that Post-Hoc tests can be performed. According to Andy Field's SPSS book [89], if there are differences in variances, the preferred tests can be Tukey, Hochberg's GT2 and Gabriel. Usually the Tukey test is chosen. When looking at the numbers in the ANOVA test applied groups, if the group numbers are equal, the Tukey test is chosen. If the number of groups is equal and there is a significant difference, Hochberg's GT2 test can be applied. If there is a difference in the number of groups, but this difference is not large, that is, the number of samples between the groups is not exactly equal, the Gabriel test can be applied. According to Andy Field's SPSS book [89], if there is no difference between variances, the most preferred and most accurate method is the Games-Howell test. With this test, data can be evaluated on a group basis.

In this thesis study, there is a significant difference compared to the ANOVA test performed according to the CV results taken at three different times on the same day and the group numbers are equal to each other. For this reason, the Tukey test was preferred. According to the Tukey Post-Hoc test performed in one-way ANOVA , the MIP group differs from the UMIP and NIP groups with a significant difference (Table 3.13). It is seen that there is no significant difference between UMIP and NIP groups. This can be explained by the fact that the MIP group has artificial receptors that recognize the valine molecule, while the UMIP and NIP groups do not have these interfaces.

Table 3.13. Tukey test results for different electrode groups.

Method	Method	Significance values
MIP	UMIP	8.05E-8 *
	NIP	4.17E-7 *
UMIP	MIP	8.05E-8 *
	NIP	0.886
NIP	MIP	4.17E-7 *
	UMIP	0.886

Table 3.14. Inter-day average, standard deviation and %RSD values of the electrodes.

Between days	Electrodes	Average	Standard deviation	%RSD
MIP	PGE-1	0.368073468	0.026926909	7.315634334
	PGE-2	0.388577028	0.031107078	8.005382529

	PGE-3	0.310200237	0.025775888	8.309435396
	PGE-4	0.390764729	0.039694432	10.15814103
	PGE-5	0.422121649	0.035785545	8.477543255
	PGE-6	0.330939648	0.018394047	5.558127222
UMIP	PGE-7	0.533702493	0.063336495	11.86737852
	PGE-8	0.425400637	0.030190197	7.096885817
	PGE-9	0.514590829	0.042257059	8.21177849
	PGE-10	0.464400055	0.033727513	7.262598753
	PGE-11	0.453788368	0.025953419	5.71927816
	PGE-12	0.447350638	0.015498949	3.464608645
NIP	PGE-13	0.411123309	0.033202749	8.076104759
	PGE-14	0.372357318	0.036375889	9.769081288
	PGE-15	0.461170852	0.028786375	6.242019651
	PGE-16	0.434129349	0.034023043	7.837075156
	PGE-17	0.429945629	0.046743109	10.87186522
	PGE-18	0.413655638	0.038671905	9.348816062

Table 3.15. Inter-day average, standard deviation and %RSD values of different electrodes.

Between electrodes	Day	Average	Standard deviation	%RSD
MIP	Day 1	0.352971019	0.038902576	11.02146449
	Day 4	0.373373975	0.044655924	11.96010613
	Day 7	0.364321014	0.064822544	17.79269963
	Day 10	0.36882284	0.066472164	18.02278953
	Day 13	0.360812243	0.053796306	14.90977847
	Day 16	0.383647207	0.047234695	12.31201332
	Day 19	0.384805861	0.048363778	12.5683578
	Day 22	0.380511599	0.041835254	10.99447543
	Day 45	0.34674938	0.035301122	10.18058693
UMIP	Day 1	0.475017423	0.058925671	12.40494947
	Day 4	0.513190674	0.063436393	12.36117416
	Day 7	0.519277126	0.066126188	12.73427699
	Day 10	0.460371721	0.058588644	12.72637761
	Day 13	0.464821821	0.059019699	12.69727368
	Day 16	0.449637035	0.022955364	5.105309821
	Day 19	0.448170903	0.0348082	7.766724573
	Day 22	0.455221813	0.042264859	9.284453752
	Day 45	0.473141013	0.030877267	6.526017868
NIP	Day 1	0.435559558	0.036251978	8.323081811
	Day 4	0.437075275	0.05194694	11.88512443
	Day 7	0.44335926	0.052839523	11.91799245
	Day 10	0.39500085	0.029846542	7.556070314
	Day 13	0.397670886	0.03552572	8.933447646
	Day 16	0.427284748	0.042710893	9.995885228
	Day 19	0.428569277	0.038320422	8.941476762
	Day 22	0.430927159	0.041056342	9.527443646
	Day 45	0.388126131	0.052369268	13.49284768

Average, standard deviation and RSD percent values calculated according to different days and according to the measurements taken on the same day are shown in Tables 3.14 and 3.15.

According to the t-test results on the same day between different electrodes of the same group, it is understood that there is no significant difference between the results of the MIP, UMIP and NIP groups within themselves. Each group seems to be consistent within itself on a day-to-day basis (Table 3.16).

As a result of the t-test, comparing the measurements of the electrodes of the MIP group on the first day with the other days, it is seen that the p values are greater than 0.05 and there is no significant change in the 45-day period compared to the first day (Table 3.17).

Table 3.16. The inter-day p values of t-test results between the same group electrodes.

Within group	p-MIP	p-UMIP	p-NIP
Day 1	0.922216275	0.17584066	0.087129315
Day 4	0.34545851	0.26901944	0.406766637
Day 7	0.24812513	0.198104547	0.555282405
Day 10	0.222598613	0.383556842	0.404870102
Day 13	0.124877667	0.462650172	0.161660039
Day 16	0.705992182	0.815114616	0.255272417
Day 19	0.457906838	0.983204178	0.28853023
Day 22	0.600928975	0.932501623	0.265803025
Day 45	0.737789687	0.275913506	0.627197

Table 3.17. Inter-day p values in the t-test results of measurements taken on the first day of the electrodes of the same group with the other days.

Between groups	p-MIP	p-UMIP	p-NIP
Day 1 – Day 4	0.418481079	0.305517436	0.954416986
Day 1 – Day 7	0.720726095	0.248998346	0.771692696
Day 1 – Day 10	0.625080469	0.675100409	0.060459978
Day 1 – Day 13	0.778252328	0.770729044	0.097418918
Day 1 – Day 16	0.247586383	0.348755281	0.72502403
Day 1 – Day 19	0.237546924	0.359277157	0.752176688
Day 1 – Day 22	0.264980293	0.518843322	0.840032546
Day 1 – Day 45	0.777660677	0.946280012	0.098102327

Two-way ANOVA was used for the statistical analysis of the 45-day process. Levene's test result examines the equality of variances. When the Significance value is greater than 0.05,

it means that the variances of the groups are equal. In this thesis study, homogeneity between variances was ensured since the significance values were greater than 0.05 according to Table 3.18 for measurements taken on different days.

First of all, significance values are examined to determine whether the results are significant. When analyzed on the basis of measurements taken on varying days according to the Table 3.19, it is revealed that there is no significant difference since the significance value is greater than 0.05. This result shows that there is no big difference between the results of the nine days from the first day to the forty-fifth day, and the electrode gives consistent results in measurements taken on different days. When the measured significance value is examined for the results given by different methods, it is revealed that this value is less than 0.05 and there is a significant difference. This result shows that there is a significant difference between the results of the MIP, UMIP and NIP groups selected as the method, as expected.

According to Cohen, when interpreting partial eta squared values, 0.01 represents small effect size, 0.06 represents medium effect size, and 0.14 represents high effect size [86]. According to this definition, when the partial eta squared values are examined in Table 3.19, it can be said that the effect of taking the measurement on different days is moderate, and the effect of preparing the electrode with different methods on the results is quite high. It is seen that the effect of ‘the day’ and ‘the method’ taken together is moderate on the results.

Table 3.18. Test of homogeneity of variances.

	Levene statistic	df1	df2	Significance values
Based on mean	0.927	26	135	0.571
Based on median	0.673	26	135	0.880
Based on median and with adjusted df	0.673	26	82.944	0.873
Based on trimmed mean	0.891	26	135	0.621

Table 3.19. Test of between subjects.

	Significance values	Partial eta squared
Day	0.163	0.082
Method	2.86E-20 *	0.487
Day*Method	0.535	0.099

Table 3.20. Tukey post-hoc test results for different days.

(I) Day	(J) Day	Significance values
1	4	0.944
	7	0.924
	10	0.996
	13	0.996
	16	1.000
	19	1.000
	22	1.000
	45	0.964
4	1	0.944
	7	1.000
	10	0.501
	13	0.488
	16	0.927
	19	0.933
	22	0.959
	45	0.291
7	1	0.924
	4	1.000
	10	0.454
	13	0.442
	16	0.904
	19	0.911
	22	0.943
	45	0.255
10	1	0.996
	4	0.501
	7	0.454
	13	1.000
	16	0.998
	19	0.997
	22	0.994
	45	1.000
13	1	0.996
	4	0.488
	7	0.442
	10	1.000
	16	0.997
	19	0.997
	22	0.993
	45	1.000
16	1	1.000
	4	0.927
	7	0.904
	10	0.998
	13	0.997
	19	1.000
	22	1.000
	45	0.975

19	1	1.000
	4	0.933
	7	0.911
	10	0.997
	13	0.997
	16	1.000
	22	1.000
	45	0.971
22	1	1.000
	4	0.959
	7	0.943
	10	0.994
	13	0.993
	16	1.000
	19	1.000
	45	0.951
45	1	0.964
	4	0.291
	7	0.255
	10	1.000
	13	1.000
	16	0.975
	19	0.971
	22	0.951

When the numbers in the ANOVA test applied groups are examined, if the group numbers are equal, the Tukey test is usually chosen. If the significance values of the Tukey Post-Hoc test results are less than 0.05, it means that there is a significant difference between the groups. According to the Tukey Post-Hoc test performed in two-way ANOVA, it is understood from the significance values that there is no significant difference between the days in the measurements taken during the 45-day period (Table 3.20). The formed electrodes gave stable results during this 45-day period. According to the Tukey Post-Hoc test, MIP, UMIP and NIP groups differed from each other with a significant difference in the 45-day period (Table 3.21).

3.21. Tukey post-hoc test results for different methods in 45-day period.

Method	Method	Significance values
MIP	UMIP	5.10E-9
	NIP	3.35E-7
UMIP	MIP	5.10E-9
	NIP	2.18E-7
NIP	MIP	3.35E-7
	UMIP	2.18E-7

Intra-day precision was made at 3 different times in a day and inter-day precision study was made for nine different days. RSD values were obtained as 2.3 percent for intra-day precision and 8 percent for inter-day precision.

Response of electrode was measured with E-8 M valine solution to determine the stability of electrode every three days for three weeks and on day 45. Current response increased to 103 percent after 7 days and 107 percent after 22 days. After 45 days electrode retained 98 percent of its signal response.

3.4. SELECTIVITY OF ELECTRODES

Selectivity analysis was performed to examine the responses of the electrodes to different molecules, aiming to demonstrate that the EIS and CV responses of the electrodes are valine specific. Au-Control (Au-NIP), Au-0.3M-Val-MIP and Au-0.3M-Val-UMIP electrodes were tested for their selectivity using the amino acids: glycine, alanine, and methionine.

Glycine (NH_2CH_2COOH), an apolar amino acid, is the simplest of the 20 amino acids found in proteins in structure. Glycine, the smallest of the amino acids, has a pKa_1 value of 2.35 and a pKa_2 of 9.78. Most of the anionic amine ($H_2NCH_2CO_2^-$) in the glycine solution is above pH 9.78, while the cationic carboxylic acid ($H_3N^+CH_2CO_2H$) is found in the solution below pH 2.35. Glycine has an isoelectric point of 6.06 [81].

Alanine, one of the most commonly used amino acids, accounts for 7.8 percent of proteins. Because it is chemically inactive, the methyl group in the domain may help the protein function in an indirect way. As a result, hydrophobic bonds between carbon and other atoms may play a role in the selectivity of the enzyme-substrate relationship [82]. Alanine has a pKa_1 value of 2.34 and a pKa_2 of 9.69. Alanine has an isoelectric point of 6.00 [81].

Only one of the 20 amino acids, methionine, contains sulfur and is an apolar amino acid as well as a lipotropic molecule that helps the body's metabolism burn fat more quickly. In enzyme reactions, S-adenosyl methionine, a methionine derivative, serves as a source of methyl groups for the enzymes [83]. Methionine has a pKa_1 value of 2.28 and a pKa_2 of 9.21. Methionine has an isoelectric point of 5.74 [81].

The electrochemical analysis of Au-Control electrode in glycine, alanine and methionine solutions were conducted at the ten different concentrations of valine in RdxPBS (Figures 3.155-3.156, 3.158-3.159, 3.161-3.162). In the absence of template molecule on the electrodes, the glycine, alanine or methionine molecules added to solution do not adhere to the electrodes and remain in solution, increasing solution conductivity and thus decreasing impedance (Figures 3.155, 3.158, 3.161), resulting in selectivity performed at the rate of 95.78 percent (Figure 3.157), 96.1 percent (Figure 3.160) and 95.04 percent (Figure 3.163) for glycine, alanine and methionine, respectively.

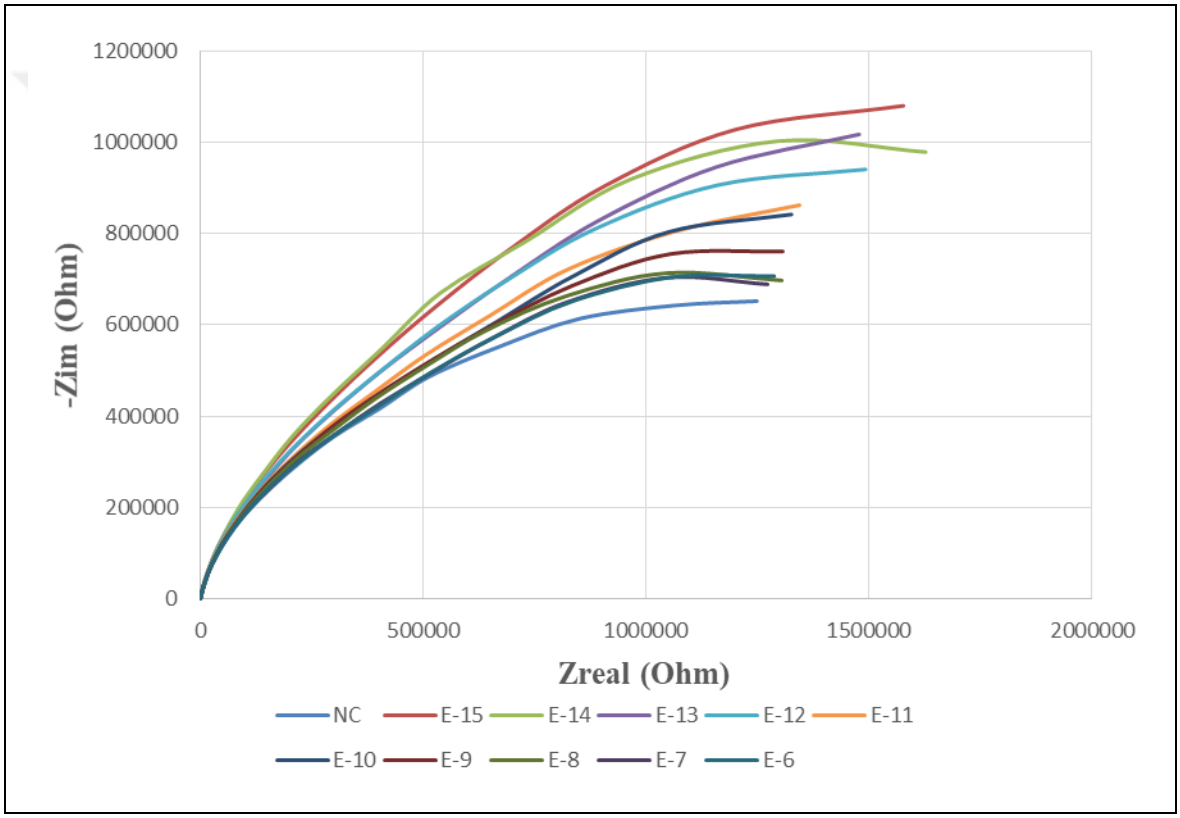

Figure 3. 155. EIS response of Au-Control electrode in glycine solution.

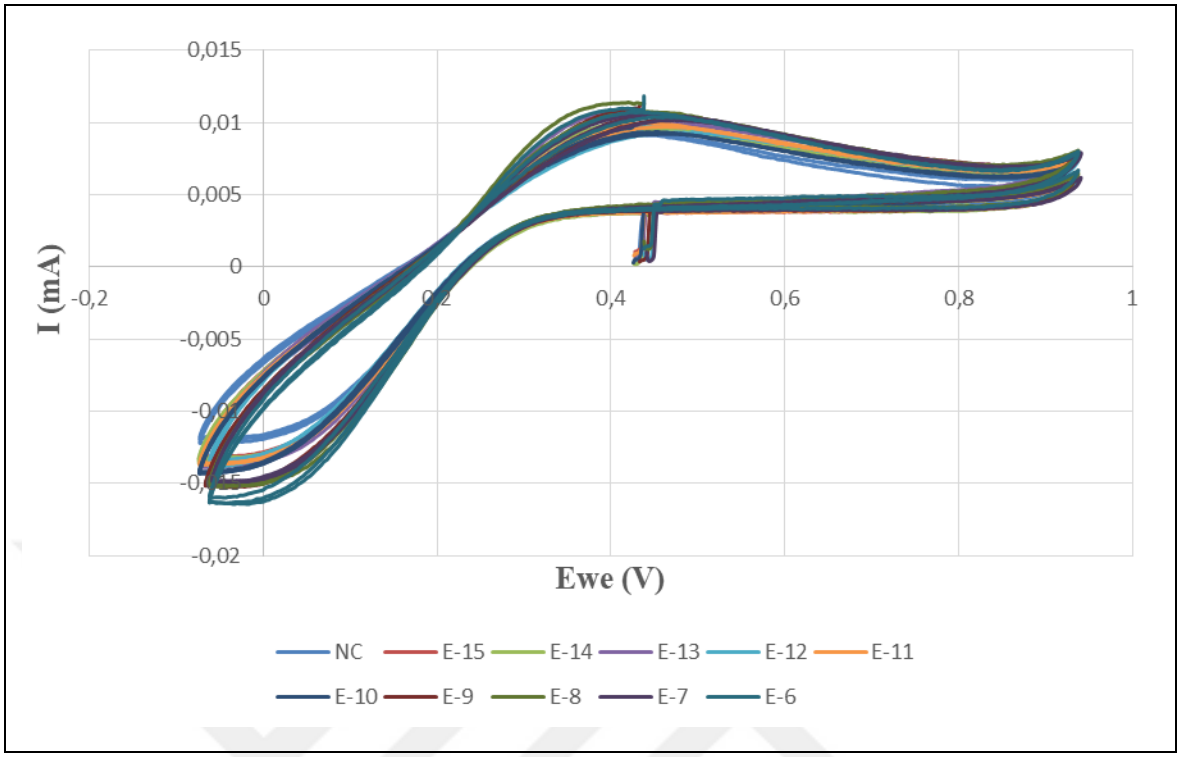

Figure 3.156. CV response of Au-Control electrode in glycine solution.

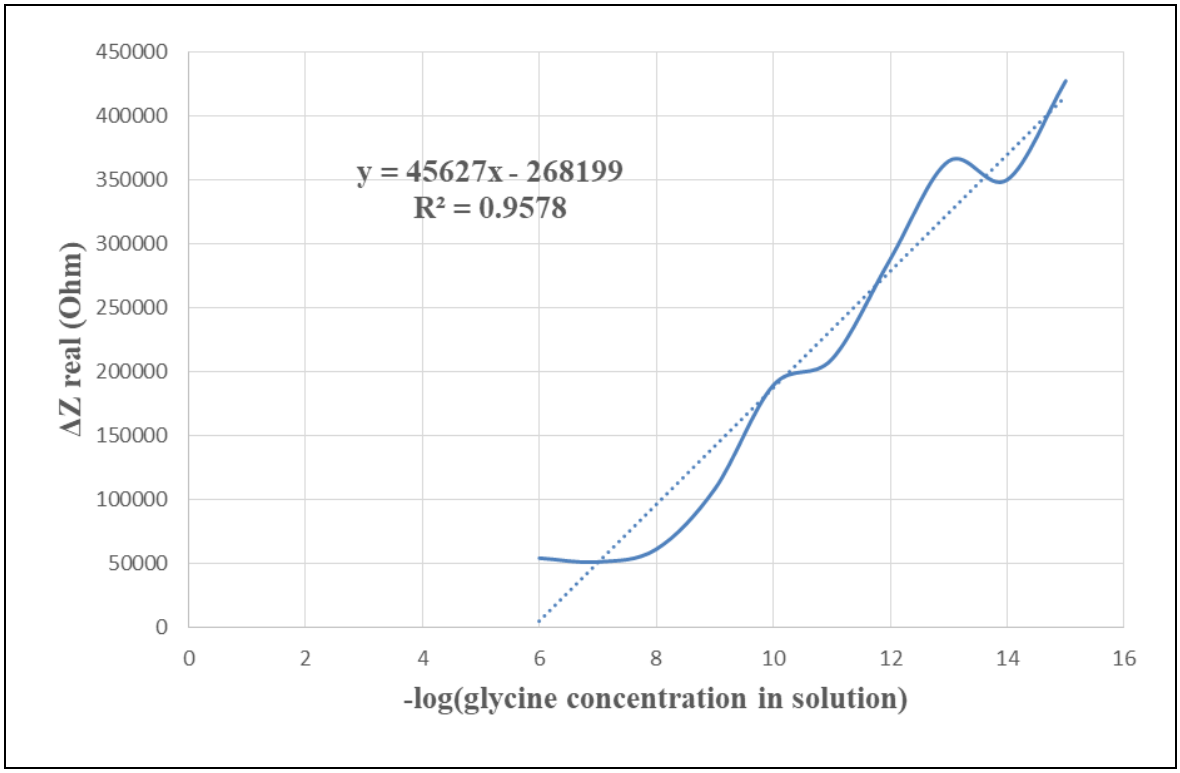

Figure 3.157. The regression curve of Au-Control electrode in glycine solution.

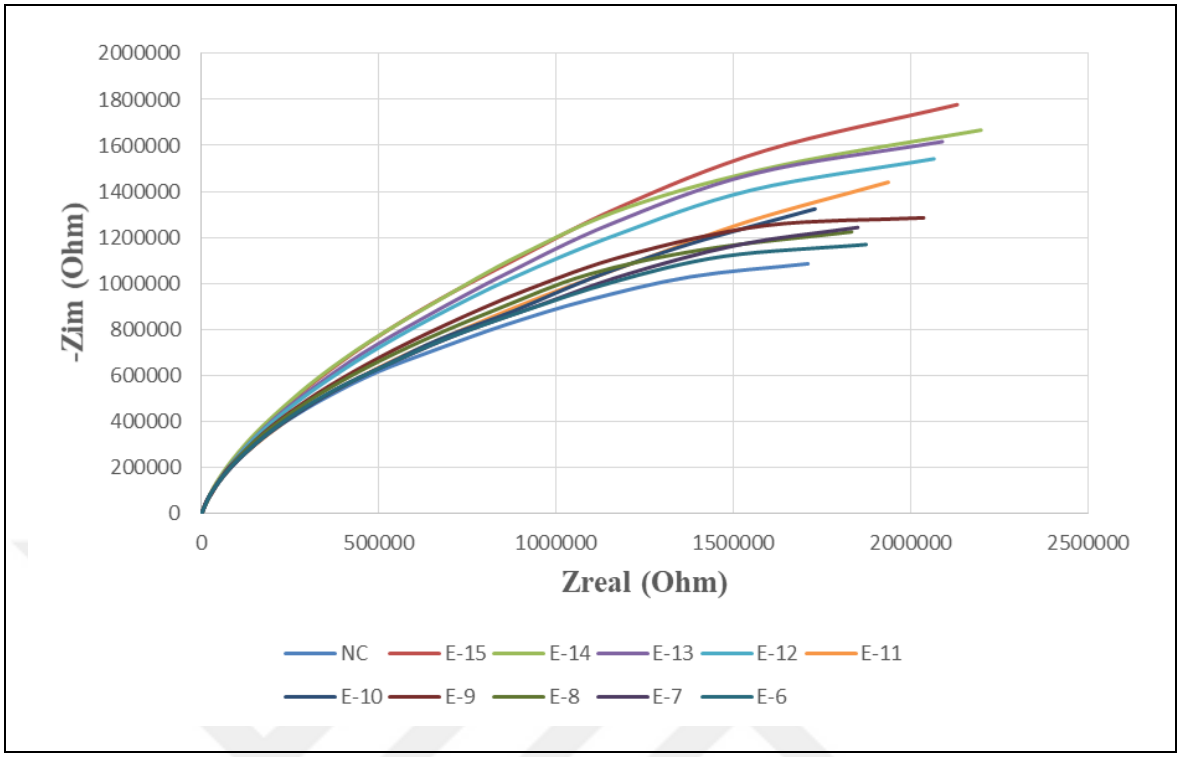

Figure 3.158. EIS response of Au-Control electrode in alanine solution.

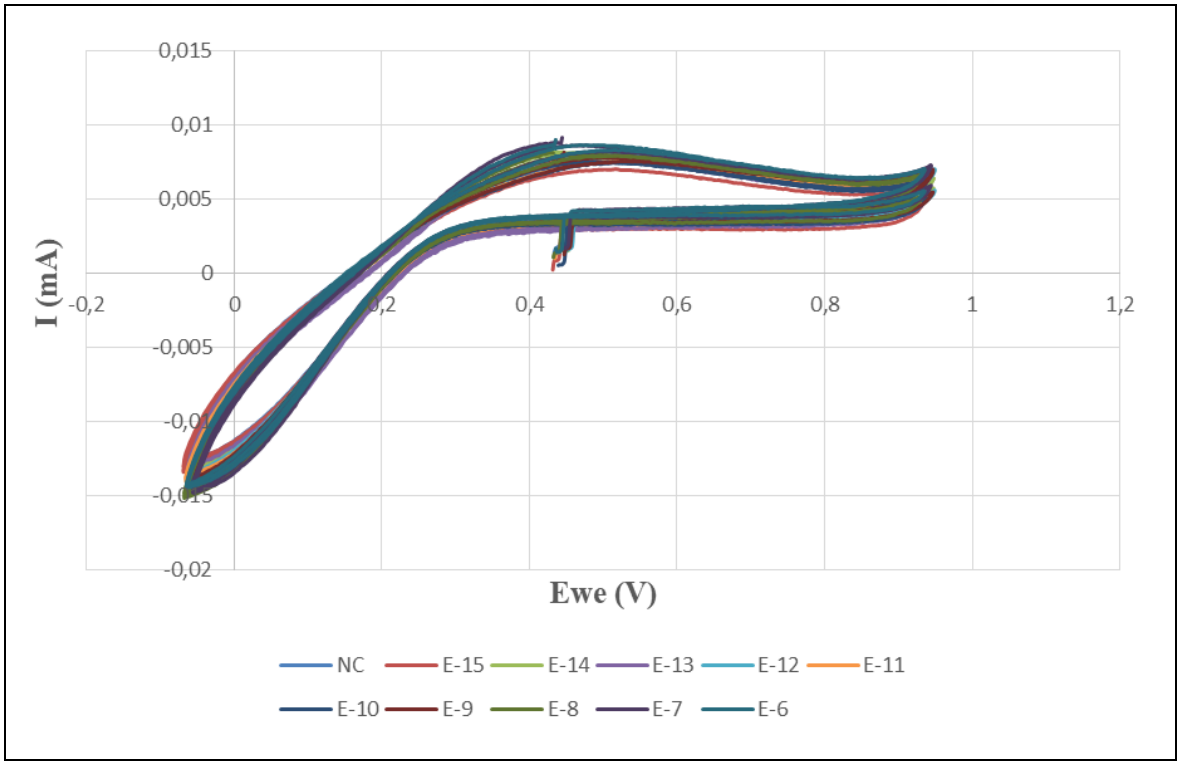

Figure 3.159. CV response of Au-Control electrode in alanine solution.

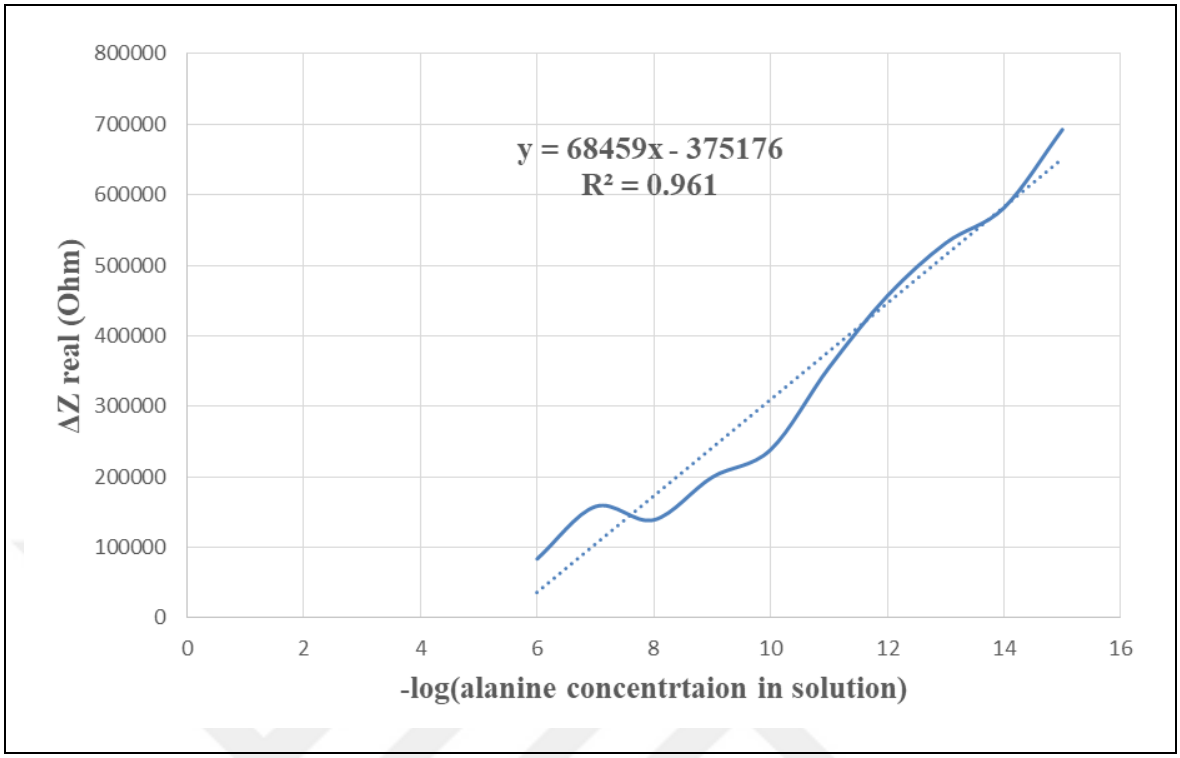

Figure 3.160. The regression curve of Au-Control electrode from alanine solution.

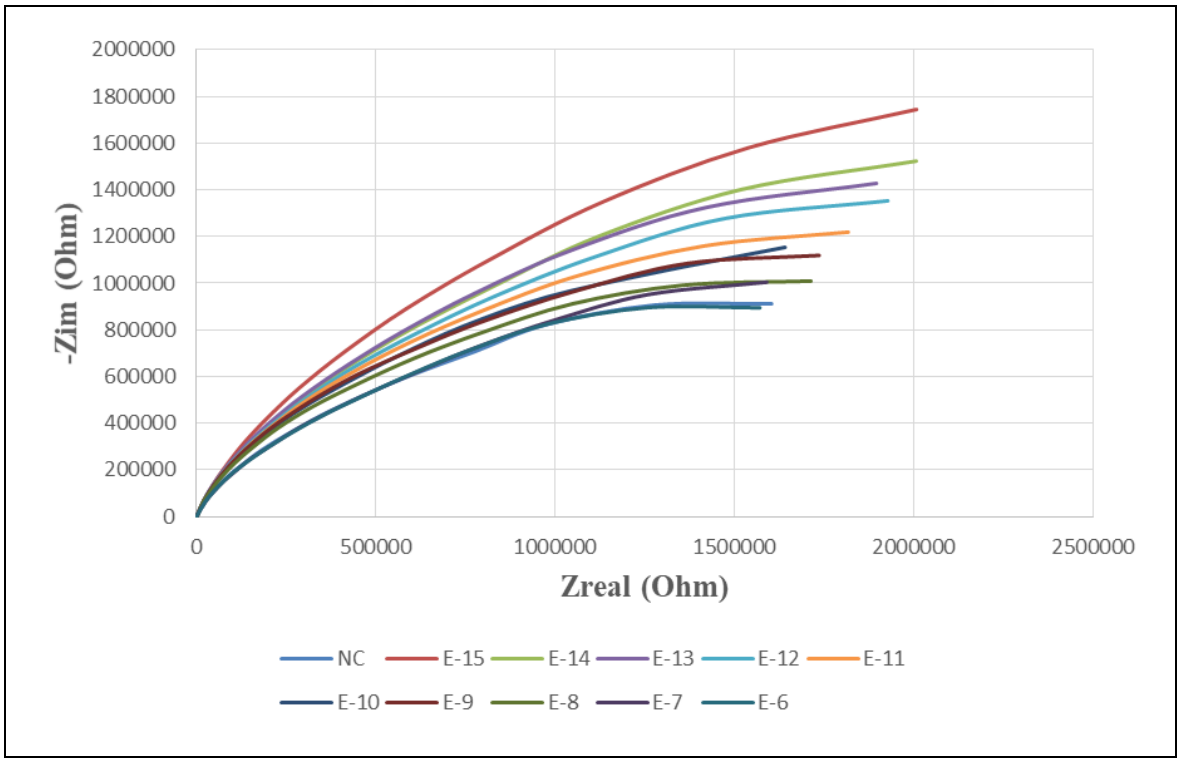

Figure 3.161. EIS response of Au-Control electrode in methionine solution.

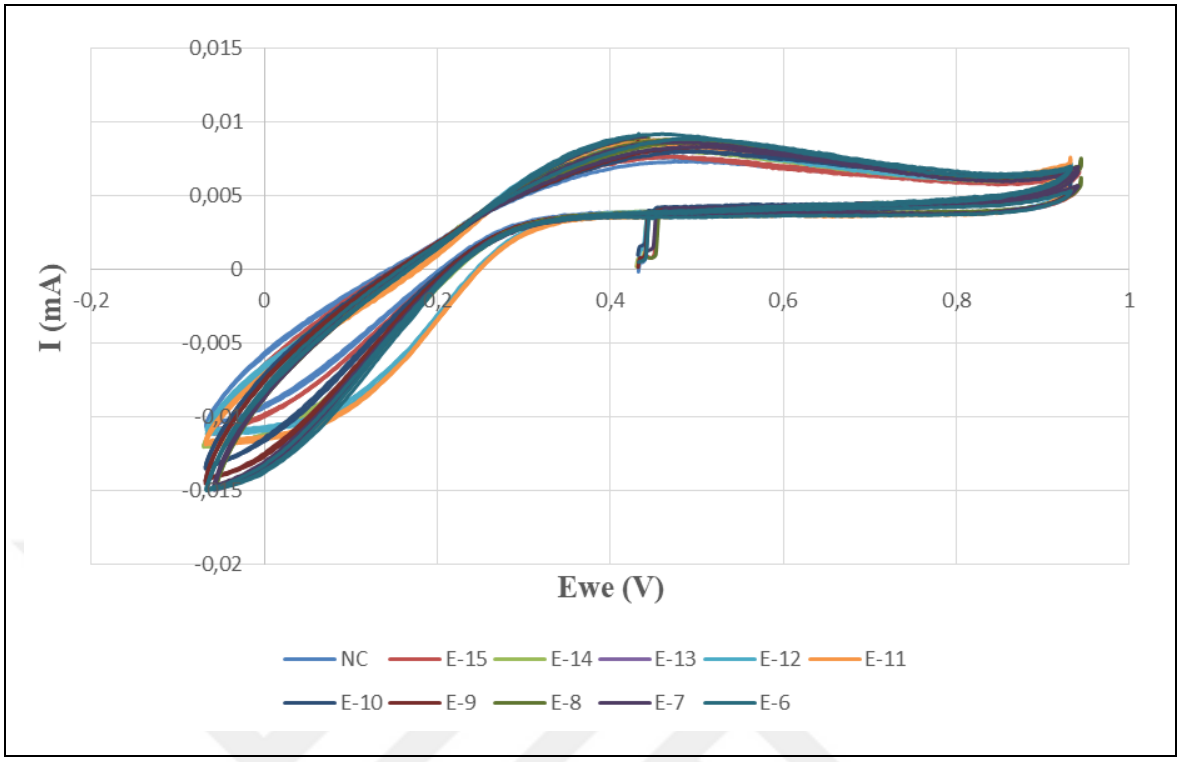

Figure 3.162. CV response of Au-Control electrode in methionine solution.

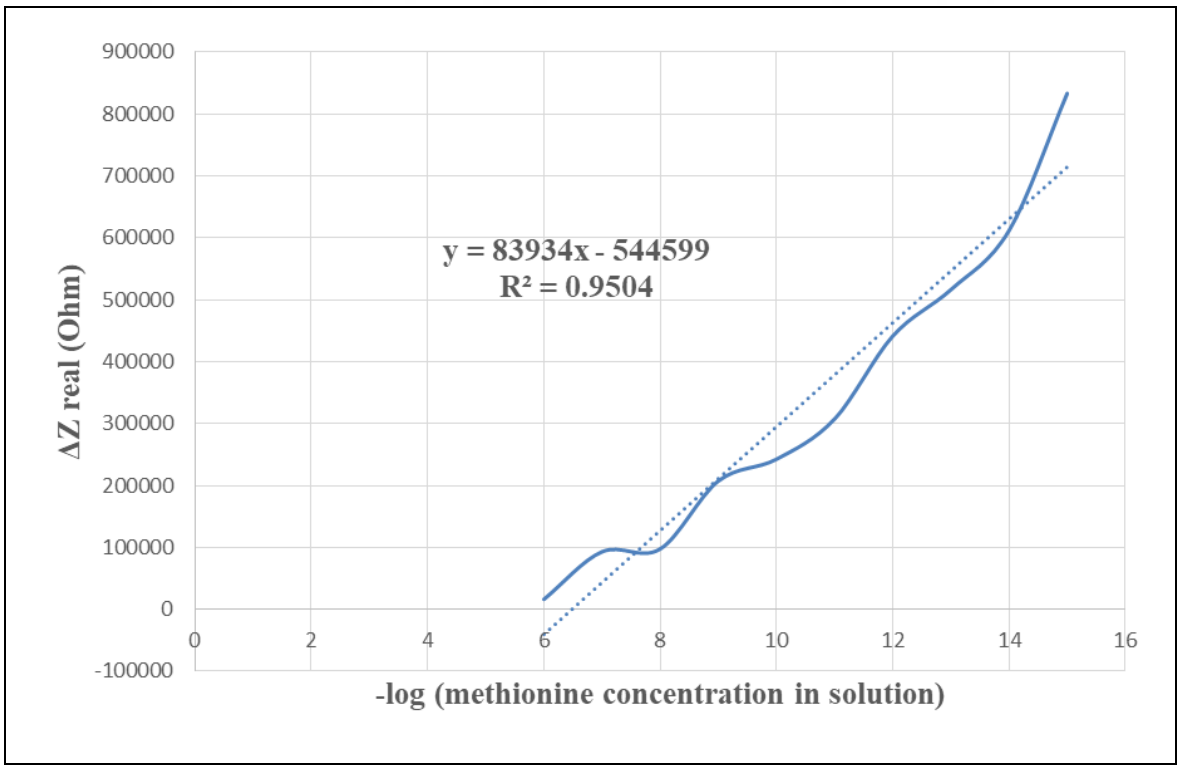

Figure 3.163. The regression curve of Au-Control electrode in methionine solution.

The analysis of Au-0.3M-Val-MIP electrode determined in electrochemical analyzes is performed with a solution containing glycine, alanine and methionine at ten different molarities as that of valine in RdxPBS solution, Figures 3.164, 3.165, 3.167, 3.168, 3.170 and 3.171 responses were obtained. Analysis of results indicates a successful selectivity analysis performed at the rate of 25.08 percent (Figure 3.166), 23.66 percent (Figure 3.169) and 1.07 percent (Figure 3.172) for against glycine, alanine and methionine, respectively, as shown in the EIS and CV plots.

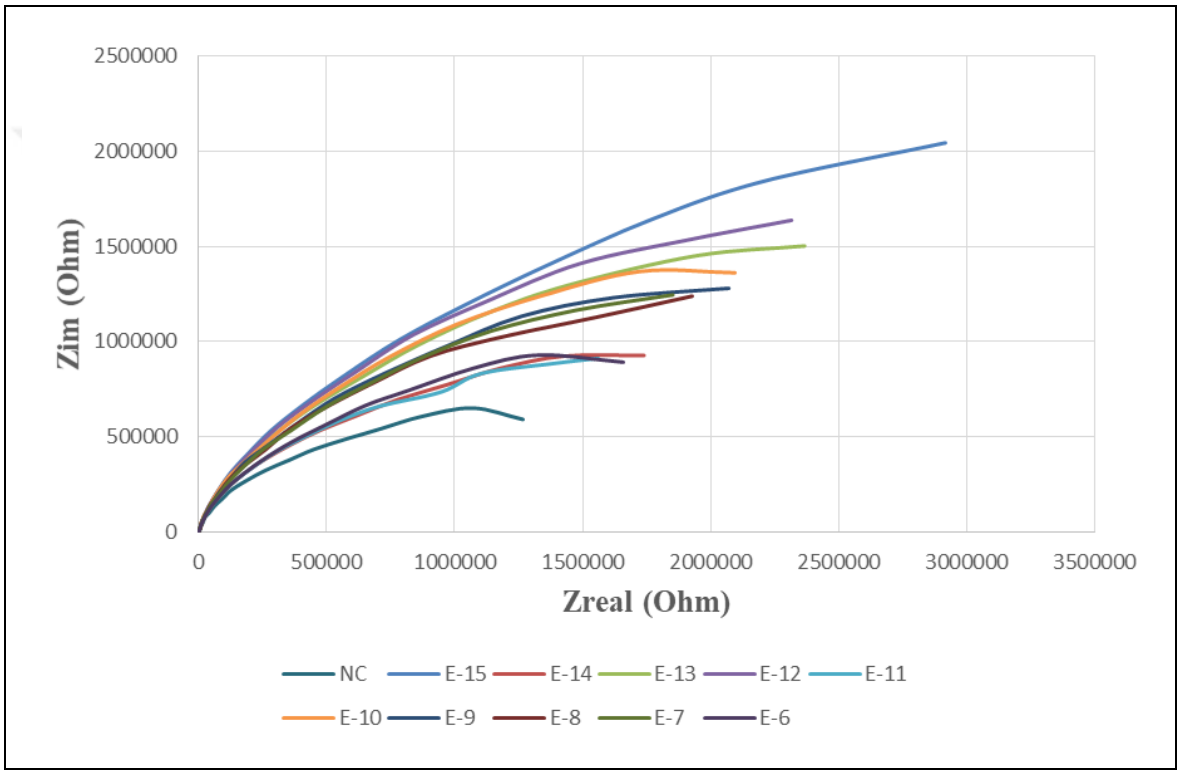

Figure 3.164. EIS response of Au-0.3M-Val-MIP electrode in glycine solution.

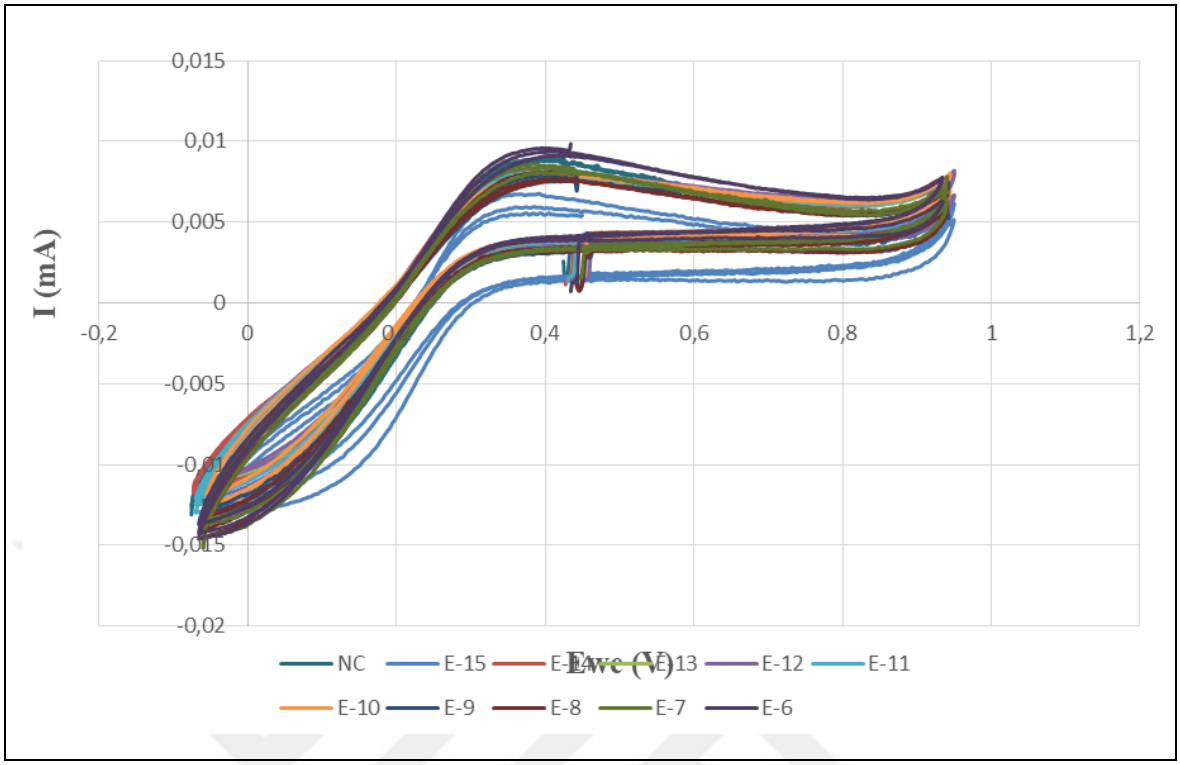

Figure 3.165. CV response of Au-0.3M-Val-MIP electrode in glycine solution.

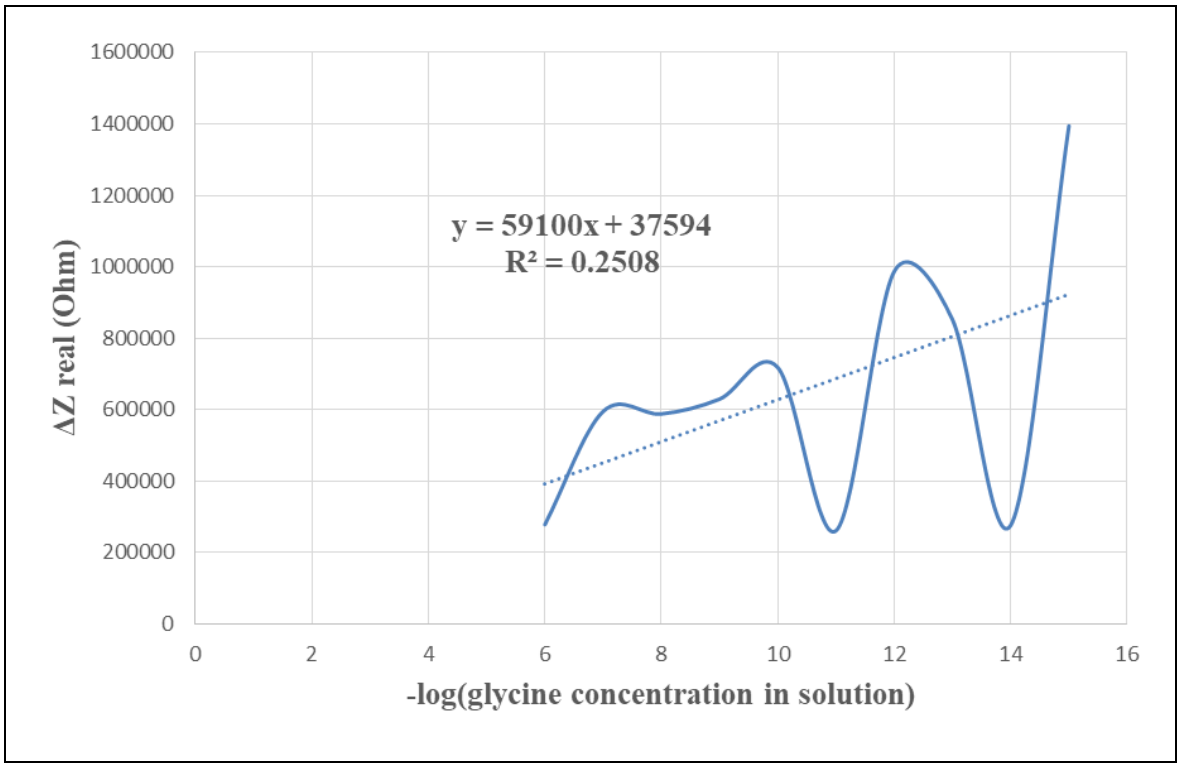

Figure 3.166. The regression curve of Au-0.3M-Val-MIP electrode in glycine solution.

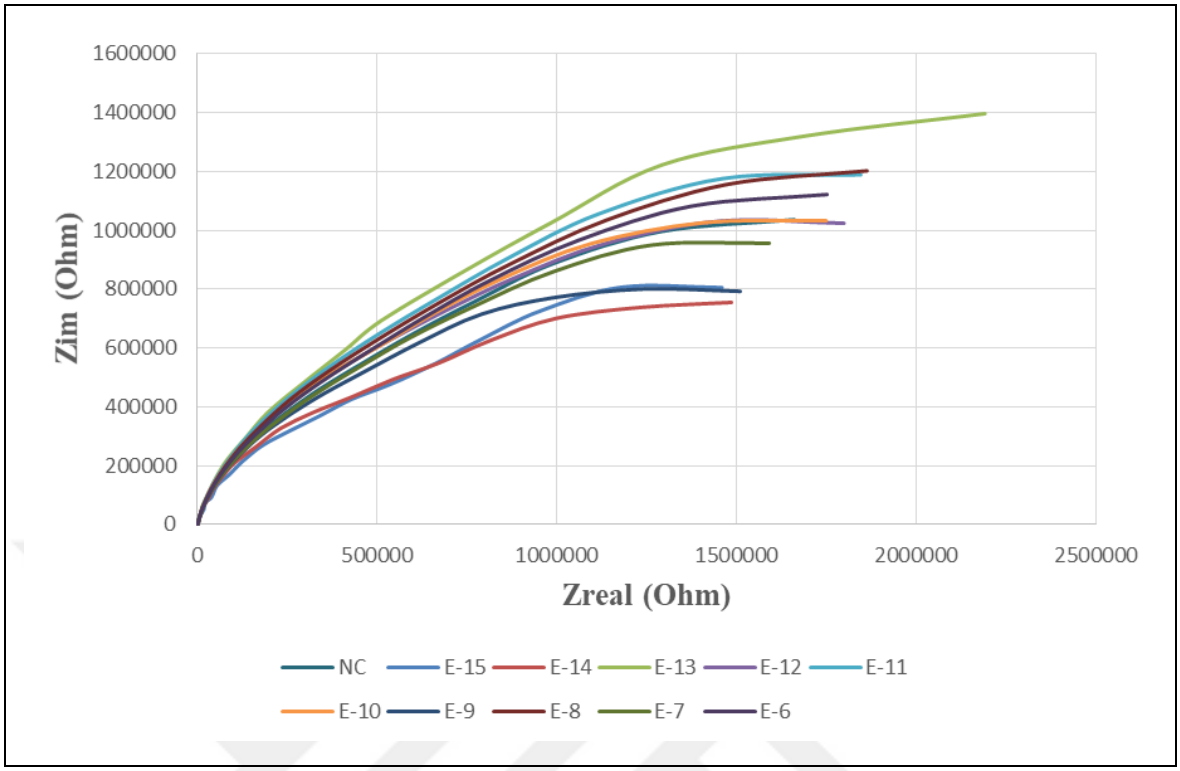

Figure 3.167. EIS response of Au-0.3M-Val-MIP electrode in alanine solution.

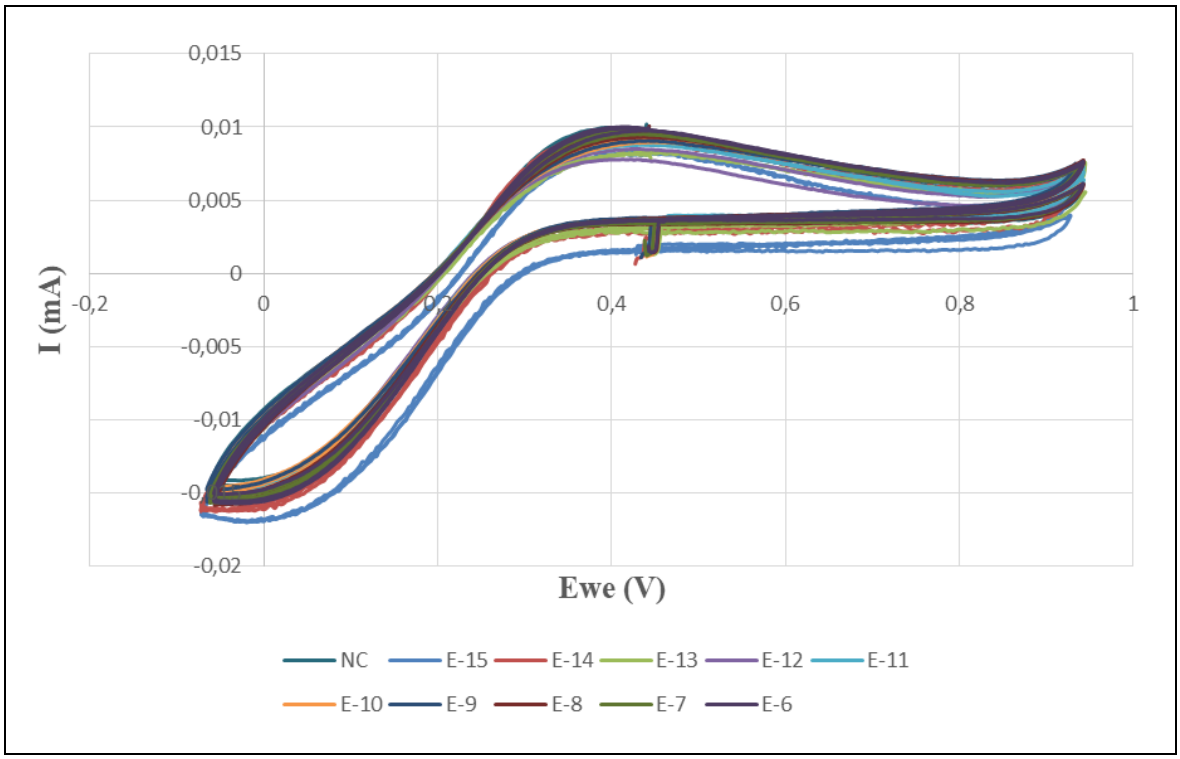

Figure 3.168. CV response of Au-0.3M-Val-MIP electrode in alanine solution.

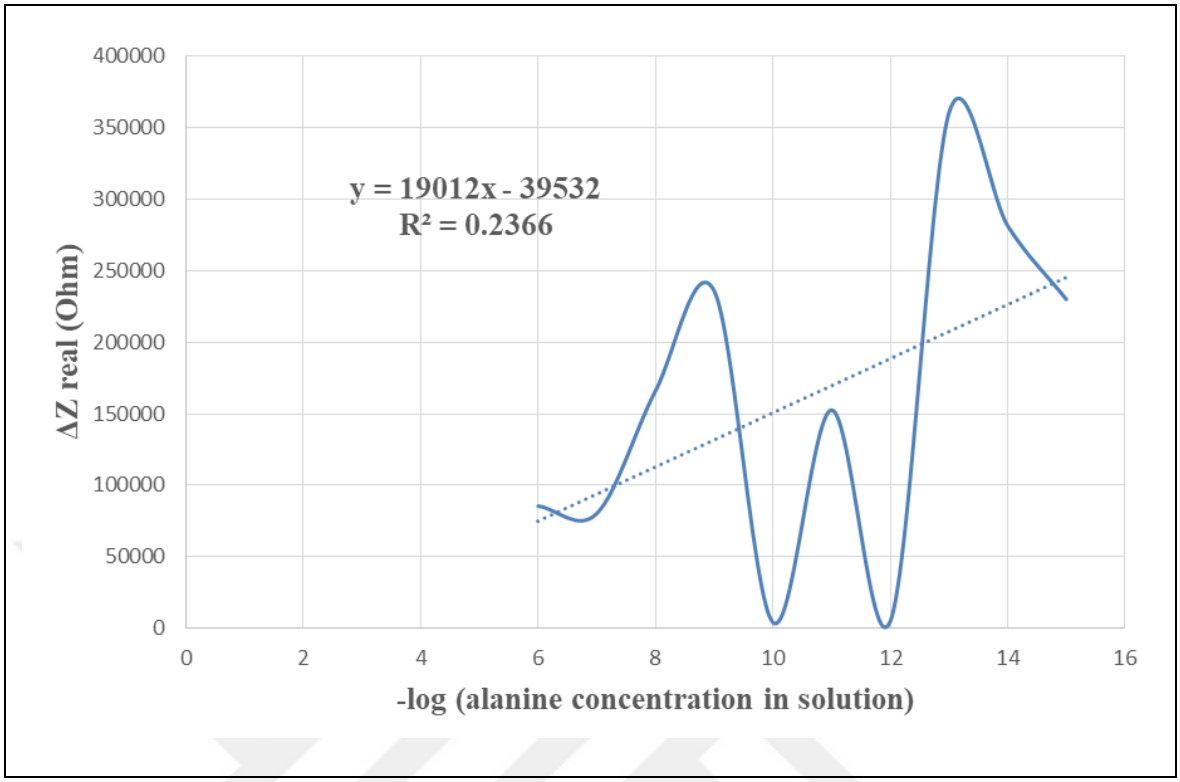

Figure 3.169. The regression curve of Au-0.3M-Val-MIP electrode in alanine solution.

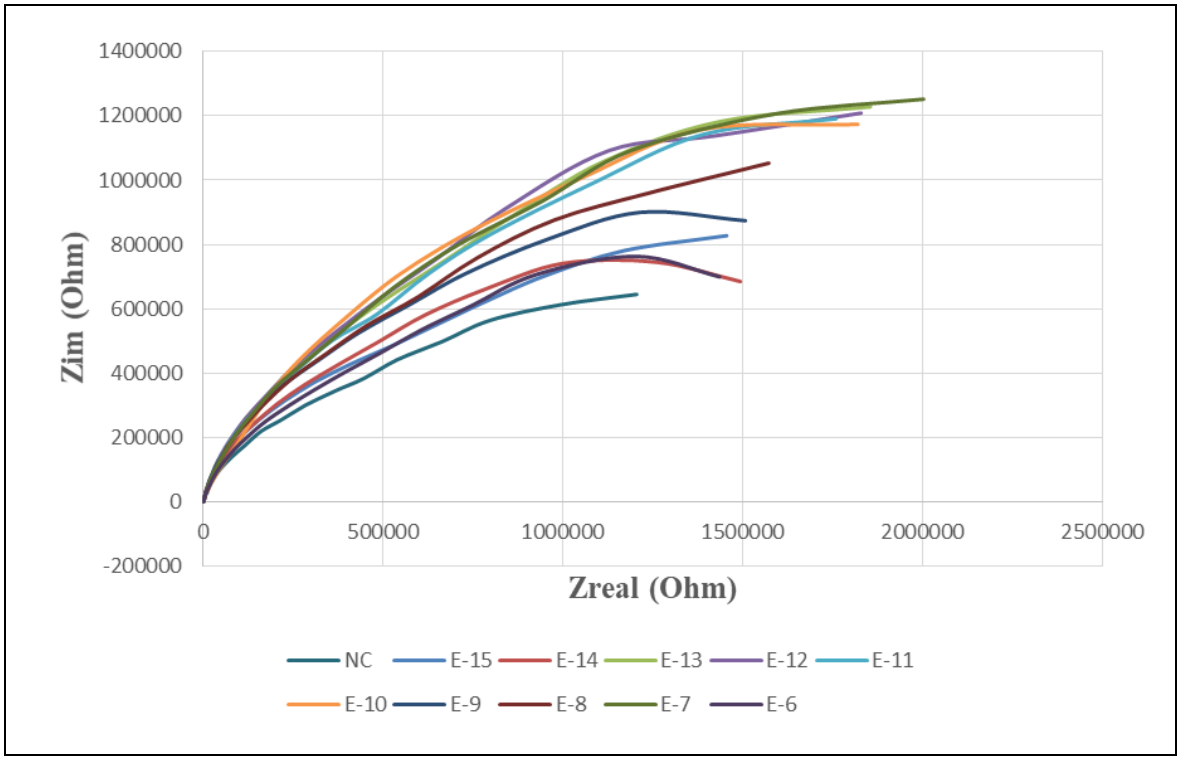

Figure 3.170. EIS response of Au-0.3M-Val-MIP electrode in methionine solution.

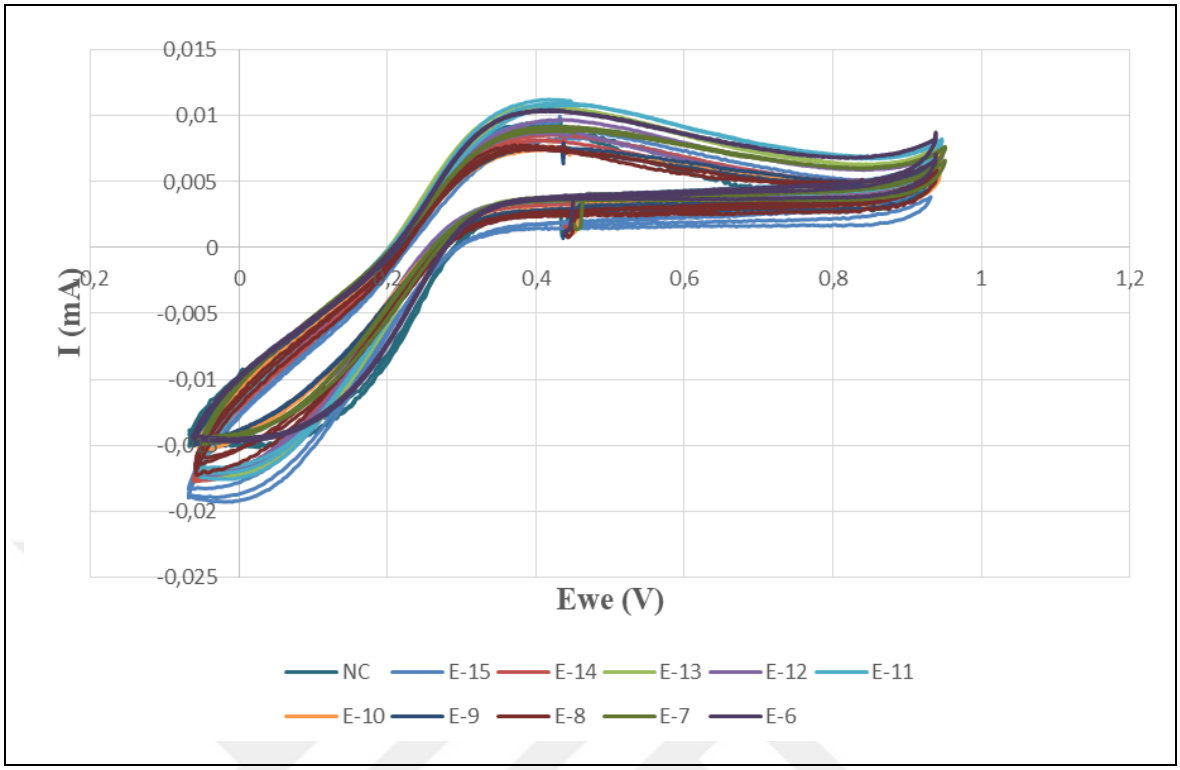

Figure 3.171. CV response of Au-0.3M-Val-MIP electrode in methionine solution.

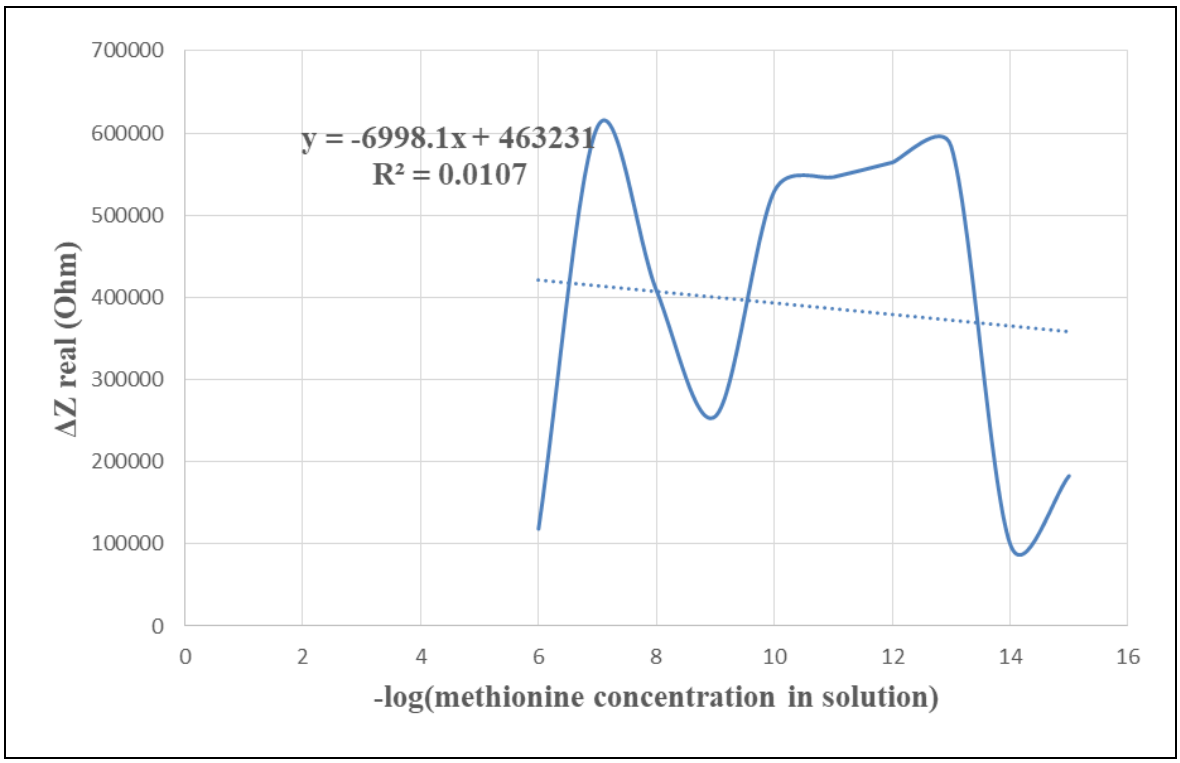

Figure 3.172. The regression curve of Au-0.3M-Val-MIP electrode in methionine solution.

The electrochemical analysis of Au-0.3M-Val-UMIP electrode in glycine, alanine and methionine solutions at ten different molarities as valine in RdxPBS solution indicated that the electrode was selective against glycine, alanine, and methionine (Figures 3.173-3.174, 3.176-3.177, 3.179-3.180) respectively at a rate of 1.28 percent (Figure 3.175), 41 percent (Figure 3.178) and 2.28 percent (Figure 3.181). This indicates that the added glycine, alanine, and methionine did not bind to valine-saturated gaps in the electrodes and failed to detect solutions of glycine, alanine, and methionine at different molarities, as shown in the EIS and CV plots.

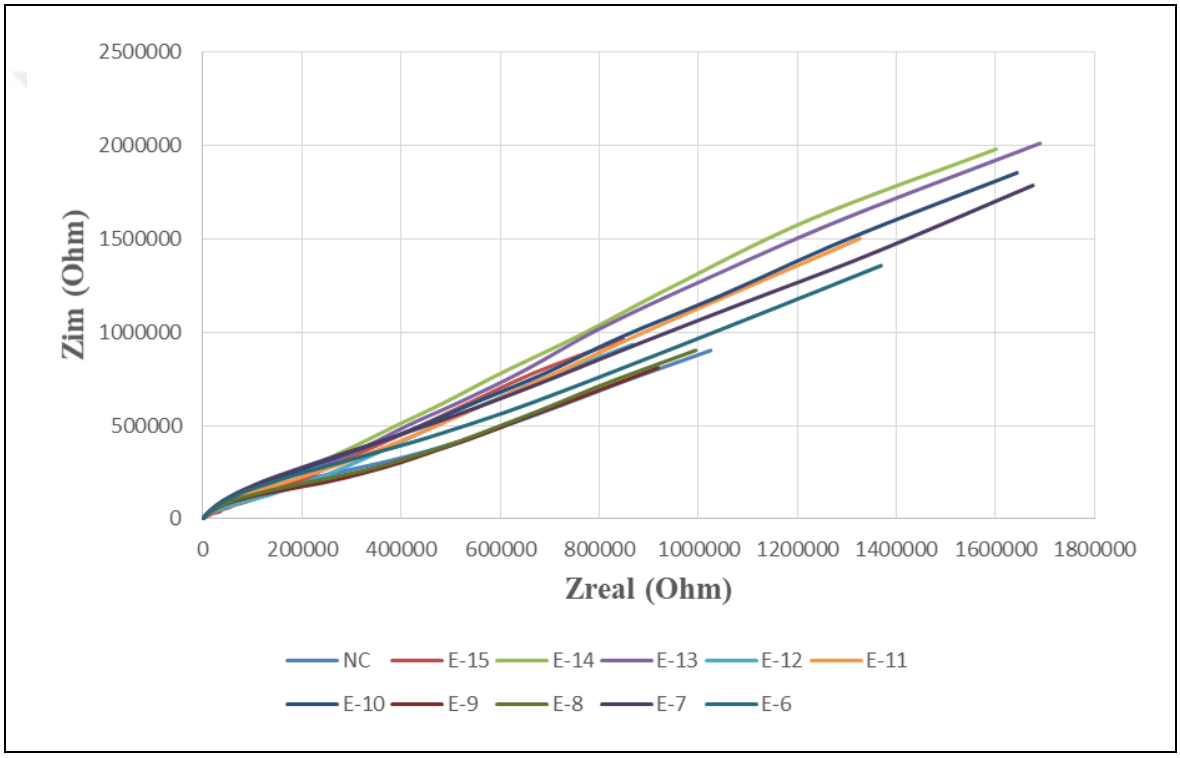

Figure 3.173. EIS response of Au-0.3M-Val-UMIP electrode in glycine solution.

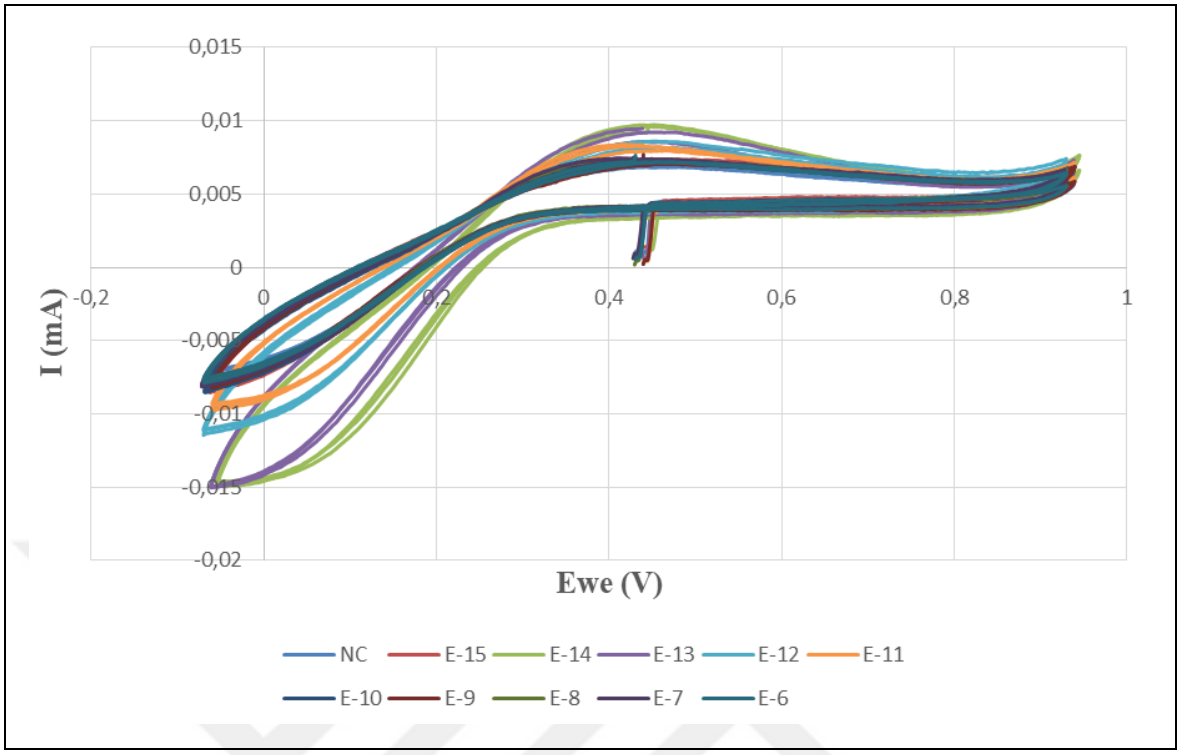

Figure 3.174. CV response of Au-0.3M-Val-UMIP electrode in glycine solution.

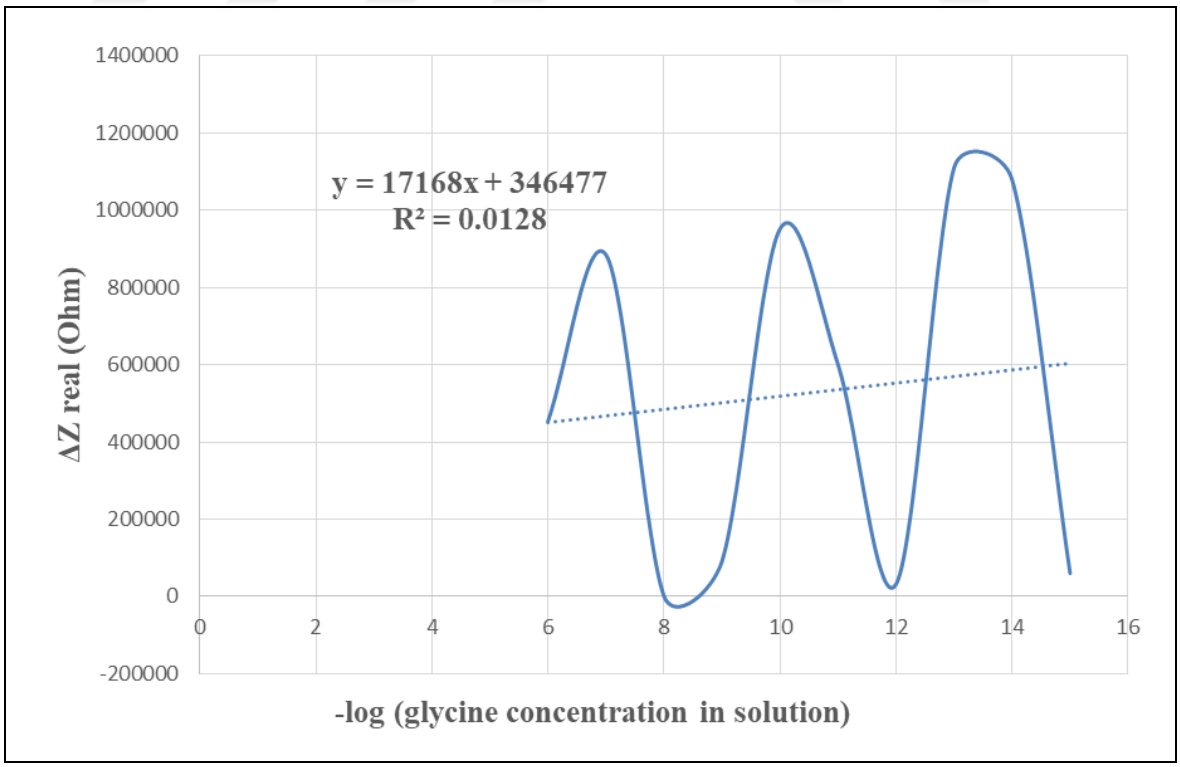

Figure 3.175. The regression curve of Au-0.3M-Val-UMIP electrode in glycine solution.

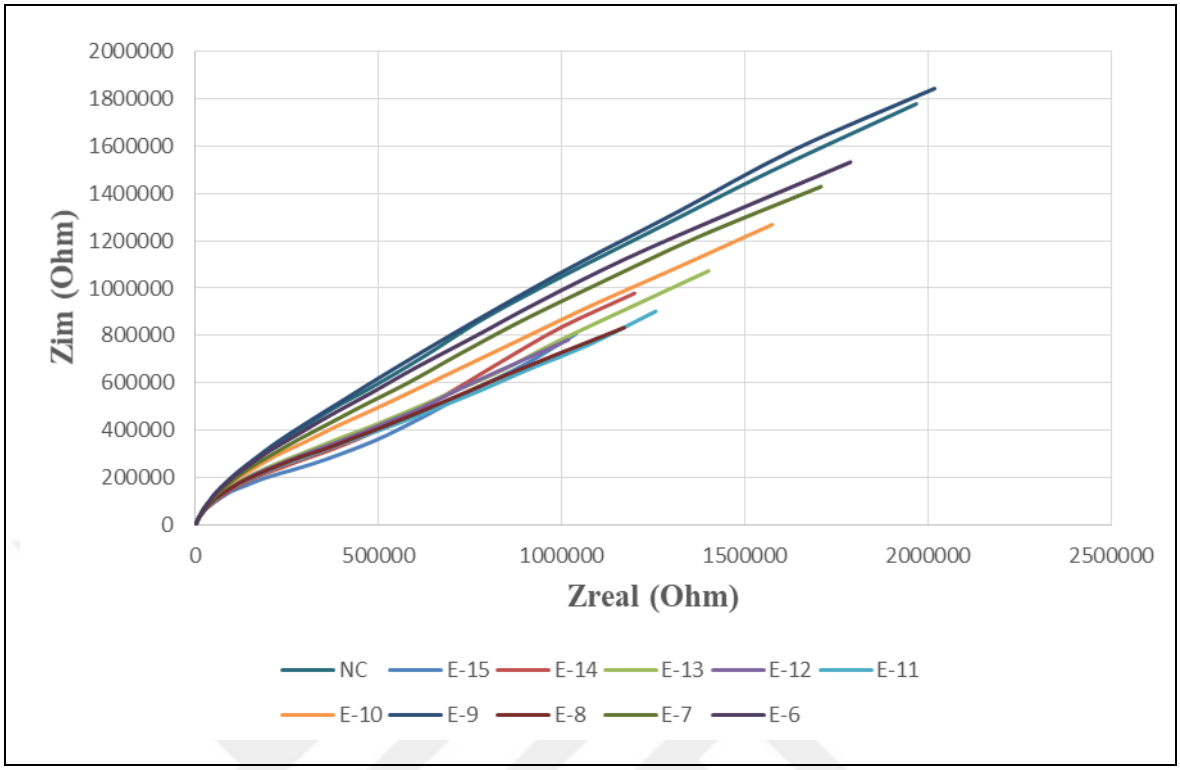

Figure 3.176. EIS response of Au-0.3M-Val-UMIP electrode in alanine solution.

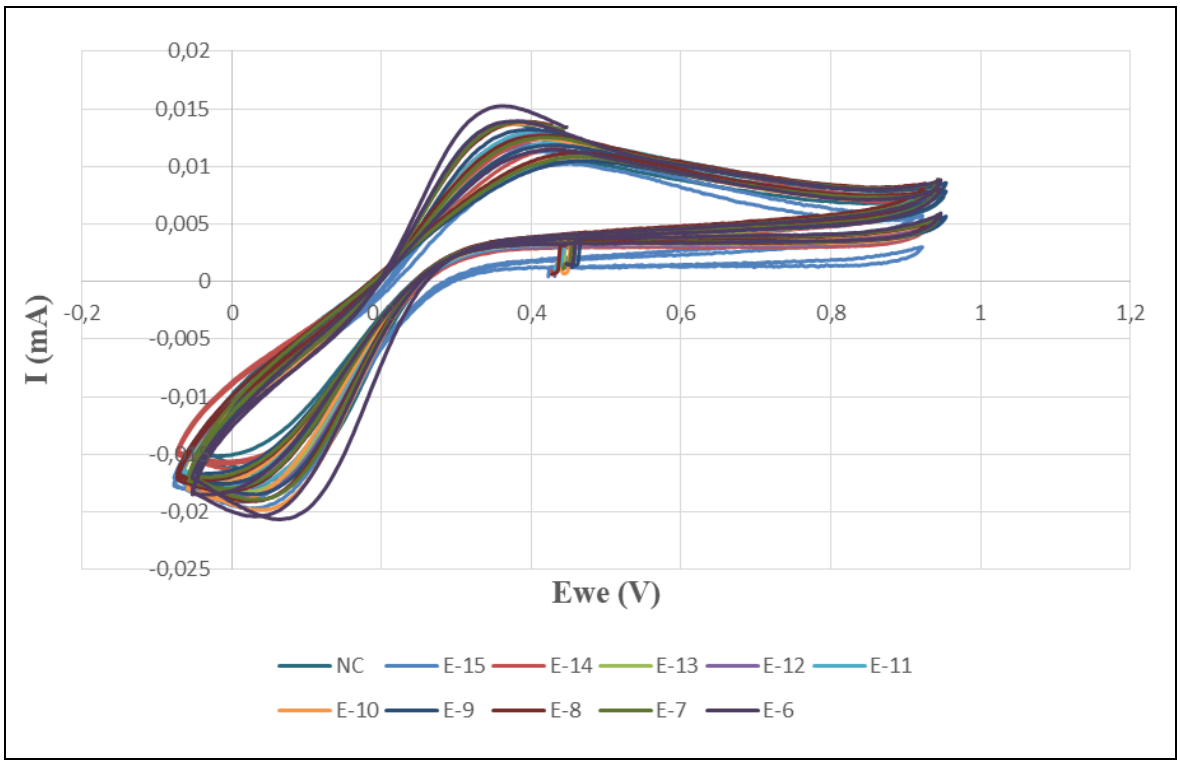

Figure 3.177. CV response of Au-0.3M-Val-UMIP electrode in alanine solution.

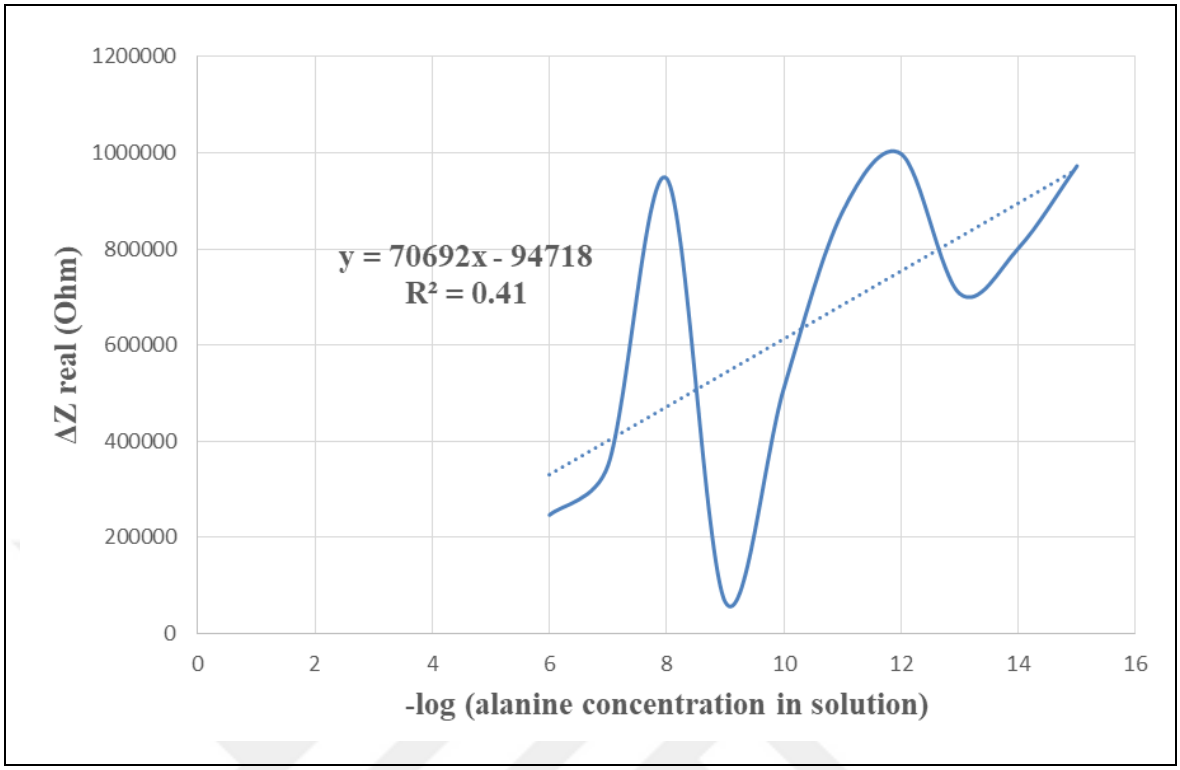

Figure 3.178. The regression curve of Au-0.3M-Val-UMIP electrode in alanine solution.

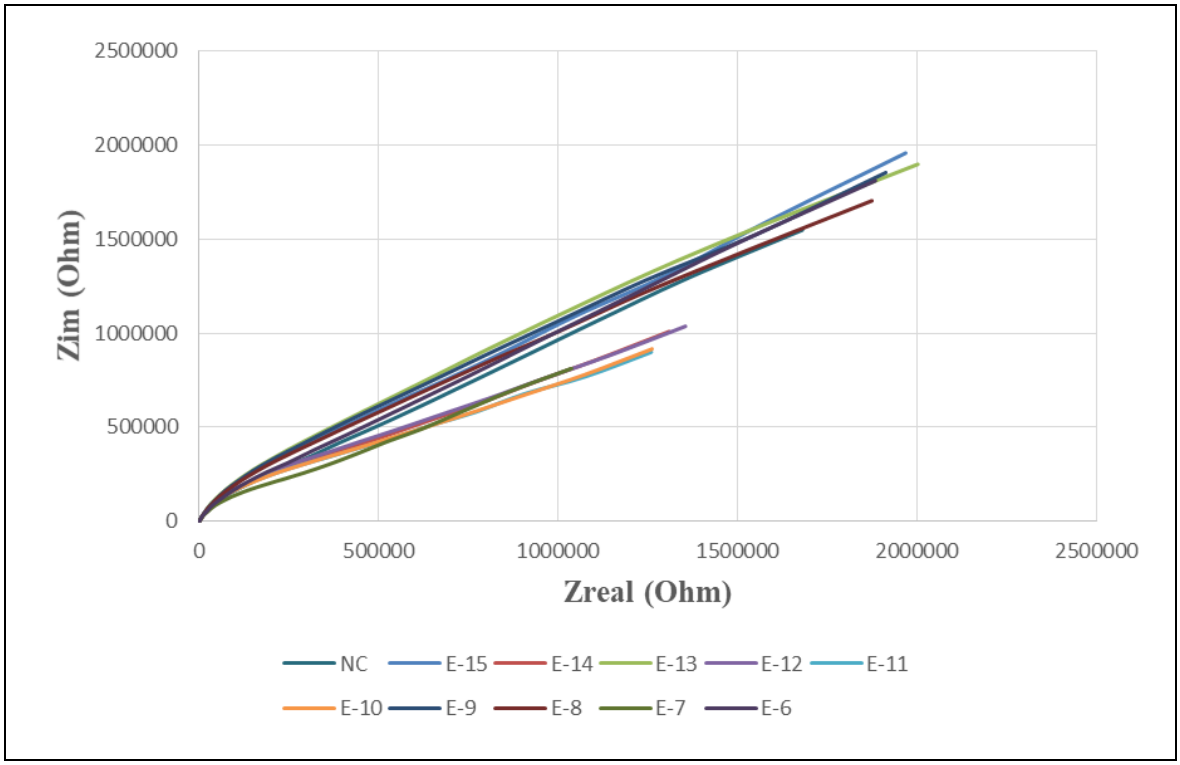

Figure 3.179. EIS response of Au-0.3M-Val-UMIP electrode in methionine solution.

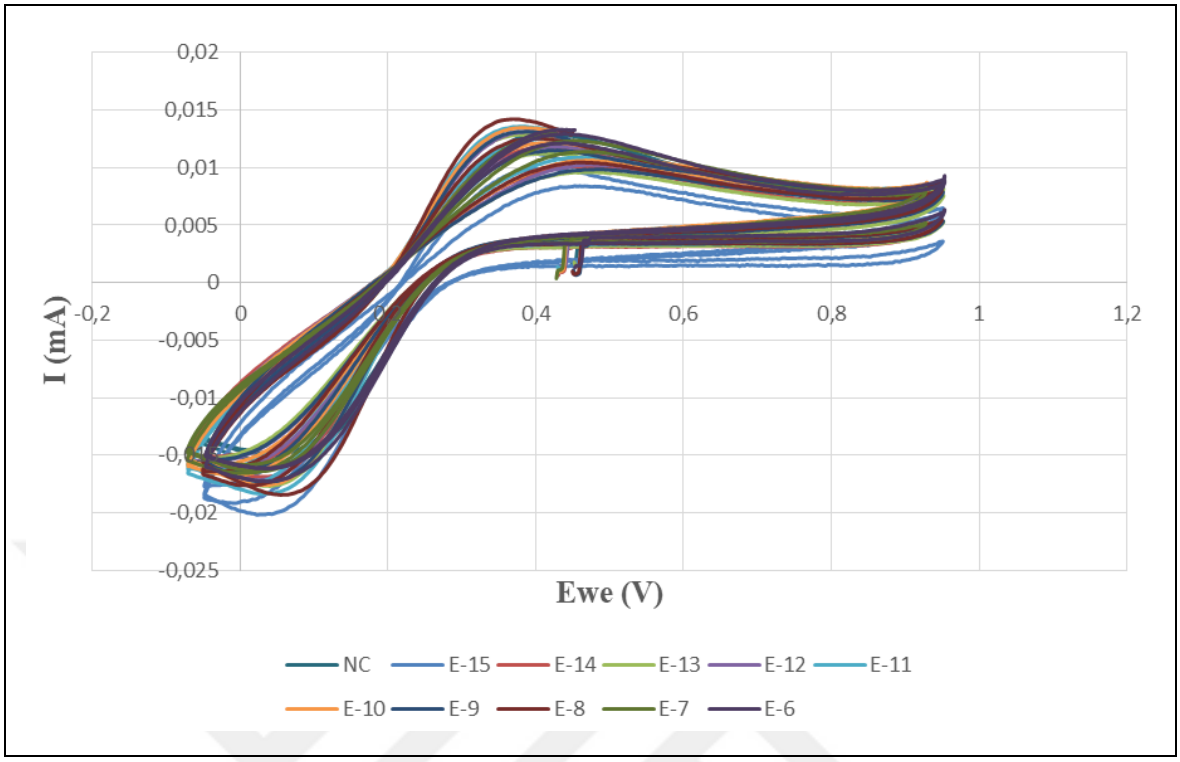

Figure 3.180. CV response of Au-0.3M-Val-UMIP electrode in methionine solution.

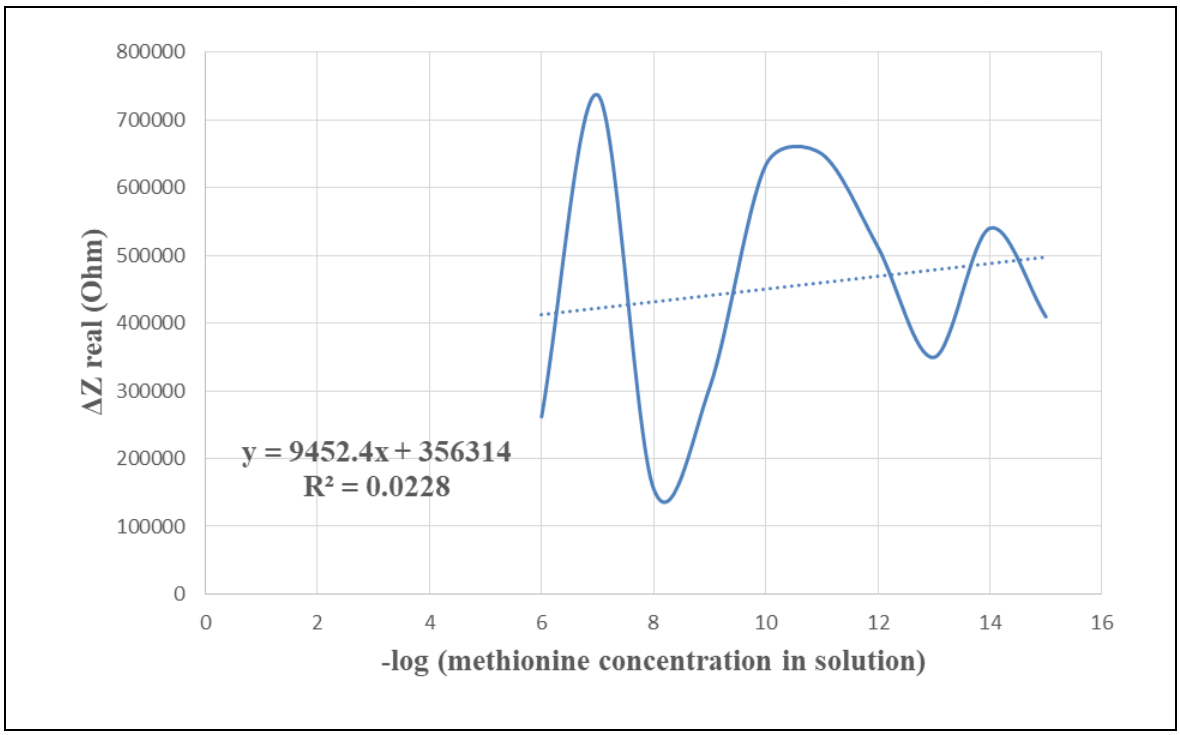

Figure 3.181. The regression curve of Au-0.3M-Val-UMIP electrode in methionine solution.

The selectivity tests conducted with glycine, alanine and methionine indicate that the Au-0.3M-Val-MIP electrode can detect valine molecules in the E-15 M to E-6 M range.

Table 3.22. The selectivity (α) and imprinting factor (β) values of Valine imprinted and non-imprinted electrode.

	MIP	NIP	MIP/NIP
	α	α	β
Glycine	3.96	0.96	4.13
Alanine	4.19	0.95	4.41
Methionine	92.76	0.96	96.63

Valine imprinted electrode was 3.96, 4.19, and 92.76 times more selective for valine than glycine, alanine and methionine, respectively, according to α values as shown in Table 3.22. Results show that valine imprinted Au electrode have higher adsorption capacity for valine in comparison to glycine, alanine and, methionine due to selective capacities in polymer structure.

According to imprinting factors (β values), valine imprinted biosensor (MIP) is more selective for valine than the control electrode (NIP), in presence of the interfering molecules glycine, alanine and methionine, at a ratio of 4.13, 4.41 and 96.63 respectively.

3.5. ANALYSIS OF ELECTRODES IN BLOOD PLASMA

Gold electrodes were analyzed in rat blood plasma sample to investigate the reliability and applicability of valine-MIP biosensors for clinical applications. The use of plasma samples for blood tests minimizes sample processing delays caused by clotting, laboratory technical challenges connected with fibrin development, and delayed results due to incompletely clotted samples. In addition, more plasma than serum can be made from the same volume of blood.

Solutions containing five different standards were prepared with the standard addition method, and EIS measurements were made starting from solution 1 to solution 5 which contain rat blood plasma with the Au-0.3M-Val-MIP electrode, which was chosen as the best electrode. This measurement was made three times from start to finish at different times on the same day (Figures 3.182-3.186), indicating that valine in blood serum binds to the

electrode's recognition interfaces increases valine concentration and impedance on the Au-0.3M-Val-MIP electrode, displaying regression curves generated using impedance data (Ohm) versus volume of standard added (mL) (Figures 3.183, 3.185, 3.187). At the end of each analysis, the electrodes were washed in 0.1M HCl and distilled water to ensure electrode reusability by removing the bound valine molecules.

In the results given below, the EIS results of the blank solution were not obtained; which was a laboratory error. In order to meet the deadlines, the experiments were not repeated and corrected for the EIS response to blank solution using an exponential equation. We think that this estimation was plausible as the average and standard deviation results of all of the three blood test measurements were close to the results obtained from the laboratory.

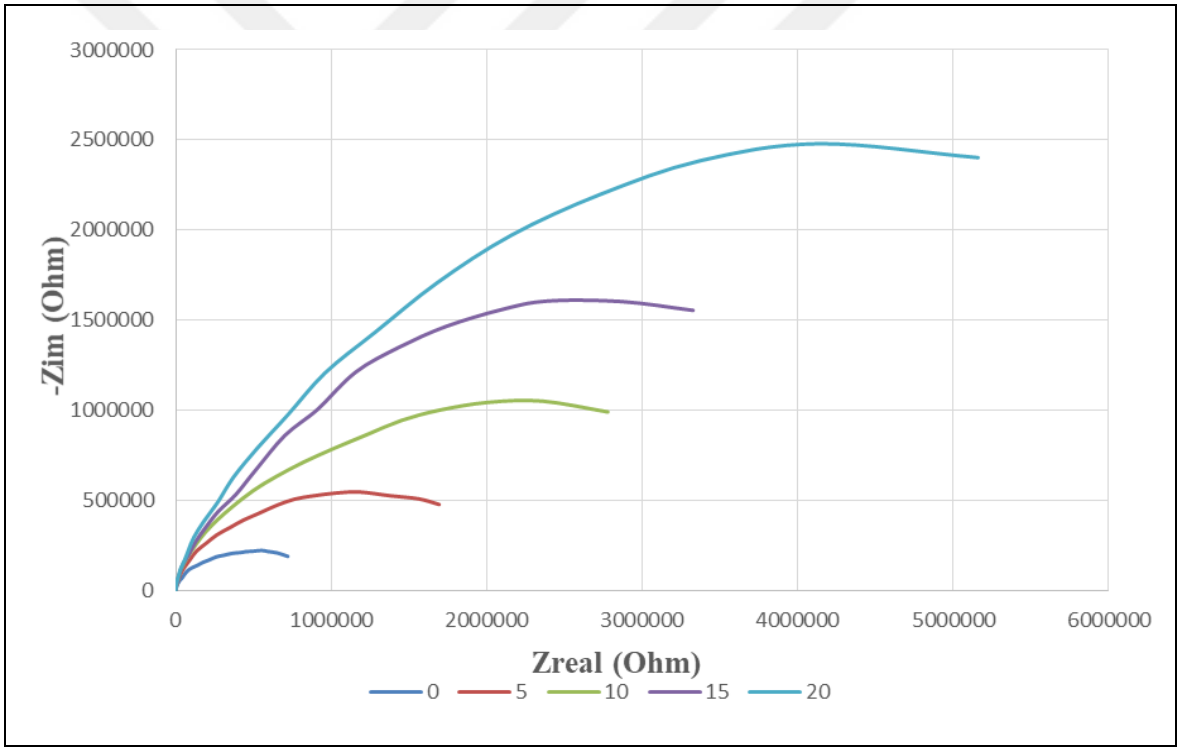

Figure 3.182. EIS response in the first measurement of the Au-0.3M-Val-MIP electrode in diluted blood plasma.

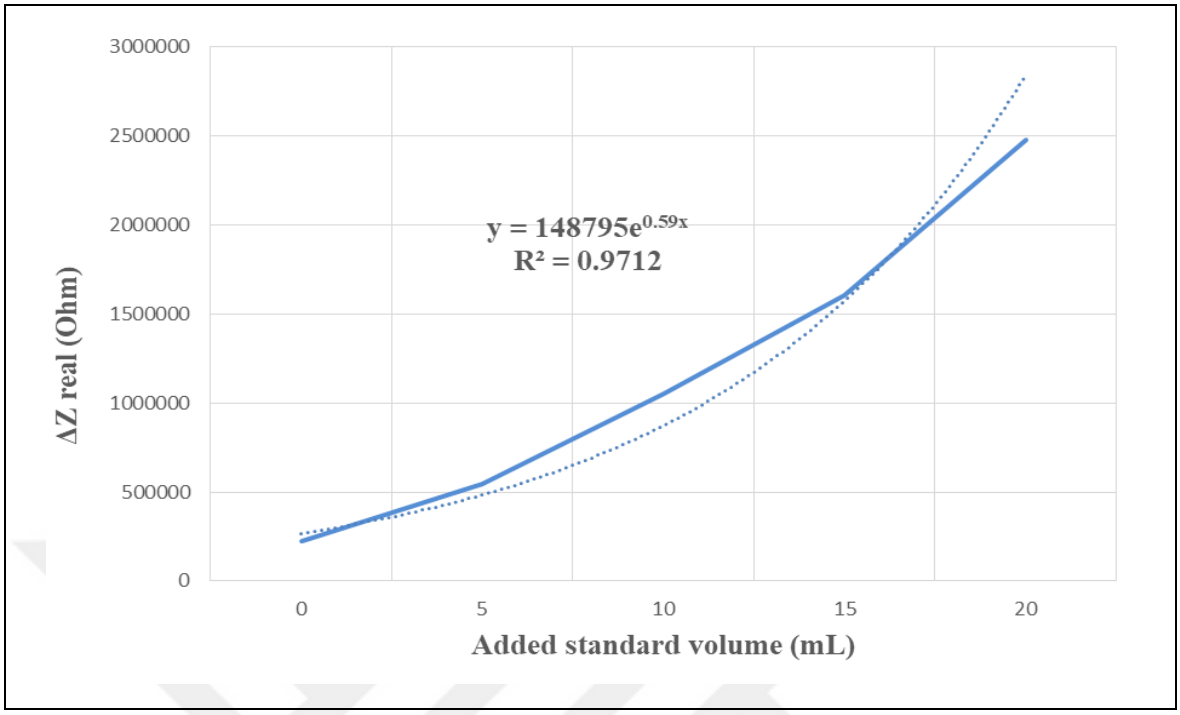

Figure 3.183. The regression curve of the Au-0.3M-Val-MIP electrode obtained in the first measurement.

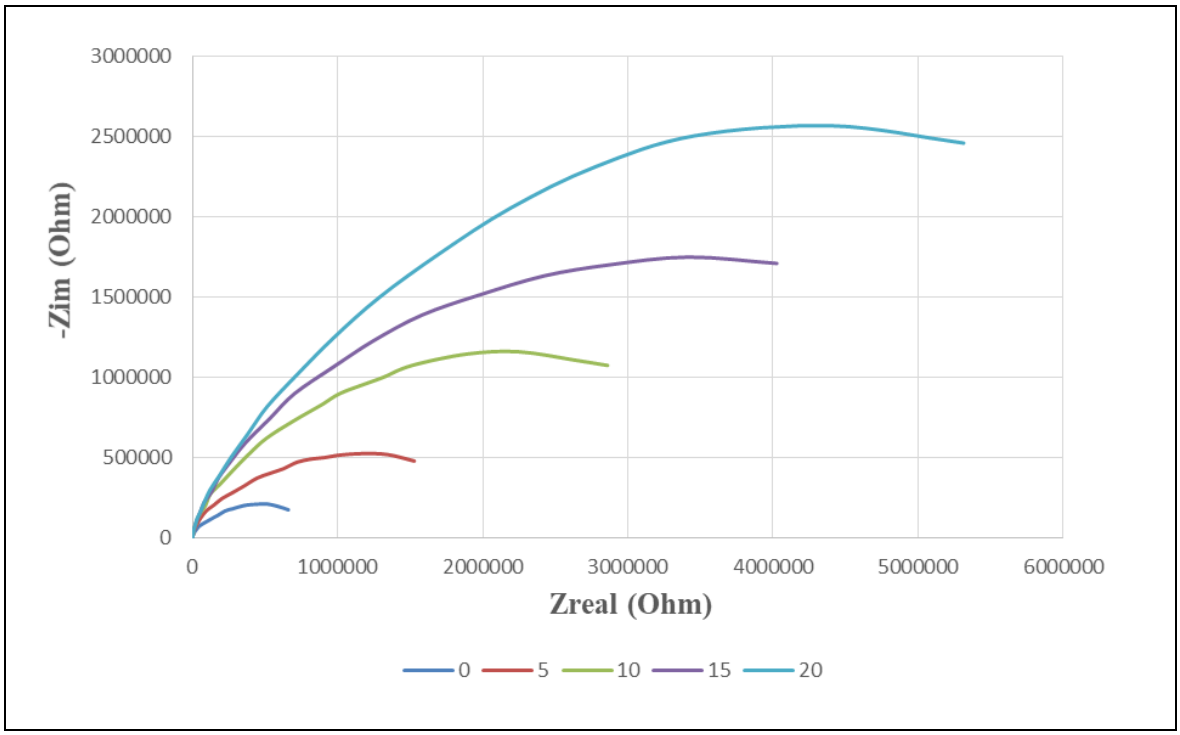

Figure 3.184. EIS response in the second measurement of the Au-0.3M-Val-MIP electrode in diluted blood plasma.

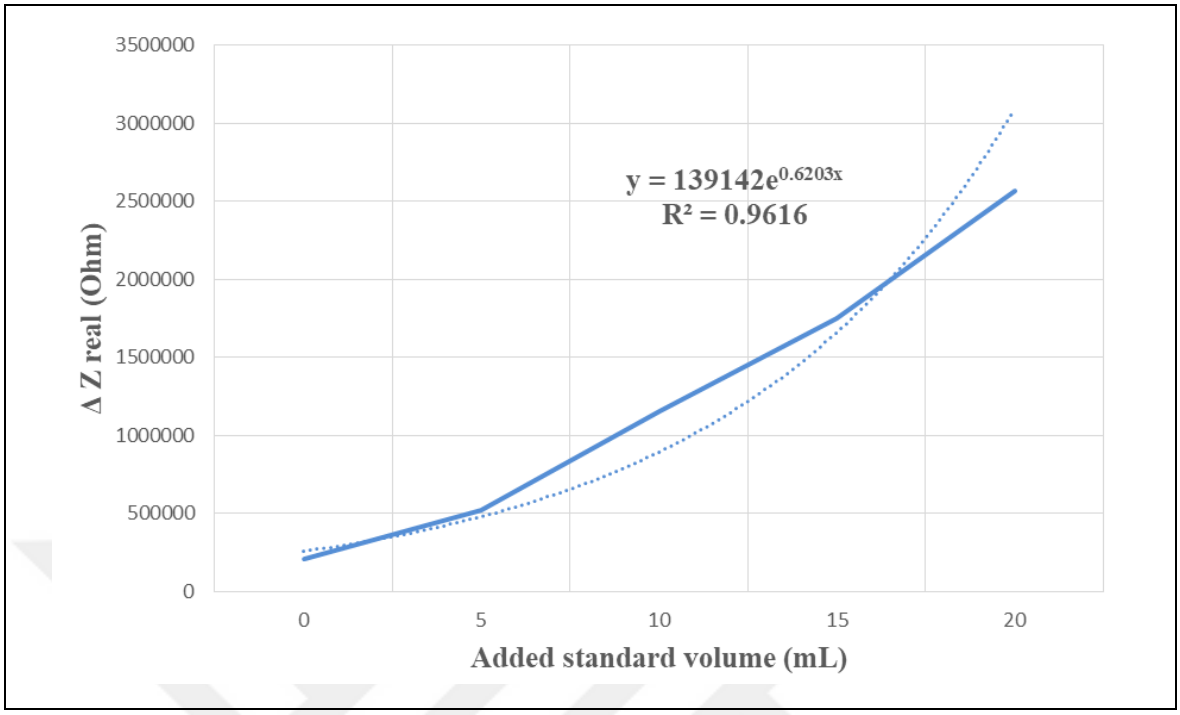

Figure 3.185. The regression curve of the Au-0.3M-Val-MIP electrode obtained in the second measurement.

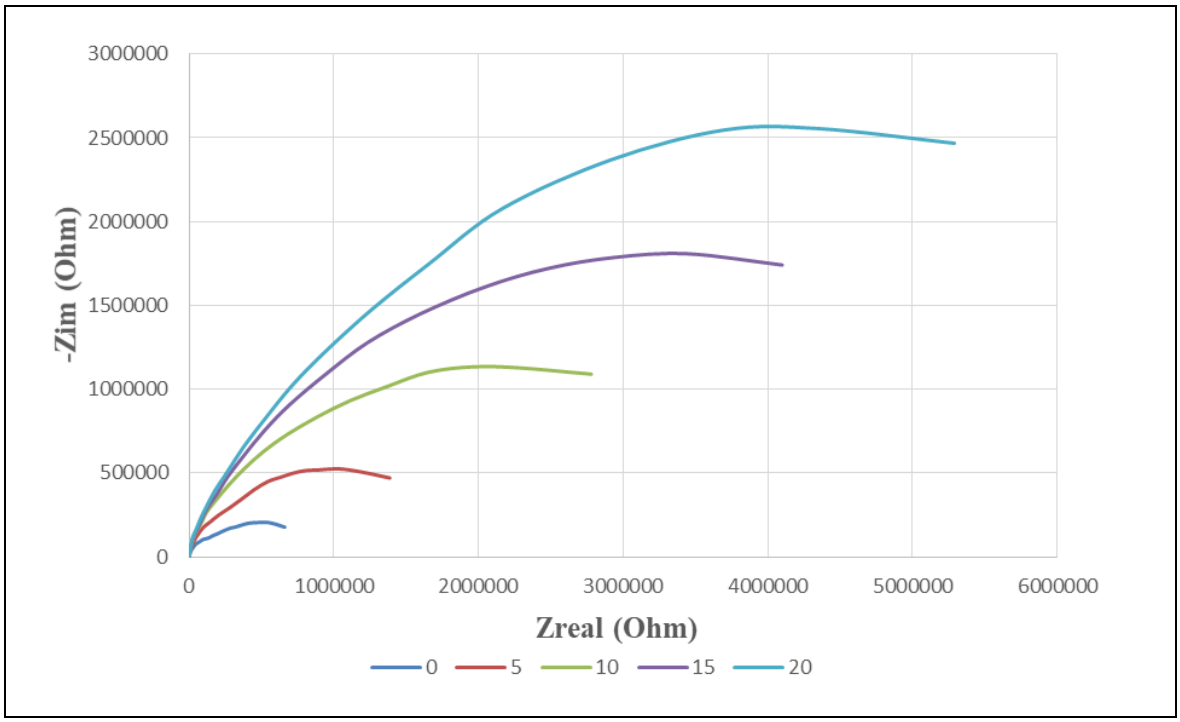

Figure 3.186. EIS response in the third measurement of the Au-0.3M-Val-MIP electrode in diluted blood plasma.

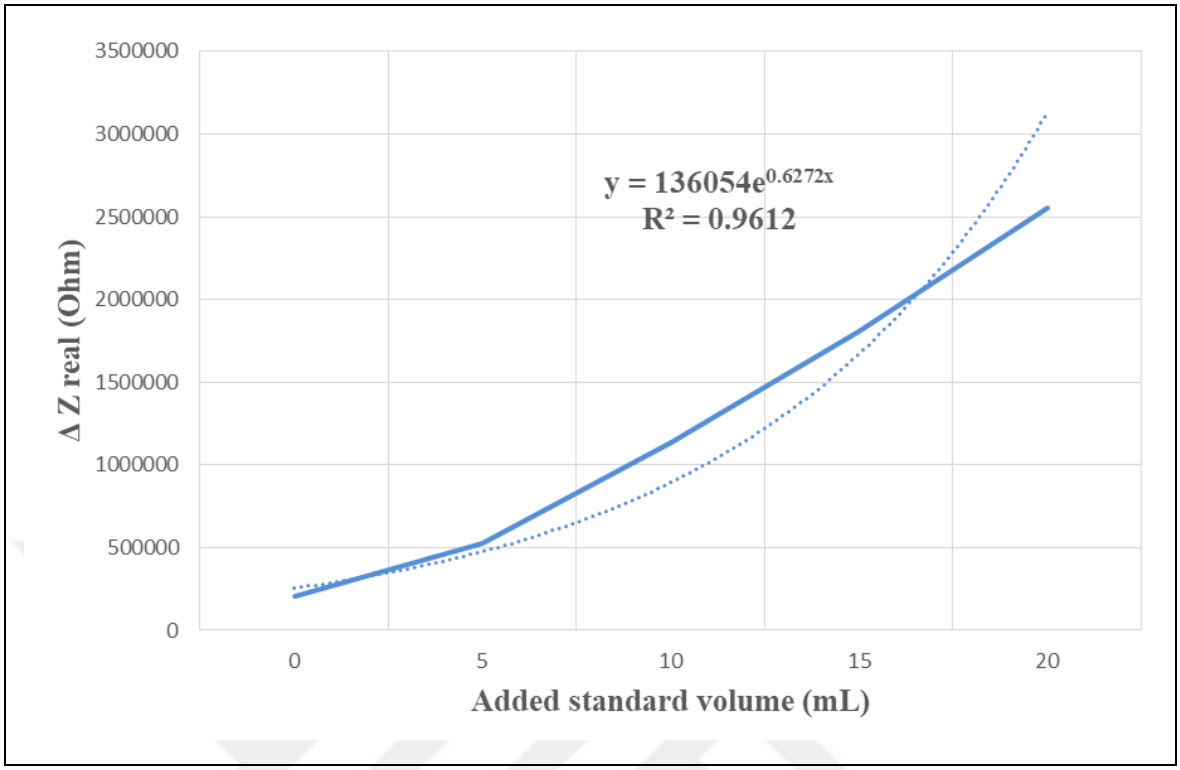

Figure 3.187. The regression curve of the Au-0.3M-Val-MIP electrode obtained in the third measurement.

The EIS graph of the Au-0.3M-Val-MIP electrode (Figure 3.182) shows that the R_{ct} values increase on a regular basis. The regression curve, displaying the change in the electrode's impedance and R_{ct} values versus the amount of standard added, shows that this electrode performed 97 percent successfully in the analysis (Figure 3.183). As the amount of standard added to RdxPBS increases, the amount of valine also increases, and accordingly, more adhesion occurs on the electrode surface. The addition of more governors to the valine recognition sites on the electrode surface raises impedance and R_{ct} values. Similarly, the second and third measurement performed with the same electrode to determine the amount of valine in the blood plasma using the standard addition method, have given correlating results, indicating regular increase in impedance at 96 percent and 96 percent regression values respectively (Figure 3.184-3.187). In the standard addition method applied to determine the unknown valine concentration in the rat blood plasma, it was determined that there was 326 µM, 304 µM and 298 µM for first, second and third measurements,respectively, valine in the plasma, according to the calculation of the analyte

concentration as shown in Table 3.3. The valine concentration in the rat blood plasma was determined as 309±14.74 µM by taking the average of these three measurements.

Table 3.3. Valine concentrations in rat blood obtained with standard addition method.

Blood tests	R^2	Valine concentration (µM)
1st measurement	0.9712	326
2nd measurement	0.9616	304
3rd measurement	0.9612	298
Average		309
Standard deviation		14.74

3.6. AFM ANALYSIS OF VALINE MIP ELECTRODE

AFM analysis was done on the hydrogel solution prepared with valine molecules used to coat the electrodes using a Park Systems XE 100 Atomic force microscope (Bio-Rad, Hercules, CA). At room temperature, images were taken in contact mode with silicon nitride tips. An image processing algorithm created by PSIA, XEI, was used to examine AFM pictures.AFM images were taken to examine the structure of the coated polymer. Control group polymer was prepared with hydrogel solution working with gold electrode without any imprinting process (Figure 3.188). The valine-UMIP group was prepared after imprinting the valine molecule at 0.1, 0.3 and 0.5 M concentrations without any removal of the template molecule (Figure 3.190, 3.192, 3.194). The valine-MIP group was obtained by imprinting 0.3 M valine, and then removing the template molecule with 0.1 M HCl and distilled water (Figure 3.196). 3D AFM images of polymers prepared by MIP and UMIP techniques for the valine molecule are shown in Figures 3.191, 3.193, 3.195 and 3.197. The surface characterization of the prepared polymers was done by scanning the 100 nm^2 surface area. There were observable differences in the topography of the NIP, MIP and UMIP electrodes both valine and choline electrodes. These differences are considered to be due to the inclusion and then removal of the template molecule. The NIP electrodes have displayed a denser topography than the MIP and UMIP electrodes.

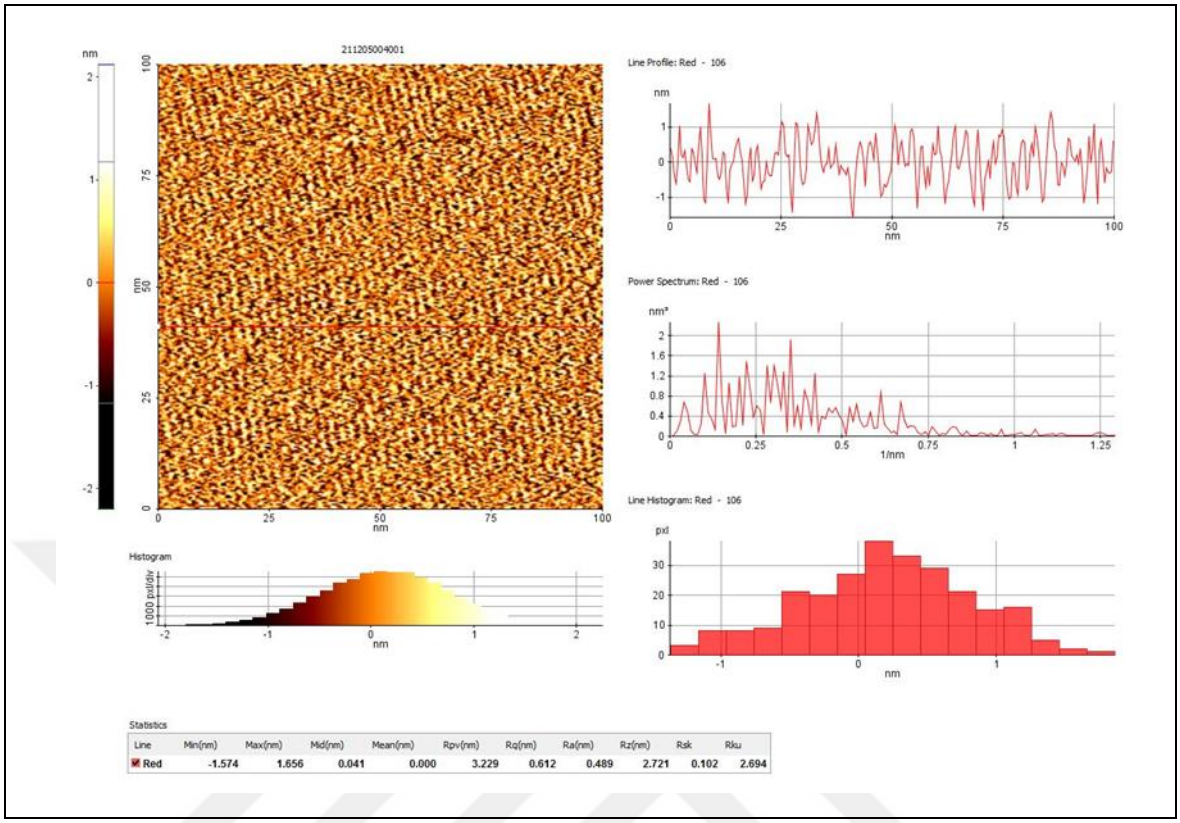

Figure 3.188. AFM image of control polymer.

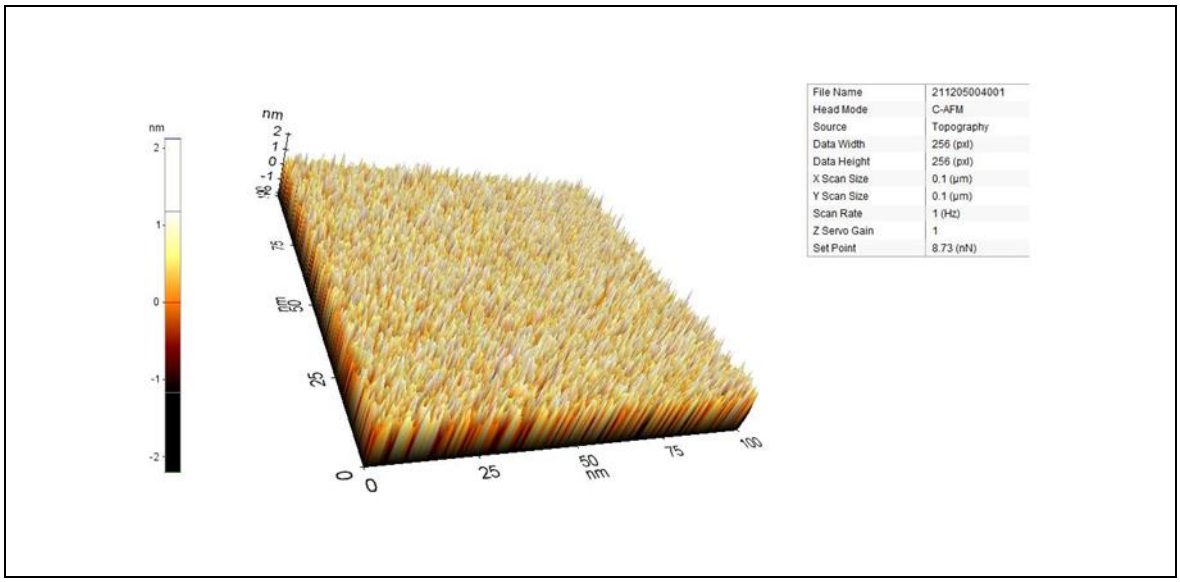

Figure 3.189. 3D AFM image of control polymer.

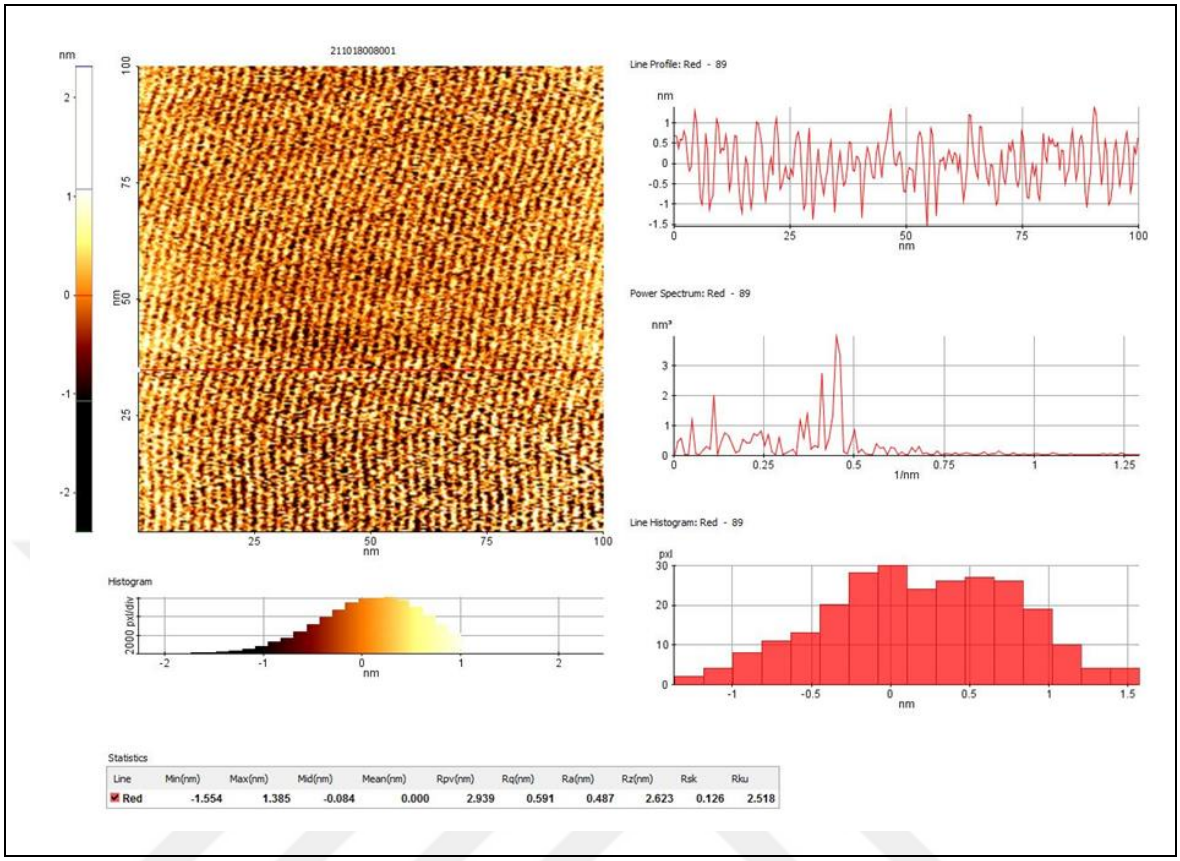

Figure 3.190. AFM image of 0.1M Valine UMIP polymer.

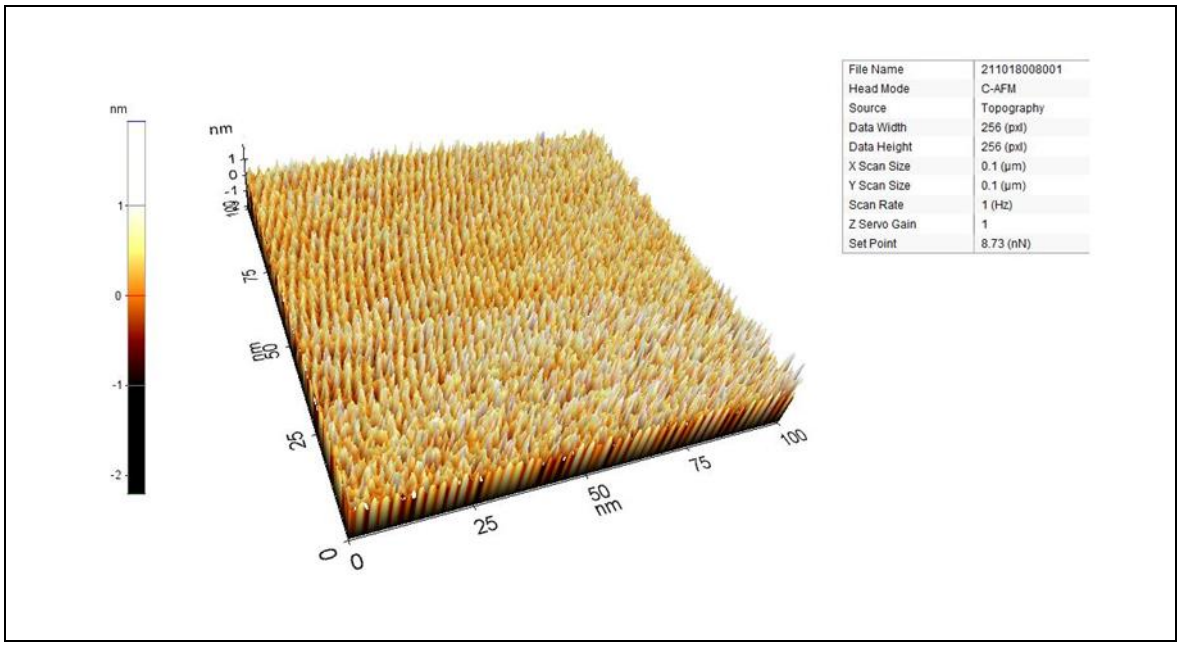

Figure 3.191. 3D AFM image of 0.1 M Valine UMIP polymer.

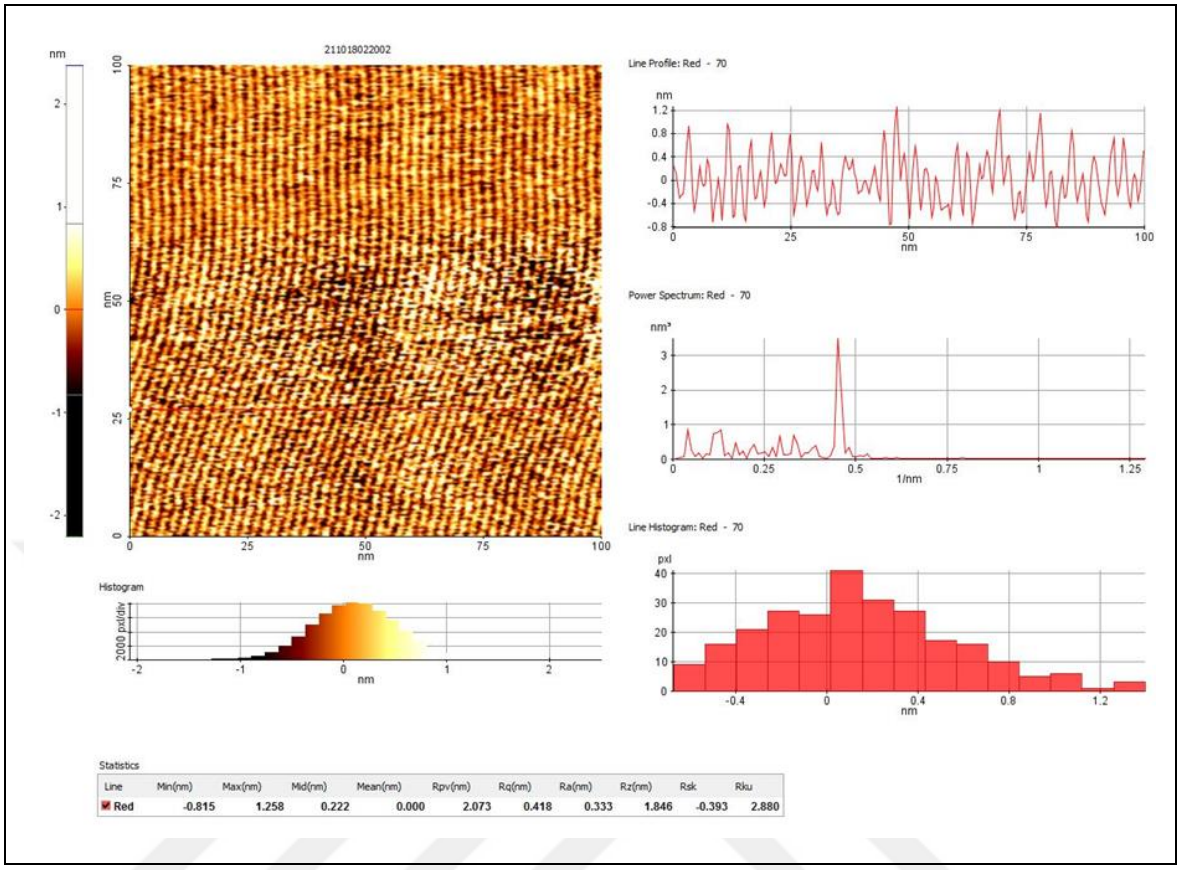

Figure 3.192. AFM image of 0.3 M Valine UMIP polymer.

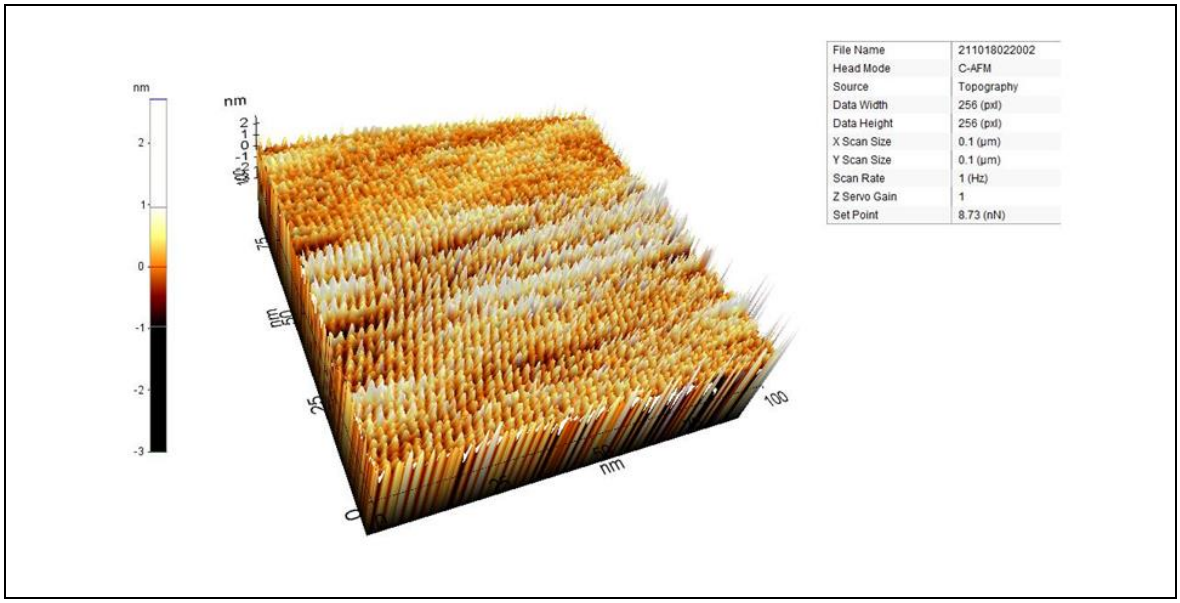

Figure 3.193. 3D AFM image of 0.3 M Valine UMIP polymer.

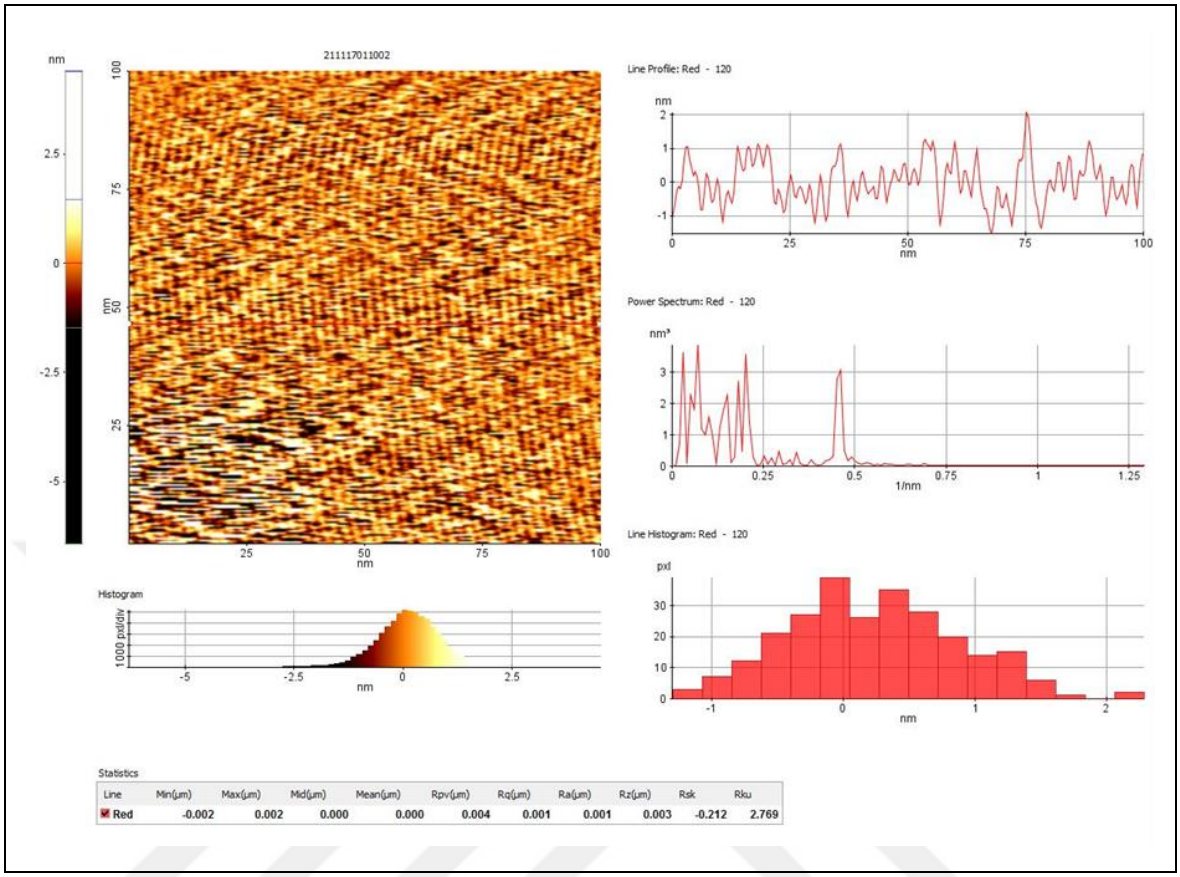

Figure 3.194. AFM image of 0.5 M Valine UMIP Polymer.

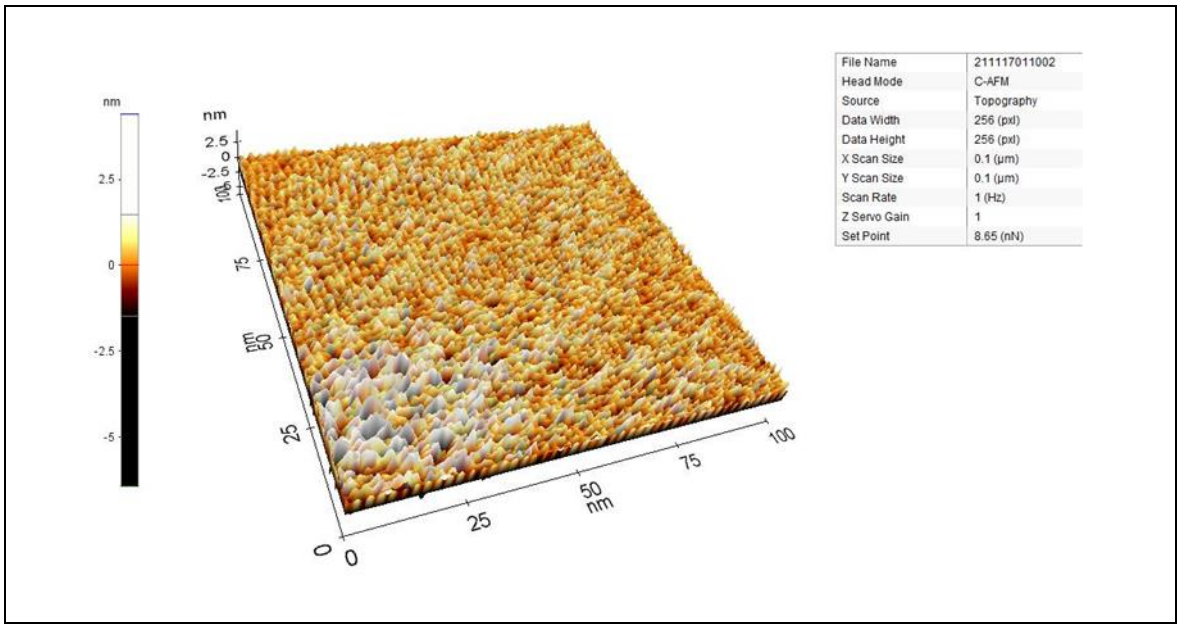

Figure 3.195. 3D AFM image of 0.5 M Valine UMIP polymer.

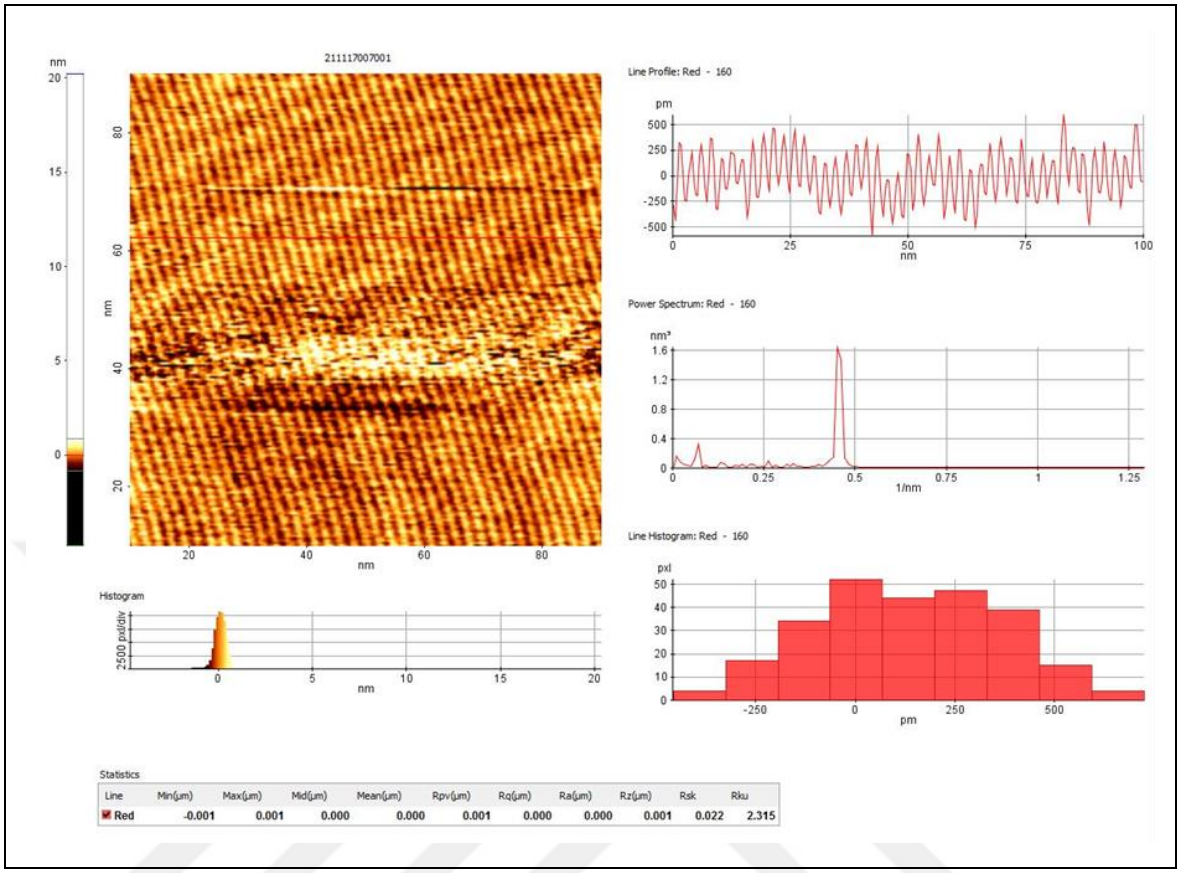

Figure 3.196. AFM image of 0.3 M Valine MIP polymer.

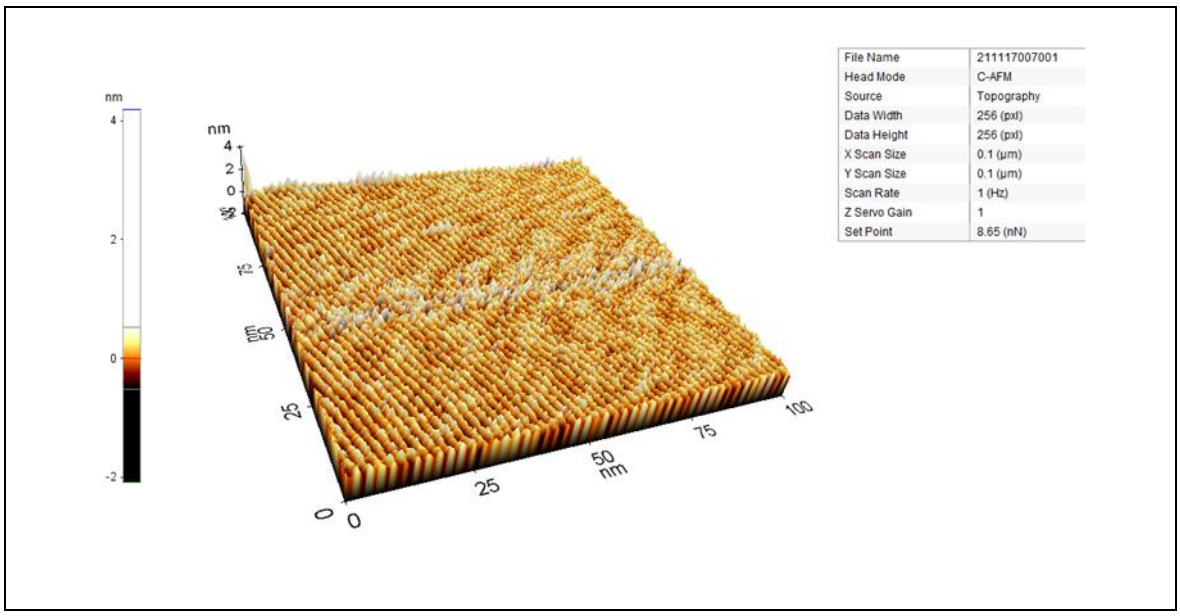

Figure 3.197. 3D AFM image of 0.3 M Valine MIP polymer.

3.7. AFM ANALYSIS OF CHOLINE MIP ELECTRODE

AFM analysis was done on the hydrogel solution prepared with choline molecules used to coat the electrodes using a Park Systems XE 100 Atomic force microscope (Bio-Rad, Hercules, CA). At room temperature, images were taken in contact mode with silicon nitride tips. An image processing algorithm created by PSIA, XEI, was used to examine AFM pictures.

AFM images were taken to examine the structure of the coated polymer. Control group polymer was prepared with hydrogel solution working with gold electrode without any imprinting (3.198). The choline-UMIP group was prepared by suppressing the choline molecule at a concentration of 0.1, 0.2, 0.3 and 0.5 M as shown in Figure 3.200, 3.202, 3.204 and 3.206. Finally, the choline-MIP group was prepared by imprinting the choline molecule at a concentration of 0.2 M and removing the template molecule as shown in Figure 3.208. 3D AFM images of polymers prepared by MIP and UMIP techniques for the choline molecule are shown in Figures 3.201, 3.203, 3.205, 3.207 and 3.209. The surface characterization of the prepared polymers was done by scanning the 100 nm^2 surface area.

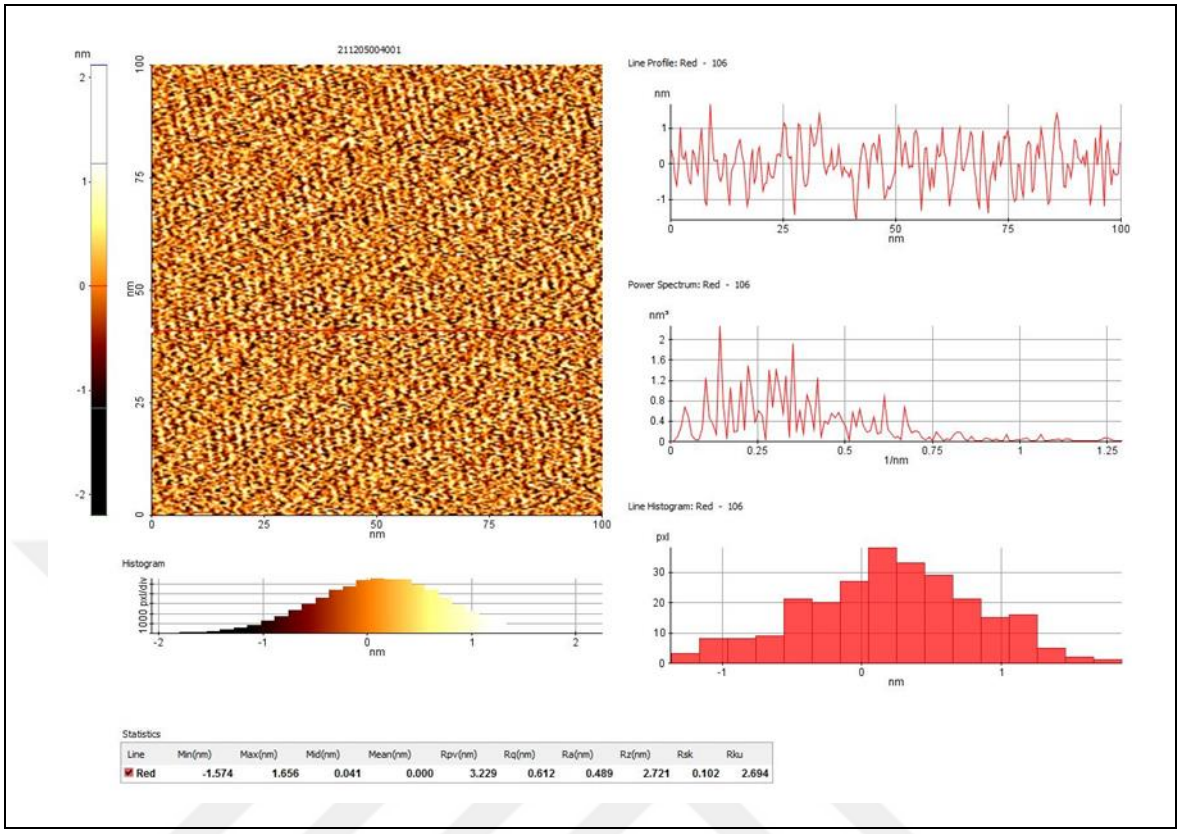

Figure 3.198. AFM image of control polymer.

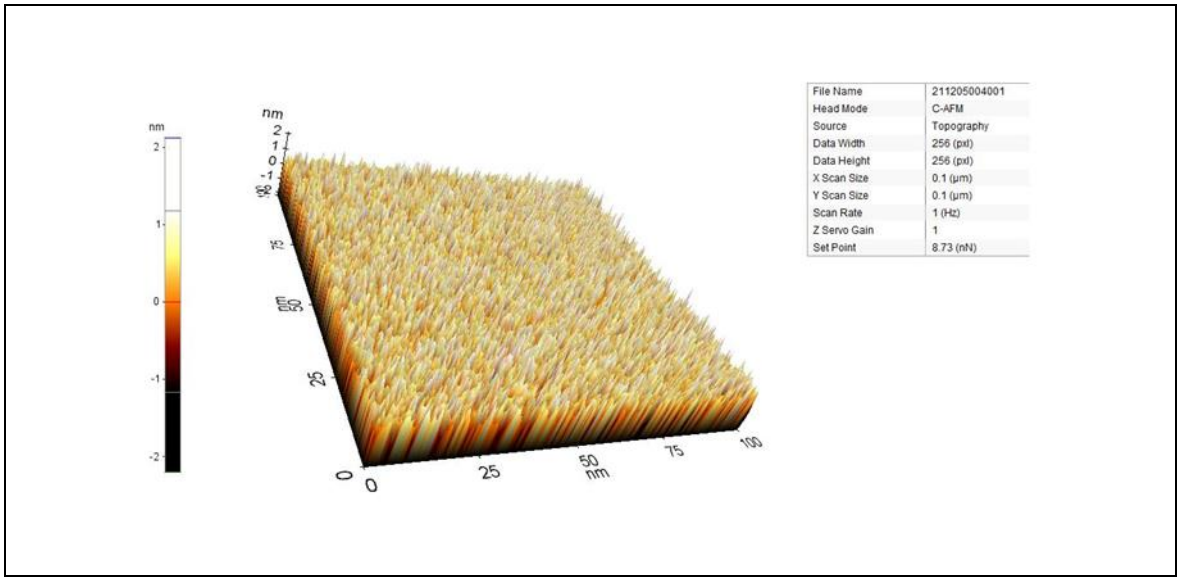

Figure 3.199. 3D AFM image of control polymer.

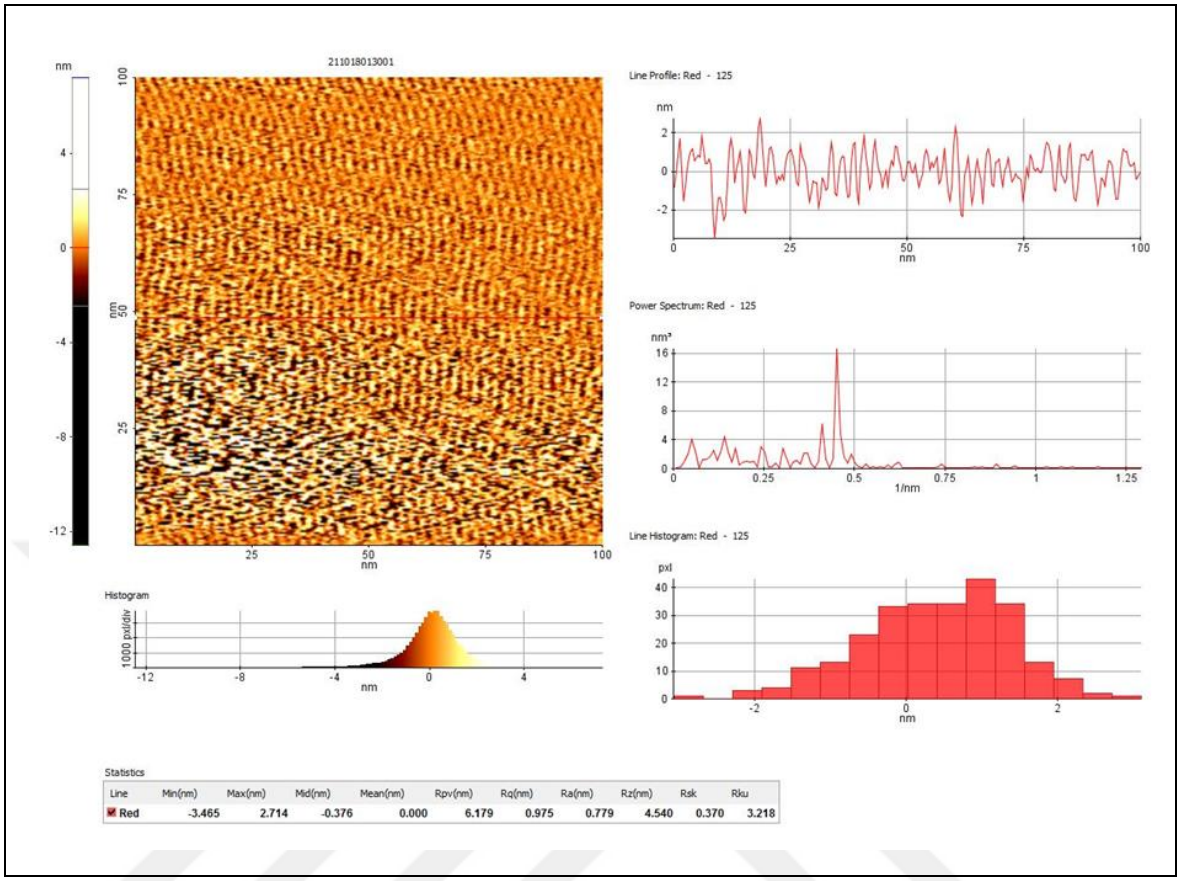

Figure 3.200. AFM image of 0.1 M choline UMIP polymer.

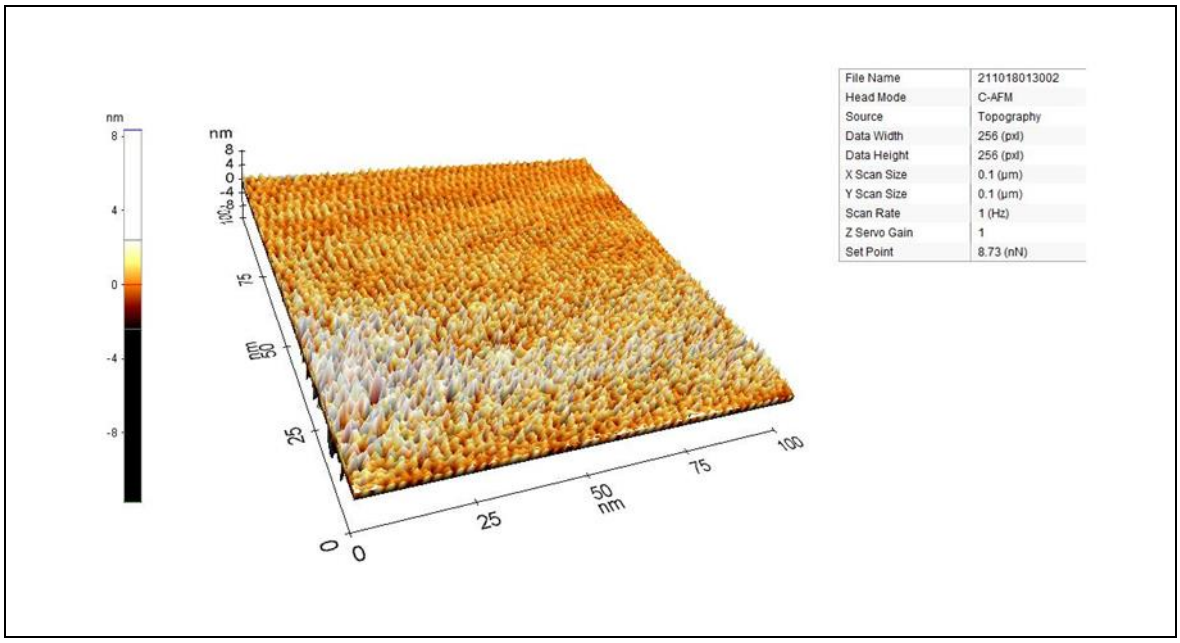

Figure 3.201. 3D AFM image of 0.1 M choline UMIP polymer.

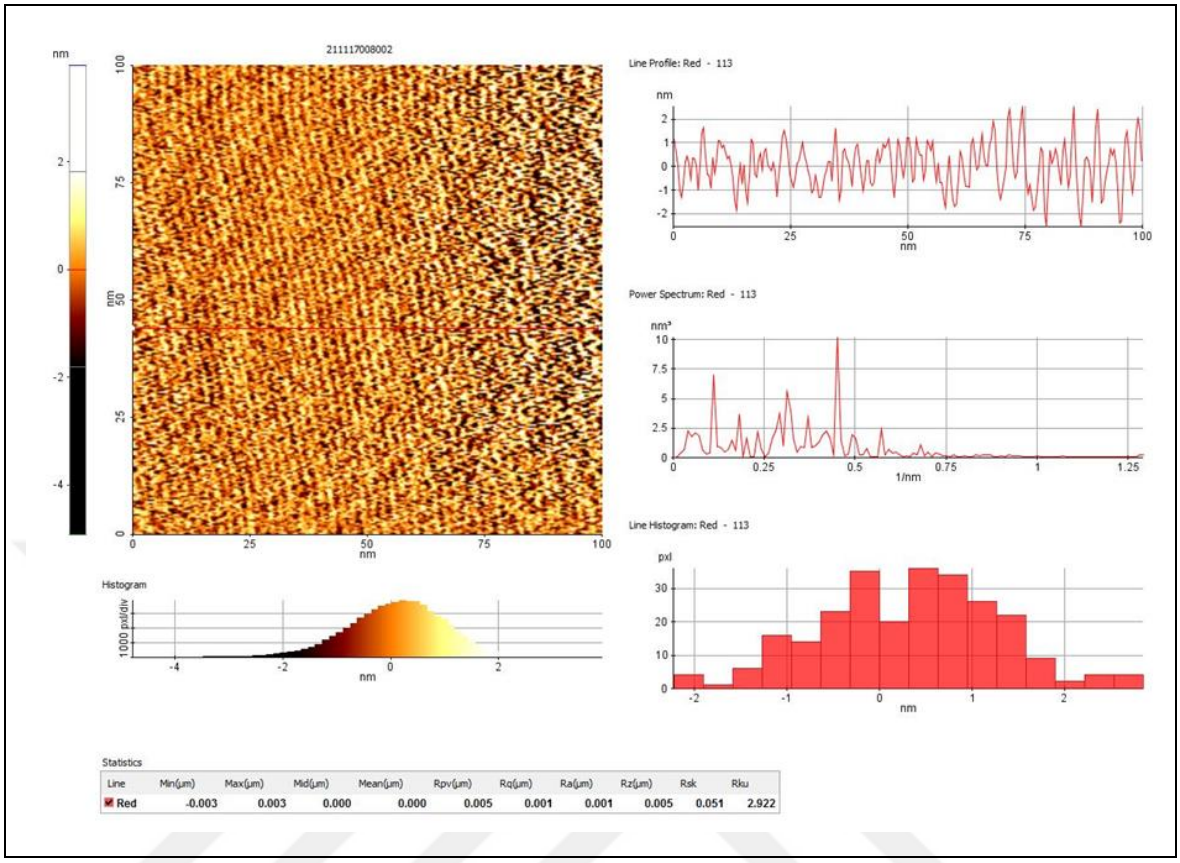

Figure 3.202. AFM image of 0.2 M choline UMIP polymer.

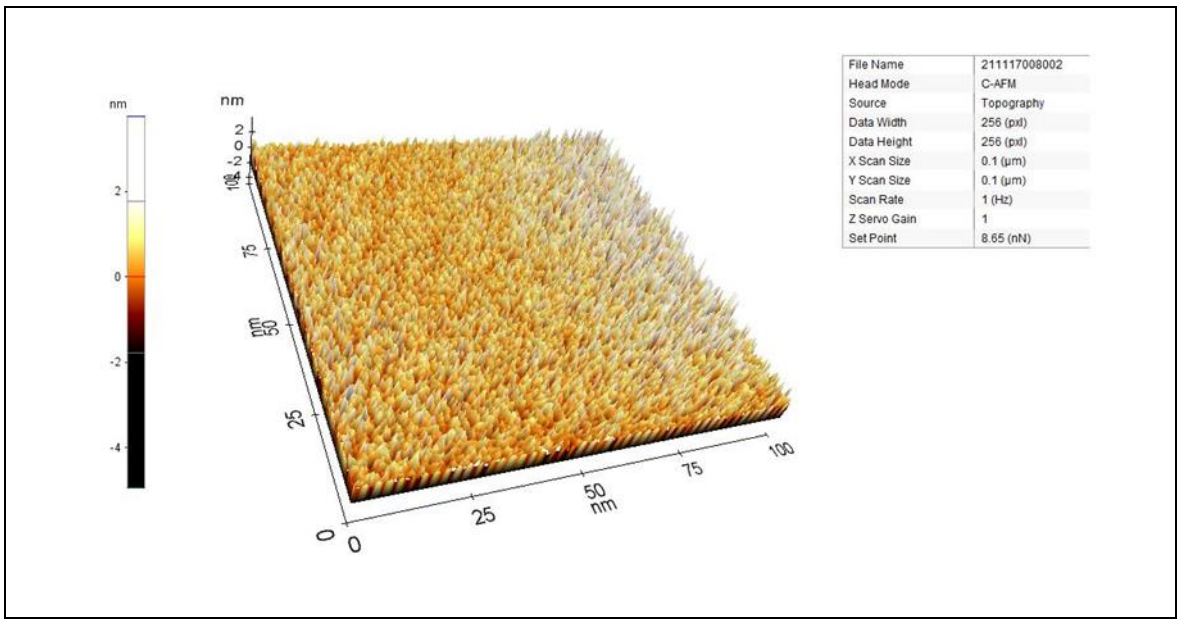

Figure 3.203. 3D AFM image of 0.2 M choline UMIP polymer.

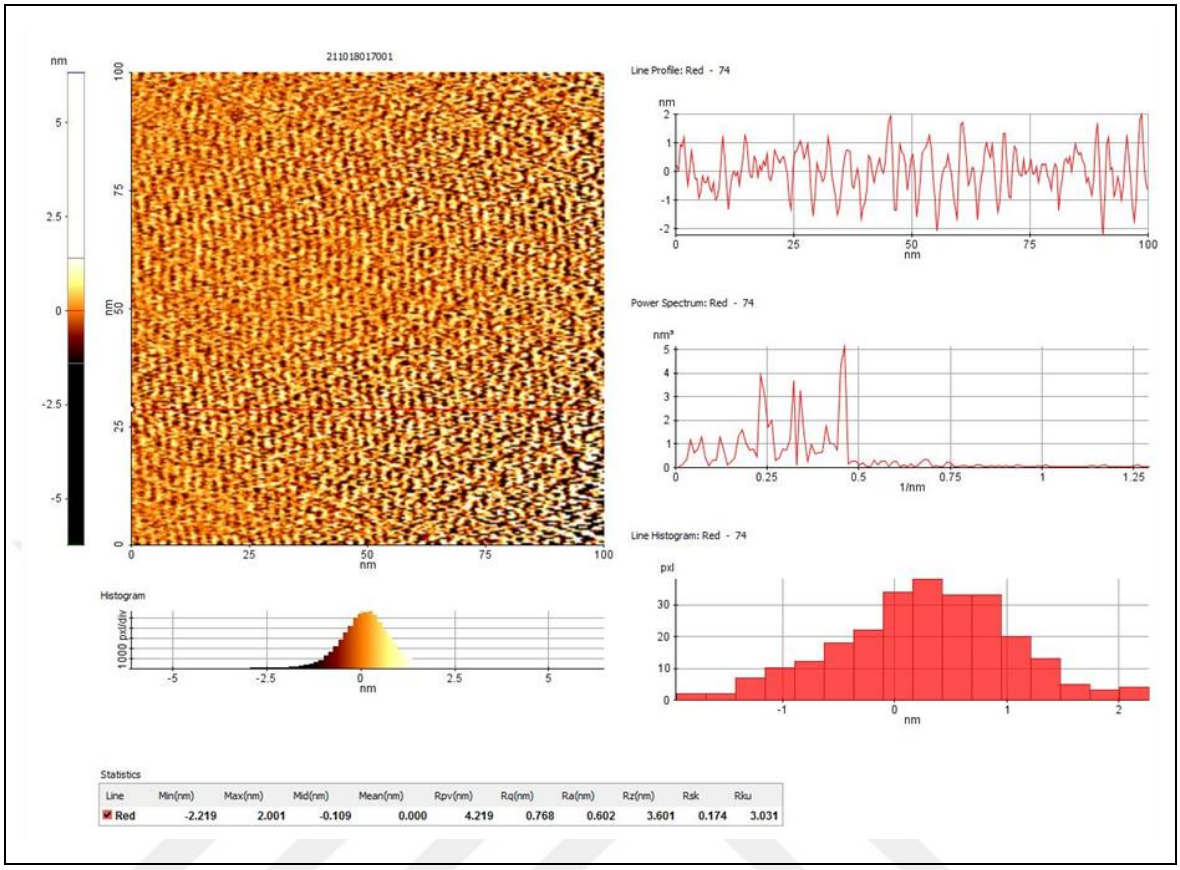

Figure 3.204. AFM image of 0.3 M choline UMIP polymer.

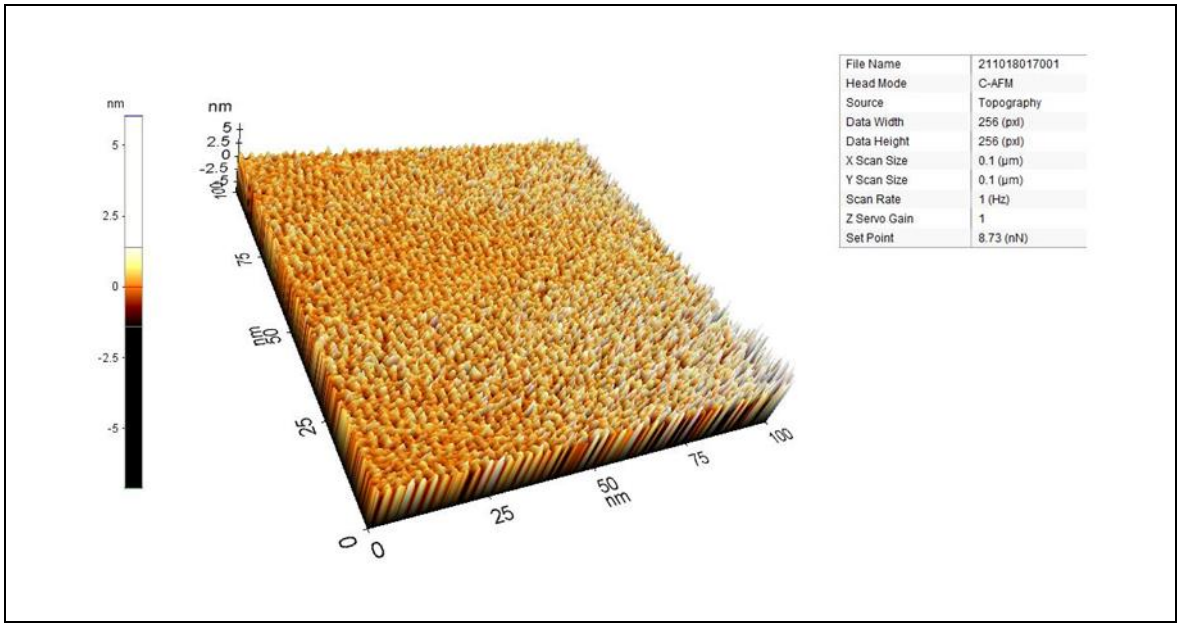

Figure 3.205. 3D AFM image of 0.3 M choline UMIP polymer.

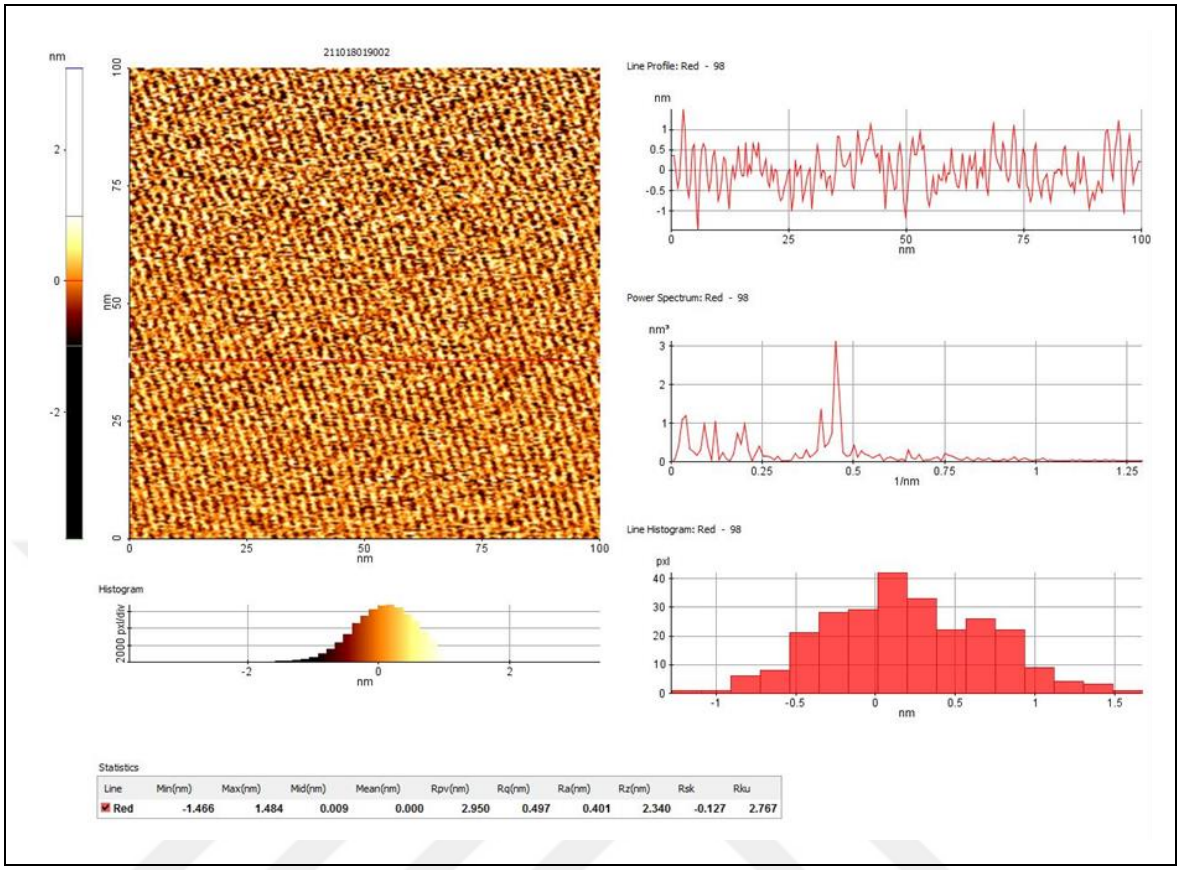

Figure 3.206. AFM image of 0.5 M choline UMIP polymer.

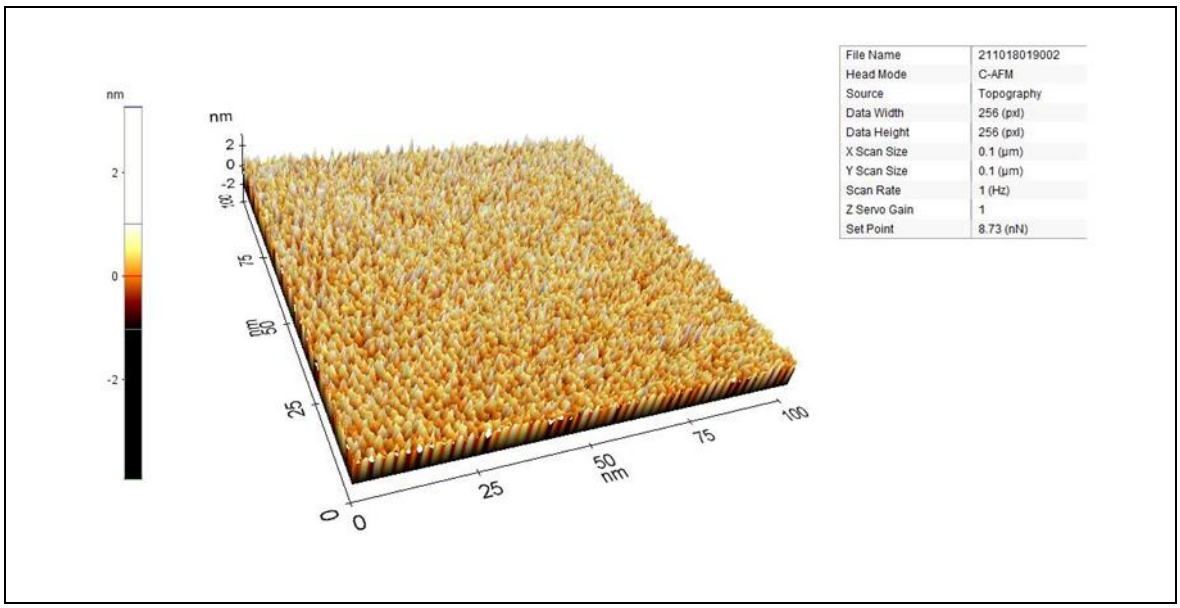

Figure 3.207. 3D AFM image of 0.5 M choline UMIP polymer.

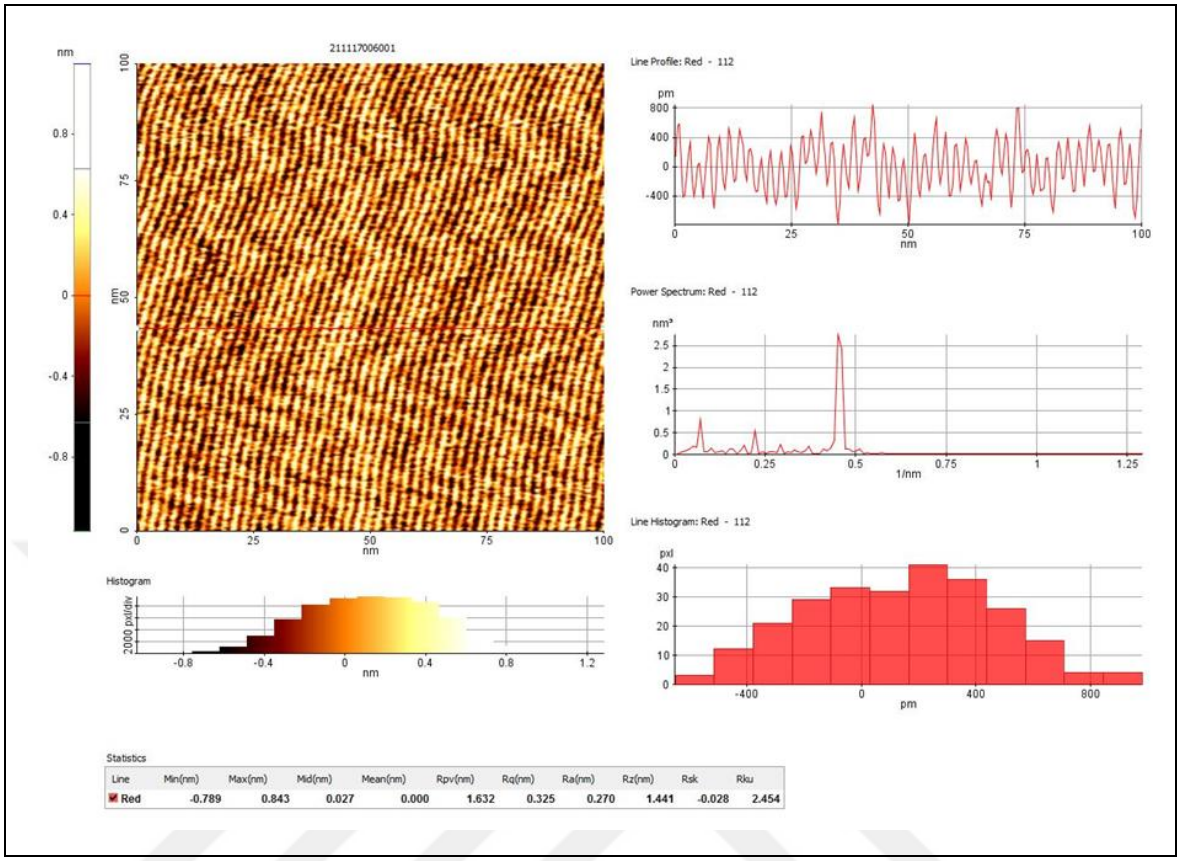

Figure 3.208. AFM image of 0.2 M choline MIP polymer.

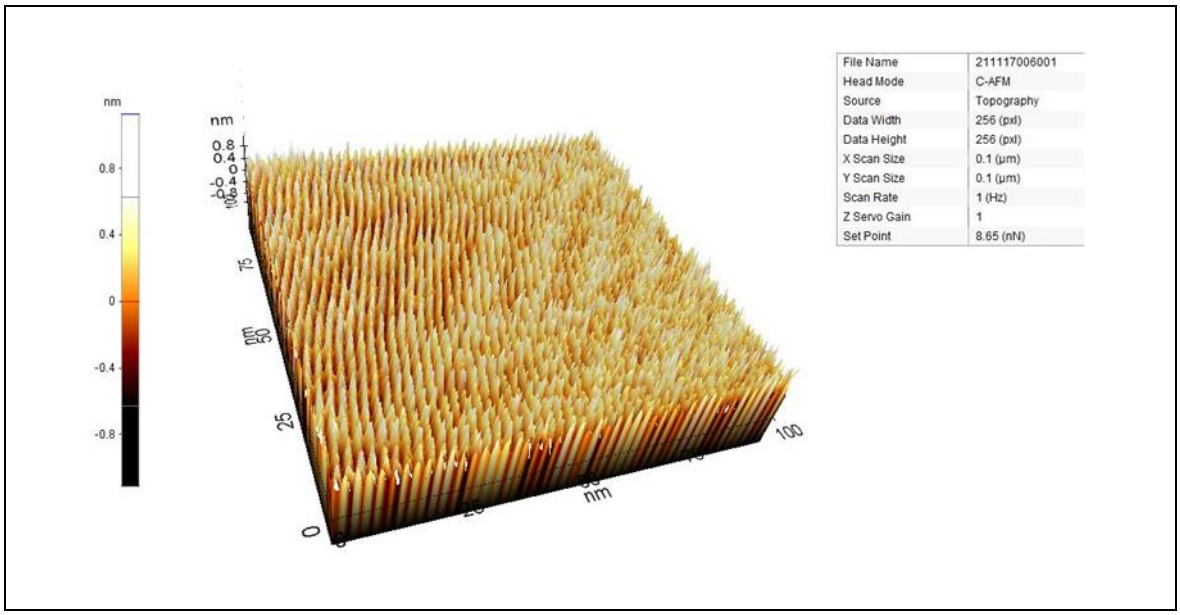

Figure 3.209. 3D AFM image of 0.2 M choline MIP polymer.

4. DISCUSSION

In this thesis, it was aimed to develop an impedimetric biosensor sensitive to valine biomarker and for this purpose, three groups of electrodes were obtained by imprinting valine on gold disc electrodes using the molecular imprinting method. Three groups of electrodes were prepared in its pure form by imprinting a valine-free hydrogel solution (Au-NIP), by imprinting and removing valine at ten different molarities (Au-MIP), and finally by imprinting and not removing valine at the same ten molarities (Au-UMIP). The appropriate hydrogel formulation for valine detection was determined and using pencil graphite electrodes optimized for pH, scan rate and response time. After selecting the appropriate hydrogel solution, valine was molecularly imprinted on gold disc electrodes and electrochemical characterization studies were carried out to determine the valine detection range of these electrodes, which were prepared in ten different molarities. As a result of these studies, the detection concentration of electrodes was finalized as 0.3 M valine, Au-0.3M-Val-MIP electrode. The Au-0.3M-Val-MIP electrode recognizes valine molecule by its affinity to Acrylamide/Bisacrylamide with the cooperative effect of H bonds, secondary forces and geometric recognition (3D shape memory) factors [90-92]. In previous studies, the response of choline imprinted electrodes using a different hydrogel solution containing MAGA, EGDMA and AIBN [84]; however, the use of PAGE hydrogel in this study prevented current drifts in CV graphs, and enabled acquisition of EIS and CV results which separated well over a wide concentration range. LOQ was calculated as 7.18E-15 M and LOD was calculated as 9.76E-17 M. The valine electrode prepared at various valine concentrations enabled detection and separation of differences in valine concentration as a result of correlating valine recognition sites in the molecularly imprinted gold electrodes. The lower concentration level has been illustrated in Au-0.15M-Val-MIP and Au-0.2M-Val-MIP electrodes (Figures 3.38, 3.44). By increasing the valine concentration, the valine recognition regions formed on the molecularly imprinted electrodes were increased and more valines were allowed to attach to these regions. When the upper concentration level imprinted on the electrode rises above a certain concentration, the saturation of the artificial receptors on the electrodes are attained as given in the EIS analyzes of Au-0.45M-Val-MIP and Au-0.5M-Val-MIP electrodes (Figures 3.86, 3.92). It can be said that less number of valine artifical receptors are formed in gold electrodes prepared by imprinting at low

concentration and the impedance is relatively lower than electrodes with high concentrations. Au-0.15M-Val-MIP, Au-0.2M-Val-MIP and Au-0.25M-Val-MIP electrodes are electrodes prepared with low valine concentration. Figures 3.40, 3.46 and 3.52 show that while there is a divergence in the impedance responses with low valine concentrations on these electrodes, the impedance responses with high valine concentrations are not able to differentiate from each other. The EIS analyzes of Au-0.4M-Val-MIP, Au-0.45M-Val-MIP and Au-0.5M-Val-MIP electrodes prepared at a high valine concentration, display close impedance values in solutions containing low valine concentration and differentiated impedance in solutions containing high valine concentration as a result of the amount of receptor formed on the electrode.

In EIS measurements made when 0.3 M valine molecule is molecularly imprinted on graphite electrode (PGE7-(TRIS-0.3M-Val-MIP)) and gold electrode (Au-0.3M-Val-MIP), the gold electrode responds at higher impedance levels and it is expressed in Figure 3.27 and Figure 3.64. This is because the resistivity of the gold electrode is higher than the graphite electrode, as it is electrically less conductive. In the selectivity tests, when the measurement is made in the solution containing a molecule other than the molecule imprinted on the gold electrode, it is seen that the impedance responses are formed in the EIS graphs, and the R_{ct} values have not been attained. It may be necessary to operate the system at lower frequencies to observe an R_{ct} value.

After selecting the electrode with the widest detection range, precision, reproducibility and stability tests , selectivity analysis and blood plasma tests were performed with this electrode (0.3M-Val-MIP). These tests were performed with pencil graphite electrodes, because we only have one gold electrode and more electrodes are required at the same time. For this, operating conditions were determined for both PGE and gold electrode. According to intra-day t-test results between different hours of the electrodes and at the same time between different electrodes, each group seems to be consistent within itself. According to the Tukey Post-Hoc test performed in one-way ANOVA, the MIP group differs from the UMIP and NIP groups with a significant difference. It is seen that there is no significant difference between UMIP and NIP groups. This can be explained by the fact that the MIP group has interfaces that recognize the valine molecule, while the UMIP and NIP groups do not have these interfaces. For Inter-day precision tests, as a result of the t-test, comparing the measurements of the electrodes of the MIP group on the first day with the other days, it is

seen that the p values are greater than 0.05 and there is no significant change in the 45-day period compared to the first day. In this thesis study, homogeneity between variances was provided for measurements taken on different days. Tukey Post-Hoc test performed in two-way ANOVA showed that there is no significant difference between the days in the measurements taken during the 45-day period. From this, it can be seen that the results of the analysis performed on different days are consistent. According to the Tukey Post-Hoc test, MIP, UMIP and NIP groups differed from each other with a significant difference in the 45-day period.

In the selectivity tests, when the measurement is made in a solution containing a molecule other than the valine molecule imprinted on the gold electrode, it is seen that the impedance responses are formed in the EIS graphs, but the R_{ct} values are not. The flat part of the graph represents the diffusion and this result is due to the conductivity of the hydrogel and the gold electrode. Semicircular part of the EIS curve may not always occur in Nyquist diagrams. The second situation is the formation of what is called pore blockage. In this case, the number of remaining vacancies is inversely proportional to the concentration of the target molecule [88]. Finally, if the bonding does not occur between the molecule imprinted on the electrode and the molecule to be detected, specific interference and impedance will not to be observed in the measurements made in solutions containing glycine, methionine and alanine is due to the fact that the Au-0.3M-Val-MIP electrode is valine-specific and does not detect other molecules (Figure 3.164, 3.167, 3.170). Since there are recognition sites specific to valine molecule on the gold electrode, it cannot select other amino acids. According to α values, valine imprinted electrode was 3.96, 4.19, and 92.76 times more selective for valine than glycine, alanine, and methionine, respectively. Valine imprinted sensor can recognize analyte, valine was 4.13, 4.41 and 96.63 times more selective than glycine, alanine and methionine according to imprinting factors (β values).

Gold electrodes were analyzed in rat blood plasma sample to investigate the reliability and applicability of valine-MIP biosensors for clinical applications. The use of plasma samples for blood tests minimizes sample processing delays caused by clotting, laboratory technical challenges connected with fibrin development, and delayed results due to incompletely clot samples. In addition, more plasma than serum can be made from the same volume of blood. Valine in blood plasma binds to the recognition sites of electrode, as well as the correlation between increasing valine concentration and impedance based on EIS response for the Au-

0.3M-Val-MIP electrode. Signal is directly proportional to analyte concentration. Ratio of concentration of analyte in initial solution to concentration of analyte plus standard in final solution is equals to ratio of signal from initial solution to signal from final solution. In the standard addition method applied to determine the unknown valine concentration in the rat blood plasma, it was determined that there was 309±14.74 µM valine in the plasma, according to the calculation of the analyte concentration. In order to determine the accuracy of the valine concentration in the blood plasma calculated with the standard addition method, the amount of valine in the same blood sample was tested with the Liquid Chromatography-Mass Spectrometry (LC–MS) method. According to the LC-MS results, the valine amino acid concentration in the blood plasma was determined as 263.94 µM.

The reason for the relatively high valine concentration in the tests performed with the Au-0.3M-Val-MIP electrode is thought to be the fact that blood plasma was added to the solution used as a blank in the calculations, even though the standard was not added. These measurements can be repeated using only Rdx-PBS for the starting solution in addition to the five solutions analyzed. In this study, it is seen that valine can be detected in the detection range of 7.16 fM – 7.16 µM in PBS. The fact that the analysis time is between 4.5-5 minutes, the validation results are consistent and the detection interval is wide shows that the biosensor developed in this study can be used effectively in the detection of valine.

According to the AFM analysis with valine and choline molecules, it is seen that there are important differences between the morphologies of the MIP, UMIP and NIP surfaces, and it is a subject worth examining more.

5. CONCLUSION

Biosensors are based on the principle that a signal proportional to the amount of analyte is formed on the transducer surface as a result of transmitting the interaction signal between the substance to be analyzed and the biocomponent on the biosensor surface to the measuring device. Biocomponents in biosensors can include enzymes, microorganisms, receptors, antibodies, and nucleic acids. A suitable transducer that converts the electrochemical signal between a biocomponent and the analyte into an electrical signal should be chosen based on the structure of the molecule to be analyzed. Providing the appropriate immobilization of a biological material is one of the biggest problems in biosensor studies. The immobilization step is critical in determining the useful life of biological material. Because of their high efficiency, biosensor systems prepared with the selection of an optimal immobilization method are widely used in the commercial field today. In the developed valine biosensor, valine molecule was immobilized with TRIS-HCl on the Au electrode surface in the presence of Acrylamide/Bisacrylamide. Optimization studies of the bioactive layer and working conditions of the developed valine biosensor were carried out. At the end of these studies, the appropriate amino acid concentration was 0.3M/ml; The optimum temperature was 37ºC, the optimum pH was 5.0, the optimum scan rate was 100 mV/s and the optimum response time was 30 seconds. It was deemed appropriate to incubate the valine molecule at 37^0C for 1 hour to form the bioactive hydrogel layer containing the valine recognition sites. In the characterization studies of the produced biosensor, the linear detection range in Rdx-PBS solution was found to be $7.16x10^{-15}$ - $7.16x10^{-6}$ M. In the selectivity tests, it was shown that the electrode formed could not detect molecules other than valine. Valine imprinted electrode was 3.96, 4.19, and 92.76 times more selective for Valine than glycine, alanine and methionine, respectively. As a result of the studies, the developed biosensor gave reproducible results for valine; it gives responses proportional to the concentration of valine in the solution in a certain concentration range; the sensitivity was also observed to be 7.16 fM.

6. FUTURE DIRECTIONS

In the literature research, it has been observed that there is no 'Au-Valine-MIP' based biosensor. Thus, the goal of this study is to save time for the patient as a result of early and accurate cancer diagnosis in pre-scans, which can specifically recognize valine with an appropriate biosensor with high electrochemical characteristics and conductivity, excellent corrosion and oxidation resistance, and a durable and stable sensor.The following items can be used to summarize the project's contribution in this context: Valine is a nano-sized molecule that has been linked to early cancer detection as well as being a cellular compound in humans. It is possible that the use of valine biosensors in clinics and patient-receiving points will aid in the early detection of cancer in screening tests. A useful and stable biosensor that can detect valine by impedance spectroscopy method (which detects different molecules in a multi-channel device in the future) has been developed in this project, and it can be used in the units where the patient is seen. The quantitative and qualitative analysis of various nano-sized molecules (metabolites) associated with different types of cancer will be performed by detecting them in current cancer studies using this electrode, which can rapidly measure blood without removing the person from the environment, saving time.

REFERENCES

1. Bulut Y. editor. Biyosensörlerin tanımı ve biyosensörlere genel bakış. *6th International Advanced Technologies Symposium (IATS'11)*; 2011:IATS.

2. Ratner BD, Hoffman AS, Schoen FJ, Lemons JE. *Biomaterials Science.* San Diego:Academic Press;1996.

3. Pacheco JG, Silva MSV, Freitas M, Nouws HPA. Molecularly imprinted electrochemical sensor for the point-of-care detection of a breast cancer biomarker (CA 15-3). *Sensors and Actuators.* 2018;256:905–912

4. Fedorov I, Korabel'nikov D, Nguyen C, Prosekov A. Physicochemical properties of l and dl valine: frst principles calculations. *Amino Acids.* (2020);52:425-433.

5. Xie G, Lu L, Qui Y, Ni Q, Zhang W, Gao Y, Risch H, Yu H, Jia W. Plasma metabolite biomarkers for the detection of pancreatic cancer. *American Chemical Society,* 2014;14:1195-1202.

6. Gümüşderelioğlu M, Karakeçili Gönen A. Nanotıp ve nano robotlar. *Bilim ve Teknik Dergisi.* 2013;20-21.

7. Aykut U. Temiz H. Biyosensörler ve gıdalarda kullanımı. *Gıda Teknolojileri Elektronik Dergisi.* 2006;3:51-59.

8. Turner A, Karube I, Wilson GS. *Biosensors: fundamentals and applications.* New York:Oxford university press;1987.

9. Blum LJ, Coulet PR. *Biosensor Principles and Applications,* New York:Marcel Dekker Inc;1991.

10. Patel P.D. (Bio)sensors for measurement of analytes implicated in food safety: a review. *TrAC Trends Anal. Chem.*2002;21:96-115.

11. Scott AM, Jedd D, Wolchok JD, Old LJ. Antibody therapy of cancer. *Nature Reviews.* 2012; 12: 278-287.

12. Akbayırlı P, Akyılmaz E. Activation-based catalase enzyme electrode and its usage for glucose determination. *Analytical Letters.* 2007; 40: 3360-72.

13. Zhou YL, Zhi JF. Development of an amperometric biosensor based on covalent immobilization of tyrosinase on a boron-doped diamond electrode. *Electrochemistry Comunications*, 2006; 8: 1811-1816.

14. Kindschy LM, Alocilja EC. A review of molecularly imprinted polymers for biosensor development for food and agricultural applications. *Trans. ASAE.* 2004; 47: 1375-1382.

15. Rogers KR, Mascini M. Biosensors for field anlytical monitoring. *Field Anal. Chem. Technol*. 1998;2:317-331.

16. Yanbin L. Biosensors. CIGR Handbook of Agricultural Engineering. 2006:52-93.

17. Heinemann WR, Anderson CW, Halsall HB. Immunoassay by differential pulse polarography. *Sci. Wash.* 1979;204:865-866.

18. Bilitewski U, Drewes W, Neermann J, Schrader J, Surkow R, Schmid RD, Bradley J. Comparison of different biosensor systems suitable for bioprocess monitoring. *J. Biotechnol.* 1993;31:257-266.

19. Delwiche M, Tang X, BonDurant R, Munro C. Improved biosensor for measurement of progesterone in bovine milk. *Trans. ASAE.* 2001;44:1997-2002.

20. Sanaikone K, Delwiche M, BonDurant R, Munro C. Quantitative lateral flow immunoassay for measuring progesterone in bovine milk. *Trans. ASAE.* 2004;47:1357-1365.

21. Rajendran M, Ellington AD. Chapter 12: Nucleic acids for reagentless biosensors. *Optical Biosensors—Present & Future*, 2002:369-396.

22. Chan SDH, Dill K, Blomdahl J, Wada HG. Non-isotopic quantitation of mRNA using a novel RNAse protection assay. Measurements of erb-2 mRNA in tumor cell lines. *Anal. Biochem.* 1996;242:214-220.

23. Karube I, Suzuki M. *Microbial biosensors. Biosensors*: A Practical Approach. Oxford, UK: Oxford University Press; 1990.

24. Chang IS, Jang JK, Gil GC, Kim M, Kim HJ, Cho BW, Kim BH. Continuous determination of biochemical oxygen demand using microbial fuel cell based biosensor. *Biosens. Bioelectron.* 2004;19:607-613.

25. Wijesuriya DC, Rechnitz GA. Biosensors based on plant and animal tissues. *Biosens. Bioelectron*. 1993;8:155-60.

26. Heinemann WR, Anderson CW, Halsall HB. Immunoassay by differential pulse polarography. *Sci. Wash*. 1979;204:865-866.

27. Liu G, Lin Y. Biosensor based on self-assembling acetylcholinesterase on carbon nanotubes for flow injection/amperometric detection of organophosphate pesticides. *Anal. Chem*. 2006;78:835-843.

28. Ziğal N. Nanolif kaplı kuvars kristal mikroterazi yüzeyler ile kütle hassas biyosensörlerin performansının geliştirilmesi (Master Thesis). Hacettepe University, Graduate School of Natural and Applied Sciences, Ankara. 2012.

29. Bergveld P. Development of an ion sensitive solid state device for neurophysiological measurements. *IEEE Trans. Biomed. Eng*. 1970;17:70-71.

30. Watson LD, Maynard P, Cullen DC, Sethi RS, Brettle J, Lowe CR. A microelectronic conductimetric biosensor. *Biosens. Bioelectron*. 1988;3:101-115.

31. Liley M. Chapter 6: Optical transducers. *Biomolecular Sensors*. 2002:121-175.

32. Delwiche M, Cox E, Goddeeris B, Van Dorpe C, De Baerdemaeker J, Decuypere E, Sansen W. A biosensor to detect penicillin residues in food. *Trans. ASAE*. 2000;43:153-159.

33. Blum LJ, Gautier SM, Coulet PR. Fiber-optic biosensors based on luminometric detection. *Food Biosensor Analysis*. 1994:101-121.

34. Rich RL, Myszka DG. Why you should be using more SPR biosensors technology. *Drug Discovery Today*: *Tech*. 2004;1:301-308.

35. Robinson GR, Attridge JW, Deacon JK, Whiteley SC. The fluorescent capillary device. *Sensors Actuators B11*. 1993:235-238.

36. Shons A, Dorman F, Najarian J. The piezoelectric quartz immunosensor. *J. Biomed. Mater. Res*. 1972; 6:565-570.

37. Kroger S, Danielsson B. Chapter 13: Calorimetric biosensors. Handbook of biosensors and electronic noses, *Medicine, Food, and the Environment*. 1997:279-298.

38. Varshney M, Srinivasan B, Tung S, Li Y. Microfluidic filter chip based chemiluminescence filter optic biosensing method for the detection of E. Coli O157:H7. *American Society of Agricultural and Biological Engineers*. 2005.

39. Ferrari M, Bashir R, Wereley S. *BioMEMS and Biomedical Nanotechnology*. USA:Springer;2007.

40. Tibbe AG, Grooth BG, Greve J, Dolan GJ, Rao C, Terstappen LW. Magnetic field design for selecting and aligning immunomagnetic labeled cells. *Cytometry*, 2002;47:163-172.

41. Tüylek Z, Biyosensörler ve nanoteknolojik etkileşim. *BEU Journal of Science*. 2017;6(2):71-80.

42. Singh N, Manshian B, Jenkins GJS, Griffiths SM, Williams PM, Maffeis TGG. Nanogenotoxicology: The DNA damaging potential of egineered nanomaterials. *Biomaterials*. 2009;30(23-24):3891-914.

43. Rasooly A. Biosensor technologies. *Methods*. 2005;37(1):1-3.

44. Eggins BR. *Biosensor: an Introduction*. Chichester: Wiley-Teubner; 1996.

45. Ratner BD, Hoffman AS, Schoen FJ, Lemons JE. *Biomaterials Science*. U.S.A: Academic Press; 1996.

46. Sharma SK, Sehgal N, Kumar A. Biomolecules for development of biosensor and their applications. *Current Applied Physics*. 2003;3(2-3):307-316.

47. Skoog D, Holler F, Nieman T. *Principles of Instrumental Analysis*. Orlando: Harcourt Brace College Pub; 1998

48. Dinçkaya E. Enzim sensörleri, biyosensörler, *Ege University Faculty of Science Press*. 1999;81-142.

49. Can F. Glukoz Oksidaz enziminin iletken polimerlere immobilizasyonu ve karakterizasyonu (Master Thesis). Mustafa Kemal University. Graduate School of Natural and Applied Sciences, Hatay. 2010.

50. Bard AJ, Faulkner LR. *Electrochemical Methods*, 2nd Ed, New York: John Wiley and Sons, Inc; 2001.

51. Bard AJ. *Integrated Chemical Systems*. New York :Wiley-Inderscience; 1994.

52. Haupt K, Mosbach K. Molecularly imprinted polymers and their use in biomimetic sensors. *Chemical Reviews*. 2000;100:2495-2504.

53. Lehn JM. *Supramolecular Chemistry: from molecular information towards self-organization and complex matter*. Weinhein : Wiley-VCH; 1995.

54. Wulff G, Poll HG. Enzyme-analog built polymers: Influence of the structure of the binding-sites on the selectivity for racemic-resolution. *Makromolekulare Chemie-Macromolecular Chemistry And Physics*, 1987;188(4):741-748

55. Saylan Y, Akgönüllü S, Yavuz H, Ünal S, Denizli A. Molecularly imprinted polymer based sensors for medical applications. *Sensors*. 2019;19:1279.

56. Aherne A, Alexander C, Payne MJ, Perez N, Vulfson EN. Bacteria mediated lithography of polymer surfaces. *Journal of the American Chemical Society*. 1996;118(36):8771-8772.

57. Kempe M, Mosbach K. Separation of amino acids, peptides and proteins on molecularly imprinted stationary phases. *Journal of chromatography A*. 1995;691(1-2):317-23.

58. Hjerten S, Liao JL, Nakazato K, Wang Y, Zamaratskaia G, Zhang HX. Gels mimicking antibodies in their selective recognition of proteins. *Chromatographia*. 1997;44:227–234.

59. Ensıng K, Berggren C, Majors RE. Selective sorbents for solid-phase extraction based on molecularly imprinted polymers. *LC-GC Europe*. 2001;19(9): 943-954.

60. Piletsky SA, Piletskaya EV, Elgersma AV, Yano K, Karube I, Parhometz YP. Atrazine sensing by molecularly imprinted membranes. *Biosensors and Bioelectronics*. 1995;10:959.

61. Rao CNR, Müller A, Cheetham AK. *The chemistry of nanomaterials: Synthesis, Properties and Applications*. John Wiley & Sons, Inc.; 2005;3:527.

62. Karim K, Breton OF, Rouillon, R, Piletska EV, Guerreiro A, Chianella I, Piletsky SA. How to find effective functional monomers for effective molecularly imprinted polymers. *Advanced Drug Delivery Reviews*. 2005;57:1795-1808.

63. Holthoff EL, Bright FV. Molecularly templated materials in chemical sensing. *Analytica Chimica Acta*. 2007;594:147–161.

64. Komiyama M, Takeuchi T, Mukawa T, Asanuma H. Molecular Imprinting, from fundamentals to applications. *Wiley-VCH Verlag GmbH & Co. KGaA*. 2003;3:527.

65. Takeuchi T, Haginaka J. Separation and sensing based on molecular recognition using molecularly imprinted polymers. *Journal of Chromatography B*. 1999;728:1-20.

66. Arshady R, Mosbach K. Synthesis of substrate-selective polymers by host-guest polymerization. *Macromolecular Chemistry*. 1981;182:687-692.

67. Vlatakis G, Andersson LI, Muller R, Mosbach K. Drug assay using antibody mimics made by molecular imprinting. *Nature*. 1993;361:645-647.

68. Wulff G, Knorr K. Stoichiometric noncovalent interaction in molecular imprinting. *Bioseparation*. 2002;10:257-276.

69. Marty JD, Mauzac M. Molecular imprinting: State of the art and perspectives. *Advanced Polymer Science*. 2005;172:1-35.

70. Katz A, Davis ME. 1999. Investigation into the mechanisms of molecular recoginition with imprinted polymers. *Macromolelers*. 1999;32:4113-4121.

71. Dong XC, Sun H, Lu X, Wang HB, Lui SX, Wang N. Separation of ephedrine stereoisomers by molecular imprinted polymers influence of synhetic condition and

mobile phase compositions on the chromatographic performance. *Analist*. 2002;127:1427-1432.

72. Asav E. Altın Elektrod yüzeyinde tek tabaka oluşumuna dayalı çift enzimli biyosensör sistemi geliştirilmesi (MSc Thesis). Ege University. 2009.

73. Harris DC. *Quantitative Chemical Analysis.Calibration methods*. New York: WH Freeman and Company; 2003.

74. Guo HM, Liu HW, Wang YL, Gao HJ, Gong Y, Jiang HY, Wang WQ. Surface structures of DL-valine and L-alanine crystals observed by atomic force microscopy at a molecular resolution. *Surface Science*. 2004;552:70–76.

75. Maia LF, Rodrigues AC. Electrical conductivity and relaxation frequency of lithium borosilicate glasses. *Solid State Ionics*. 2004;168(1-2), 87-92.

76. Vermoyal JJ, Frichet A, Dessemond L, Hammou A. AC impedance study of corrosion films formed on zirconium based alloys. *Electrochimica Acta*. 1999;45(7):1039-1048.

77. Yue D, Jia Y, Yao Y, Sun J, Jing Y. (2012). Structure and electrochemical behavior of ionic liquid analogue based on choline chloride and urea. *Electrochimica Acta*. 2012;65:30-36.

78. Cormack PAG, Elorza AZ. Molecularly imprinted polymers: Synthesis and characterization. *Journal Chromatography B*. 2004;804:173-182.

79. Sellergren B. Enantiomer separation using tailor-made phases prepared by molecular imprinting. *Practical Approach Chiral Separaton Liquid Chromatography*. 1994:69-93.

80. Chapuıs F, Pıchon V, Hennıon MC. Molecularly imprinted polymers: Developments and applications of new selective solid-phase extraction materials. *LC-GC Europe*. 2004;17(7):408-417.

81. Plimmer RHA, Hopkins FG. *The chemical constitution of the proteins*. London:Longmans; 1908.

82. Jakubke HD. *Aminoacid, Peptide, Proteine*. Weinheim:Verlag Chemie; 1982.

83. Brown-Borg HM, Rakoczy SG, Wonderlich JA, Rojanathammanee L, Kopchick JJ, Armstrong V, Raasakka D. Growth hormone signaling is necessary for lifespan extension by dietary methionine. *Aging Cell*. 2014;13(6):1019–1027.

84. Polat T. Molecular imprinting polymer based biosensor for choline (Thesis). Yeditepe University, Engineering Faculty, İstanbul. 2017.

85. Ranjbar MRN, Luo Y, Poto C, Varghese RS, Ferrarini A, Zhang C, Sarhan N, Soliman H, Tadesse HM, Ziada DH, Roy R, Ressom HW. GC-MS based plasma metabolomics for identification of candidate biomarkers for hepatocellular carcinoma in Egyptian cohort. *Plos One*. 2015:10(6)

86. Cohen J. Eta-squared and partial eta-squared in fixed factor ANOVA designs. *Educational and Psychological Measurement*. 1973;33:107–112.

87. Tekin S. Platin elektrot yüzeylerine tutturulmuş organik moleküllerin elektrokimyasal tekniklerle pK_a değerlerinin tayini (Thesis). Ankara University, Graduate School of Natural and Applied Sciences, Ankara. 2008.

88. Peeters M, Eersels, K, Junkers, T, Wagner P. Molecularly imprinted polymers: synthetic receptors for diagnostic medical devices, in molecularly imprinted catalysts. *Elsevier*. 2016;253-271.

89. Field A. *Discovering Statistics Using IBM SPSS Statistics*. Sage; 2018.

90. Anfinsen CB. Studies on the principles that govern the folding of protein chains. *Chemistry*. 1972;55-71.

91. Pedersen CJ. Cyclic polyethers and their complexes with metal salts. *Chem. Soc*. 1967;89:2495-2496.

92. Cram DJ, Cram JM. Host-Guest Chemistry: Complexes between organic compounds simulate the substrate selectivity of enzymes. *Science*. 1974;183:803.

APPENDIX A: ETHICAL COMMITTEE APPROVAL FORM

T.C. YEDİTEPE ÜNİVERSİTESİ
Hayvan Deneyleri Yerel Etik Kurulu (HADYEK)

ETİK KURUL KARARI

Protokol No	Toplantı Tarihi	Toplantı Sayısı	Karar No	Proje Yürütücüsü
2021-046	10.08.2021	2021/08	2021/08-9	Dr. Öğr. Üyesi Feride Şermin Utku
'Altın Disk Elektrod Üzerine Yapılandırılan Mıp Tabanlı Valin Biyosensörü' isimli proje oy birliğiyle etik açıdan uygun görülmüştür.				

Hayvan Türü / Irkı	Toplam Hayvan Sayısı	Hayvanın Cinsiyeti
Sıçan / Spraque Dawley	6	Erkek veya Dişi

Görevi	Adı Soyadı	Katılım Durumu
Başkan	Prof.Dr. Bayram YILMAZ	
Başkan Vekili	Prof.Dr. Erdem YEŞİLADA	
Üye	Dr. Veteriner Hekim Engin SÜMER	
Üye	Prof.Dr. M. Ece GENÇ	
Üye	Prof.Dr. Rukset ATTAR	
Üye	Prof.Dr. Gamze TORUN KÖSE	
Üye	Prof.Dr. Özlem MALKONDU	
Üye	Doç.Dr. Aylin YABA UÇAR	
Üye	Doç.Dr. Burcu GEMİCİ BAŞOL	
Üye	Atakan Mücahit YAVUZ	
Üye	Ahmet ŞENKARDEŞLER	

APPENDIX B: LC-MS ANALYSIS WITH RAT BLOOD PLASMA

TIBBİ LABORATUVAR TETKİK SONUÇ RAPORU

(ORİJİNAL RAPOR)

Laboratuvar Ruhsat No(667-B)

Adı Soyadı	**: AYSEL ARAT**	**Cinsiyeti / Yaşı**	: Kadın / 21
T.C. Kimlik No	:	**Doğum Tarihi**	: 01.01.2001
Dosya Numarası	: 8066960	**Numune Türü**	: Serum
Örnek Numarası	: 33605349	**Adresi**	:
Rapor Numarası	: [123].[33605349].[2021]	**Rapor Basım**	: 06.01.2022 15:43
Referans ID	: 3748253		
İsteyen Hekim/Merkez	: LABORATUVAR DOKTORU	**Tetkik İstem Tarihi**	: 31.12.2021 10:06
Kurum	: REFERANS LABORATUVARI İSTANBUL	**Numune Alma Tarihi**	: 31.12.2021 10:06
		Lab. Kabul Tarihi	: 31.12.2021 13:32

Triptofan	**120.74**	**umol/L**	10 - 140	LC-MS/MS (1)
Tirozin	**107.02**	**umol/L**	34 - 112	LC-MS/MS (1)
Sistin	**45.52**	**umol/L**	33 - 55	
Valin	**263.94**	**umol/L**	119 - 336	

Yorum: Normal plazma amino asit analizi

Plazma amino asit analizi açıklaması:
Referans değerler 10-12 saatlik açlık sonrası alınan numune için geçerlidir. Kan aminoasit düzeyleri değerlendirilirken aşağıdaki kriterler kullanılmaktadır.
Aminoasit düzeyi, referans aralığının dışındaysa; Tek bir aminoasitte üst sınırın %50 üzerine kadar olan artışlar diagnostik olmayabilir. Üst sınırın %50-150 üzerindeki değerler orta düzeyde artmış, üst sınırın %150 sinden yüksek olan değerler ise ileri derecede artmış olarak değerlendirilir ve yeni alınacak numune ile testin tekrarı önerilir.

Uzm. Dr. Kamil Cengiz Bali
Biyokimya ve Klinik Biyokimya Uzmanı
Diploma No: 2570 - 31924/35232
e-imza

Uzm. Dr Altan YALÇINER
Biyokimya ve Klinik Biyokimya Uzmanı
Diploma No:17236/20704
e-imza

APPENDIX C: HYDROGEL FORMULATION

Table C.1. Hydrogel formulations used for MIP process.

Formula Name	Formulation
H513	513 µl Acrylamide/Bisacrylamide (30%) 225 µl EGDMA 61 µl HEMA 179 µl TRIS (1.5 M, pH 4.8) 20 µl APS (10%) 2 µl TEMED
H600	600 µl Acrylamide/Bisacrylamide (30%) 250 µl TRIS (1.5 M, pH 4.8) 10 µl APS (10%) 1 µl TEMED
H767	767 µl Acrylamide/Bisacrylamide (40%) 200 µl TRIS-HCl (3.5 M, pH 4.8) 30 µl APS (10%) 3 µl TEMED
H853	853 µl Acrylamide/Bisacrylamide (40%) 125 µl TRIS-HCl (3.5 M, pH 4.8) 20 µl APS (10%) 2 µl TEMED